AD-A170 002 FRACTURE AND VISCOELASTIC CHARACTERISTICS OF THE HUMAN 1/3
CERVICAL SPINE(U) BETH ISRAEL HOSPITAL BOTTON MASS
W T EDWARDS ET AL. 1986 AFOSR-TR-86-0453
UNCLASSIFIED F49620-81-K-0010 F/G 6/16 NL

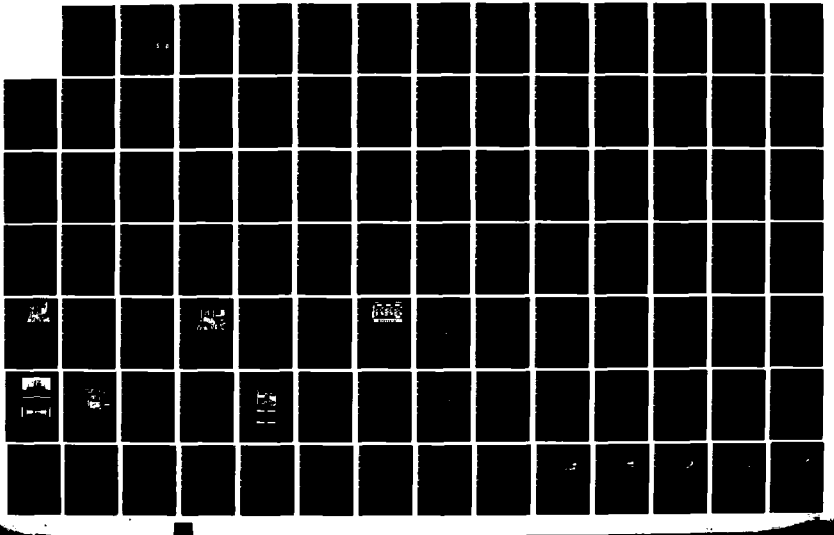

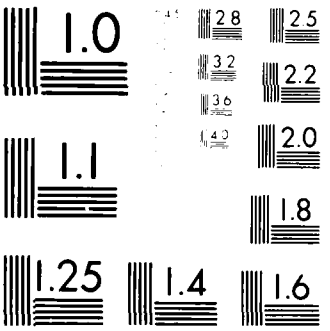

AD-A170 002

DTIC FILE COPY

REPORT DOCUMENTATION PAGE

READ INSTRUCTIONS BEFORE COMPLETING FORM

1. REPORT NUMBER: AFOSR-TR- 86-0453	2. GOVT ACCESSION NO. / 3. RECIPIENT'S CATALOG NUMBER
4. TITLE (and Subtitle): FRACTURE AND VISCOELASTIC CHARACTERISTICS OF THE HUMAN CERVICAL SPINE	5. TYPE OF REPORT & PERIOD COVERED
	6. PERFORMING ORG. REPORT NUMBER
7. AUTHOR(s): W.T. Edwards, W.C. Hayes, Y.F. Kou, M.S. Coffee, and A.A. White III	8. CONTRACT OR GRANT NUMBER(s): F49620-81-K-0010
9. PERFORMING ORGANIZATION NAME AND ADDRESS: Beth Israel Hospital, 330 Brookline Avenue, Boston, MA 02215	10. PROGRAM ELEMENT, PROJECT, TASK AREA & WORK UNIT NUMBERS: 61102F 2312/A2
11. CONTROLLING OFFICE NAME AND ADDRESS: Air Force Office of Scientific Research (AFSC), Bolling Air Force Base, DC 20332	12. REPORT DATE
	13. NUMBER OF PAGES
14. MONITORING AGENCY NAME & ADDRESS (if different from Controlling Office)	15. SECURITY CLASS. (of this report)
	15a. DECLASSIFICATION/DOWNGRADING SCHEDULE

16. DISTRIBUTION STATEMENT (of this Report)

Approved for public release; distribution unlimited.

17. DISTRIBUTION STATEMENT (of the abstract entered in Block 20, if different from Report)

18. SUPPLEMENTARY NOTES

19. KEY WORDS (Continue on reverse side if necessary and identify by block number)

cervical spine; motion segments; lumbar spine; multiaxial testing; failure condition; creep; three-dimensional motion transducer

20. ABSTRACT (Continue on reverse side if necessary and identify by block number)

Cervical spine segments were tested both nondestructively and destructively to determine the load-displacement relationships and vertebral strength. For this study, a sevro-hydraulic multi-degree of freedom material testing machine was designed and constructed. This new system, called the Planar Testing Apparatus (PTA), was used to generate motions needed to characterize the sagittal response of spine segments. A study of the viscoelastic properties of two vertebrae lumbar spine segments was conducted following the completion of the PTA to check and demonstrate the test system. The results from seven lumbar specimens were also

DD FORM 1 JAN 73 1473 EDITION OF 1 NOV 65 IS OBSOLETE

UC

SECURITY CLASSIFICATION OF THIS PAGE (When Data Entered)

20. ABSTRACT (cont.)

included in this report.

The cervical spine segments consisted of three vertebrae and their interconnecting soft tissue, discs, and ligaments. The three vertebrae specimens were taken from the mid cervical region and from the lower cervical spine. A noninvasive electro-mechanical displacement measuring apparatus was constructed to monitor the six degree of freedom motion of the middle vertebral body as it moved relative to the two adjacent vertebrae during the mechanical tests. Kinematic equations were derived to compute the three-dimensional translations and the Eulerian rotations at the center of the moving vertebra.

Results for cervical spine specimens indicated that at low displacement rates (less than 5 mm/sec or 5 deg/sec) there was no dependence of spinal segment stiffness on displacement rate. Curves for load vs. displacement (both axial and shear) and moment vs. sagittal bending displayed large regions of small load and low slope as displacements increased. All specimens were stiffer in compression than in tension. Specimens taken from the upper cervical region showed greater stiffness for posterior motion compared to anterior motion considering motion of the inferior vertebrae with respect to the superior vertebrae in the specimen. They also showed greater stiffness to axial and shear displacement than specimens from the lower region. All specimens displayed soft tissue failure before bony fracture for loading in flexion. The application of axial compression in combination with flexion was required to produce fracture. With the spinal testing techniques developed here, it was possible to precisely quantify the multidimensional biomechanical properties of the spine.

AFOSR-TR- 86-0453

PREFACE

This report describes the research completed as a result of the contract F49620-81-K-0010 awarded to Beth Israel Hospital, Boston, Massachusetts by the Air Force Office of Scientific Research (AFOSR). The contract technical monitor (CTM) during the development of experimental equipment was Col. Irving, and during the later part of the project was Dr. Berry.

The delay in the completion of this contract was due to two principal reasons:

1) The development and construction of the multi-axial materials test system required for the testing of spine segments was more complex and time consuming than anticipated.

2) Administrative problems placed constraints on the budget which delayed hardware development and limited personnel.

An Interim report was submitted to the contract technical monitor in August, 1981 describing the design analysis of test hardware.

The authors acknowledge the contribution of several individuals who participated in this work. The assistance of Joe Lelli is acknowledged for his help during the early development of test system hardware. Y. K. Kou is gratefully acknowledged for design of the central interface between the testing system and the computer. Further appreciation is due Dr. Berry for his understanding and patience while this report was being prepared.

The support provided by the National Institutes of Health through Grant AM33066, and by a Grant from General Motors Research Laboratory after the expiration of this contract made possible the completion of the work reported here.

TABLE OF CONTENTS

LIST OF TABLES

LIST OF FIGURES

1. INTRODUCTION

1.1 BACKGROUND

Reduction of the risk of injury to the cervical region of the spine resulting from extreme loading conditions of the type observed in motor vehicle accidents and emergency ejection from military aircraft is of concern to many. Detailed data of the relationship between loads and displacements, the vertebral strength, and the modes of injury in the spine are required to define the tolerance of the spine to injury.

Experimental methods previously used for in vitro biomechanical studies of the spine have been limited. Methods developed to simulate the complex combination of loads and displacements in the spine generally employ small loads in comparison to the normal physiologic and fracture conditions. Other methods for study of spinal fracture employ uniaxial material testing machines. A primary goal of this project was to develop a multiaxial materials testing system capable of simulating the load displacement conditions for sagittal motions and load specimens to failure. This new multiaxial testing system was used to investigate the mechanics of the cervical spine and the tolerance of the cervical spine to injury.

1.2 PROGRAM SUMMARY

The objectives of this research were: 1) to construct a multiaxial spinal testing apparatus for measuring the material properties of the spine, 2) to determine the geometry of human cervical spine segments, 3) to measure the viscoelastic load-displacement properties of the cervical spine, and 4) to model the cervical spine. A multiaxial testing apparatus was constructed with three independent components of displacement input and six independent components of load measurement. This system, called the Planar Testing Apparatus (PTA), can generate planar motions needed to characterize the sagittal response of spine segments. A study of the viscoelastic properties of two vertebrae lumbar spine segments was conducted following the completion of the PTA to check and demonstrate the test system. The results from seven lumbar specimens were also included in this report.

Seven cervical spine segments were tested both nondestructively and destructively to determine the relationships between loads and displacement, vertebral strength, and modes of failure. The Planar Testing Apparatus was used to measure the mechanical properties of specimens by applying controlled loads or displacements in the sagittal plane. The spine segments consisted of three cervical vertebrae and their interconnecting soft tissue, discs, and ligaments. Three specimens were taken from the upper cervical region, one from the central (C3-C5) region, and three from the lower cervical spine.

A noninvasive electro-mechanical displacement measuring apparatus was developed which monitored the six degree-of-freedom motion of the middle vertebral body as it moved relative to the two adjacent fixed bodies. Kinematic equations were derived to compute the three-dimensional translations and the Eulerian rotations at the center of the moving vertebra. The results included in this report are presented in three parts: A) the development of the Planar Testing Apparatus, B) the viscoelastic properties of lumbar spine segments in compression (a pilot study), and C) the viscoelastic and strength properties of cervical spine segments.

2. PLANAR TESTING APPARATUS DEVELOPMENT

The Planar Testing Apparatus (PTA) is a multi-degree-of-freedom material testing machine (Fig. 1). The concept and kinematic design were originated by W.T. Edwards and Y.F. Kou at the Orthopaedic Biomechanics Laboratory and developed under this grant. The interface of the testing machine to the PDP 11/03 microcomputer and the control protocol of the testing machine were also developed during this project.

The general layout of the Planar Testing Apparatus is similar to most electrohydraulic material testing machines (such as, INSTRON model 1331) in that it contains a moving test stage and a stationary load cell. The test specimens installed on the test stage can be loaded independently in the vertical direction (tension/compression, z-axis), the horizontal direction (shear, x-axis), and rotated about the axis perpendicular to the vertical and horizontal axis (y-axis). Figure 2 shows the orientation of the coordinate axes with respect to the test stage. For this project, functional spinal unit specimens were placed on the test stage such that x-z plane represented the sagittal plane and positive x was in the anterior direction of the specimen (Fig. 3)

2.1. HARDWARE

2.1.1. Load Frame

Test specimens are mounted on the Planar Testing Apparatus load frame between a moving test stage below and a stationary load cell above. The load cell is bolted to a 76x127x940 mm cross head which is mounted on two 61 mm diameter stainless steel poles. The crosshead is clamped onto each of the stainless steel poles by 2 sets of nuts and bolts. The crosshead can slide freely on the poles when the nuts and bolts are loosened, but is secured by tightening the nuts and bolts. Specimens up to 914 mm in length and 254 mm in width can be mounted on the Planar Testing Apparatus for testing. The maximum dimensions of the Planar Testing Apparatus are 2000 mm in height, 660 mm in width and 952 mm in length.

2.1.2. Load Cell

A multi-component load cell (Robert A. Denton, Inc. Model 1687 Serial# 75) was mounted onto the crosshead. This load cell is a cylinder of 140 mm in diameter and 76 mm in height. The load cell can resolve a maximum of 17,792 N in the z direction (tension-compression), a maximum of 8,896 N in the x direction (anterior-posterior shear) and a maximum of 1,129 N-m about the y axis (sagittal bending). Signal conditioning for the load cell is obtained with Vishay 2120 strain gage conditioners.

2.1.3. Test Stage

The test stage (Figure 4) is a 140x254 mm moving platform supported from below by three linear hydraulic actuators. The three hydraulic actuators are arranged so that two of the actuators are attached to one axle of the test stage and the third actuator attached to the remaining axle. Tapered roller bearings are used on the axles to reduce any play in the actuators and test stage attachment mechanism. Extreme care was taken during the assembly of the test stage and bearings to properly align the three actuators in the plane of motion. Holes are drilled and taped on the surface of the test stage for installation of test fixtures to support the specimens.

2.1.4. Hydraulic Actuators

The hydraulic actuators used on the Planar Testing Apparatus have three main components.

(a) the servovalve;

(b) the piston; and

(c) the LVDT position sensor.

The servovalve responds to the incoming electrical current and directs the oil flow path to extend or to retract the actuator piston. The position of the hydraulic actuator is sensed by a linear variable differential tranducer (LVDT) which is installed within the actuator's housing. A MOOG power oscillator (MOOG 123-105) is used to provide excitation for the LVDT.

Three high performance MOOG (MOOG, Inc., East Aurora, N.Y.) cylinder-servovalve assemblies (model A085-233) were used. This actuator has 710 mm^2 piston crossectional area and 152 mm stroke. The servovalve is rated at 207 kPa maximum supply pressure with a maximum no-load velocity of 1244 mm per second (at 137 kPa supply) and an equivalent first-order time constant of 0.002 second (MOOG Inc. : MOOG A085 Servoactuators, Data sheet no. 850-382).

2.1.5. Electro-hydraulic Controller

MOOG 122-104 analog controllers are used to control the position of the hydraulic actuator. A demodulator is built into the controller to condition the A.C. signal from the LVDT, providing D.C. signal proportional to the actuator position. The D.C. signal indicates the position of the hydraulic actuator and serves as the feedback in the control circuit. The inputs to the closed-loop control circuit are the mean level voltage and the command voltage. The mean level voltage offsets the positions of the actuator so that the full range of the actuator can be used (Figure 5). Once the mean level voltage has been set, it remains unchanged during the test sequence. The command voltage is the voltage which actually controls the motions of the test stage. The control block diagram of the MOOG 122-104 analog servo controller is shown in Figure 6.

2.1.6. Display Panel

A display panel allows manual control of the Planar Testing Apparatus, (Figure 7). The panel contains three identical sets of knobs, indicators and circuits which correspond to the three hydraulic actuators. Four LEDs are used to indicate the range setting (100%,50%,10%,5%). The 100% range corresponds to a maximum actuator range of motion of +75 mm. Digital voltmeters (DVM) are used to display the position of the hydraulic actuators in percent of the maximum displacement of the selected range. Selection switches are used to select the DVM display options. The display on the digital voltmeter can be the input command signal, the mean level setting, the LVDT feedback signal, the error signal or the actuator's limit setting. This information is also displayed in percent of the maximum actuator displacement of the selected range.

In addition to displaying the status of the hydraulic actuator, the display panel also interprets the command signal and the range selection signal from the PDP 11/03 microcomputer. The range selection signal activates the analog switches in the circuit and directs the command signal to appropriate potentiometers where the incoming signal is dropped to the proper range. The resulting signal from the panel's input to the MOOG controller. The upper and lower limits of the actuator displacement can be set on the panel. When a pre-selected limit is exceeded, the reed relay on the MOOG D.C. level detector (Model 123-103) shuts off the hydraulic supply to the actuators. The mean level voltage is also set on the display panel. Figure 8 shows the signal flow diagram of the Planar Testing Apparatus.

2.1.7. PDP 11/03 Microcomputer

A PDP 11/03 microcomputer (Digital Equipment Corp., Maynard, MA) is used both as a calculating and a controlling device. The functions of the microcomputer used by the Planar Testing Apparatus including start up, range selection, range calibration, open-loop test stage position control, closed-loop load control and data acquisition. The

microcomputer is set up to take 18 channels of data. The maximum data rate is 10 data points per second for displacement control and 7 data points per second for load control. The control cycle rate is 100 Hertz and 30 Hertz for displacement control and load control respectively. A block diagram of the complete system is shown in Figure 9.

2.2. GEOMETRIC CONSIDERATION

Since the Planar Testing Apparatus is capable of three degree-of-freedom motions, a reference point on the x-z plane (sagittal plane) is necessary to define the position and the orientation of the test stage. Figure 10 shows a simplified drawing of the test stage and the hydraulic actuators. Points E and D are the two axles of the test stage and Points A, B and C are the three axles on the base frame to which the three hydraulic actuators are attached. Parameters ES and TS are input by the user to define the reference point T. The reference point T is the center of rotation and represents the test stage position on the x-z plane. The origin 0 is defined at the mid-point between A and C. The position of point T on the x-z plane (with respect to the origin 0), and the angle theta (defined by DE and the horizontal line), define the spatial position of the test stage. This configuration is referred to as the absolute orientation.

2.3. SYSTEM PRECISION

The main factor affecting the precision of the Planar Testing Apparatus system is the resolution of the A/D and D/A modules on the PDP 11/03 microcomputer. The PDP 11/03 is a 16- bit machine and the MINC software uses the 4 most significant bits as status bits, leaving 12 bits to resolve the analog voltage signal. The full range of the D/A module is +10V with a resolution of 0.0048V per bit The full range of the A/D module is +5.1175V with a resolution of 0.0025V per bit. The MOOG 122-104 servo-controllers have been modified such that the LVDT reading of +5V indicates the full stroke (+76.2 mm) of the hydraulic actuators and the command voltage of +10V moves the hydraulic actuator +75 mm at 100% range setting. This arrangement allows the highest possible resolution with the available equipment. The PDP 11/03 can thus detect a change in actuator displacement of 0.037 mm and can control an actuator displacement of 0.0018 mm at 5% range setting with all actuators near mid-stroke.

Assuming that the time constant of the electronic control circuitary is negligible compared to the time constant of the hydraulic actuator and that the inertia of the actuator is negligible, the system can be represented by the first order system shown in Figure 11. The gain of the servocontroller (K) can be adjusted from between 1 to 20 with the present circuit design. From experiment, the rise time of the hydraulic actuator with no mass attached is 0.06 second with a unit step voltage input. The system is stable throughout the complete range of the gain adjustment. With the test stage mounted on the hydraulic actuators, the added mass of the test stage cannot be neglected and the system becomes second order. Hence,

the stability is affected by the gain setting [24]. Different gain settings have been tried and gain settings under 10 were found to be stable.

2.4. RANGE OF MOTION AND LOAD CAPACITY

The configuration of the Planar Testing Apparatus has been optimized to meet the motion range and load capacity required for tests in spinal mechanics [10]. The kinematic design minimizes the gross actuators motion. The maximum horizontal range is 330 mm, the maximum horizontal force is 36,474 N, the maximum vertical force is 42,256 N and the maximum moment is 31,610 N-m. The ranges of motion and the load capacity of the test stage at different orientation are tabulated in Tables 1 to 3 respectively.

2.5. SOFTWARE

2.5.1. Organization

The control program is organized on three levels. The main program contains the menu of all the available options for the control of the apparatus. The second level is the control programs. All the command signals are generated at this level. Data acquisition and storage also take place at this level. The third level includes the utility programs. This level manages interfacing between the software and the laboratory hardware.

2.5.2. Start Up Routine

A range-calibration provides the voltage relationship between the D/A output voltage and the voltage actually seen by the hydraulic controller. There are four range-calibration data files which correspond to the four ranges (100%,50%,10%,5%) used for hydraulic control. During start up, one of the four range calibration data files is read into the computer program. At the same time, a data file defining actuator location vs the LVDT feedback voltage is also read in. A voltage is then output to the hydraulic controller so that the error signal becomes zero (Figure 12). This voltage is simply governed by the operational-amplifier equation :

$$0.0=(E_{com}/R_{com})+(E_{mean}/R_{mean})+(E_{LVDT}/R_{LVDT}) \qquad (1)$$

where,

E : voltage
R : resistance
com : command
mean : mean level
LVDT : LVDT feedback

The appropriate output voltage (E_{com}) can be calculated from Equation (1) and output through the D/A module to the MOOG hydraulic controller, after the LVDT feedback voltage (E_{LVDT}) and the mean level voltage (E_{mean}) are read into the computer. Error indicating LEDs on the display panel go dark when it is safe to actuate the hydraulic actuator.

2.5.3. Open-Loop Control Routine

The role of the computer in the control scheme defines open or closed loop control. An open-loop control routine is used to position the test stage. The user can input the desired translational and angular displacement or input the final absolute orientation of the test stage. To facilitate testing, portions of this information can also be input through a data file. A ramp function is generated by the control program to move the test stage from the current orientation to the specified orientation and the corresponding output voltage stored in an integer array. A test sequence of ten different orientations can be specified and the routine generates functions to command the test stage to the positions in sequence. The voltage information array is reused for data storage to reduce the core memory required to run the control routine. Nevertheless, a rate of 10 data samples per second can still be attained for 18 channels of data. The open-loop routine can also use the recorded data file to reproduce the displacement history from the particular test.

2.5.4. Closed-Loop Control Routine

The closed-loop control routine changes the orientation of the test stage so that the load (tension-compression, shear and bending moment) specified by the user can be obtained. This routine uses an integral control scheme (Figure 13) so that small disturbances do not affect the final load value. The control algorithm makes a uni-directional search until the loads reach the pre-determined values. The toe region of the load-displacement response for biological tissue does not affect the machine in searching for the loads. The feedback path is completed by the three-component load cell and the signal conditioner (Figure 8). The user is required to supply the desired loads, the test stage velocity limit and the feedback gain. The magnitude of the feedback gain is dependent upon the stiffness of the specimen. For higher stiffnesses, a lower feedback gain is required to maintain stability. Since the routine uses an integal control scheme, a high gain can result in load oscillation [24].

A linearized version of the test stage position control calculation is used to reduce computation time during each closed-loop cycle. The sampling frequency (sweeping rate) of the closed-loop control cycle is set at 30 Hz. The control strategy employed assumes no coupling effect between different components of loads.

2.5.5. Calibration Routine

There are four potentiometers in each of the three sets of circuits in the display panel. These potentiometers reduce the D/A signal to one of the four range settings (100%,50%,10%,5%) selected by the user. The calibration routine serves to calibrate the potentiometer settings to ensure an accurate relationship between the D/A voltage output and the voltage actually seen by the hydraulic controller. The routine utilizes the existing range calibration data to move the hydraulic actuators to different points along the whole displacement range of the actuator. The LVDT feedback voltages at these points are recorded. By using Equation (1), the voltage seen by the hydraulic controller can be calculated. A linear regression is then used to relate the D/A module output to the voltage calculated. The result is then stored in a new range-calibration data file.

2.5.6. Set Mean Level Routine

The mean level voltage is used to offset the position of the individual hydraulic actuators so that an experiment can be performed at the most convenient region of the stroke range. Figure 5 shows a simplified illustration of the operation of the mean level voltage. The displacement shown in Figure 5 can be translational or rotational displacement. Since the Planar Testing Apparatus has three degrees of freedom, the mean level setting for the three hydraulic actuators cannot be randomly selected. This routine allows the users to set the mean level voltage such that a zero command voltage corresponds to the current orientation or to any specified absolute orientation of the test stage.

2.5.7. Test Stage Position Adjustment Routine

Adjustment of the test stage position is necessary during installation of the specimen. The adjustment routine independently moves the test stage in the z, the x directions or rotates the test stage about the y axis. The adjustment has fine and coarse control and can be terminated instantly by the users during the execution of the routine.

2.6. SUMMARY OF PLANAR TESTING APPARATUS

The Planar Testing Apparatus provides a new approach to biological material testing. In the past, tests of multi-axial, coupled spinal mechanics generally used static weights applied with cables and pulleys. The displacement was measured by mechanical or electro-mechanical devices. For equipment of this type, there is no effective way to control the displacements of the specimen in more than one axis.

The ability of the Planar Testing Apparatus to perform load or displacement control in a multi-degree-of-freedom environment not only makes more realistic physiological testing possible, but has opened several new areas of interest. For example, the response of the intervertebral joint to different combinations of displacement directions and rates can be evaluated. It should now be possible to evaluate the stiffness matrix of the intervertebral joint directly instead of inverting the flexibility matrix [25]. With the use of the multi-component load cell, the coupling effect can also be evaluated.

3. VISCOELASTIC PROPERTIES OF THE LUMBAR SPINE

Following the development of the Planar Testing Apparatus, a brief project was undertaken to refine the testing capabilities of this system. The lumbar region of the spine was selected for this study because the specimens were available for testing and the cervical spine specimens could be in this way saved for the main part of the study, presented in the next section of this report, and because the biomechanical properties of the lumbar spine are relevant to the better understanding of both low back pain and injuries to the spine.

3.1 REVIEW OF THE LITERATURE

Compressive loads applied to the spine are supported anteriorly by the intervertebral disc and the longitudinal ligaments, and posteriorly by the facet joints and the posterior ligaments. The intervertebral disc and the facet joints in the lumbar region of the spine have both been identified as possible sites of mechanically induced pain. Excessive mechanical stress can produce pain and injury in the anterior or the posterior spine components. Increased anterior load can promote disc degeneration, disc herniation, or disc proplase. Increased posterior loading may produce soft tissue injuries or osteoarthritis of the facet joints. An understanding of the load distribution characteristic of the intervertebral joint is thus an important step in understanding the etiology of low back pain and the mechanisms of injury in the spine.

Low back pain is one of the most frequent and costly medical complaints in this country [13,33,34]. Kelsey, et al. [13] showed that the back and spine disorders were the most frequent causes of activity limitation in persons under age 45 with a decrease of 28.6 days a year in work capacity per 100 subjects age from 25 to 44 in the United States. Low back pain affects more than half of the working population at some time during their working careers [33]. Based on data from 237 long-term male employees just before their retirement at age 62- 65, Rowe found that 56% of workers experience low back pain sufficient to require medical treatment [30]. Drivers, material handlers and office workers are amoung the highest risk groups for low

back pain [33,34]. Even though drivers and office workers do not usually participate in heavy lifting, both kinds of jobs involve long period of sitting. Therefore, the time dependent load distribution characteristic of the intervertebral joint cannot be neglected when considering the cause of low back pain.

In-vivo measurements indicate that large forces occur in the lumbar spine during the activities of daily living. Nachemson measured interdiscal pressure in-vivo and compared the result with the pressure obtained from cadaver specimens [22]. He pointed out that the pressure in the L3-L4 disc corresponds to a force as high as 2.5 times body weight when the subject is sitting or standing at 20 degrees flexion. His experiment also established that the interdiscal pressure is related to the mechanical stress applied to the intervertebral joint [23]. Since the load supported by the lumbar disc is high, it has been hypothesized that mechanical stresses play an important role in the pathogenesis of low back pain. However, the specific mechanisms involved are poorly understood [37].

Both the anterior and posterior portions of the intervertebral joint display nonlinear, coupled viscoelastic load-displacement properties [29]. We may hypothesize that a difference in the viscoelastic properties of the disc and the facets can cause a re-distribution of load between these functional spinal unit components in response to sustained compressive load. Thus, when a constant axial compressive load is applied to the intervertebral joint, the relative load distribution between the intervertebral disc and the facet joints vary with time.

The objectives of this investigation of the lumbar spine were to assess the time dependent load distribution characteristics of the intervertebral joint using physiological combinations of displacements and loads. The specific objectives were:

1) Measure the creep response of intact lumbar functional spinal units;

2) Determine the fraction of total applied load supported by the disc and the facets; and

3) to generate an idealized viscoelastic model for the lumbar functional spinal units.

The advanced testing methodologies needed for these biomechanical measurements were developed for the Planar Testing Apparatus and demonstrated using this system.

3.2 MATERIALS AND METHODS

The load-displacement and creep characteristics of 7 lumbar functional spinal units (FSU) were studied. Physiologic load conditions were selected to test the distribution of compressive load between anterior and posterior functional spinal unit components over time.

3.2.1. Pretest Preparation

Two vertebrae, lumbar functional spinal units (FSU) of L1-L2 and L3-L4 were used in this experiment. Human spines were obtained from donated cadavers from the Harvard Medical School Anatomical Gifts Program. These specimens were collected within 48 hours after death and were placed into tightly sealed plastic bags to prevent dehydration and were frozen at -20 degrees Celsius until needed. X-rays were taken of each specimen to screen out those with metastatic bone disease, previous spinal fractures or other disorders known to alter the mechanical properties of the spine. Prior to testing, the spines were thawed over night at room temperature. Excess soft tissues were cleaned from the specimens leaving the interconnecting ligaments intact. The spines were then divided into L1-L2 and L3-L4 functional spinal unit specimens by dissection of the adjacent discs. The exposed discs at the T12-L1, L2-L3 and L4-L5 levels were graded from 0 (normal) to 3 (degenerated) using the grading method of Galante [9].

Seven lumbar specimens were used for this experiment. The age, sex, disc grade, and causes of death for these cadaver specimens are shown in Table 4a.

3.2.2. Test Fixture and Mounting Protocol

A special test fixture was designed for the load- displacement and creep tests Figure 14. With this fixture, a constant reference configuration was exactly reproducible during repeated removal and installation of the fixture in the Planar Testing Apparatus. The two identical parts of the fixture were constructed from a rectangular, 25 mm thick aluminium plate. An aluminium ring 31.8 mm in height with an outer diameter of 133.3 mm and 12.7 mm wall thickness was attached to the center of each plate. Four 63.5 mm long set screws positioned 90 degree apart were screwed through the wall into the aluminium ring radially from the outside. Another four socket head screws were screwed into the wall along the axial direction of the ring to secure the aluminium ring onto the plate. Epoxy was used to seal the gap between each ring and plate so that there was no leakage through the cup formed by the ring and the plate.

One vertebra of the functional spinal unit pair was mounted in each of the fixture halves. One long metal bolt was screwed horizontally through each of the superior and inferior vertebral bodies in the frontal plane. A wood screw was screwed through the

superior and inferior spinous processes of each vertebra. Half of the inferior vertebral body of the specimen was then placed into the cup on the lower plate of the fixture. By using the long set screws around the aluminium cup, the specimen was carefully positioned so that the mid-plane of the intervertebral disc was parallel to the lower plate. Resin ('Castolite' Buehler Ltd. No. 20-8120-009) was then poured into the aluminium cup until the resin covered the long metal screw in the inferior vertebral body, the wood screw in the spinous process, and the four set screws of the ring, all of which served to secure the spinal specimen within the resin. The resin hardened in about 1.5 hours.

The specimen was kept moist at all times. For mounting, wet cotton padding was wrapped around the specimen and periodically injected with water by a syringe to maintain a moist environment. During the test, an additional plastic saranite film was placed around the specimen. Radiographs were used to verify proper positioning of the spinal specimens in the test fixture, Figure 15. Four threaded rods were screwed superior-inferiorly into the four corners of the lower plate and four aluminium tubes of equal length (82.5 mm) were sleeved over each rod. The upper plate was then placed onto the fixture with the cup facing down toward the specimen and the four threaded rods through the four corresponding holes on the upper plate. The upper plate was supported by the four equal length aluminium tubes and became parallel to the lower plate. Nuts were put onto the rods to secure the two plates in position. The length of the aluminium tubes were selected so that about half of the superior vertebral body was embedded in the cup on the upper plate. The superior vertebral body was held in place by the set screws of the upper aluminium cup while resin was poured into the cup to secure the superior vertebral body.

After the resin was set, the lower and upper plates together with the threaded rods and aluminium tubes were mounted to the test stage and the load cell of the Planar Testing Apparatus (Figure 16). The functional spinal unit was positioned on the test stage of the Planar Testing Apparatus so that the sagittal plane of the specimen was in the same plane as the plane of motion (x-z) of the Planar Testing Apparatus. This initial orientation of the test stage was referred to as the set up orientation.

3.2.3. Neutral Point

Most biological tissues (including the intervertebral joint) are viscoelastic and non-linear. Figure 17 shows a typical load-displacement response of a functional spinal unit for one complete cycle of displacement. The flat region around the zero load point has been called the toe region or the neutral zone. Several different definitions have been given for the neutral zone and the neutral point [8,29]. In our tests, the neutral point for each functional spinal unit was defined as the mid-point between the two intersections of the hysteresis curve with the zero load line (points A and B in Figure 17). The neutral point and neutral zone were defined for the three

components of sagittal displacement by measuring the load-displacement response for each independent motion. The neutral orientation was defined as the position of the test stage where all three components of displacement (axial translation : x, anterior-posterior translation : z, and sagittal rotation : Θy) were located at their neutral points. The initial translation (x=0, z=0) and initial rotation (theta=0) for all experiments on each specimen were also defined at the neutral orientation.

After the specimen was placed in the Planar Testing Apparatus and the set up orientation defined, complete cycles of motions in x,z translation and sagittal rotation were executed on the testing machine to generate hysteresis curves for the specimen. The three load-displacement (tension-compression, translational shear and sagittal bending) curves were plotted on the CRT of the computer. The displacements from the set up orientation to the neutral orientation were estimated from the CRT display and recorded. The test stage was then moved to this neutral orientation and the orientation stored into memory for the remainder of the tests.

3.2.4. Functional Spinal Unit Geometry

For these experiments, the superior and inferior vertebral bodies were assumed to be rigid. The dimensions of the set up of the specimen and fixture were obtained from the lateral radiograph (Figure 15). The magnification factor of the radiograph was calculated by comparing the actual dimensions between two markers placed on the fixture and its images on the X-ray. The conventions used to define the geometry of the superior and inferior vertebral bodies are shown in Figure 18. The center of the vertebral body was defined as the intersection of the two lines connecting the mid-points of AB, CD and AD, BC. The loads applied to the specimen were resolved to the center of the superior vertebral body. The center of rotation of the test stage was placed at the center of the inferior vertebral body.

3.2.5. Experimental Protocol

The experiment was divided into five parts. Part I involved defining the neutral point and setting up the experiment. The load-displacement responses of the intact functional spinal unit and the isolated anterior components were measured in Parts II and IV, respectively. The creep responses of the intact function spinal unit and the anterior portion of the function spinal unit were measured in Parts III and V.

The geometry of the functional spinal units was measured from the radiographs, and the data is presented in Table 4b.

Part I - Neutral Point Location

After the fixture with the intact spinal specimen was installed onto the test stage, the aluminium tubes and the threaded rods were removed. The x,z coordinates and the sagittal angle were recorded as

the set up orientation. Starting from the set up orientation, the specimens were cycled through compression and tension, anterior and posterior shear (at a rate of 0.5 mm per second), and sagittal bending (at a rate of 1 degree per second). Each component of motion was applied separately so that three series of measurements were made. The translations and rotation between the set up orientation and the neutral orientation were determined from the load-displacement curves. The test stage was then moved to the neutral orientation.

Part II - Hysteresis Curves

Starting from the neutral orientation, the specimens were subjected to compression and tension, and anterior and posterior shear at a rate of 0.5 mm per second and to sagittal bending at a rate of 1 degree per second. These tests generated hysteresis curves in the z ,x directions and sagittal rotation respectively. The hysteresis curves were used to verify the material properties and served as a reference for other parts of the experiment.

Part III - Intact Functional Spinal Unit Testing

This part of the test used the Planar Testing Apparatus to simulate a constant axial load applied to the intact functional spinal unit. A mixed load-displacement control option was used. The functional spinal unit specimens were loaded in compression while controlling the anterior-posterior shear load at zero and the flexion-extension angle at a constant setting. The final axial compressive load was set at 1200 N using a displacement ramp function limited to 0.1 mm per second. The anterior- posterior shear load was set at 0 N and the rate of sagittal rotation was set at 0 degrees per second. A feedback gain of 0.001 mm per N was chosen for the experiments. For each specimen, tests were performed at fixed flexion-extension angles of 0 degrees, 2 degrees extension and 2 degrees flexion in sequence. The test lasted 1 hour for each setting. After each test, the test stage was returned to the neutral orientation and the specimen was relaxed for 1 hour between tests. The displacement history throughout this part of the experiment was recorded by the computer and stored into data files for future use.

Following these tests of intact functional spinal units, the four aluminium tubes and threaded rods were re-installed and the fixture together with the specimen were removed from the test stage of the Planar Testing Apparatus. The intact specimen was then stored in the cold room at four degrees Celsius for 12 hours until the next part of the experiment.

Part IV - Isolated Intervertebral Disc

The load-displacement curves of the intervertebral disc were measured in this part of the test. The specimens were reinstalled into the Planar Testing Apparatus. The aluminium tubes and threaded rods were removed from the fixture and the test stage moved to the

neutral orientation obtained from Part I. The load-displacement in tension-compression, translational shear and sagittal bending (Part II) were repeated and the data compared with previous data. The test fixture was then removed from the test stage and the resin casting removed from the aluminium fixture by unscrewing the set screws around the aluminium ring. The posterior elements with the embedding material were then transected by cutting vertically through the pedicles. The intervertebral discs were then placed back into the fixture and the set screws were used to obtain the previous fixture dimensions. Automobile body putty was then used to fill the gap left open by the removed embedding material. The fixture together with intervertebral disc, the aluminium tubes and threaded rods were re-installed onto the testing machine. The test stage was moved to the neutral orientation based on the data obtained previously. Hysteresis curves were generated in x, z directions and in sagittal rotation about the y axis.

Part V - Creep History Test - Isolated Anterior Components

After the response of the isolated anterior components was obtained (Part IV), the displacement history recorded in Part III was used to deform the isolated intervertebral disc. The load resulting from this deformation was recorded and stored for later comparisons with the intact specimens. The testing sequence of 0 degrees flexion-extension, 2 degrees extension and 2 degree flexion, and the relaxation time of one hour between tests were the same as in Part III.

3.2.6. Analysis

The data transducers allowed simultaneous recording of the three components of load, the positions of the three hydraulic pistons and time. Six channels on the PDP 11/03 computer were used. A data acquisition rate of 0.25 seconds per data point was used during the load transient and a rate of 30 seconds per data point was used during creep. After each test, the data obtained were stored on floppy diskettes. The files were then transferred from the diskettes to the VAX 11/750 computer for further analysis. From these six channels of data, translations in the x,z directions and the sagittal plane rotation as well as the three components of load were calculated. These data were then read into the RS/1 statistics package for plotting and function fitting (RS1 Bolt, Beranek and Newman Research Systems, Cambridge, Massachusetts).

The x,z displacements and the sagittal angle were defined as zero at the neutral orientation. The three components of load reading at the neutral orientation were used as an offset and were substracted from the corresponding component of load reading so that the loads always read zero at the neutral orientation.

Equation (2) was used to represented the response of two parallel 3-parameter Kelvin solid models (Fig. 19). Our experiment used a ramp displacement of 0.1 mm/sec until the axial compressive load of 1200 N was obtained. Hence, a standard step input response function could not be used to fit the experimental data. In this case, the data was fit from the initial time (t_o when the constant axial load (1200 N) was just obtained and the term representing the initial conditions was incorporated into the step response function equation. From the equation, it is clear that the effect of the initial condition gradually diminishes. In fact, the values of the constants (A,B,C,D) calculated using the step response function were very close to the values of the constants calculated from Equation (2).

$$S=A(1-\exp(-(t-t_o)/B)+C(1-\exp(-(t-t_o)/D)+E(\exp(-(t-t_o)/B)+$$
$$(S_o-E)\exp(-(t-t_o)/D) \qquad (2)$$

where,

A,B,C,D,E	=	constant
S	=	displacement
t	=	time
t_o	=	initial time
S_o	=	initial displacement

For our test conditions, the response described by this equation is equivalent to the response of a system with two times constants and an initial elastic response, a 5-parameter solid. Because of this similarity, this model will be referred to as the 5-parameter model below. Equation 2 was fit to the displacement versus time curve of the intact intervertebral joint using the Marquardt-Levenberg method from the RS1 statistics package. This technique combines the advantages of the high convergence rate of the Gauss-Newton procedure and the simple alogrithm of the method of steepest descent in calculation of the least-square solution.

When the displacement history of the intact intervertebral joint (Part III) was reapplied to the transected specimen (Part V), the recorded load represented the portion of load supported by the intervertebral disc during the previous test with the intact intervertebral joint. The difference between the constant applied load and the load recorded from the transected specimen was then taken as the load supported by the facet. Since the data acquisition rate for these two experiments (III,V) was the same. The data could be processed point by point, i.e. without interpolation.

3.3. RESULTS

The results of this study of the lumbar FSU show that the axial compression tests at 0 degrees flexion-extension angle were most consistent throughout the experiment. The data presented here focuses on the results for the 0 degree flexion flexion-extension angle, although data for the 2 degrees flexion and 2 degrees extension tests are also shown. The results of the load distribution experiments are presented here in the following order:

(a) the hysteresis characteristic of the functional spinal units,

(b) the displacement versus time for the intact functional spinal unit;

(c) the axial load across the intervertebral disc versus time;

(d) the percent of total applied load supported by the disc versus time; and

(e) the load-displacement of the intervertebral disc during the load transient.

3.3.1. Hysteresis

Figure 20.1-5 shows the hysteresis curve of the functional spinal unit specimens. These were obtained before the first series of load control creep tests (Part III) and just before the displacement history test (Part V). The hysteresis curves are used to compare the material properties of the functional spinal units.

3.3.2. Displacement versus Time - Intact Functional Spinal Unit

Functional spinal unit specimens (at 0 degrees flexion-extension) under a constant axial load of 1200 N displayed the typical behavior of a Kelvin solid. Seventy percent of the total displacement observed over the hour of testing occurred within the first 30 seconds of the test. This initial response was followed by a slower creep period which continued throughout the remainder of the loading period. The displacement versus time plot of the intact functional spinal units are shown in Figures 21.1-5. The measured data of the 0 degrees flexion-extension tests were fit with the Kelvin solid model Equation (2), using the Marquardt-Levenberg method. These best fit curves are shown in Figures 22.1-5 along with the experimental data.

There are two time constants in the 5-parameter Kelvin solid model, Equation 2. For 7 specimens, the long time constant had a mean of 2620.0 seconds (S.D. _ 769 seconds) and the short time constant had

a mean of 79.6 seconds (S.D. ± 32.6 seconds). The results of the curve fitting are tabulated in Table 5. For the five-parameter Kelvin solid model, the data were fit from the initial time, t_o where the axial force just attained a steady load at 1200 N. The initial conditions of the displacement at time, t_o were incorporated into the fitting procedure.

3.3.3. Intervertebral Disc Load

The displacement during the closed-loop cycle in Part III of the experiment was compared with the open-loop cycle in Part V to confirm that the displacement of the intact functional spinal unit was repeatable in Part V of the test, The displacements were reproduced to within 0.05mm. Typical results are plotted in Figure 23.

Figures 24.1-5 show the axial load supported by the intervertebral disc at all three sagittal rotation angles by replicating the motions of the intact specimen from Part III. The disc load level of the 2 degrees flexion test is consistently higher than that of the 2 degrees extension test. However, the disc load level of these two tests were not consistently higher or lower than the 0 degrees flexion-extension tests. The disc load level of the 0 degrees flexion-extension tests varied from about 1000 N to 1150 N where as the 2 degrees flexion tests and the 2 degrees extension tests varied from 400 N to 1400 N.

Figures 25.1-4 show the time dependent characteristics of the axial load across the isolated intervertebral disc at 0 degrees flexion-extension angle. The load on the anterior components is expressed as a percentage of the total applied axial load. The transient response during the first 30 seconds of the test was not consistent between specimens. The load supported by the intervertebral disc alone may range from 50% to 150% during the transient period following the application of load. Thus, the first 30 seconds of data is not shown in Figure 25. The remaining data were fit by a linear least squares method and are also shown in the figures. For 4 specimens, the mean initial loads supported anteriorly was 77.2% (S.D. ± 9.7%) of the total intact load. The mean load after one hour was 88.8% (S.D. ± 4.0%) of the total intact load (specimens B,D,G,, Table 6. The gradual increase in the anterior load was observed for all but one (specimen F) functional spinal unit specimen. Stiffening of the disc was observed with specimen C. In this case, the load supported by the intervertebral disc was higher than the applied load. This violates static equilibrium. Hence, specimen F and C were not used in the calculation of the mean load and its standard deviation.

3.4 DISCUSSION

3.4.1. Planar Testing Apparatus

In previous studies, application of unidirectional loads were always accompanied by motions in more than one direction due to coupling effect. Panjabi, et al. [25,26] measured the flexibility matrix of thoracic functional spinal units and noted a significant coupling motion between axial and anterior-posterior translation. Schultz, et al. found that sagittal bending and anterior-posterior shear are coupled in the lumbar spine [31]. Lin, et al. [17] and Yang and King [38] used wedge shape knife edge to apply eccentric load to spinal specimens. Adams and Hutton [1] Cyron and Hutton [5] use rollers and plates to simulate flexion and extension. These load application methods inevitably generate anterior-posterior shear during axial compression. The Planar Testing Apparatus developed for this project was able to eliminate coupling forces and generate a unidirectional load of physiological magnitude (1200 N). The advantages of the Planar Testing Apparatus over other testing systems were demonstrated.

In these lumbar spine experiments, a mixed load and displacement control scheme was used to control anterior and posterior shear. The center of rotation was defined at the center of the inferior vertebral body. When the spinal specimen is extended or flexed, anterior-posterior shear is generated due to the deformation of the intervertebral disc. *In extension, a posteriorly directed shear* force is exerted on the inferior vertebral body. In the same fashion, specimens under flexion generate an opposite response. The Planar Testing Apparatus maintained a zero anterior-posterior shear by translating the inferior vertebral body posteriorly during extension tests and by translating anteriorly during flexion. The typical anterior-posterior translation (x) of the specimen needed to produce zero anterior-posterior loads under flexion and extension conditions is shown in Figure 26. In this was a pure unidirectional compressive load was produced.

The displacement resolution of the testing machine can affect the stability of the closed-loop load control of the Planar Testing Apparatus. At 100% range setting, the resolution of the hydraulic actuator is 0.036 mm. When there is an error in load detected, a minimum change in actuator length of 0.036 mm is necessary. The actual translation in the x, z directions and sagittal plane rotation varies depending on the test stage position. For stiff materials, small changes in displacement produce large changes in load, and thus may result in load oscillation. The resolution of the linear displacement and the rotational displacement of the Planar Testing Apparatus at 10% range setting (0.0036 mm per bit) proved to be stable in our experiments.

The gain can also affect the stability of load control, Figure 11. High gain can induce load oscillation and a low feedback gain

increases the rise time of the system [24]. The gain setting of 0.001 was selected for stability and reasonable rise time (approximately 12 seconds) for the one hour experiments.

One control cycle is defined as the process to acquire data, to calculate and to execute the command. A high control cycle frequency is required to avoid large step change in displacement. Large step change in displacement can cause "overshoot" in the motions of the test stage. Even though the three components of load are coupled, this coupling is reasonably small, and the control algorithm can assume that the three components of load are not coupled. A linearized version of test stage position calculation is also used. These algorithms are used to reduce the computation time so that a high control cycle frequency can be attained. Control cycle frequency of 30 Hz can be obtained using the PDP 11/03 microcomputer. With the computer interface, variations of this study can be accomplished with minimal changes in the software of the system.

3.4.2. Load Distribution

The findings of these lumbar creep studies suggest that an increasing fraction of the total axial load applied to the intervertebral joint is supported by the intervertebral disc as the joint creeps. This increase in anterior load observed at 0 degrees flexion-extension angle, with zero A/P shear is probably a combined effect from sliding of the facet joints, and from the differences in material properties between the intervertebral disc and the facet capsules. The results suggest that the facets slide along their articular surfaces, passing load to the facet capsules, which then relax.

This study is the first to measure the time dependent distribution of the anterior-posterior loads in the spine. Facet loads of 25% reported by Yang and King [38] and 20% reported by Nachemson [21] for quasi-static conditions are comparable to our result of 23% at the onset of loading. Previously, however, there was no direct evidence of how axial load is being supported by the facet joint. Yang and King [38], Adams and Hutton [1], and Andersson [3] have suggested that the capsular ligament plays an important role in supporting the axial compressive load across the facet joint. They suggested that the ligament is visco- elastic and relaxes when the deformation of the capsular ligament is held constant. As each facet slides along the surface of the adjacent facet in response to an axial load, the capsular ligament is stretched, so as to resist further sliding. However, the relaxation time constant of the capsular ligament and the intervertebral disc are different. The results of our experiments suggest that the relaxation time constant of the facet is shorter than that of the intervertebral disc. This indicates that the capsular ligament relaxes faster than the intervertebral disc when both are held under the same deformation. The long and short time constant calculated from the Kelvin solid model seem to agree with this hypothesis.

3.4.3. Relaxation of Lumbar Specimens

In these experiments, the spinal specimens were tested in creep at 0 degrees flexion-extension, then at 2 degrees extension, and finally at 2 degrees flexion. Each creep test lasted for 1 hour and the specimens were allowed to relax for 1 hour between tests. Before relaxation, the specimens were positioned at the original neutral orientation in the Planar Testing Apparatus.

The experimental data show that the specimens did not recover completely from the creep test in one hour and that the disc load level of the 2 degrees extension and the 2 degrees flexion were not consistent between tests, Figure 24. In addition, the disc load at 2 degrees flexion did not support a load close to 100% of the total applied axial load (1200 N) as was suggested by Adams and Hutton [1]. However, the first test performed after 12 hours of relaxation (0 degrees flexion- extension) always produced a consistent level of load starting at 77% of the total applied load and finished at 89% of the total applied load, Figure 25. This phenomena was confirmed for one specimen when the displacement history was repeated on the intact specimen [15]. The results show that the load history (constant at 1200 N) was reproducible after the intact specimen relaxed for 12 hours, but the load history was not reproducible if the specimen relaxed for only 2 hours.

Koeller has reported that the deformation was less when the specimen was creep tested a second time [13]. However, according to Koeller, the difference in displacement between the first and the second test was very small. Figure 21 shows that the displacement of the 0 degrees flexion-extension test is consistently the lowest and the 2 degrees flexion test is the highest. If the intervertebral specimens are not given enough time for relaxation, a change in viscoelastic material properties of the intervertebral joint will occur. Even though the change of load distribution characteristic due to insufficient relaxation cannot be determined from these experiments, the data shows that there is an increase in deformation of the intervertebral joint. Based on these findings, the relaxation time between tests changes the load-displacement characteristic of the spinal specimens. However, more data are needed to further understand the change in material properties of the intervertebral joint due to repeated creep tests.

3.4.4 Neutral Orientation

Earlier stiffness tests of the intervertebral joints were done using constant load with series of strings and pulleys [17,25,26,31]. In a typical stiffness test, the specimen is displaced by a constant static load and measurement of the displacement made after 5 to 10 minutes. Then the load is removed and the specimen is allowed to recover for 10 to 15 minutes. The orientation of the specimen after the recovery period is defined as the new neutral orientation. During

relaxation, the specimen may or may not return to its original height depending on the specimen conditions such as disc grade, moisture, and the duration of the experiment. Hence, the new neutral orientation may not be the same as before.

The design of our test fixture allows creep tests to start at the same neutral orientation in every test so that the same displacement condition can be repeated after the posterior elements are transected. A well defined neutral orientation is important because a shift in the neutral orientation can lead to misintepretation of the data especially at high load or high rates of loading where hysteresis is pronounced and the test is carried out beyond the toe region of the load-displacement curve.

3.5. SUMMARY OF LUMBAR SPINE STUDY

These experiments suggest several important features of the load distribution behavior of lumbar intervertebral joints.

(1) The fraction of the axial load supported by the intervertebral disc increases with time when a constant axial compressive load is applied to the intervertebral joint. At 0 degree flexion-extension angle, the increase in the intervertebral disc load is linear with time. The initial load supported by the disc is at 77% of the total applied load and increases to about 89% in one hour. At 2 degrees flexion, the intervertebral disc supports nearly all of the total applied axial compressive load. At 2 degrees extension, the intervertebral disc load increases exponentially with time and approaches an asymptotic value. The final load supported by the disc is less than the final load supported by the disc at 0 degree flexion-extension angle.

(2) Exactly defined neutral orientation and sufficient relaxation time between creep tests is key to consistent test results. For a 1 hour creep test, 12 hours of relaxation at 4 degrees Celsius is sufficient if the spinal specimen is returned to its original geometric configuration in a fixture. Insufficient relaxation of the spinal specimen causes higher than normal deformation of the specimen. The load-displacement curve of an insufficiently relaxed specimen demonstrates a greater toe region and greater slope than the sufficiently relaxed specimen.

(3) Mechanisms for low back pain cannot be directly interpreted from these mechanical tests. However, it appears that at 2 degree extension, the tip of the facet joint may touch the lamina of the adjacent vertebral body. This is a potential mechanism which may produce pain after long periods of standing. The back pain elicited after prolong erect sitting may be caused by the high stress exerted on the intervertebral disc when load is transfered to the disc from the facet joints.

The material presented here demonstrates the time dependent load distribution characteristis of the lumbar intervertebral joint. The experiment has shown that time is an important factor when considering the load distribution of the intervertebral joint. However, more studies of this aspect of spinal biomechanics are needed to gain further understanding of the causes of low back pain.

4. VISCOELASTIC AND STRENGTH PROPERTIES OF CERVICAL SPINE

The study of spinal mechanics provides clinically useful information for the analysis of movement disorders arising from congenital malformation or injury. Detailed data defining the kinematics, the relationship between loads and displacements, the vertebral strength, and the modes of failure of the normal spine are required to define the tolerance of the cervical spine to injury and to determine when and if surgery or other treatment is necessary to repair an abnormal spine. This part of the project focused on the measurement and quantification of cervical spinal motion under physiologic loading in vitro in both non-destructive and failure testing situations. Testing was done on eight cervical spines taken from cadavers. Cervical spines were tested nondestructively to gather load vs. displacement data and destructively in a combination of flexion and compression.

4.1 REVIEW OF THE LITERATURE

4.1.1 Anatomy

The human spine is composed of the cervical, dorsal (thoracic), lumbar, sacral, and coccygeal segments. The upper segments consist respectively of seven, twelve, and five separate vertebrae, while the sacrum and the coccyx consist respectively of five and four vertebrae fused in the adult. The spinal column has four curves when viewed laterally. In the cervical and the lumbar segments, the spine is convex anteriorly, and in the thoracic and sacral segments, it is concave anteriorly. Each cervical, thoracic, and lumbar vertebrae consists anteriorly of a vertebral body and posteriorly of a neural arch containing four articular, two transverse, and one spinous process, Figure 27. The arch provides a protective canal for the spinal cord and nerves.

Vertebrae are connected to one another anteriorly through the longitudinal ligaments and the fibrocartilagenous intervertebral discs, and posteriorly through the interspinous and superspinous ligaments and the facet joints. The facet joints are formed by the two inferior articular processes of one vertebra and the two superior articular processes of the vertebra below it. The transverse processes project laterally and serve as attachment sites for the muscles which control rotation and lateral bending of the spinal

column. The spinous process projects dorsally and distally and serves as an attachment site for the muscles of extension and rotation. Several texts present a thorough description of the anatomy of the normal cervical spine, and White and Panjabi present a comprehensive description of the biomechanics of the entire spine [28].

Spinal movements occur between motion segments, also called functional spinal units (FSU's), consisting of two adjacent vertebrae and their interconnecting tissue and ligaments. The FSU is the smallest basic spinal structural unit which exhibits biomechanical characteristics similar to the entire spine. In the cervical region the seven vertebrae are designated C1 through C7. The cervical spine consists of 7 FSU's beginning with articulation between the head (occiput) and C1, Occ-C1, and ending with C6-C7. Motion between vertebrae takes place in all three anatomic planes, the sagittal, transverse (horizontal), and coronal (frontal) planes. The four predominant motions of spine are flexion-extension, compression-tension, axial rotation, and lateral bending.

4.1.2 Biomechanical Considerations

Based on these anatomic considerations, the spine is an articulated column composed of structural units of complex geometries and material properties. The load characteristics (along with the multiaxial nature of the applied loads) result in additional complexities at the structural level. These complexities of spinal column motion are: 1) coupled motions, 2) non-linearities in load versus displacement behavior, and 3) time dependent load-displacement responses. These were recognized in previous mechanical studies of connective tissue and spinal segments. White and Panjabi discuss in detail the biomechanically relevant anatomy [28].

Lysell [19], Panjabi et al [25,26], and Markoff [20] and others showed that spinal motions in all three mobile regions are generally coupled. That is, motion (translations or rotations) in one anatomic direction is accompanied by motion in at least one other direction. For example, in left lateral bending of the distal cervical spine, the vertebrae also rotate axially bringing the spinous processes away from the direction of bending. Coupling also occurs in the cervical region between flexion-extension and sagittal anterior-posterior translation [19]. The coupling of spinal motions is due to the geometry of the vertebrae, the orientation of the intervertebral disc and facet articulation, the interconnecting ligaments, and the curvature of the spinal column.

The load vs. displacement response of the spine is also non-linear [7,27,36]. When forces and moments are applied to the spine and the resulting displacements are measured, the slope of the load vs. displacement curve increases with increasing load, Figure 28. Therefore, displacement measurements made in uniaxial loading situations cannot be summed in order to indicate the response during simultaneous loading along more than one axis [7]. Combined loading conditions should therefore be used experimentally whenever possible.

The rate of loading also influences the load-deflection behavior of the spine [12,15,16]. This is a result of the viscoelastic characteristics of the ligaments, discs, and muscle. The rate of displacement is directly related to the loads produced by these components. The slope of the load vs. displacement curve increases at higher loading rates and the forces generated are generally higher at well. Therefore, a thorough study of spinal motion should include several loading rates. A second result of viscoelasticity is the hysteresis evident in the load-deflection behavior of spines loaded cyclically. This is due to energy loss during each load cycle, Figure 17.

4.1.3 Objectives

Detailed information on the load vs. displacement response of the spine can best be gathered through in-vitro testing. Past spinal mechanics investigators have generally studied two vertebrae segments (FSU's). In the present studies, we have chosen spinal segments consisting of three vertebrae and their interconnecting ligaments and discs (FVS's). With these segments, upper and lower vertebrae can be manipulated while the middle vertebra is allowed to move in a way physiologically similar to the in vivo condition, with intervertebral discs and ligaments being the only constraints.

Due to the nonlinear and viscoelastic nature of the spine and the complex loading to which it is subjected, a meaningful test procedure must include a multi degree-of-freedom loading apparatus and a displacement measurement device which does not interfere with the natural modes of spinal motion. The Planar Testing Apparatus, described above, is capable of generating either controlled loads or controlled displacements. These two control methods make possible the measurement of all of the parameters necessary to define independently specimen stiffness and specimen flexibility.

The displacement measuring apparatus developed for this project consists of three precision LVDT's and six precision RVDT's grouped so as to continuously monitor the position of three small balls on a collar rigidly affixed to the specimen. The collar is clamped around the free vertebra so that there is no motion of the collar relative to the specimen. However, the collar is designed so that the bone is not punctured, thus avoiding unphysiologic stresses. The transducer groups are designed to add minimal loading to the specimen, and are capable of measurement over the complete range of normal movement. The displacement collar is attached only to the moving vertebra and does not interfere with the natural motion of the specimen. The output voltages of the transducers are recorded via an on-line computer. With this apparatus, a highly accurate, continuous and noninvasive method of displacement measuring is possible.

The motion of the moving vertebra with respect to the fixed can be described as a translation along and Eulerian rotation about, a fixed orthogonal axes system with its origin at the center of the moving body. The three Euler angles very nearly describe lateral bending, flexion-extension, and torsion rotations, and are easily visualized, particularly for planar motion. This method is well suited for the description of spine kinematics.

The specific objectives of this cervical spine study presented in this report were:

A) Develop experimental techniques needed for mechanical testing of human cervical spine specimens.

B) Define algorythyms to calculate the rigid body translations and Euler rotations of the moving vertebra relative to a fixed reference.

C) Measure the nonlinear mechanical properties of intact cervical spine specimens considering sagittal loading and displacements for conditions up to including failure of the vertebrae and rupture of the soft interconnecting tissues.

A final objective was to quantify the change in mechanical properties and strength of cervical spine segments due to axial rotation applied in combination with flexion and compression.

4.2 MATERIALS AND METHODS

4.2.1 Planar Testing Apparatus

The Planar Testing Apparatus (PTA) described in this report is a multi degree-of-freedom materials testing machine capable of multiaxial load or displacement control. The PTA allows in-vitro simulation of the full range of in-vivo spinal motions. It is capable of producing simultaneous multiaxial displacements and loads at constant or variable rates. System software presents real time load vs. displacement data for monitoring test parameters. While in load control, direct measurement of the variables required to determine spinal segment flexibility can be made. In displacement control, measurement of the variables necessary to determine spinal stiffness is possible.

4.2.2 Displacement Measurement Device

A complete description of the motion of a single vertebra is defined by measurement of the position of three non-colinear points fixed to the moving vertebra. An electromechanical transducer system was developed for use with the PTA for the measurement of the absolute 3-D motion of the center vertebra in a three vertebrae cervical spine segment [4]. The 3 vertebrae segments which include all of the interconnecting ligaments and discs will be referred to as Functional Vertebral Segments (FVS's), Figure 29.

This six degree of freedom motion measurement system consisted of three identical transducer groups that monitored the position of three points attached to the moving vertebra. Each transducer group was composed of a linear variable displacement transducer (LVDT) and two rotational variable displacement transducers (RVDT's) (Schaevitz Engineering, Cat. No. 2000LW and R30A). One transducer group is illustrated in Figure 30. The tip of the rod from the transducer was attached to a point on a collar around the free vertebra being monitored. The transducer rod and LVDT housing were free to rotate about the axis of RVDT 1 and RVDT 2. RVDT 1 was mounted onto the LVDT housing so that it measured motion of the body in the vertical plane. RVDT 2 was mounted onto the housing such that it measured motion of the LVDT in a horizontal plane. The LVDT core guide was attached to the rod which was supported in two precision, linear instrument bearings housed in aluminum blocks attached to the LVDT body. This arrangement prevented the core guide from being stressed during testing. A teflon block was attached to the back of the LVDT and to the supporting rod thus allowing free translation of the rod along the LVDT body with no lateral displacement or rotation of the core of the LVDT in the LVDT body. The output from the RVDT's was linear to within 0.25% of their range and were calibrated with a sensitivity of 0.25 volts per degree over a range of 40 degrees. The LVDT's were linear to within 0.25% of their range and were calibrated with a sensitivity of 0.25 volts per mm with a range of 40 mm.

Each transducer group was rigidly attached to an aluminum bridge mounted on the PTA load frame. Figure 31 illustrates the orientation of the transducer groups on the bridge with respect to the specimen and the load frame. The groups were mechanically balanced so that no loads were applied to the specimen when the transducers were attached. With the nine transducer system, it was possible to independently determine the 3-D location of three non-colinear points attached to the specimen. With nine transducers monitoring the motion of a specimen moving with 6-DOF, redundant measurements were available to check accuracy and to provide back-up measurements in case of transducer failure.

4.2.3 Specimens

Human spines were collected within 48 hours of death from Harvard Medical School through its Anatomical Gifts Program (Table 7). The spines were separated into lumbar, thoracic, and cervical segments, placed in plastic bags, sealed, and frozen at -20°C. Freezing and thawing cycles have been shown by others not to affect the properties of the bone [32], the disc [11], or the ligamentum flavum [2]. Before testing, the cervical segments were allowed to thaw overnight at 5°C. Anterior-posterior and lateral radiographs were then taken. Specimens showing any abnormalities, fracture, or bone disease were excluded. The specimens were then separated by dissection at the discs into three functional vertebral segments (FVS's), either C2-C3-C4 and C5-C6-C7 segments or C3-C4-C5 and C6-C7-T1 segments. The segments were cleaned of excess soft tissue while leaving the ligaments intact. Two

steel pins 1.75 mm in diameter were inserted laterally through the inferior and superior bodies at their midlines. The pins helped to secure the bodies in a castolytic resin ('Castolite' Buehler Ltd. No. 20-8120-009) in which they were ultimately embedded.

4.2.4 Test Fixture

The cervical spine holding fixture constructed for use with the PTA consisted of an aluminum cup 114 mm in diameter, 12.7 mm wall, rigidly attached to a 25.4 mm thick aluminum plate. This fixture assembly was rigidly attached to the test stage of the PTA. Four set-screws 9.5 mm in diameter positioned 90^{o} apart were screwed through the cup wall to position the specimen and insure that the resin remained attached to the cup. Figure 32 illustrates the test fixture. The inferior body was positioned in the center of the lower cup so that the plane of the disc was parallel to the cup edge and to the lower plate. Resin was then poured into the cup covering the 4 set screws, 2 pins, and approximately 3/4 of the height of the body. The 2 exposed vertebrae were wrapped in water soaked cotton sheeting and covered with saranite film to prevent dehydration while the resin dried, approximately 6 hours at 5^{o} C. This technique prevented specimen dehydration and preserved the properties of the disc and the longitudinal ligaments [11,37].

A collar made of galvanized steel was used for attachment of the LVDT's to the middle vertebra, Figure 33. Three 3.9 mm diameter balls from a ball and cup linkage set ('Du-Bro' Cat. No.18D) were screwed into the collar in a radially symmetric pattern to provide the three reference points. The cups were attached to the tips of each LVDT rod. The ball linkages provided for approximately 50 degrees of rotation with very little friction. Along each edge of the collar were cut numerous teeth-like projections about 3 mm in length which held securely onto the vertebra about its midline without puncturing the bone. The collar was placed around the body and fastened in place. Its length was adjusted to fit varying sizes of specimens.

Once the collar with its 3 balls was positioned, the specimen was again radiographed laterally, anterior-posteriorly, and axially so that the exact 3-D orientation of the balls with respect to the midpoint of the free vertebra could be determined. For determining the magnification of the image, 2 small pins were placed into the walls of the inferior aluminum cup at about the midline. The actual distance between pins was compared to the measured distance on the image to determine a magnification factor. The radiographs were checked to see that the collar was in contact only with the center vertebra of the specimen and its posterior elements. The superior body was then positioned and embedded in a second cup-plate fixture. The upper and lower plates were spaced at the proper distance for embedding the specimen and held parallel through the use of aluminum tubes of the required height. The tubes were held in place by threaded rods and bolted onto the upper and lower plates. Anterior-posterior and lateral radiographs were taken of the test fixture and the specimen so that the orientation of the center of the body of the

middle vertebra with respect to the test fixture could be determined. The fixture provided a method for securely holding the specimen so that it could be remounted for each test in exactly the same position. Figure 34 shows a collared specimen in the test fixture on the test stage of the PTA.

4.2.5 Test Setup

The test fixture was bolted onto the test stage and onto the load cell. The load control option of the PTA was used to position the test stage such that all three sagittal loads were approximately zero immediately after bolting the specimen fixture on the PTA. The aluminum tubes and the threaded rods which supported the upper and lower plates of the fixture while mounting the specimens were then removed.

Specimen load-displacement response and failure test data were referenced to the neutral point of the load-displacement curves. The neutral point is defined as the position on the load-deflection curve where virtually no load results for small displacements. The neutral point falls within the flat region of the hysteresis curve. For these tests, the neutral point was defined as the condition midway between the two zero load points along the loading curve and the unloading curve using 1mm/sec and 1 deg/sec displacement input rates. At this point, there were no forces or moments applied to the specimen. Once the neutral point had been determined from the uniaxial load-deflection curves, the test stage was moved to bring the specimen to the neutral orientation. Again, the test stage was moved in small uniaxial increments and the resulting load-deflection curves checked to see that the specimen was at the neutral orientation. The test stage location was then recorded so that the specimen could be repositioned at the original neutral orientation for future testing.

The geometry of the entire specimen was defined from the lateral radiographs of the specimen in the test fixture Figure 35 and the definition of the neutral point condition. The center of the fixed vertebral body, S_f, was defined as the intersection of the midpoints of the distances f1 and f2. The translation and rotation of the geometric center of the moving vertebral body, S_m, was referenced to this point. The loads were resolved to, and the moving specimen rotated about, Sm. This point is at the intersection of the midpoints of m1 and m2. For all subsequent testing, the PTA was able to resolve the specimen loads to the neutral point and to generate motions of the test stage with reference to this point.

4.2.6 Test Protocol

Nondestructive Testing

Seven specimens were tested nondestructively to obtain load vs. displacement behavior at two different displacement rates. Using the load control option of the PTA, a compressive load of about 10% body weight was first applied to account for the weight of the head and the

stiffness of the missing muscles. Hysteresis curves were generated using the displacement control option of the PTA. The specimen was subjected to compression and tension and anterior and posterior shear at a quasistatic rate of 1 mm per second and to sagittal bending at a rate of 1 degree per second. Each test was repeated three times and the third data set from each test was recorded. This was to ensure that the results were repeatable. The test sequences were then repeated at a rate of 3 mm per second and 3 degrees per second. The third data set from each test was recorded to determine the influence of displacement rate on the load-displacement response.

Destructive Testing

After completion of the nondestructive test sequences, each specimen was subjected to flexion angles of up to 42^{o} at a rate of 6^{o} per second until failure occured. If there was no evidence of ligamentous or bony failure, the specimen was then compressed while held at maximum flexion until failure occurred. The forces and moments for these test conditions were recorded throughout these tests. Radiographs were taken after the test sequences were complete to document evidence of failure.

4.2.7 Kinematic Analysis

A FORTRAN program was used to calculate the relative motions between the fixed and the moving vertebra. The three dimensional translation vector of the center of the moving vertebral body, S_m, with respect to the center of the fixed vertebral body, S_f, and the Eulerian rotations of the moving body (Appendix B) were calculated. The translation equations and the rotation equations will be discussed separately.

Translation

The 3D displacements of the 3 balls, A, B, and C, on the collar were determined with respect to the pivot points of their respective transducer groups, A_o, B_o, and C_o. The transducer voltages were measured and transformed into distances (mm) and angles (radians) based on the available instrument calibration information (Appendix A). Figure 36 illustrates the vector relationships between the center of the fixed and moving vertebra (S_f, S_m), one of the balls attached to the moving vertebra, (A), and the pivot point of one transducer group, (A_o). The vector $\mathbf{(A-A_o)}$ can be determined from

$$\mathbf{(A-A_o)} = [Zs]_A\,[Y]_A\,[Z]_A\,\mathbf{(L)_A} \qquad (3)$$

where

$\mathbf{(A-A_o)}$ is the vector in the pivot reference frame from the point A_o to the ball A;

$[Z_s]_A$ is a coordinate rotation matrix whose columns contains direction cosines of the transducer group axes relative to their calibration orientation;

$[Y]_A$ is a coordinate rotation matrix whose columns contain the direction cosines of the angle determined by R1;

$[Z]_A$ is a coordinate rotation matrix whose columns contain the direction cosines of the angle determined by R2; and

$(L)_A$ is the vector along X_A to the point A whose length is determined by L1.

The elements of Equation (3) are given in detail in Appendix B. Similar equations relate B to B_o and C to C_o.

The positions of the points A_o, B_o, and C_o with respect to the center of the fixed body, S_f, were determined from the PTA geometry and from radiographs of the specimen in the test fixture. The vector position of ball A with respect to S_f was then determined from

$$(A) = (A_o) + (A-A_o) \qquad (4)$$

where

(A) is the vector in the fixed reference frame, S_f, from the origin of the fixed frame to the point A; and

(A_o) is the vector in the fixed reference frame, S_f, from the origin of the fixed frame to the point A_o.

The position vectors from ball A to S_m and from ball A to S_f were determined from radiographs. The equation for the position vector from S_m to S_f is

$$(S) = (A) + [R](S)_A \qquad (5)$$

where

(S) is the position vector from the origin of the moving reference frame, (S_m) to the origin of the fixed frame, (S_f);

(A) is the position vector in the fixed reference frame from the origin of the fixed frame, S_f, to the ball A;

$[R]$ is the rotation matrix whose elements represent successive rotations of S_m about X_m, Y_m, and Z_m; and

(S_A) is the position vector, in the balls reference frame, of S_m with respect to A. The elements of S_A were determined from radiographs.

Eulerian Rotations

Figures 36 and 37 illustrate the vectors used to calculate the unknown Euler rotations of the point S_m. A method was chosen that simultaneously determines both the three translations of S_m with respect to the fixed coordinate system, X_f, Y_f, Z_f, and the successive Eulerian rotations about the fixed axes. This method was used previously by Dieudonne, et al. at NASA [6] to determine the position and orientation of a payload platform of a motion simulator relative to a fixed platform, and used by Koogle, et al. [14] to describe the motions of a special transducer system. The resulting translations were compared with those determined in the previous section to check on the accuracy of the methods. The nomenclature presented by Dieudonne, et al. was used here.

X_m, Y_m, Z_m mutually perpendicular set of unit vectors defining the moving reference frame with its origin at the center of the moving vertebral body, S_m;

X_f, Y_f, Z_f mutually perpendicular set of unit vectors defining the fixed reference frame with its origin at the center of the fixed vertebral body, S_f;

$\mathbf{A_i}$ vector fixed in the moving reference frame from S_m to the balls A, B, and C; i=1,2...6;

A_{ix}, A_{iy}, A_{iz} *components of vector* $\mathbf{A_i}$;

$\mathbf{B_i}$ vector fixed in the fixed reference frame from S_f to points A′, B′, and C′ on the PTA frame; i=1,2...6;

B_{ix}, B_{iy}, B_{iz} components of the vector $\mathbf{B_i}$;

$\mathbf{S}$ vector in the fixed reference frame from S_f to S_m;

x, y, z components of the vector $\mathbf{S}$;

$\mathbf{l_i}$ vector in the fixed reference frame from points A′, B′, and C′ to the points A, B, and C; i=1,2...6;

l_{ix}, l_{iy}, l_{iz} components of the vector $\mathbf{l_i}$;

$|\mathbf{l_i}|_a$ magnitude of $\mathbf{l_i}$ representing the actual length as determined from the PTA geometry and the locations of A, B, and C;

ψ, θ, ϕ component rotations of the moving body about the X_f, Y_f and Z_f axes respectively;

[R] rotation matrix representing component rotations of the moving body relative to the fixed body;

$\mathbf{f(\alpha)}$ vector function;

0 null vector;

α unknown parameter vector.

From the transducer outputs, the components of the vectors l_i are known. This vector can also be given by

$$l_i = [R]\, A_i + S - B_i, \quad i=1,2...6. \tag{6}$$

Determination of the relative orientation of S_m with respect to S_f involves solving six simultaneous nonlinear equations represented by Equation 6 for the six unknowns (x, y, z, ψ, θ, ϕ). The Newton-Raphson iteration method was used to compute the vector root, α, of the equation

$$f(\alpha) = 0. \tag{7}$$

This function is defined as

$$f_i(\alpha) = l_i^T l_i - |l_i|_a^2. \tag{8}$$

The iteration formula is

$$\alpha_{n+1} = \alpha_n - \left[\frac{\partial f(\alpha_n)}{\partial \alpha_n}\right]^{-1} f(\alpha_n) \tag{9}$$

where

$$\alpha_n = \begin{bmatrix} x \\ y \\ z \\ \psi \\ \theta \\ \phi \end{bmatrix}_n \tag{10}$$

and

with $\dfrac{\partial f(\alpha_n)}{\partial \alpha_n}$ and $f(\alpha_n)$ defined in detail in Appendix B.

Given the six l_i values and initial guesses for x, y, z, ψ, θ, and ϕ, Equation 6 is used iteratively until a given convergence criteria is reached which defines the position and orientation of the center of the moving body, S_m relative to the center of the fixed body, S_f. The convergence criterion was

$$tr|\alpha_{n+1} - \alpha_n| \leq 0.0001$$

where $tr(\alpha)$ is the sum of the components of α.

4.3 RESULTS

The results are presented in the form of load vs. displacement curves made from a) the data obtained from the load cell, b) the transducers monitoring the motions of the test stage, and c) the specimen collar. The curves for all specimens are plotted using the same scale. An expanded form of each curve is presented in Appendix D. The three components of load (anterior-posterior shear, tension-compression force, and flexion-extension moment) were resolved from the load cell to the center of the middle vertebral body, and are plotted against the displacements of the middle vertebra with respect to the center of the fixed vertebra above it. Data were obtained throughout the nondestructive test sequences and for the destructive test sequences when angles of rotation were below 15^{o}. For higher angles of rotation, the displacement measuring collar was removed. For destructive test sequences, the loads are plotted against test stage displacement.

The data analysis focuses on two biomechanical considerations: coupling of spinal motions and the effect of displacement rates on stiffness. The data are divided into two groups, one obtained from the upper cervical region, (specimens C, F, H, and E), and the other for lower cervical region, (specimens B, D, and G).

4.3.1 Nondestructive Axial Tests

The results of the compressive force vs. axial displacements are shown for the two levels of the cervical spine in Figures 38.1-38.4 (for the upper cervical region) and in Figures 38.5-38.7 (for the lower cervical region). The three vertebrae specimens were loaded at compressive rates between 0.5 mm/sec to 5 mm/sec. For those specimens loaded at more than one rate, the results are presented on the same curve.

The compressive response of all specimens displays a large region of low load with negligible slope near the neutral point. The slope increases beyond the neutral zone in both tension and compression. Compressive forces are shown positive. The slopes of the curves from 0.5 mm to 0.7 mm in tension and 0.4 to 0.6 mm in compression were used to estimate the specimen axial stiffness. If more than one

displacement input rate was tested, the results from the lower rate curve were used. From these measurements, all specimens were stiffer in compression than in tension. In the specimens taken from the upper cervical region, the estimated stiffnesses ranged from 145 to 325 N/mm for tension, and from 500 to 3500 N/mm for compression (Table 8). Two of these compression specimens (F and H) exhibited very high stiffness values. No specific reason for this behavior could be identified, but bone on bone contact could have been a possibility. In the specimens taken from the lower level of the spine, the estimated stiffness ranged from 25 to 35 N/mm in tension and from 200 to 360 N/mm in compression. There was no difference in the slope or position of these curves as the rate of loading was increased.

Figures 39.1-7 compare coupled response of the vertical and shear forces vs. vertical displacement. The curves of shear force vs. Z-displacement display a large region of low load and zero slope near the neutral point. When the stage was displaced along Z (compression-tension), the shear forces were zero in tension but there was slight posterior shear associated with compression.

Figures 40.1-7 compare displacements of the center vertebra along X, Y, and Z with the inputs of the test stage displacement along Z. There were only slight displacements along Y in tension and compression for all specimens, however there was relatively large posterior displacement associated with tension for specimens C, F, and G and anterior displacement associated with compression for specimens C and F.

4.3.2 Nondestructive Shear Tests

Figures 41.1-7 show the measured shear force plotted against the anterior-posterior X-displacements. These force vs. displacement trends are similar to those in the axial force vs. Z-displacement plots. The slopes were near zero for small displacements, and increased as anterior or posterior displacement increased. Estimates of the stiffness of the specimens was measured from the slope of the curves between 0.5 mm to 0.7 mm of anterior motion and 0.6 mm to 0.8 mm of posterior motion. For the specimens taken from the lower level of the spine, the anterior stiffness (25 N/mm-30 N/mm) was greater than the posterior stiffness (5 N/mm-14 N/mm), although all stiffnesses were fairly small. In the specimens taken from the upper levels, specimens F, H, and E dis layed much higher posterior stiffnesses than anterior stiffnesses The estimated stiffnesses ranged from 30 N/mm to 70 N/mm for anterior shear, and from 35 N/mm to 250 N/mm for posterior shear in the specimens from the upper levels. The slope of these curves did not suggest a dependence of estimated stiffness on displacement rate for the rates tested.

The axial and shear forces generated by X-displacements are compared in Figures 42.1-7. When the stage was displaced posteriorly along X, the compressive forces generated were approximately 50% greater than those generated in shear except for specimens B and D. When the stage was displaced anteriorly, there were little or no vertical forces generated.

The curves in Figures 43.1-7 show the resulting rotations for anterior-posterior displacement inputs. When the lower vertebra and test stage was displaced posteriorly along X, the middle vertebra of each specimen rotated positively about Y, Figure 29. When the stage was displaced anteriorly along X, the vertebra rotated negatively about Y. There was no region of low moment and zero slope near the neutral point of the curves. Specimens G, E, and H show some lateral bending associated with anterior-posterior shear.

4.3.3 Nondestructive Flexion-Extension Tests

Figures 44.1-7 show the flexion-extension moment plotted against sagittal rotation curves for each specimen. The flexion moment and rotation are shown negative. The results of the bending tests show significant scatter at the low angles of rotation shown. For moment vs. rotation data, the stage was rotated 1.5^{o} to 6^{o} in flexion-extension. Based on the data collected by White and Panjabi [38] this is about 15% of the range of motion of the typical cervical FVS. In general, the specimens were stiffer in extension than in flexion.

The axial and shear forces generated when the specimen was rotated in flexion-extension are shown in the curves in Figures 45.1-7. A small amount of compression resulted with extension rotation and tension was measured with flexion, except for specimen H which was under compression in both flexion and extension.

4.3.4 Destructive Tests

Figures 46.1-6 show the sagittal moment resulting from large flexion angle inputs. A modified test protocol was used for two of the specimens, C and E. Specimen C was not tested at large angles of flexion. Specimen E failed after the initial nondestructive testing was complete and was then tested at large angles of flexion for comparison purposes. The load-displacement data for specimen E at the time of failure are not available. Specimen E displayed only -800 N-mm of moment for a sagittal rotation of -30^{o}.

As shown, for example in Figure 46.1, the neutral zone extends from 0^{o} to at least 10^{o} before the slope of the curve increases. When a rotation did not produce evidence of failure, the specimen was returned to its neutral position. The stage was then rotated to a higher angle. The curves for each test are shown on the figure. This procedure was followed for specimens F, G, and H, and Figures 47.1-3. The curves showing the moment resulting from each flexion sequence are also shown. Each time the test was repeated to a higher angle, the slope of the load-displacement curve decreased. There was no clear evidence of failure on the moment vs. sagittal rotation curves for any specimen.

The curves in Figure 48.1-6 show the vertical and shear forces generated for large sagittal rotations. There was a slight tensile force generated for low angles of flexion. This axial force became

compressive and increased markedly as the angle of flexion was increased, however the force remained far below the maximum compressive force of 1750 N presented by Panjabi, et al. [28] for cervical spine from C3-C7. A negative shear force was generated as the angle of flexion increases. Specimen E, which was broken before these tests, showed the opposite trends.

If there was no evidence of yield on the moment vs. sagittal rotation curves in the destructive tests, the stage was rotated to the maximum flexion position possible with the test fixture and then compressed. Yield on the load-displacement curves was measured at the point of zero slope, maximum load, however only specimen D displayed clear evidence of failure on the curve showing vertical force vs. vertical displacements, Figure 49. This occured at an angle of -27 deg and 6.5 mm of compression, resulting in a compressive force of 2600 N.

All specimens were examined visually to determine which elements had failed when he test sequences were complete. In all cases, there was complete failure of posterior ligaments and both discs adjacent to the middle vertebral body. The specimens were then radiographed to determine if bony failure had occured. The radiographs of specimens D and H showed anterior fracture of the middle vertebral body as well as complete posterior element failure. The radiograph of specimen G showed fracture of the anterior superior vertebral body, fracture of the superior part of the middle vertebral body, and complete posterior element fracture. The radiographs for the remaining three specimens showed no bony fracture.

4.4 DISCUSSION

4.4.1 Test Results-Cervical Segments

All specimens show greater stiffness in compression than in tension based on estimates of the slopes of the load displacement curves. This was typical of segments from both regions of the spine. This is apparently due to the compression resistance offered by the discs and the compressive stiffness of the facet joints. Specimens F and H showed extremely high compressive stiffnesses. At only 0.6 mm of vertical compression, these specimens were subjected to the maximum force that cervical vertebrae can withstand, according to White and Panjabi [37], yet they showed no obvious signs of failure. The reasons for this are not apparent, however bony interaction between the adjacent vertebra in the most plausible explanation.

The vertical (compression-tension) stiffnesses decrease from the upper cervical levels to the lower cervical levels. This trend is evident even without considering specimens F and H. Liu, et al. [18] studied the biomechanics of cervical FSU's at rates of 0.0085 mm/sec and 85 mm/sec. They compressed a FSU steadily until a load of 880 N was reached and then returned the specimen to its original configuration at the same rate. In tension, a maximum displacement of 1.25 mm was recorded. Liu, et al. reported that axial stiffness

increases in more distal segments of the spine. To determine how his stiffness data from FSU's compared stiffnesses of FVS's, we summed the stiffnesses from two adjacent FSU's as if they were springs in series (k_1k_2/k_1+k_2). The results of this calculation showed no evidence of increasing or decreasing stiffness in the cephalocaudal direction.

The displacement rates used in the nondestructive test sequences here were relatively low and can all be considered quasistatic. This explains why there was no dependence of estimated stiffness on displacement rate for either axial or anterior-posterior loading. Tests conducted at rates from 0.5 mm/sec to 5 mm/sec showed no significant changes in the load-displacement response. Dynamic testing is generally done at rates approaching 100 mm/sec to simulate pilot ejection or automobile crash environments and generally show an increase in the slope of load-displacement curves. While the PTA is capable of rapid displacements, we were not able to take high speed data during these tests due to the data limitations of the MINC computer.

Shear stiffnesses were consistently lower than axial stiffnesses. This finding is typical also of the thoracic and lumbar regions. The compressive forces are generated by the interaction of the facet joints and are generally larger than the shear forces generated by negative X-displacements. As the middle vertebra is displaced anteriorly with respect to the fixed vertebra, little or no vertical forces are generated.

In the specimens from the upper cervical levels, stiffnesses were higher in posterior shear than in anterior shear, with the exception of specimen C. This is due to the interaction of the apophyseal joint members as the middle vertebra is moved posteriorly with respect to the fixed vertebra above it. This trend is reversed in the specimens from the lower levels, although the stiffnesses displayed in both anterior and posterior shear in the lower segments were very low. Liu, et al. [18] reported that posterior shear stiffnesses were higher than anterior shear stiffnesses for all levels of the cervical spine.

The shear stiffness also decreases from the upper cervical levels to the lower levels, with the exception of specimen C. This may be due to the changing geometry of the more distal posterior elements. Liu, et al. [18] reported the opposite trend. When his data from two adjacent FSU's are summed (k_1k_2/k_1+k_2), there does not seem to be any evidence of increasing or decreasing stiffness as one descends the cervical spine.

The middle vertebra rotated positively about Y (extension) as the vertebra below was displaced in the negative X-direction, again due to the interaction of the facet joints and to the stiffness of the anterior ligament. It rotated negatively about Y as the vertebra below was displaced in the +X-direction due to the anterior compression of the discs and to resistance offered by the posterior ligaments. The coupling of horizontal displacements and sagittal rotations of cervical spinal segments has been shown by Liu, et al.

[18] and Panjabi, et al. [27]. Panjabi applied a horizontal load of 25% body weight to cervical FSU's and measured the resulting sagittal rotation. He reported maximum X-displacements of 2.7 mm and maximum Y-rotations of 10.7°. In the present study, a compressive preload of 10% body weight was added to the FVS and a maximum of 5° extension resulted from a maximum of 1.5 mm of displacement of the lower vertebra posteriorly, in the negative X-direction (Fig. 20.3). The amount of preload may greatly affect the degree of rotation associated with horizontal (X) displacements. There was a small amount of axial rotation about Z also, most notably for specimens E, G, and H. This was due most probably to irregularities in these specimens. Specimens G and H are from the same cervical spine.

The widest scatter in our data between specimens was measured in the curves of sagittal moment vs. sagittal rotation (Fig. 21.1-21.7). The angles of rotation are too low to detect any trends. In quasistatic A-P bending tests on cervical FSU's, Liu, et al. [18] also found bending moments to vary widely. For flexion and extension angles of 5°, he found maximum extension moments ranging from 400 N-mm to 7500 N-mm and maximum flexion moments ranging from -800 N-mm to -9000 N-mm with no dependence on cervical spinal level. In future testing, the angles of rotation should be increased to at least 30% of the physiologic range of motion of cervical FVS's to provide better description of the flexion-extension properties.

There were compressive forces generated at the middle vertebra when the specimens were rotated in extension due to the interplay of the facet joints and the intervertebral discs. Compressive forces were less than 80 N for angles of extension of less than 1.5°, Figure 45.2.

There is no evidence of sudden failure of FVS's at high angles of flexion. This is clear from the curves showing moment vs. stage rotation, Figures 46.1-6. When comparing the forces generated in X and in Z for these large flexion angles, Figures 48.1-6, it is clear that these forces alone cannot account for failure of the specimens. However, the study of Figures 47.1-3 suggest that each time the specimens are rotated to successively higher flexion angles, the soft tissues and the posterior ligaments become less stiff. In this way, the failure of the specimen may be a gradual giving way of many structural elements at once.

When specimen D was compressed while held at 27° of flexion, there was a bony fracture at 2600 N. Liu, et al. [18] found a maximum compressive strength (without flexion) of 1020 N for a FSU consisting of C6-C7.

4.4.2 Displacement Measurement

The PTA allows simulation of the full physiologic range of spinal motions. This machine provides continuous and repeatable loading or displacement capabilities. Together with the displacement measuring collar, this makes possible the measurement of all necessary

parameters for the definition of the complete biomechanical response of the spine, including both specimen stiffness and flexibility and low rate viscoelastic properties. The displacement collar provided an ideal means of monitoring motion. It held firmly yet non-invasively around the middle vertebra.

Electromechanical transducer assemblies have the advantage over dial gage systems of highly accurate and continuous real-time recording of motion. Previous investigators have attached electromechanical devices or balls to the moving member of a FSU with bone screws or Steinmann pins. While these methods are valid for non-destructive testing, they would most likely affect the outcome of failure testing due to increased stresses at the site of the screw or pin. Further, Panjabi, et al. [28] noted difficulty in keeping his transducers in contact with the balls attached to the moving member. He overcame this difficulty by adding rubber bands, or by adding low pressure compressed air to the back of the LVDT coils. This, together with the weight of the relatively large balls, could apply additional stresses to the specimen.

The six degree of freedom displacement measuring apparatus used here combines the accuracy of precision transducers with a lightweight and virtually friction free gimbaled assemblies. This system provides a non-invasive yet rigid attachment to the specimen needed for accurate measurements without hampering normal motions. Since a total of nine transducers are used, three more transducers than are necessary to determine the spatial location of three noncolinear points, there is a backup system in the event that one or more transducer becomes non-operational during testing.

A trial displacement collar was used to determine the accuracy of the entire displacement measurement system involved the use of. By using the collar in conjunction with the PTA, it was possible to determine the errors from this apparatus for a situation identical to specimen tests. Curves were plotted which show displacement collar motion and test stage motion vs. time (Appendix C). Minimum errors of close to 0% were recorded for X and Y translation directions. Minimum errors of 3% were recorded for measurement of rotation about the X and Z axes. Maximum errors of 1.2^{o} for a stage rotation of 10^{o} about Y and 0.4 mm for Z stage translations of 3 mm were recorded. In addition to transducer error, other possible sources for this error included motion of the displacement collar, position of the assembly on the PTA bridge, or in the determination of the position of the assembly origins with respect to the global reference system.

4.5 SUMMARY OF CERVICAL SPINE STUDY

This study of the cervical spine measured the biomechanical load-displacement properties of specimens up to failure using a combination of refined experimental and analytical methods. Previous biomechanical investigations of spine segments and the current investigation have shown that the spine displays complex nonlinear, coupled, viscoelastic properties. Therefore, to best examine this

response, physiological load-displacement conditions must be reproduced in vitro, and the resulting three dimensional motions measured and analyzed.

The use of three-vertebrae Functional Vertebral Segments (FVS) in mechanical tests offered advantages over both two vertebrae segments (FSU's) and whole cervical spines. Tests of the FSU involve fixing one vertebra and applying loads to the second, taking into account the motions about one joint only. Accurate strength measurements cannot be obtained from FSU's. For the FVS, the middle vertebra is jointed naturally to the two adjacent vertebrae, providing for more physiological end conditions. Unlike whole cervical spine specimens, motions of each vertebra can be controlled and directly measured. The use of the Functional Vertebral Segment is recommended in future studies which include failure investigations.

A valid test apparatus for the study of spinal motions must be able to produce simultaneous motions in more than one plane and to measure loads and displacements in three dimensions. Liu, et al. [18] subjected cervical FSU's to individual modes of loading (axial, shear, bending, and torsion) with a material testing machine and recorded motions with strain gages. The Planar Testing Apparatus used here is capable of producing controlled loading or three components of controlled displacements simultaneously. The PTA, in conjunction with the displacement measuring apparatus, allows for three dimensional motion and motion measurement, and direct data analysis.

The three dimensional motion measurement system and analysis of Eulerian rotations were developed and refined from the techniques presented in several previous studies to monitor the displacements of the FVS specimens. Tenser, et al. [35] used a displacement measuring apparatus very similar to the one developed here. Measurement errors due to the assembly design and limitations on the range capabilities of his transducers were reduced in the improved system by mounting transducers in a gimbaled arrangement.

Methods were developed here for the precise calculation of translations along and Eulerian rotations about an orthogonal axis system with its origin at the center of the moving member of a FVS. This method of describing three dimensional motion of one body relative to another is simple and understandable. Koogle, et al. [14] used the kinematic analysis developed by Dieudonne, et al. [6] for the calculation of Eulerian rotations of his test fixture but had difficulty with the elastic strain gages used to monitor displacements and with the design of the fixture to hold spine specimens. The analysis used in the present study is well suited to our displacement measuring apparatus.

Load-displacement tests of seven cervical FVS's yielded several interesting results. There was no dependence of stiffness on displacement rate at the rates used in this study. This study suggests that velocities greater than 5 mm/sec or 5 deg/sec are required to observe viscoelastic effects. Curves showing axial and

shear forces vs. axial and shear displacements, and moment vs. rotation, displayed large neutral zones, or regions of small load and low slope as displacements increase. All specimens were stiffer in compression than in tension, and the specimens from the upper cervical region were stiffer in response to shear and vertical motions than specimens from the lower region. Specimens taken from the upper cervical region showed greater stiffness to posterior motion than to anterior motion.

Few previous *in vitro* investigations on cervical spine have been performed, and the tolerance of this region to injury is not well established. For this reason, cervical FVS's were rotated in flexion to increasingly higher angles to determine the fracture behavior of the cervical spine. All specimens showed soft tissue failure before bony fracture, and in three of six cases, no bony fracture was evident even at flexion angles of 30^{o}. In addition to high flexion angles, compressive loads of 150 N or more were necessary for fracture of the specimens. It appears that there was a gradual giving way of all structural elements, instead of a catastrophic fracture of a particular structure, for the experimental condition used.

5. SUMMARY OF PROJECT

The methodologies developed using first lumbar and then cervical spine segments here will serve as a basis for further sagittal investigations of the spine. Tests of additional cervical spine specimens will establish the statistical significance of the results gathered thus far. Future tests should consider more severe load combinations. The sagittal results presented here and the results from these future tests will provide a comprehensive description of the cervical spine and its tolerance to flexion type injuries. The Planar Testing Apparatus, displacement measuring device, and kinematic analysis are an advanced biomechanics testing system suited to studies of spine, as well to investigations into the behavior of the knee, wrist, shoulder or other complex anatomic joints.

6. REFERENCES

1. Adams MA, Hutton WC: The Effect of Posture on the Role of the Apophysial Joints in Resisting Intervertebral Compressive Forces. J. Bone Joint Surg. 62-B:358-362, 1980.

2. Akerbolm B: Standing and Sitting Posture. Forlag, Stockholm A/B Nordiska Bokhandel, 1948.

3. Andersson GBJ: The biomechanics of the posterior element of the lumbar spine. Introductory comment. Spine 8:326, 1983.

4. Coffee MS: Measurement of three-dimensional spine motion kinematics and failure properties. Cambridge, Mass. Inst. of Tech., 1986.

5. Cyron BM, Hutton WC: Articular tropism and stability of the lumbar spine. Spine 5:168-172, 1980.

6. Dieudonne JE, Parrish RV, Bardusch RE: An Actuator Extension Transformation for a Motion Simulator and an Inverse Transformation Applying Newton-Raphson's Method., NASA, TND-7067, 1972.

7. Edwards WT, Hayes WC, Mass R, Posner I, White AAIII: Variation of lumbar spine stiffness with load. J Biomech Eng :in press.

8. Fung YC: Biomechanics: Mechanical properties of living tissues. New York, Springer-Verlag, 1981.

9. Galante JO: Tensile Properties of the Human Lumbar Annulus Fibrosis. Acta Ortho. Scand., Suppl. 100 :, 1967.

10. Hayes WC, White AAIII, Edwards WT, Lelli J: Fracture and viscoelastic characteristics of the human cervical spine: Kinematics of the 3 actuator system. Grant # F49620-81-K-0010 Aug:, 1981.

11. Hirsch C, Galante J: Laboratory conditions for tensile tests in annulus fibrosis from human intervertebral discs. Acta Ortho. Scand. 38:148-162, 1967.

12. Kazarian LE, Graves GA: Compressive strength characteristics of the human vertebral centrum. Spine 2:1-14, 1977.

13. Koeller W, Funke F, Hartmann F: Biomechanical behavior of human intervertebral discs subjected to long lasting axial loading. BioRheology 21:675-686, 1984.

14. Koogle TA, Piziali RL, Nagel DA, Perkash I: A motion transducer for use in the intact in-vitro human lumbar spine. Trans of the ASME Aug:160-165, 1977.

15. Kou YF: Time dependent load distribution characteristics of lumbar intervertebral joint. Cambridge, Mass. Inst. of Tech., 1985.

16. Lafferty JF, Winter WG, Gambaro SA: Fatigue characteristics of posterior elements of vertebrae. J Bone Joint Surg 59-A:154-158, 1977.

17. Lin HS, Liu YK, Adams KH: Mechanical response of the lumbar intervertebral joint under physiological (complex) loading. J. Bone Joint Surg. 60-A-1:41-55, 1978.

18. Liu YK, Krieger KW, Njus G, Ueno K, Conners M, Wakano K, Thies D: Cervical Stiffness and Geometry of the Young Human Male., AFAMRL, 1982.

19. Lysell E: Motion in the Cervical Spine. Acta Ortho. Scand., Suppl. 123, 1969.

20. Markoff KL: Deformation of the thorascolumbar intervertebral joints in response to external loads: A biomechanical study using autopsy material. J. Bone and Joint Surg. 54-A:511-533, 1972.

21. Nachemson AL: Lumbar Interdiscal Pressure. Acta Ortho. Scand., Suppl. 43, 1960.

22. Nachemson AL: Electromyographic studies on the vertebral portion of the psoas muscle. Acta Orthop Scand 37:177, 1966.

23. Nachemson AL: The Lumbar Spine an Orthopaedic Challenge. Spine 1-1:59-71, 1976.

24. Ogata K: Modern Control Engineering. Englewood Cliffs NJ, Prentice-Hall, Inc., 1970.

25. Panjabi MM, Brand RA, White AA III: The three dimensional flexibility and stiffness properties of the thoracic spine. J. Biomech. 9:185-192, 1976.

26. Panjabi MM, Krag MH, White AA III, Southwick WO: Effects of preload on load displacement curves of the lumbar spine. Orthop. Clin. of North America 8:181-192, 1977.

27. Panjabi MM, White AA III, Johnson RM: Cervical spine mechanics as a function of transaction of components. J. Biomech. 8:327, 1975.

28. Panjabi MM, White AA III, Keller D, Southwick WO, Friedlaender G: Stability of the cervical spine under tension. J Biomech 11:189-197, 1978.

29. Pope MH, Wilder DG, Matteri RE, Frymoyer JW: Experimental measurements of vertebral motion under load. Orthop. Clin. North America 8-1:155-167, 1977.

30. Rowe ML: Low back disability in industry. Updated position. J Occup Med 12:476-478, 1971.

31. Schultz AB, Warwick DN, Berkson MH, Nachemson AL: Mechanical properties of human lumbar spine motion segments. Part I: Responses in flexion extension, lateral bending, and torsio. J. Biomech. Eng. 101:46-52, 1979.

32. Sedlin E, Hirsch C: Factors affecting the determination of the physical properties of femoral cortical bone. Acta Orthop. Scand. 37:29-48, 1966.

33. Snook SH: Low Back Pain in Industry. In: AAOS Symposium on Idiopathic Low Back Pain, ed by AA White, III, SL Gordon, St. Louis, Mosby, 1982. pp 23-38.

34. Steinberg GG: Epidemiology of low back pain. In: Chronic low back pain. ed by M Stanton-Hicks, RA Boas, Raven Press, 1982, pp 1-13.

35. Tenser AF, Ahmed AM: The Role of Secondary Variables in the Measurement of the Mechanical Properties of the Lumbar Intervertebral Joint. ASME J. Biomechical Eng. 103:129-137, 1981.

36. Tenser AF, Ahmed AM, Burke D: Some static mechanical properties of the lumbar intervertebral joint, intact and injured. J. Biomech. Eng. 104: 193-201, 1982.

37. White AA III, Panjabi MM: Clinical Biomechanics of the Spine. Philadelphia, Pa., J.B. Lippincott, Co., 1978.

38. Yang KH, King AI: Mechanism of facet load transmission as a hypothesis of low back pain. Spine 9(6):557-565, 1984.

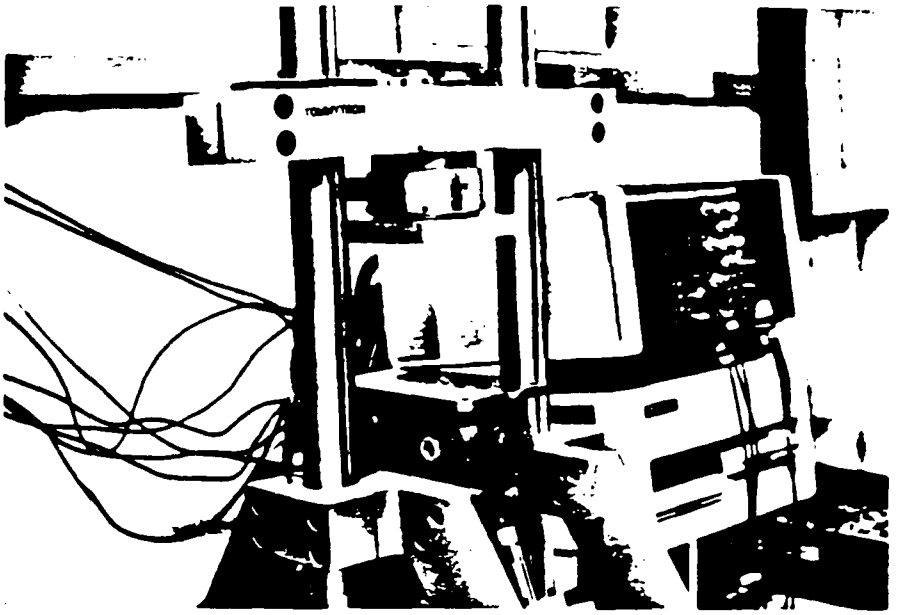

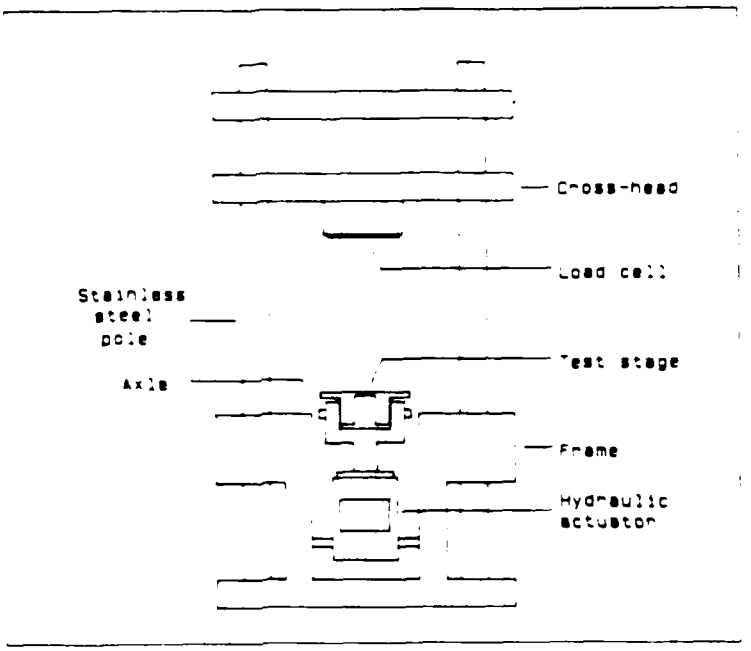

Figure:1 Planar Testing Apparatus

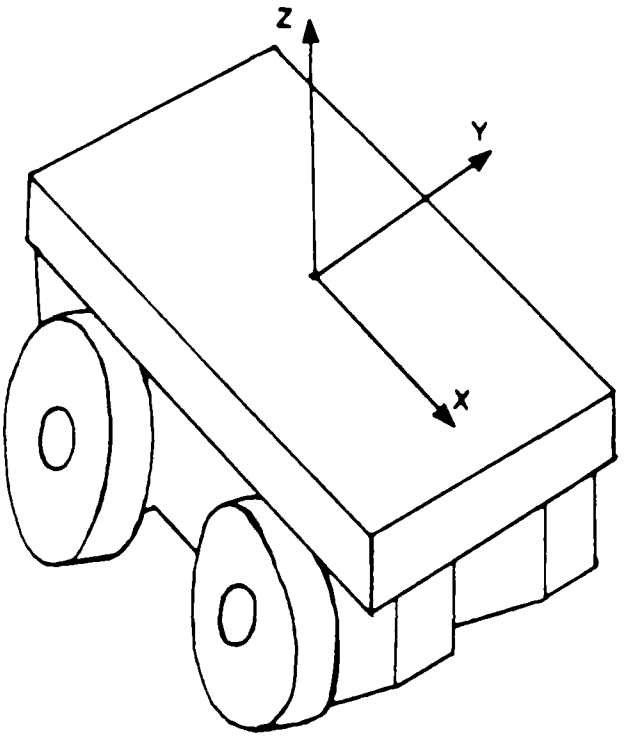

Figure:2 Three-dimensional coordinate system employed for the test stage of the Planar Testing Apparatus.

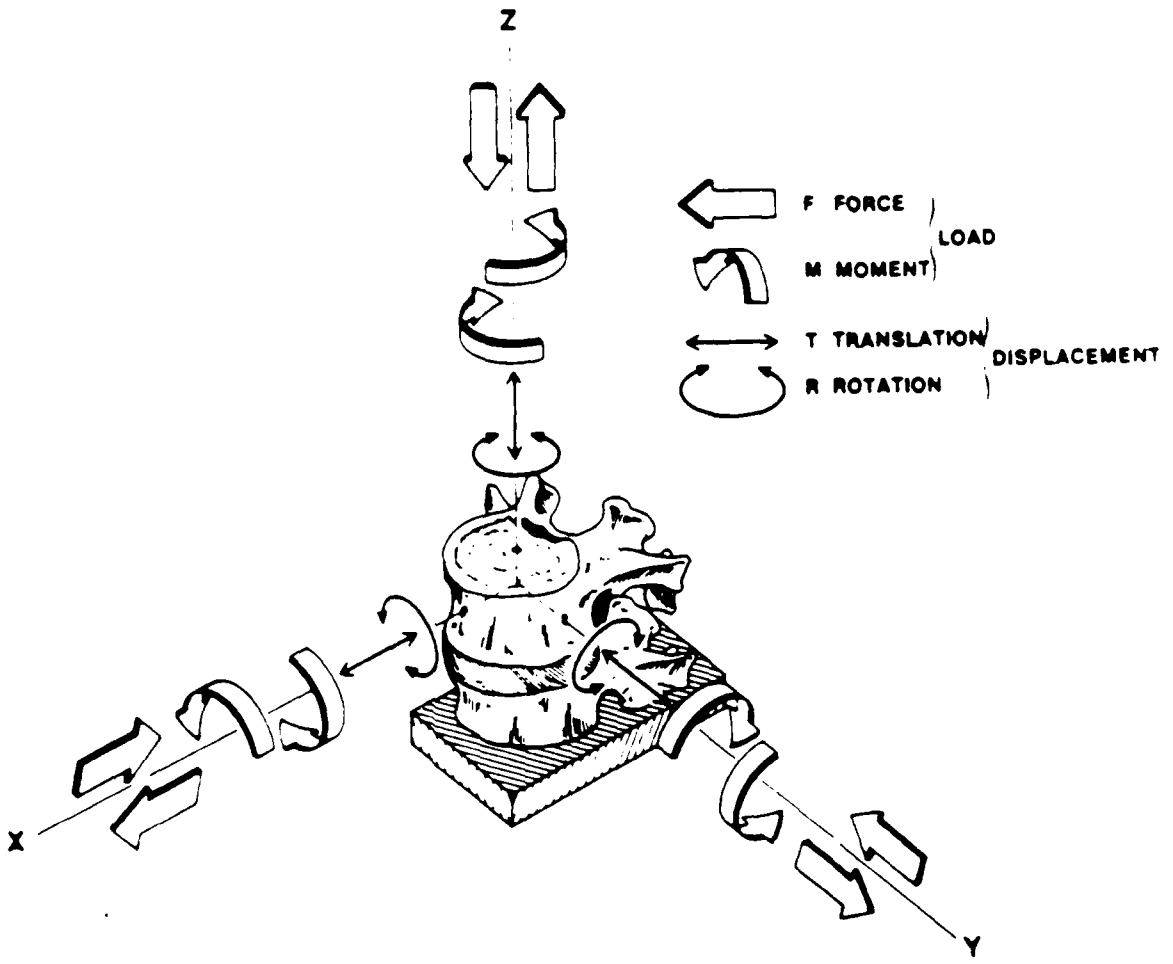

Figure:3 Three-dimensional coordinate system employed for the spinal specimen

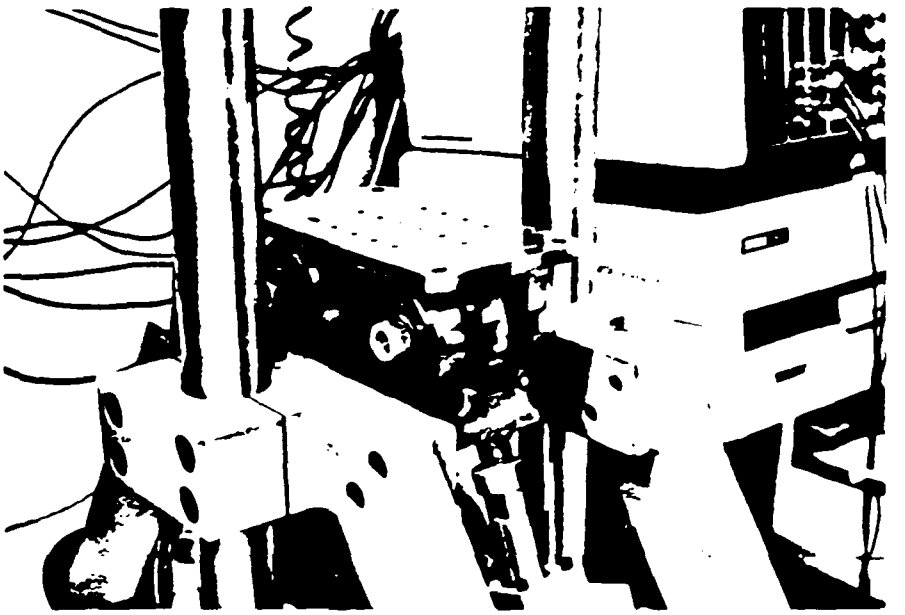

Figure:4 Test stage of the Planar Testing Apparatus

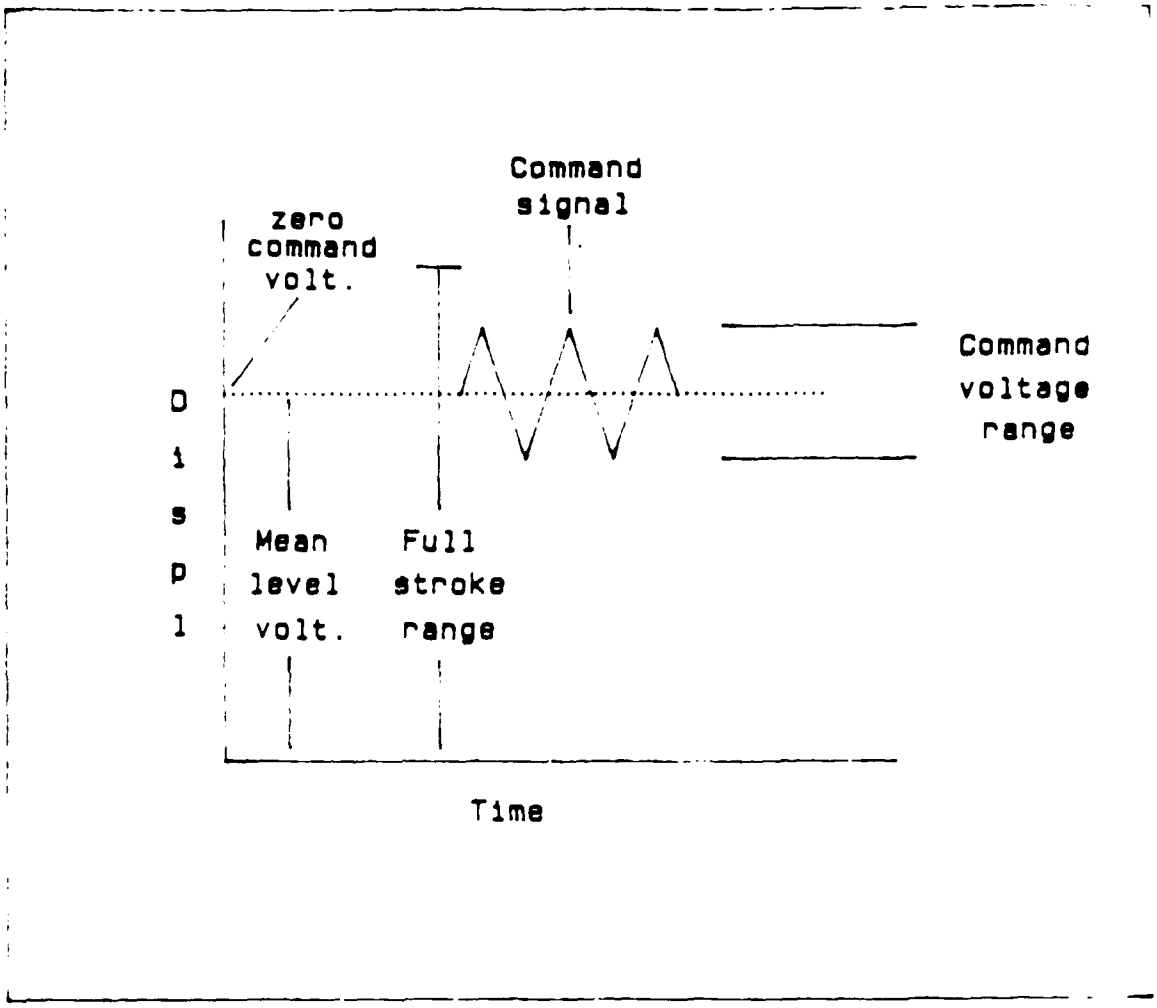

Figure:5 Mean level adjustment.

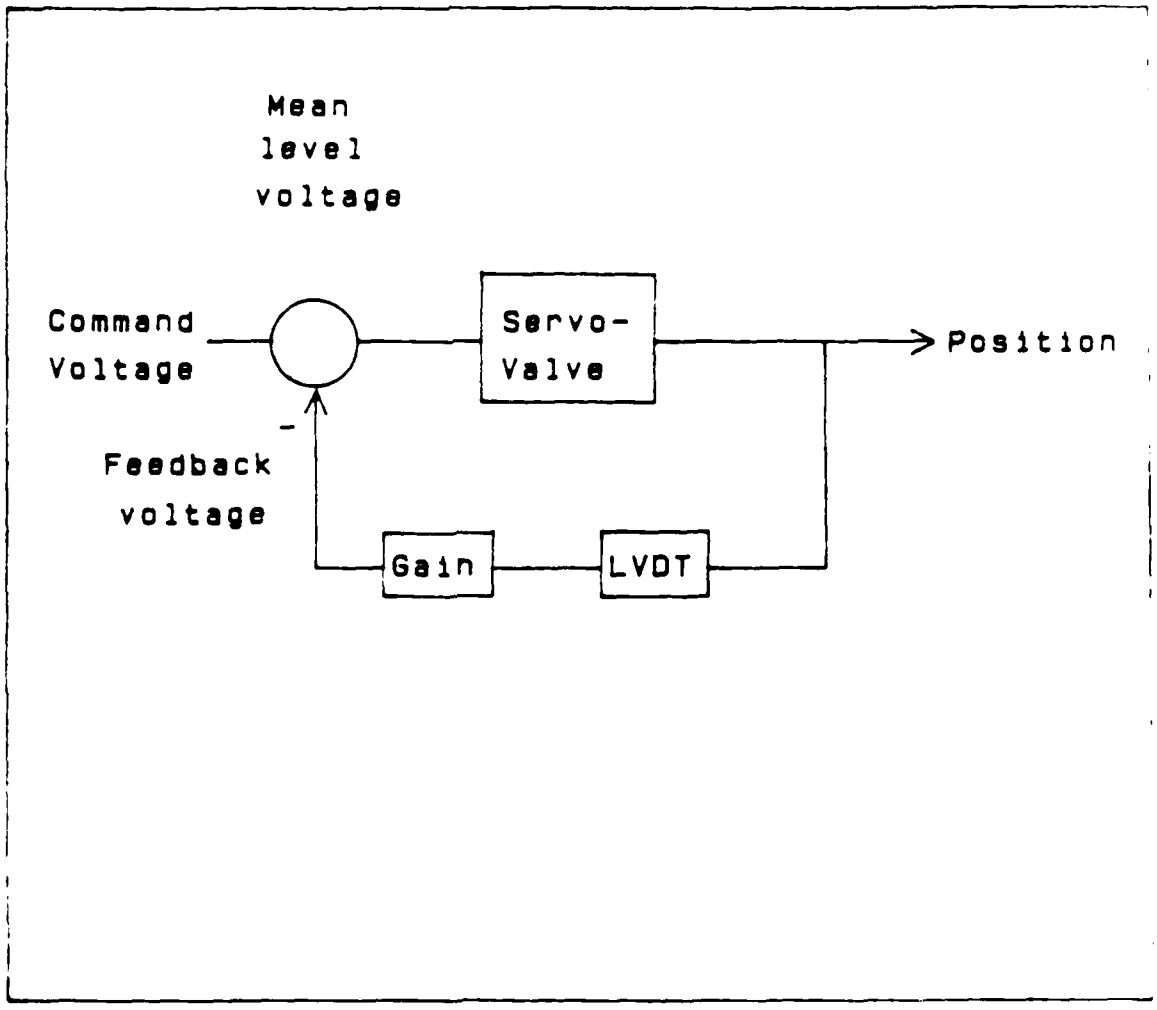

Figure:6 Control block diagram of the MOOG 122-104 analog controller.

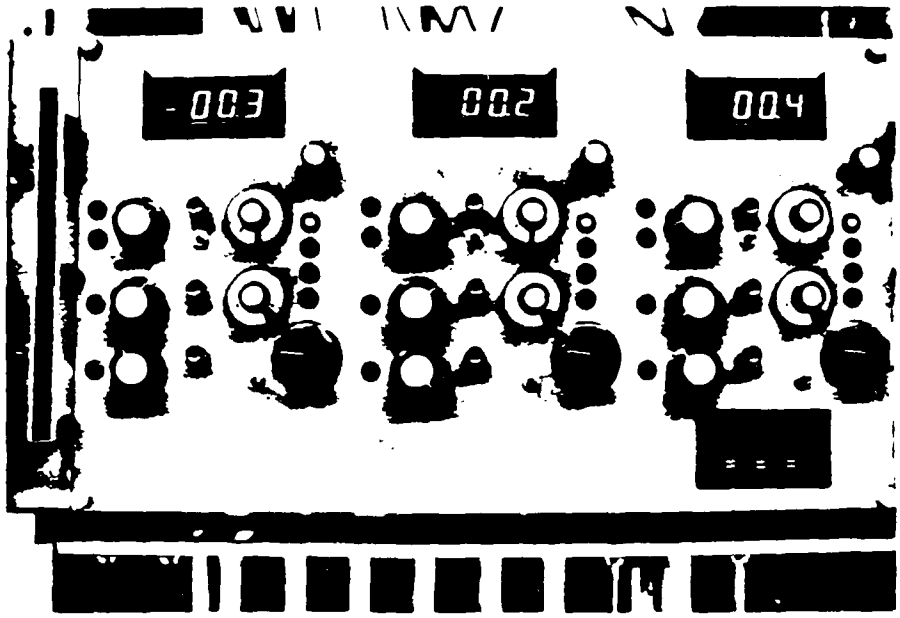

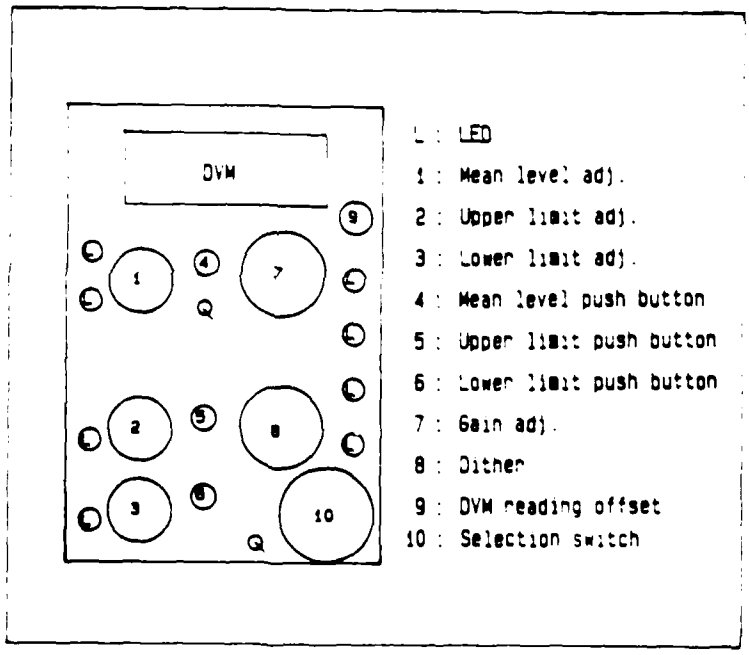

Figure:7 Display panel of the Planar Testing Apparatus.

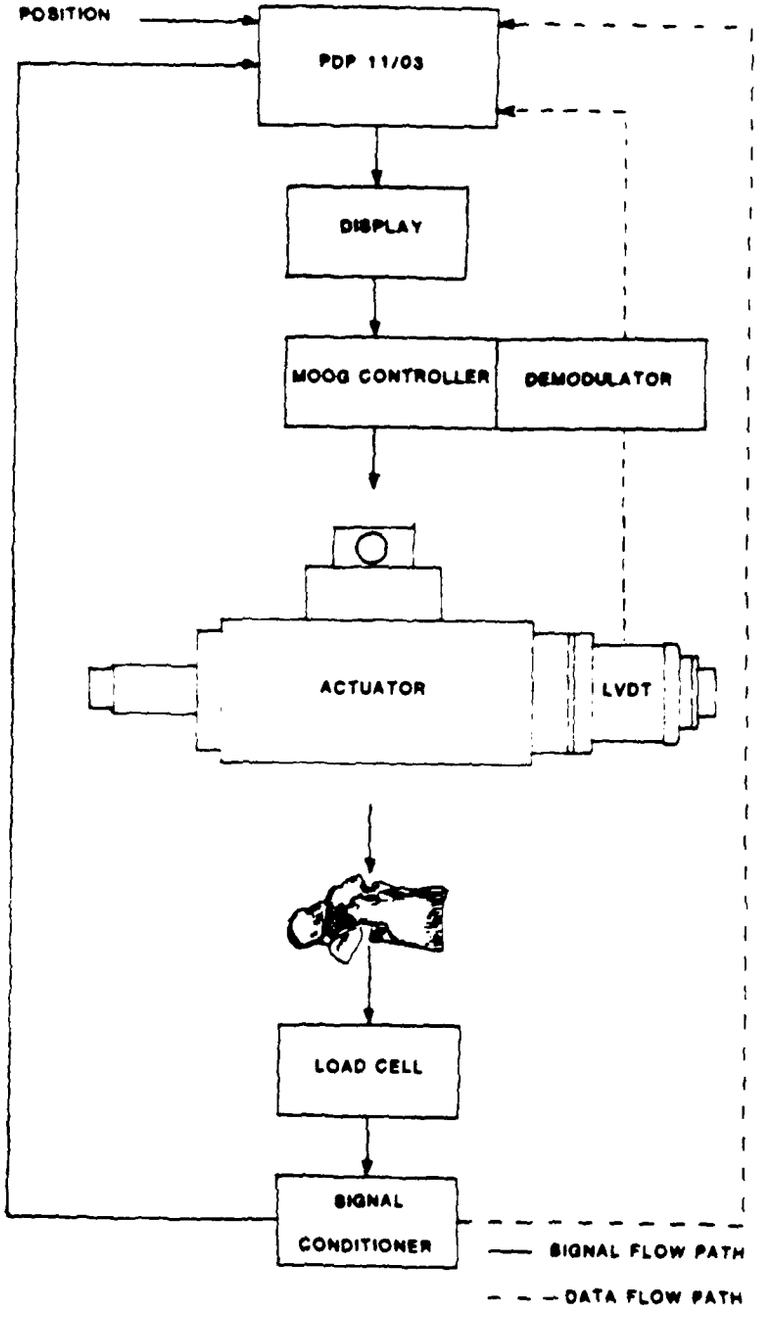

Figure:8 Planar Testing Apparatus signal flow diagram

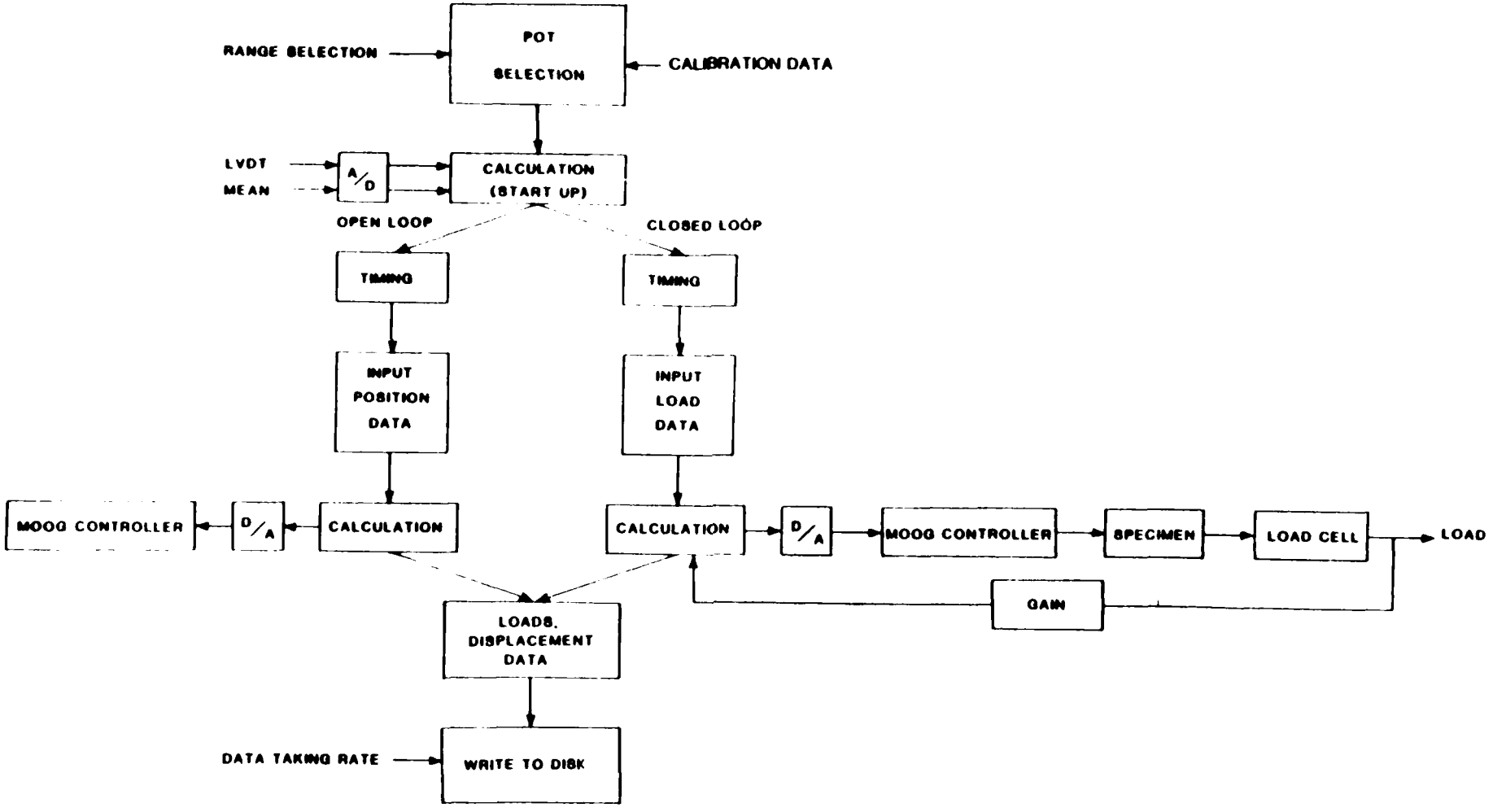

Figure:9 Overall system block diagram.

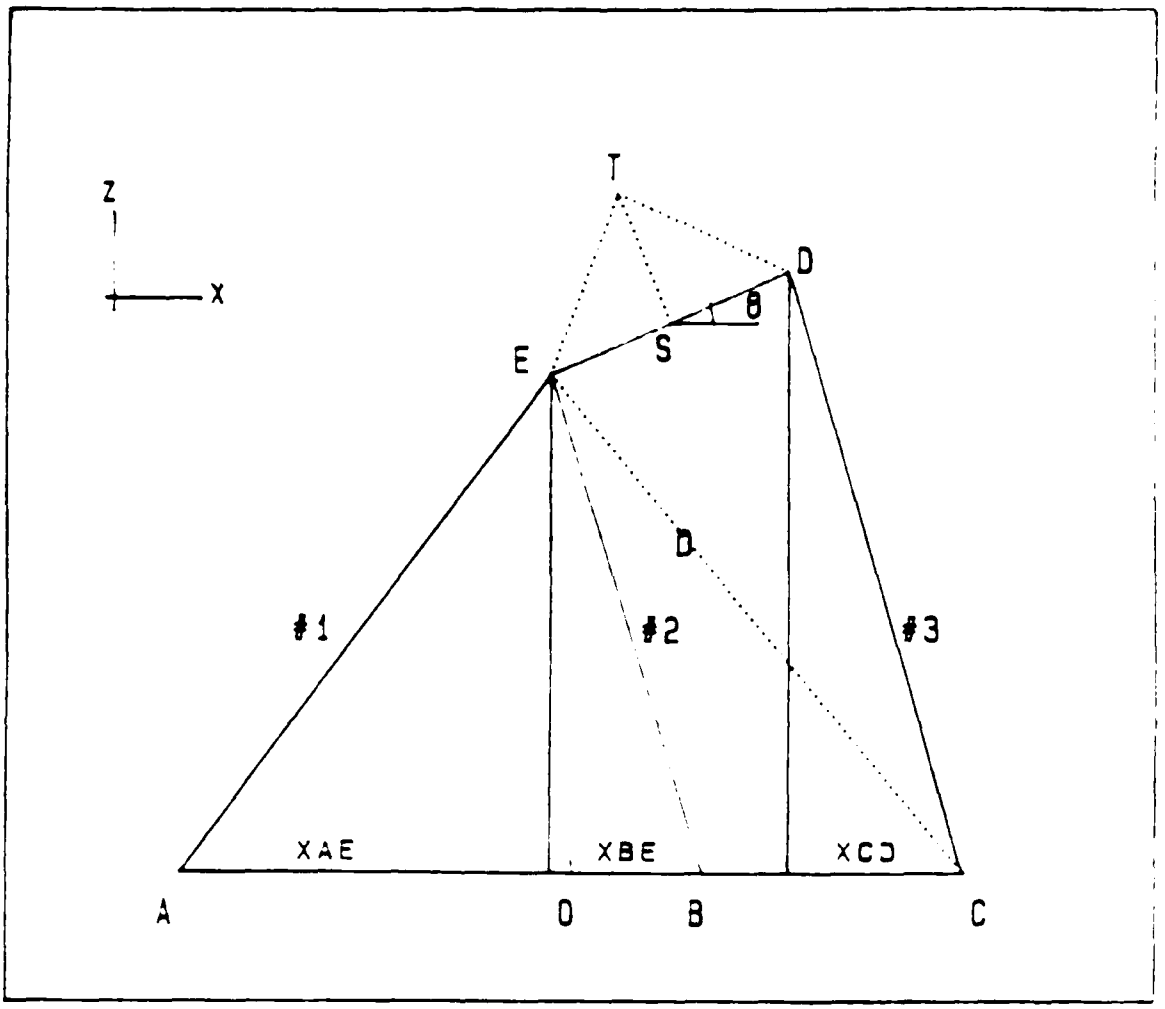

Figure:10 Test stage geometry

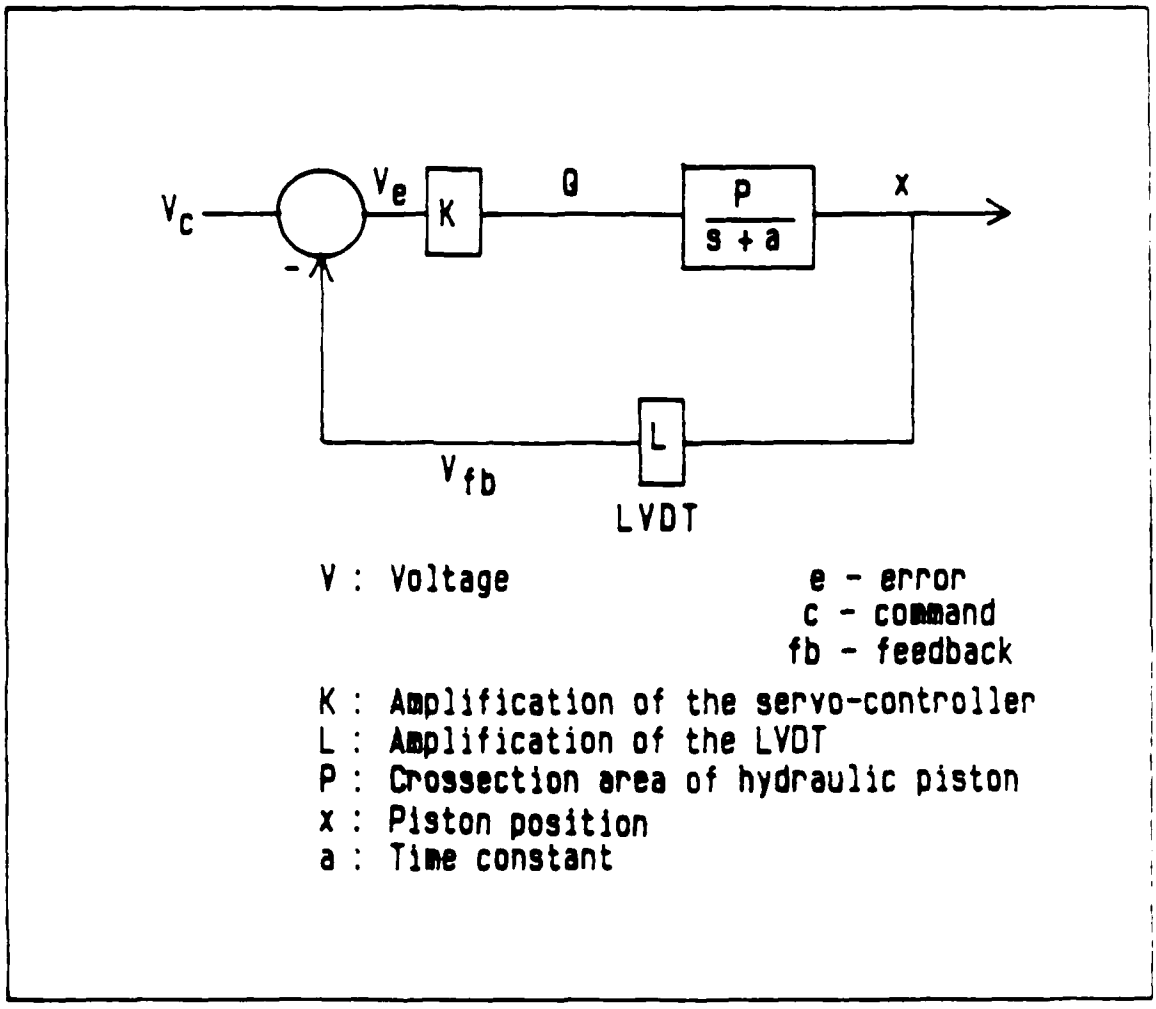

Figure:11 Displacement control system block diagram.

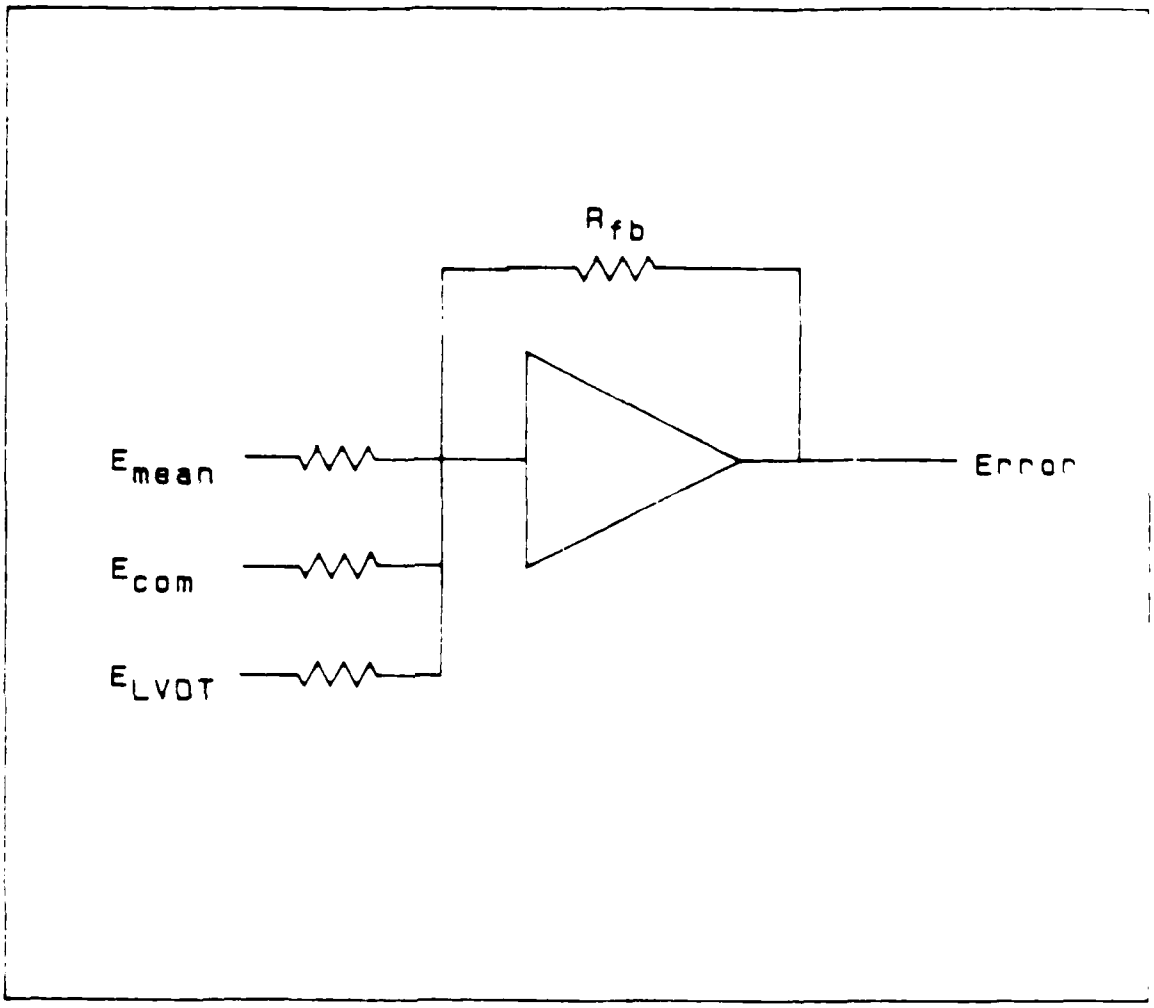

Figure:12 Summing junction of an operational-amplifier.

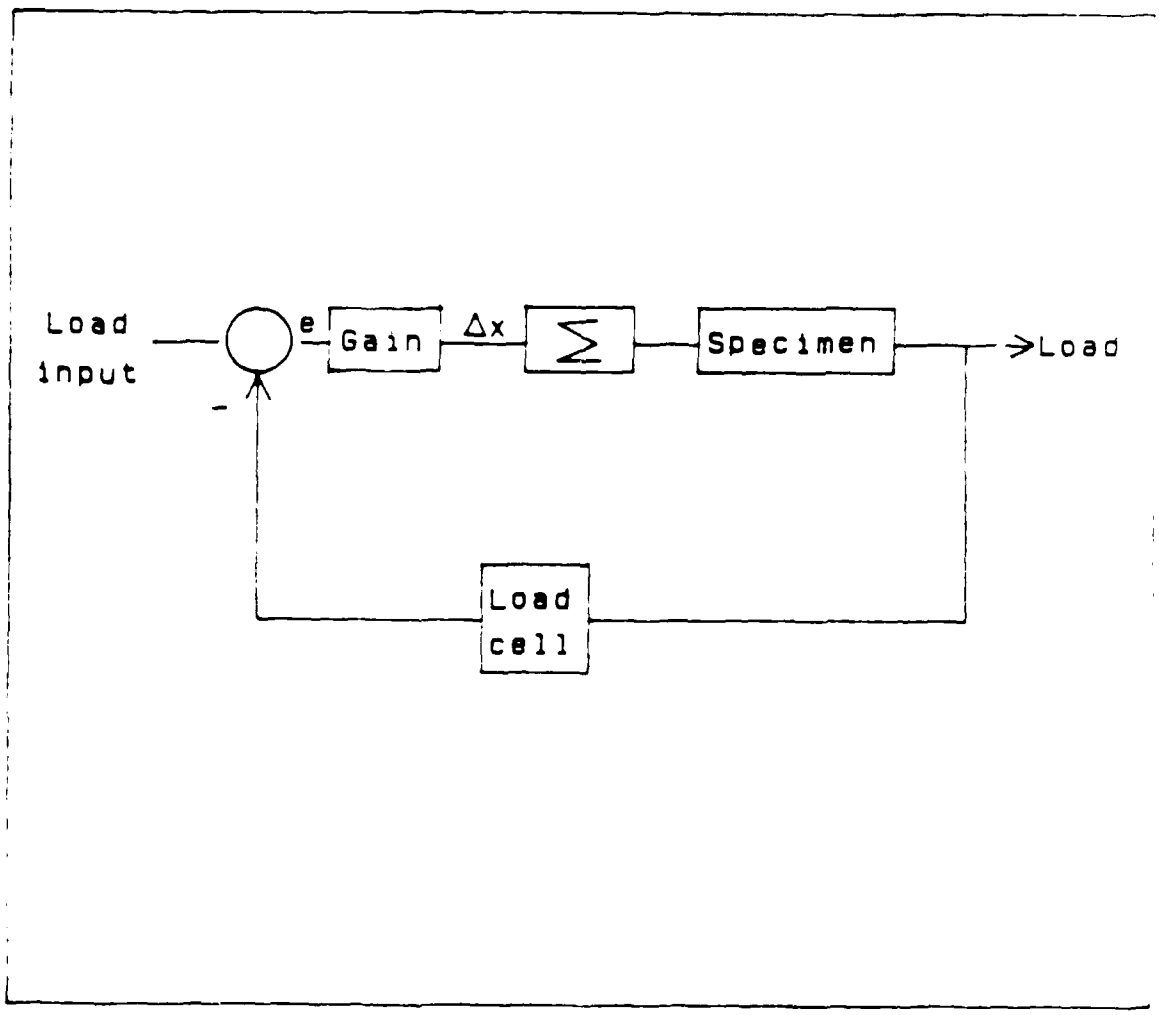

Figure:13 Load control system block diagram.

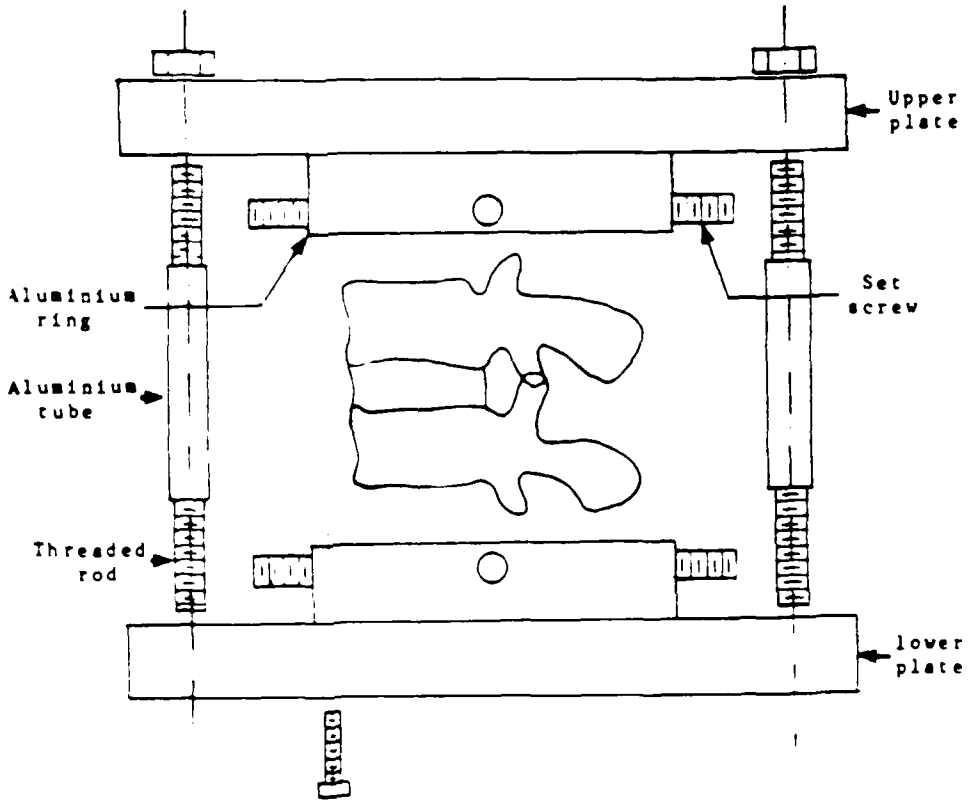

Figure:14 Test fixture for mounting of spinal specimen.

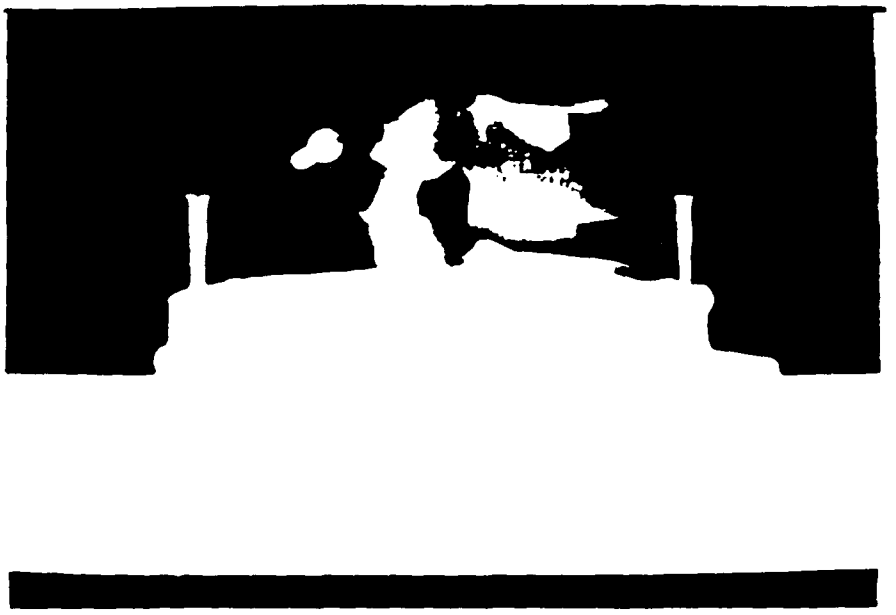

(a)

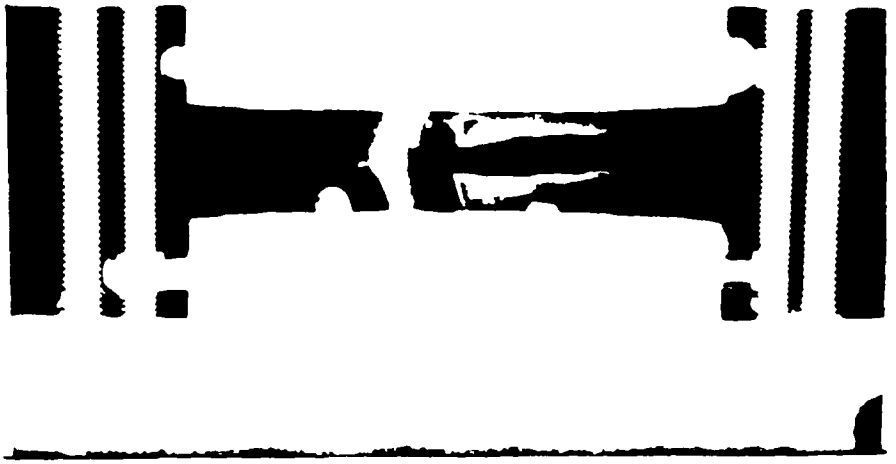

(b)

Figure 15 (a) X-ray of functional spinal unit embedded in the test fixture without the upper plate. The two wire screws on the rim of the aluminum ring served as a marker to determine the magnification factor. (b) X-ray of function spinal unit embedded in the test fixture with the upper plate.

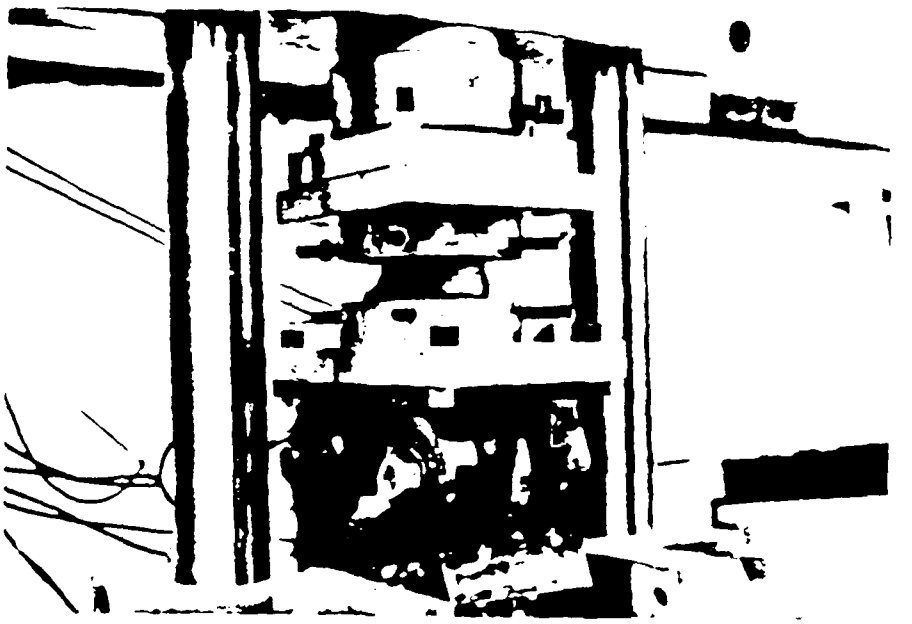

Figure:16 Picture of test fixture with functional spinal unit specimen installed on the test stage of the Planar Testing Apparatus

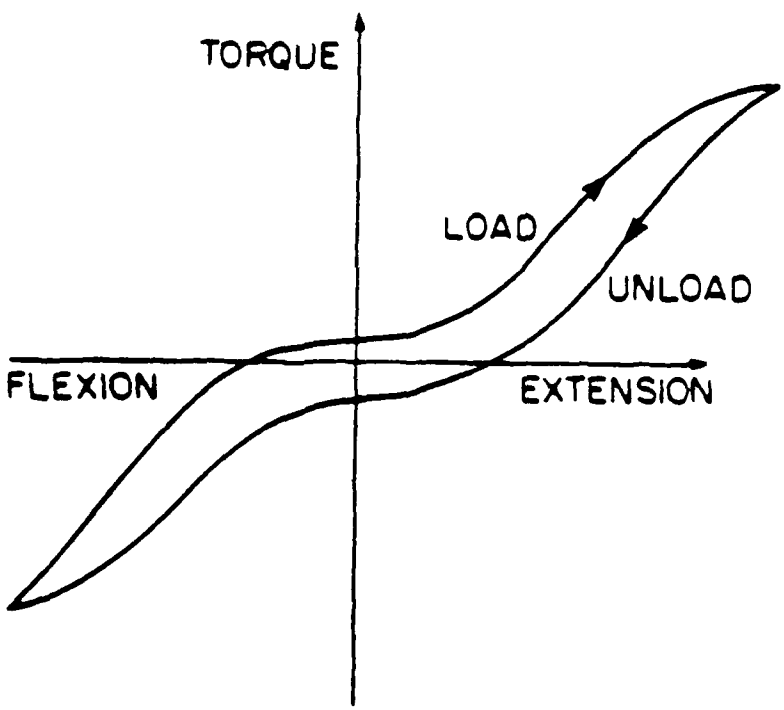

Figure:17 Hysteresis behavior of a functional spinal unit

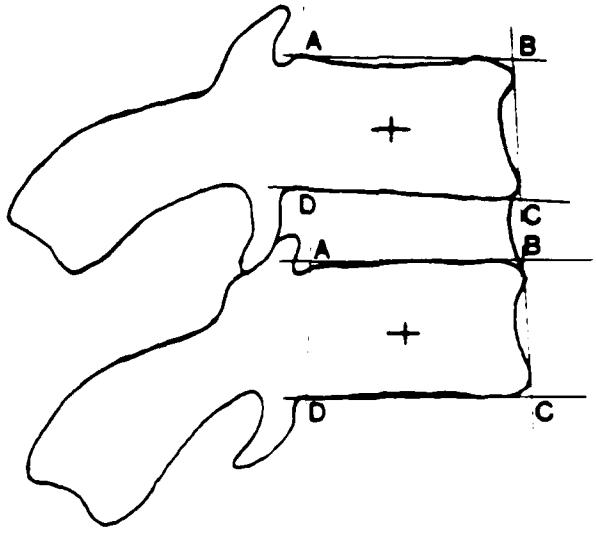

Figure:18 Geometrical consideration of the functional spinal unit.

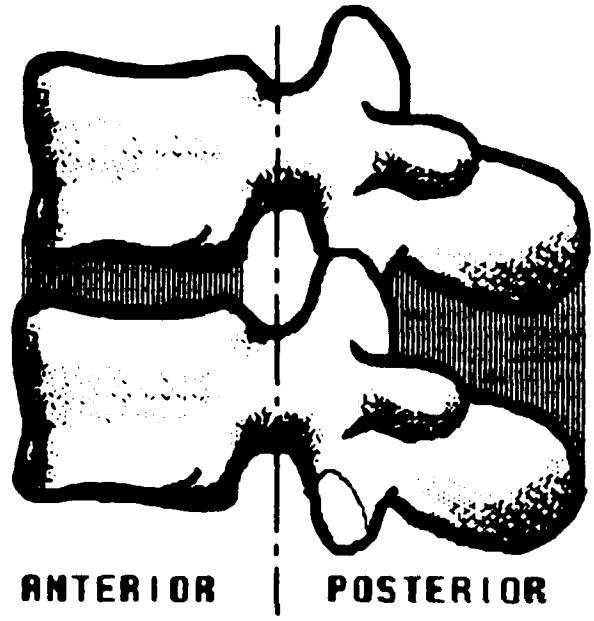

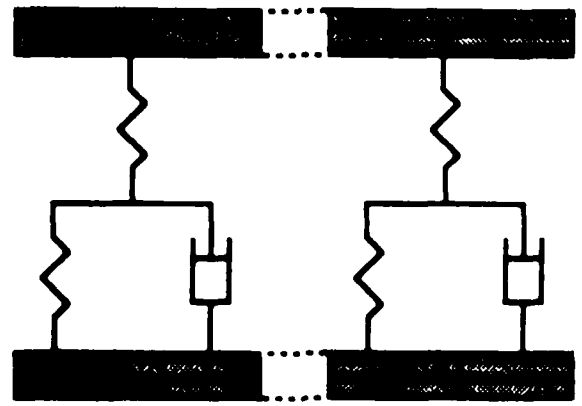

Figure:19

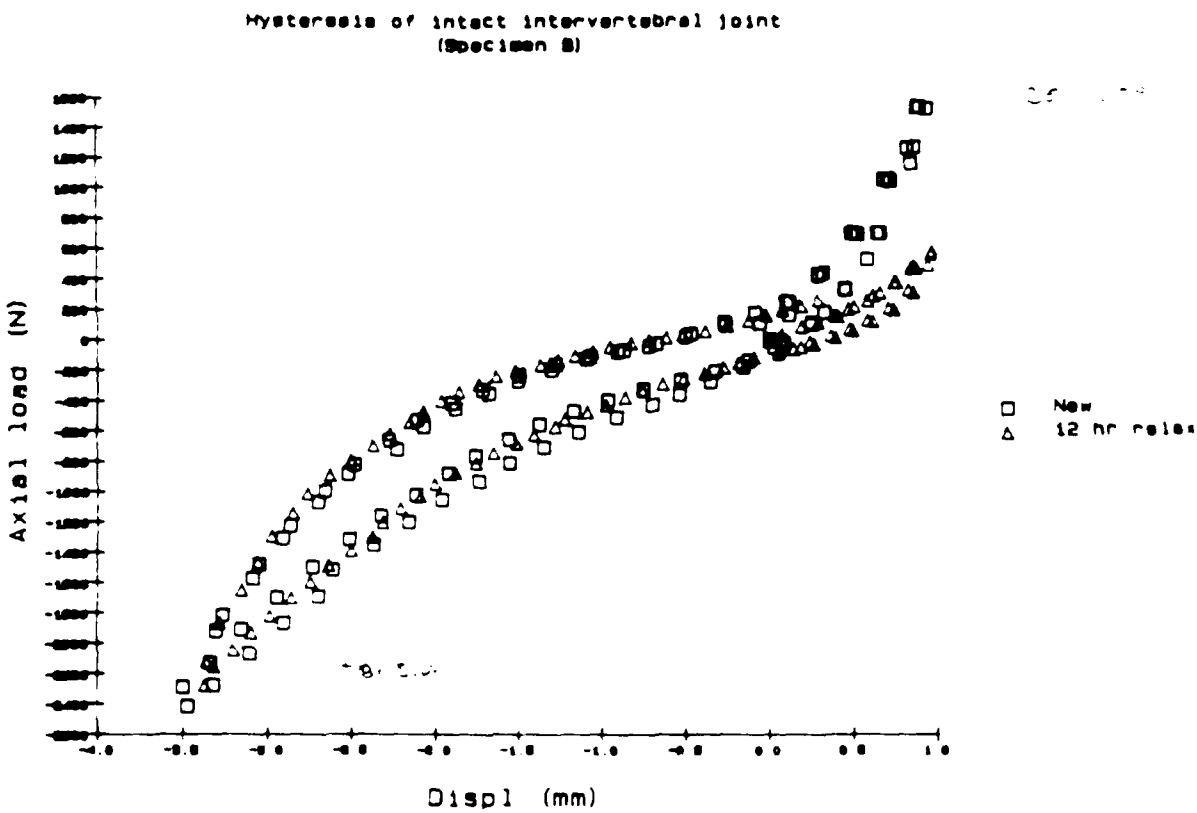

Figure:20.1 Hysteresis of intact intervertebral joint

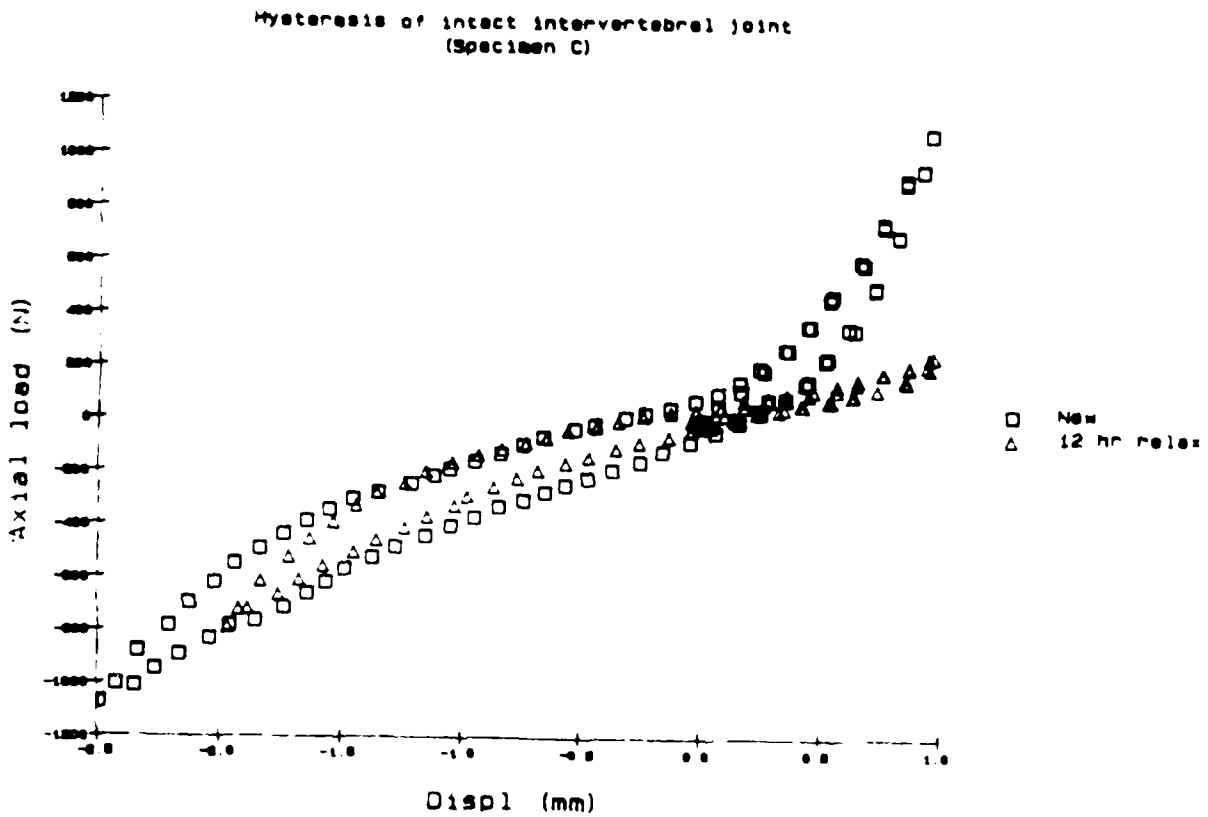

Figure:20.2 Hysteresis of intact intervertebral joint

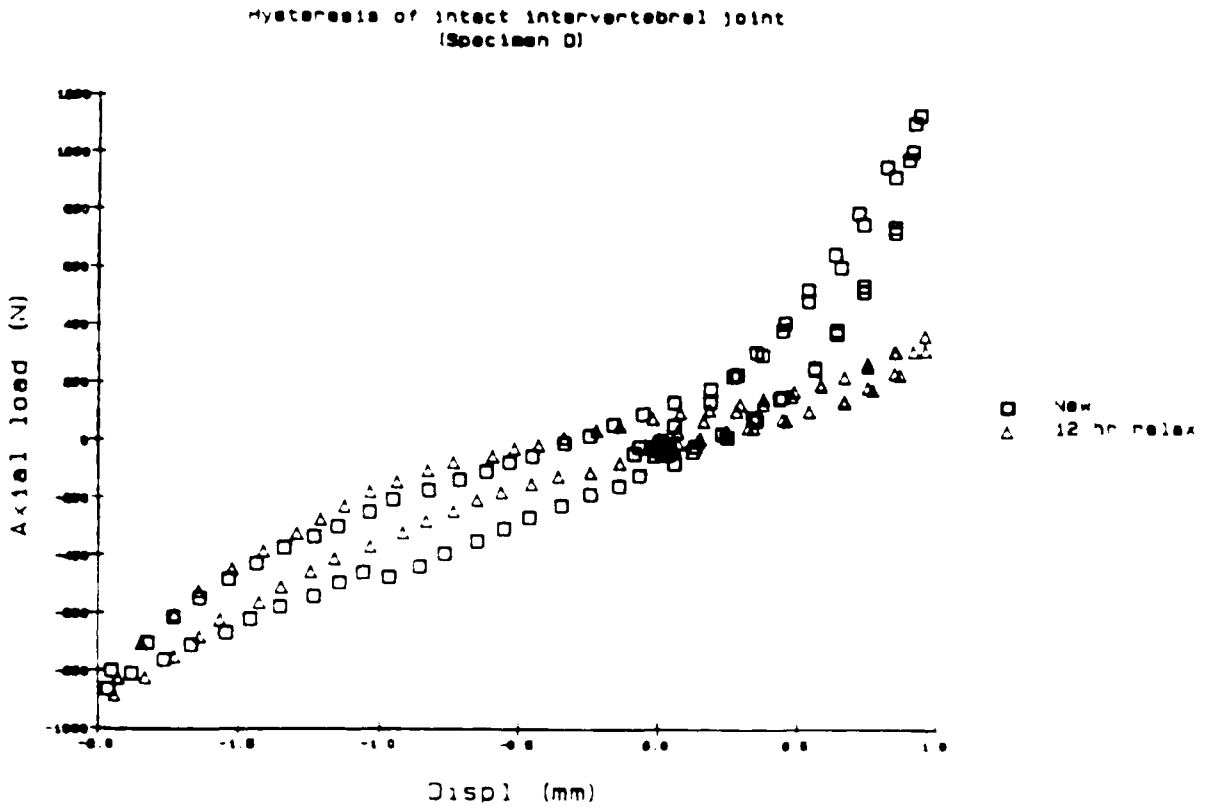

Figure:20.3 Hysteresis of intact intervertebral joint

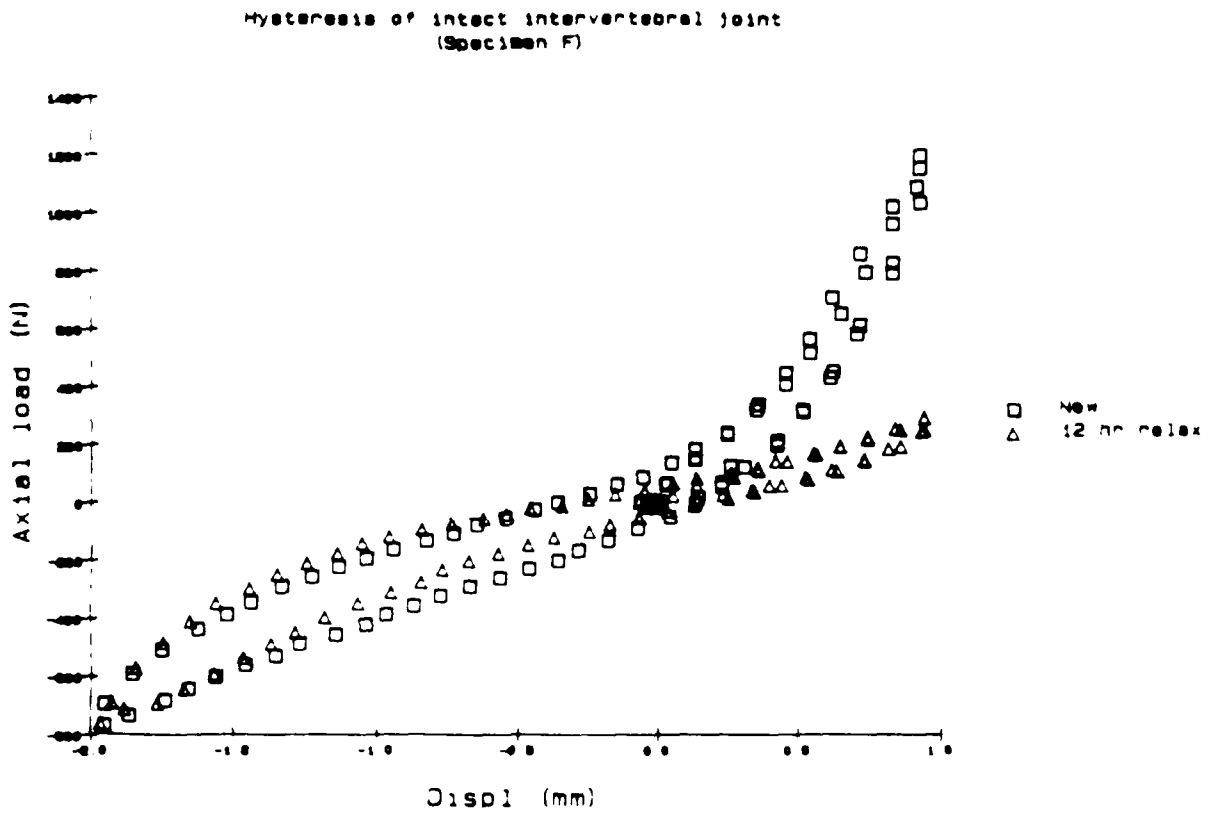

Figure:20.4 Hysteresis of intact intervertebral joint

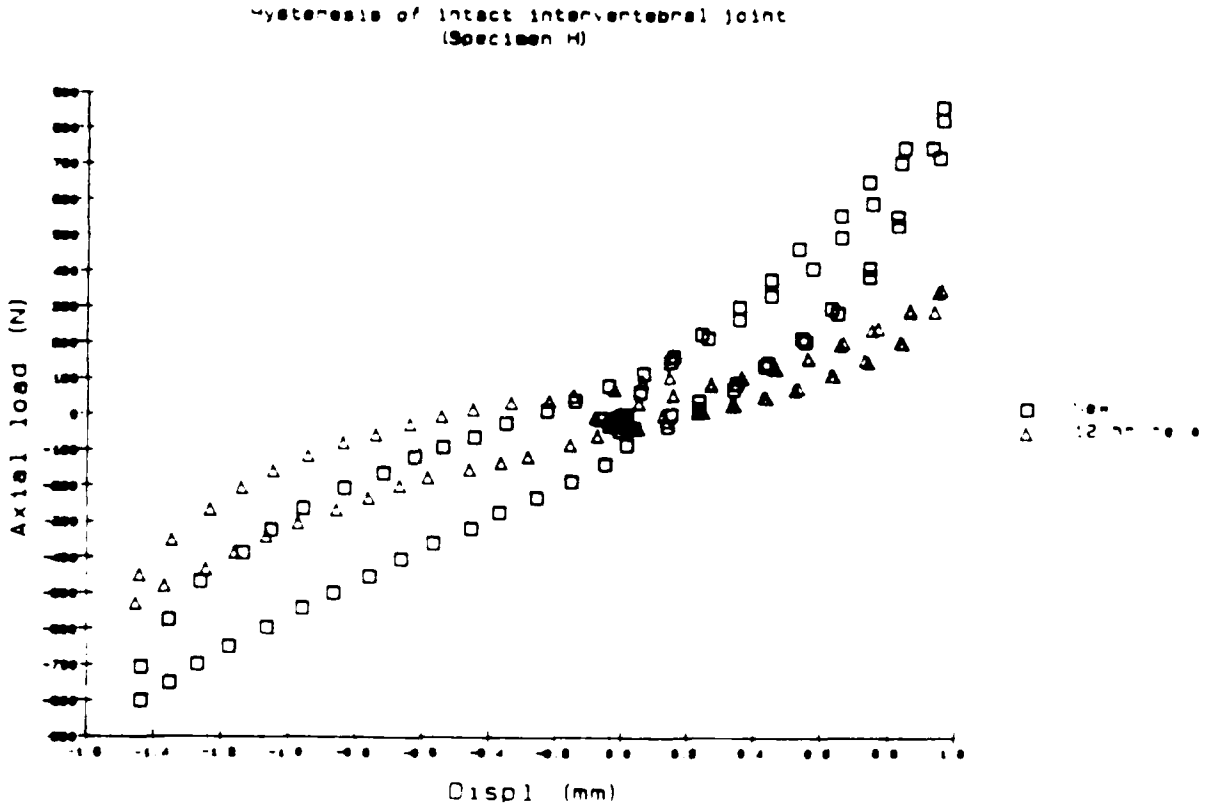

Figure:20.5 Hysteresis of intact intervertebral joint

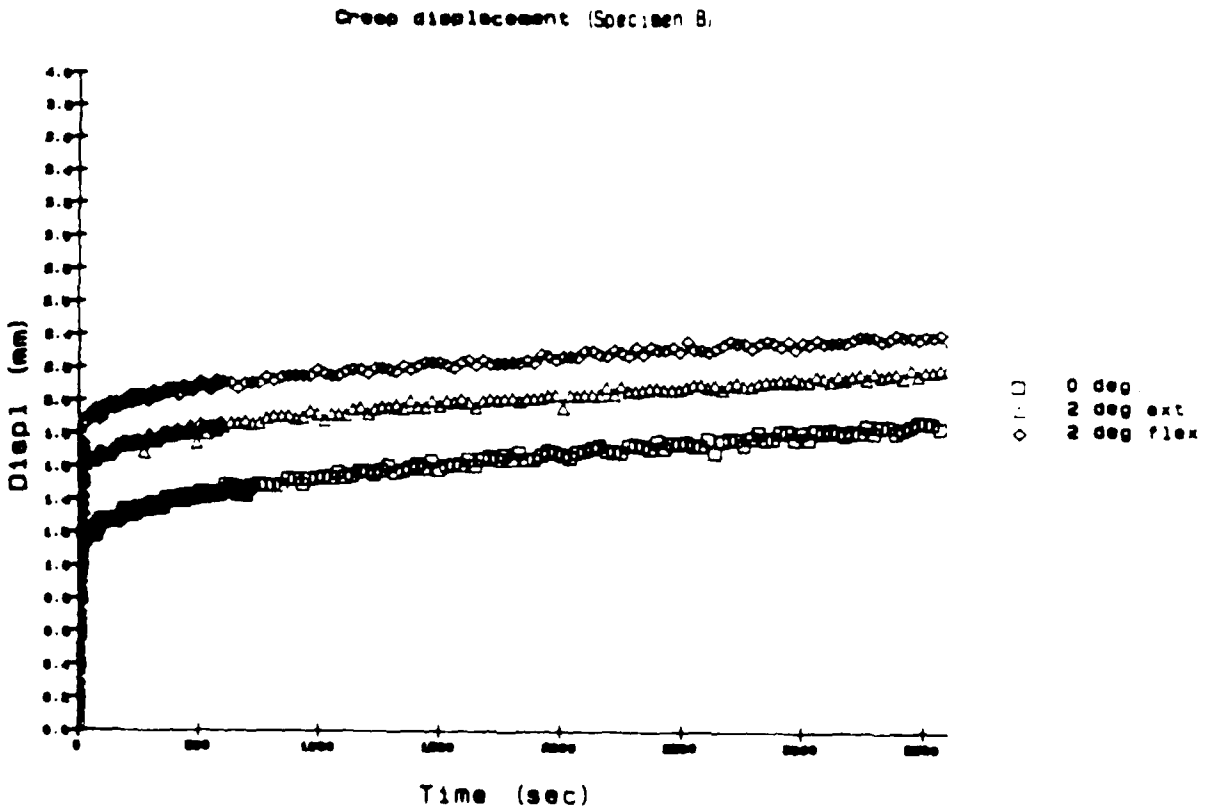

Figure:21.1 Creep displacement of intervertebral joint at three sagittal rotational angle settings.

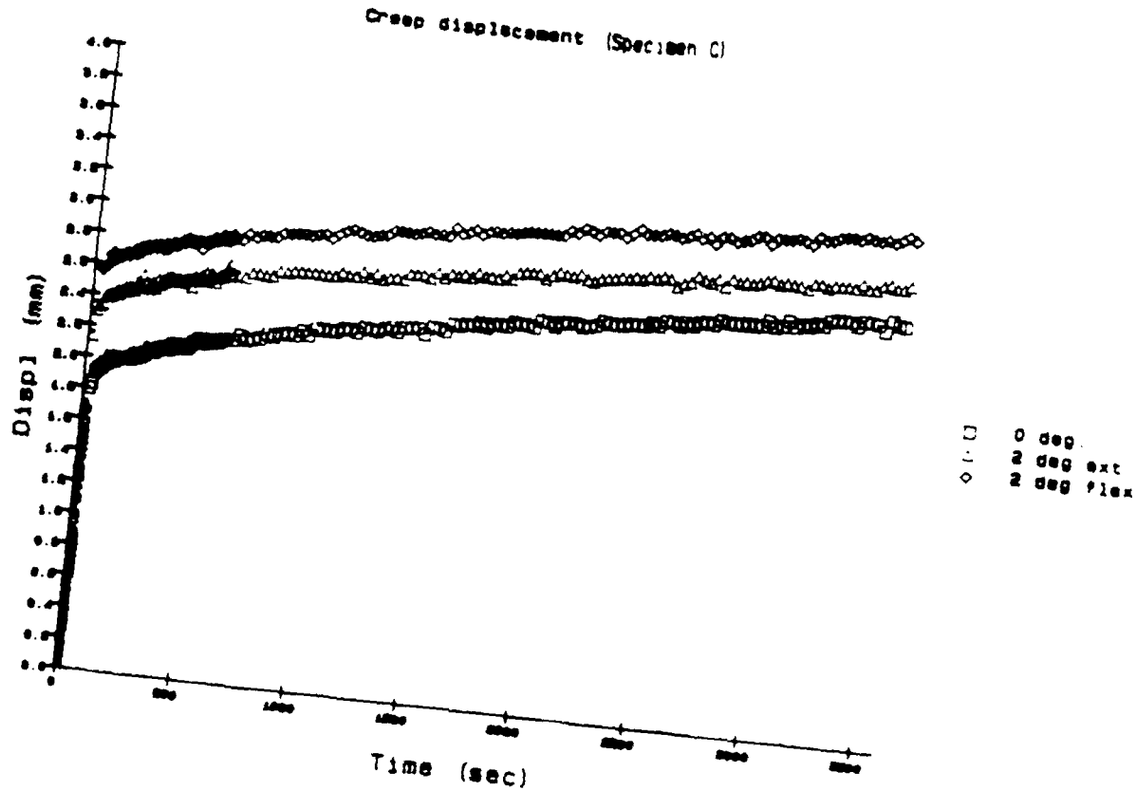

Figure 21.2 Creep displacement of intervertebral joint at three sagittal rotational angle settings.

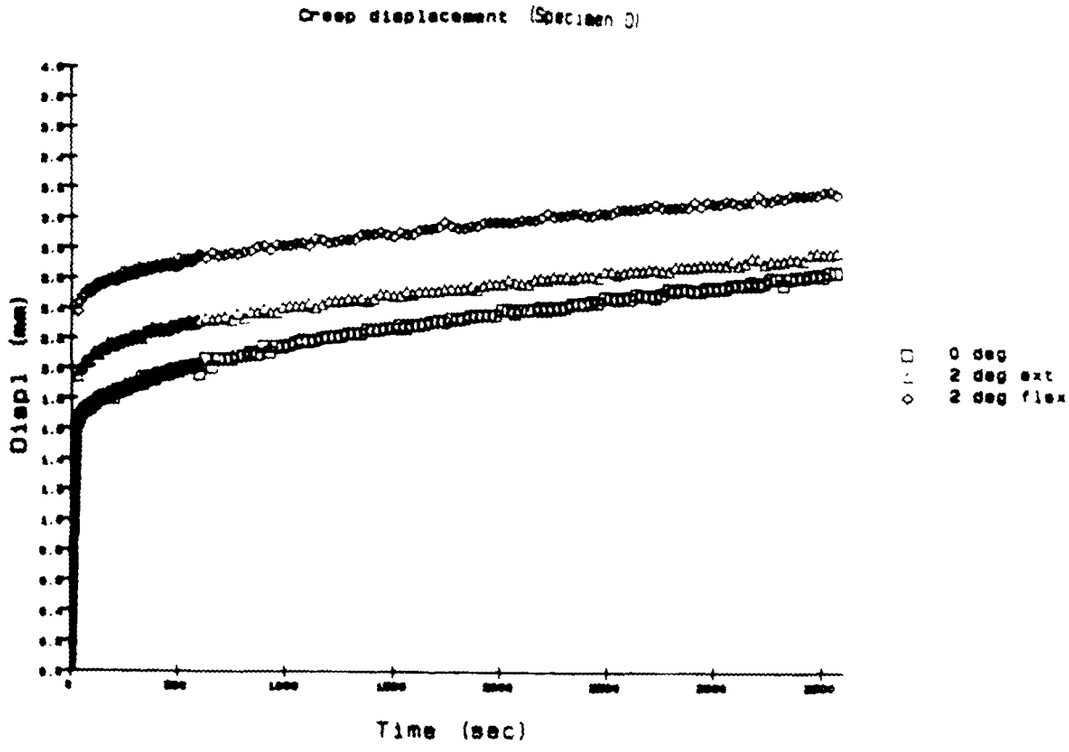

Figure 21.3 Creep displacement of intervertebral joint at three sagittal rotational angle settings.

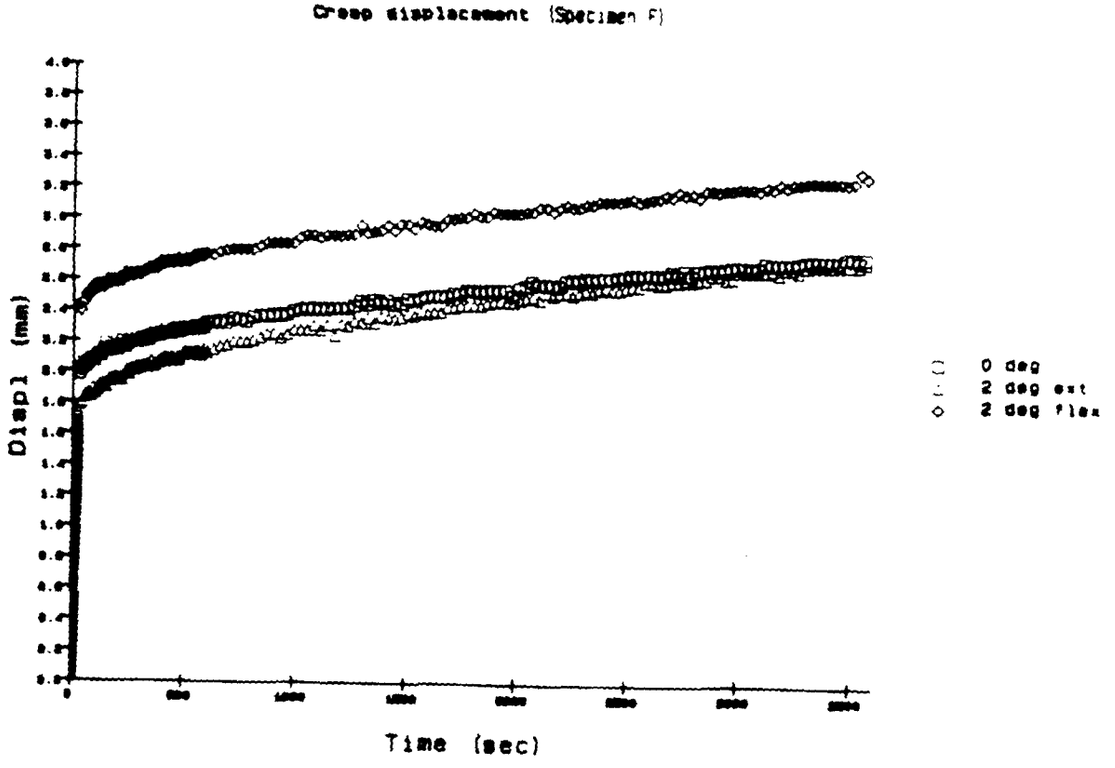

Figure:21.4 Creep displacement of intervertebral joint at three sagittal rotational angle settings.

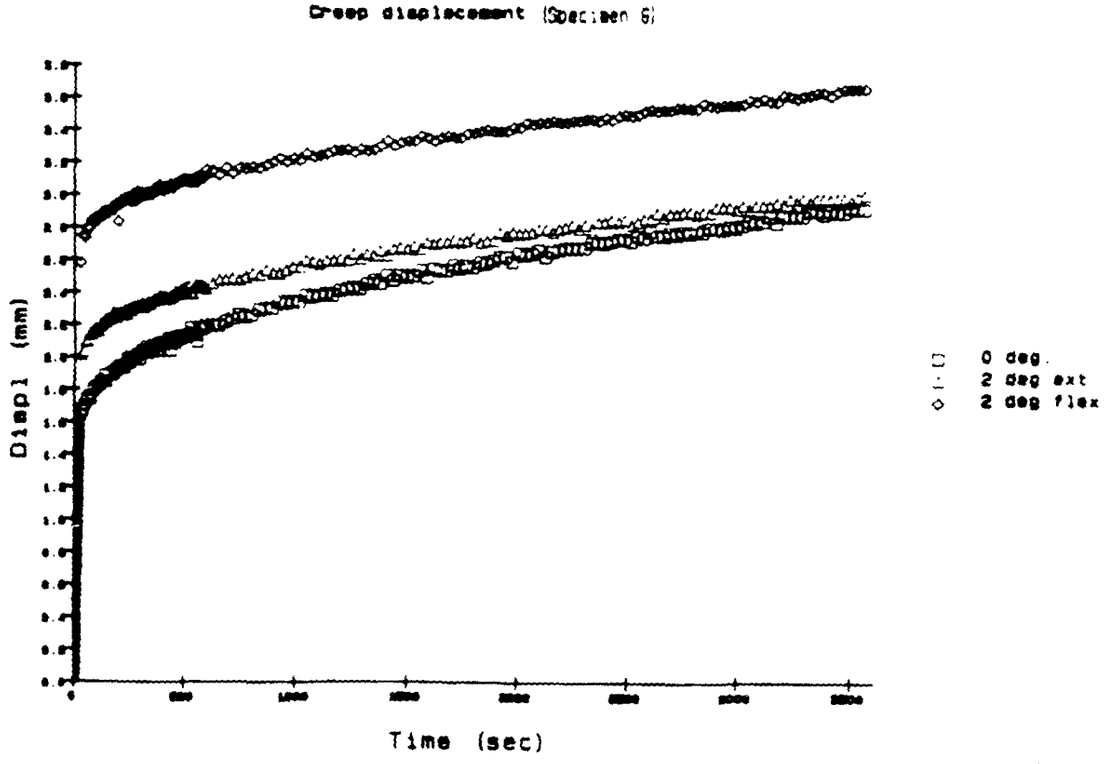

Figure 21.6 Creep displacement of intervertebral joint at three sagittal rotational angle settings.

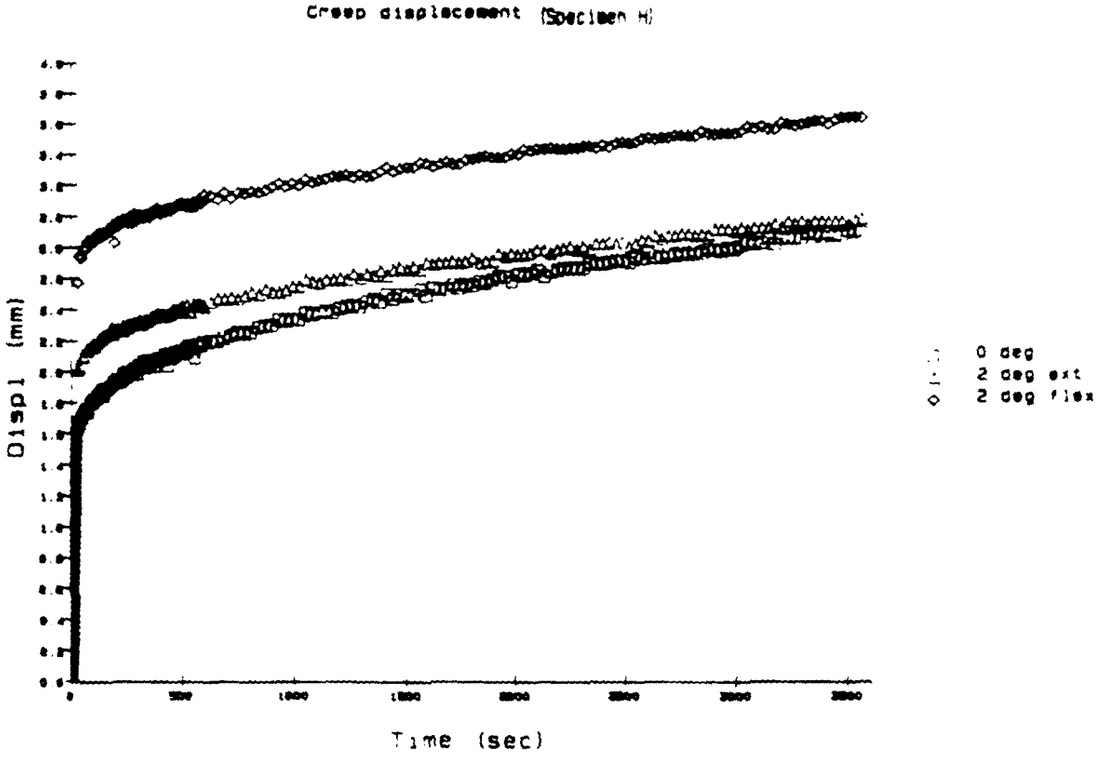

Figure:21.6 Creep displacement of intervertebral joint at three sagittal rotational angle settings.

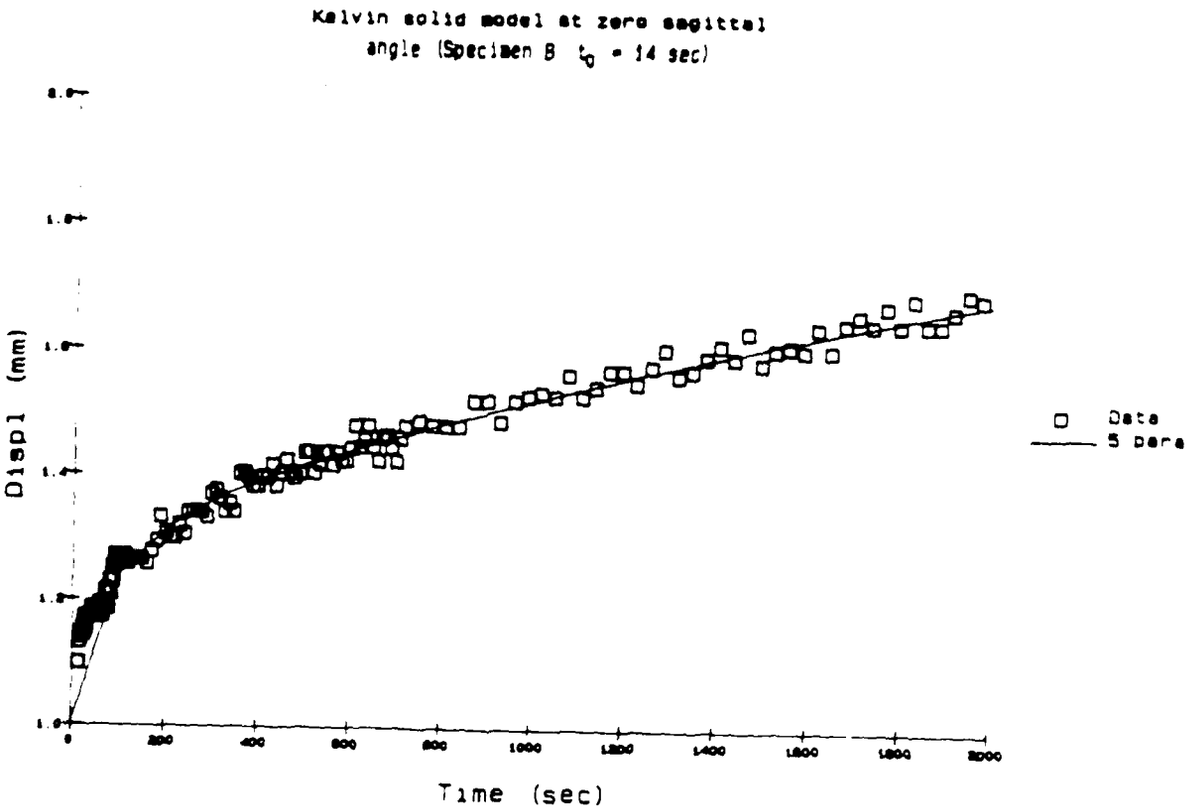

Figure:22.1 Creep displacement response with exponential fit of 5-parameter Kelvin Solid Model in parallel of the intact intervertebral joint. (to:time at initial condition)

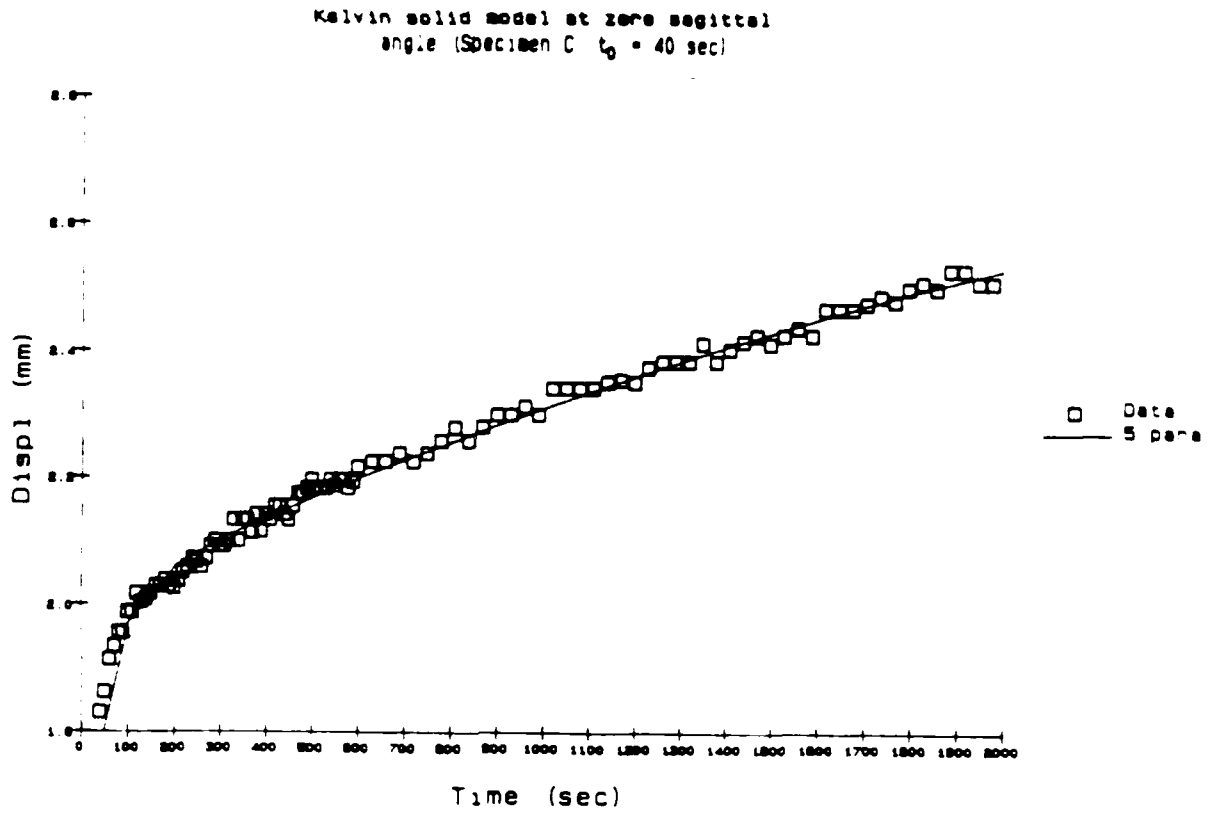

Figure:22.2 Creep displacement response with exponential fit of 5-parameter Kelvin Solid Model in parallel of the intact intervertebral joint. (to:time at initial condition)

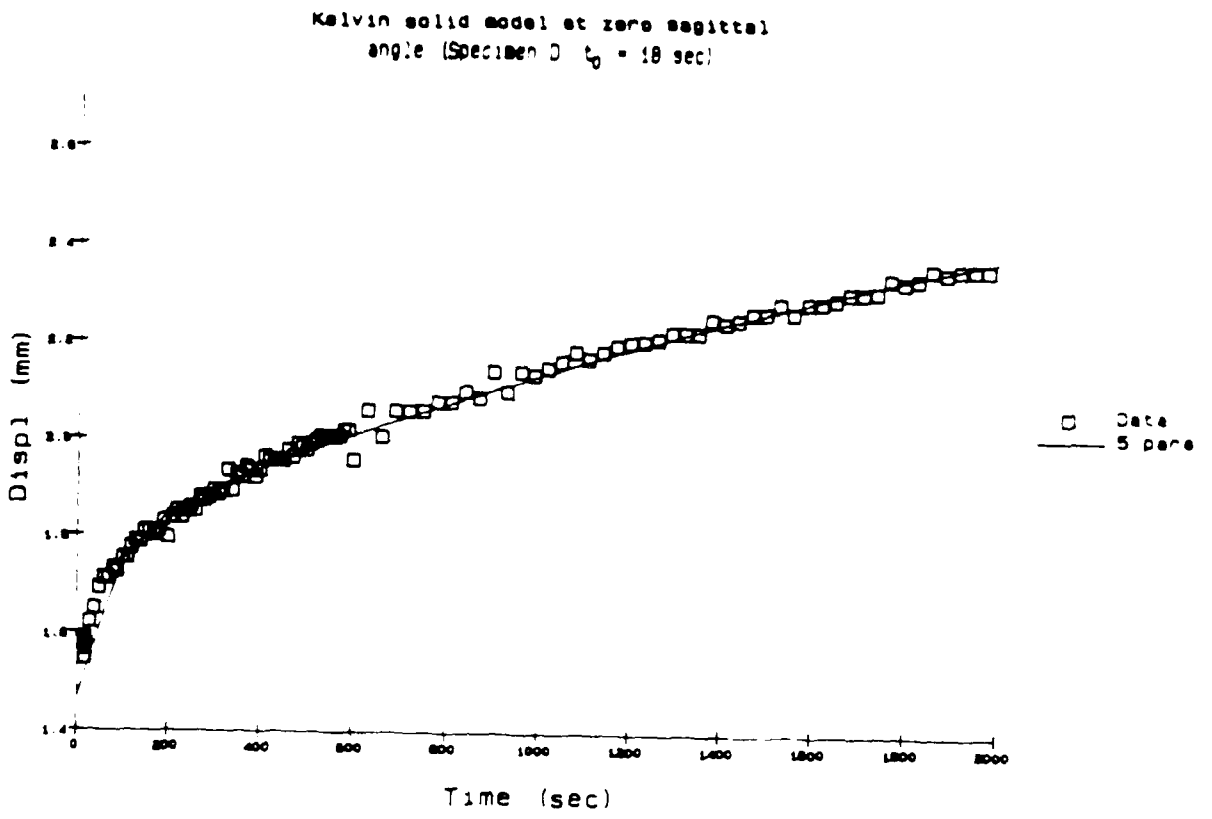

Figure:22.3 Creep displacement response with exponential fit of 5-parameter Kelvin Solid Model in parallel of the intact intervertebral joint. (to:time at initial condition)

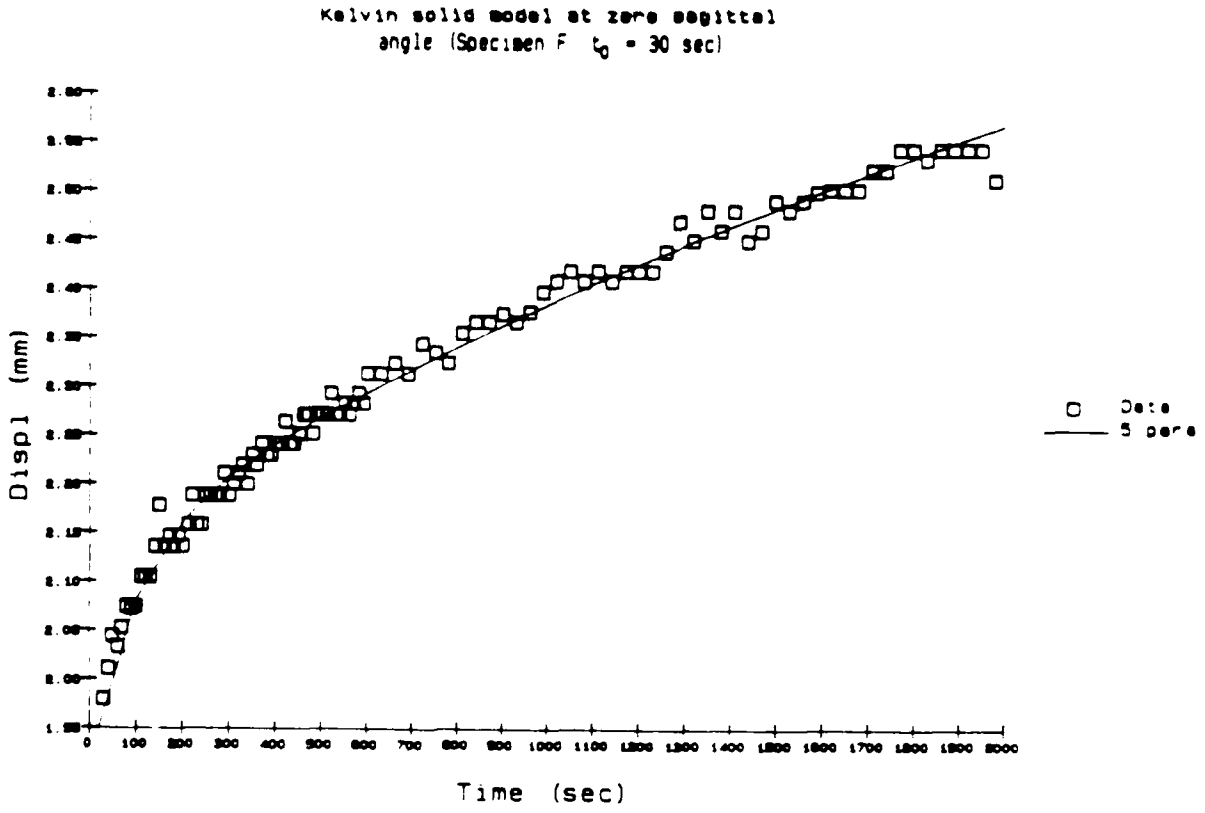

Figure:22.4 Creep displacement response with exponential fit of 5-parameter Kelvin Solid Model in parallel of the intact intervertebral joint. (to:time at initial condition)

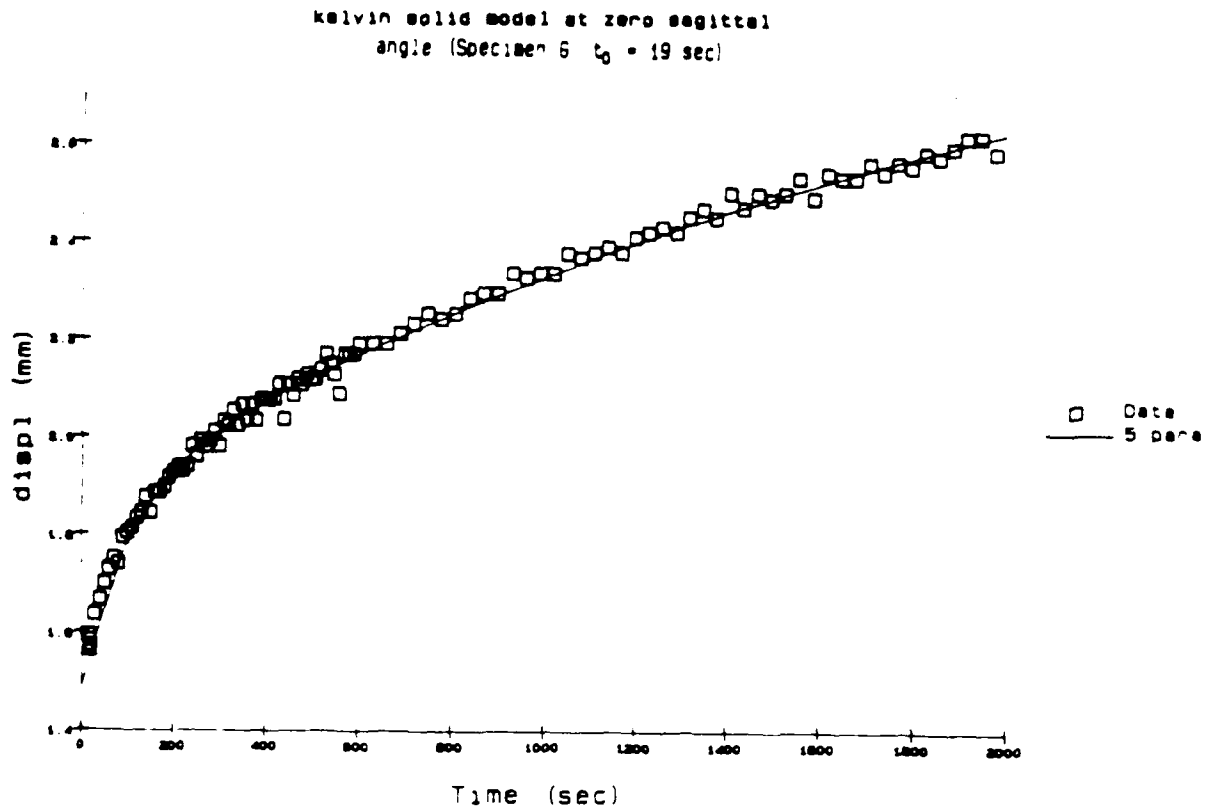

Figure:22.5 Creep displacement response with exponential fit of 5-parameter Kelvin Solid Model in parallel of the intact intervertebral joint. (to:time at initial condition)

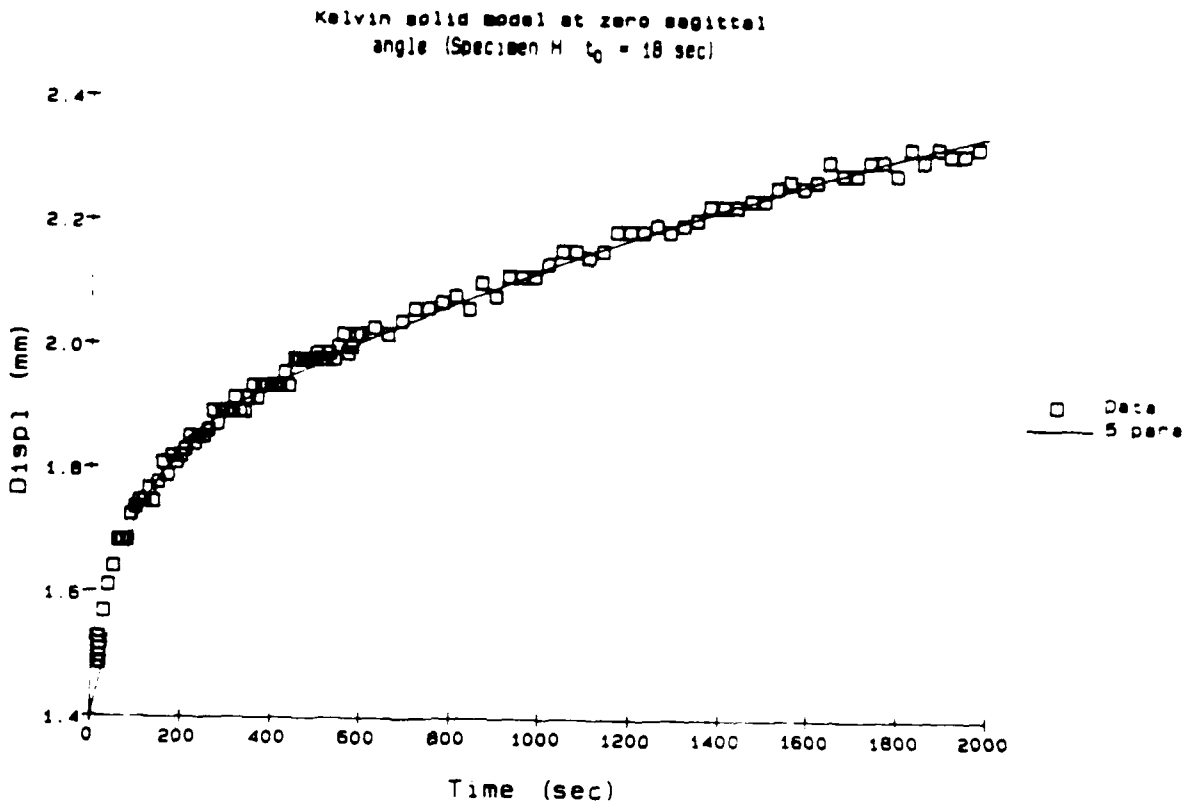

Figure:22.6 Creep displacement response with exponential fit of 5-parameter Kelvin Solid Model in parallel of the intact intervertebral joint. (to:time at initial condition)

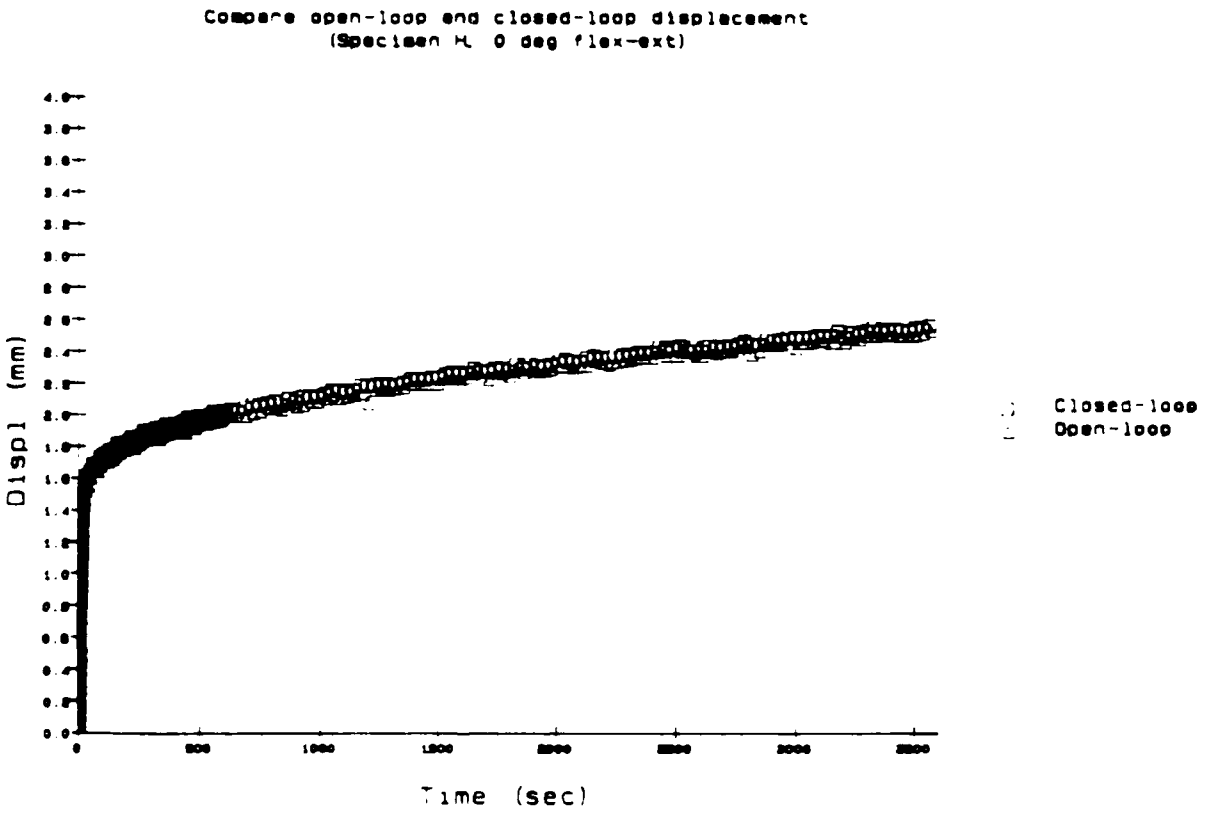

Figure:23 Repeatability of displacement between closed-loop and open-loop tests.

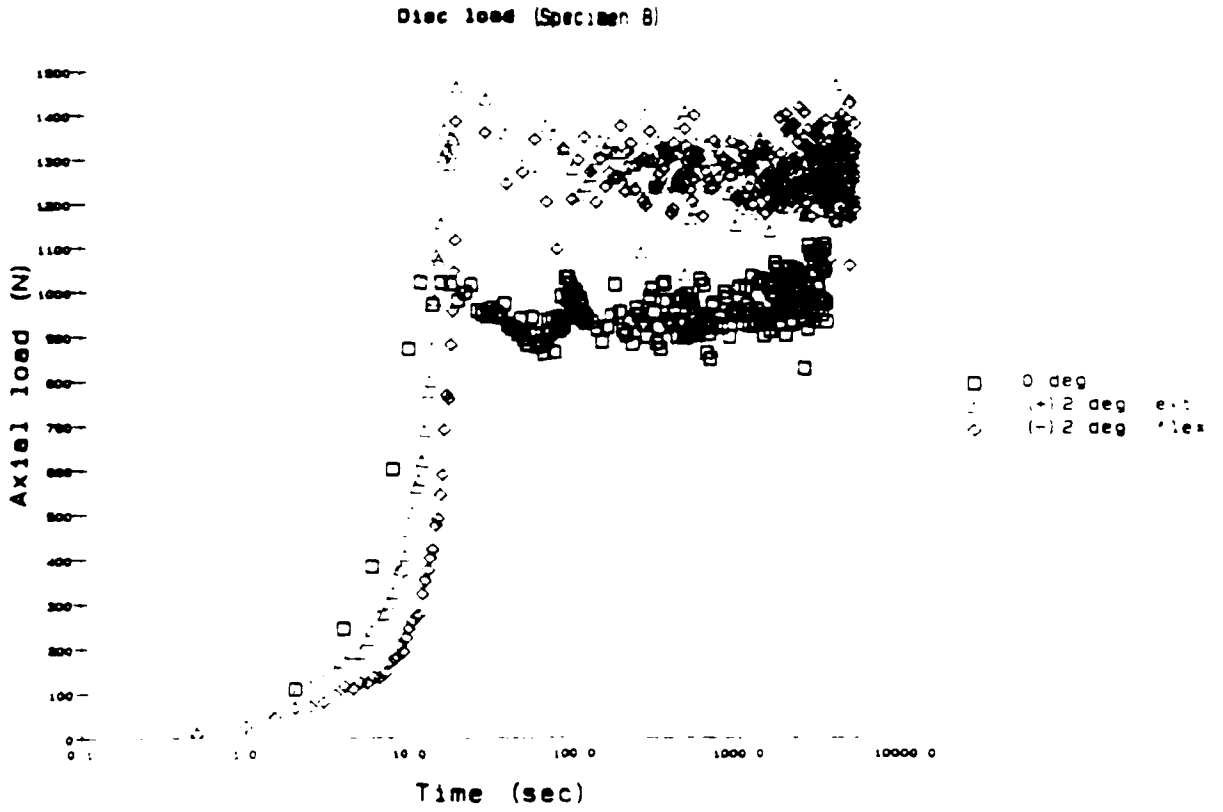

Figure:24.1 Load supported by the intervertebral joint at three sagittal rotational angle settings.

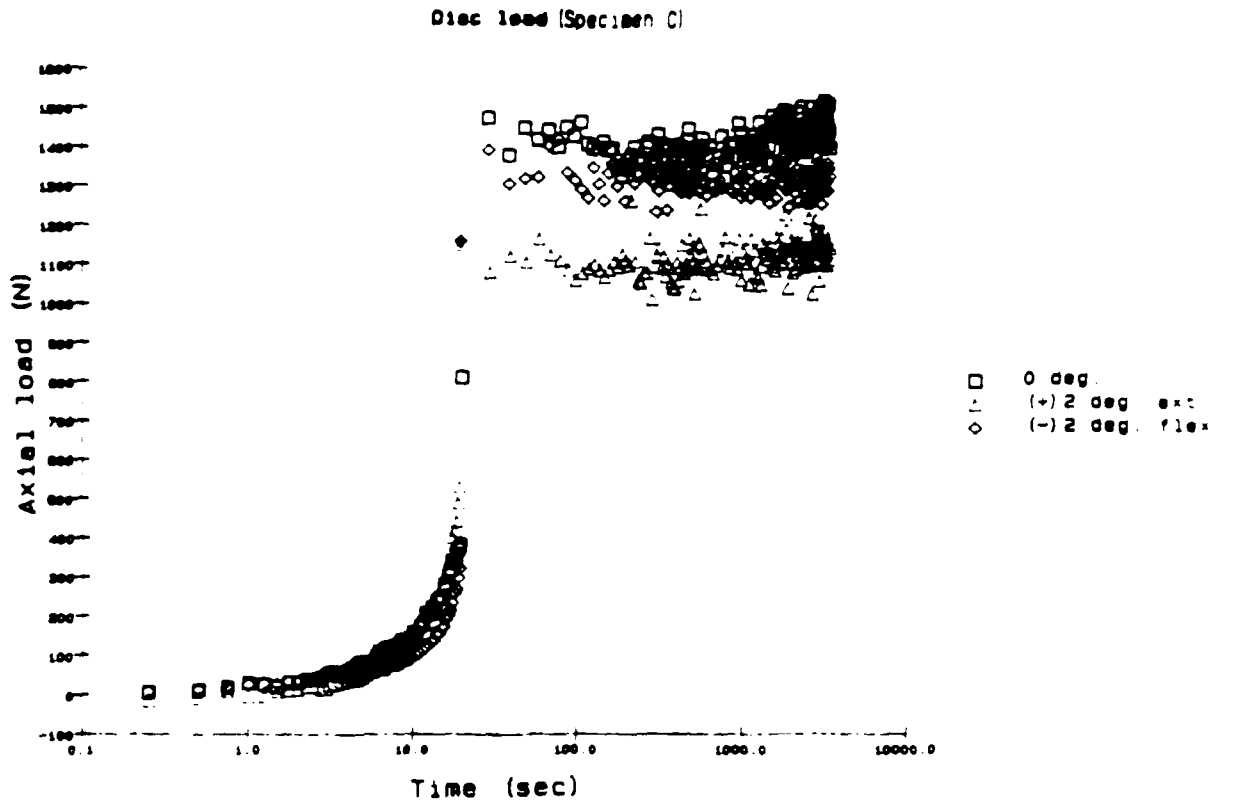

Figure:24.2 Load supported by the intervertebral joint at three sagittal rotational angle settings.

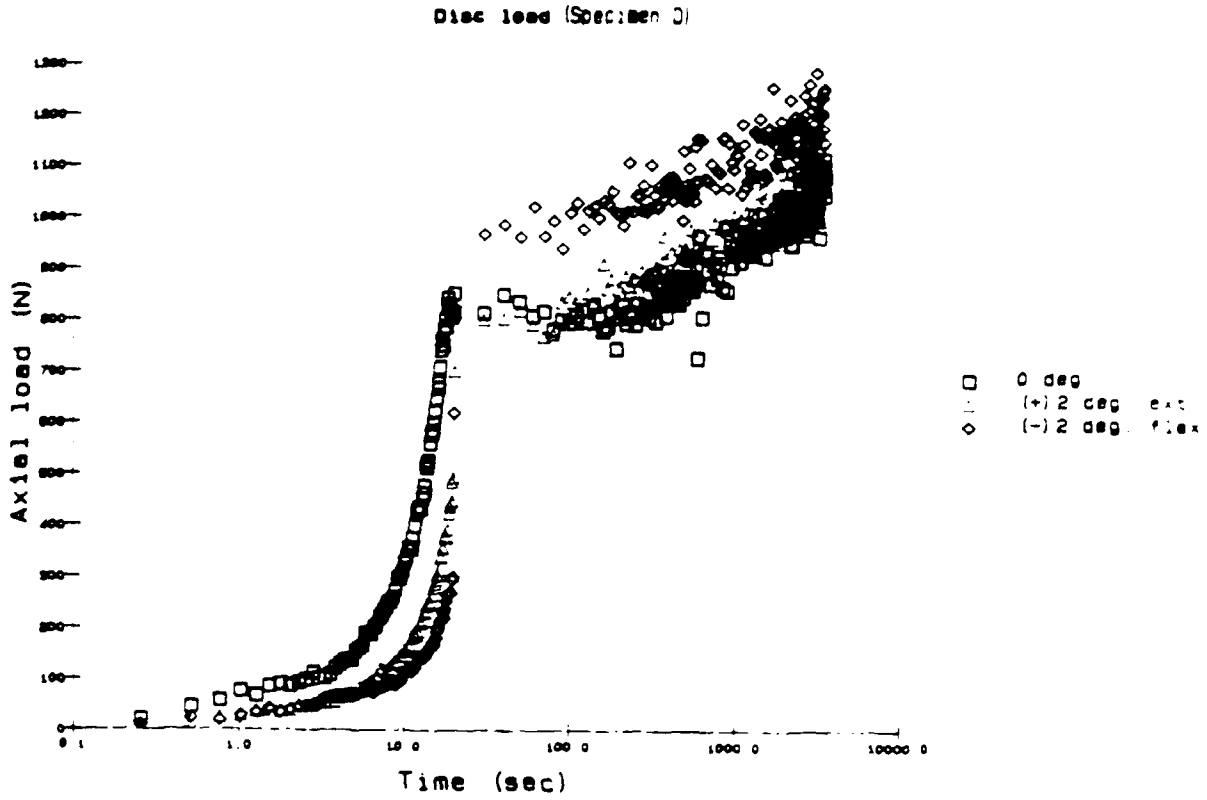

Figure:24.3 Load supported by the intervertebral joint at three sagittal rotational angle settings.

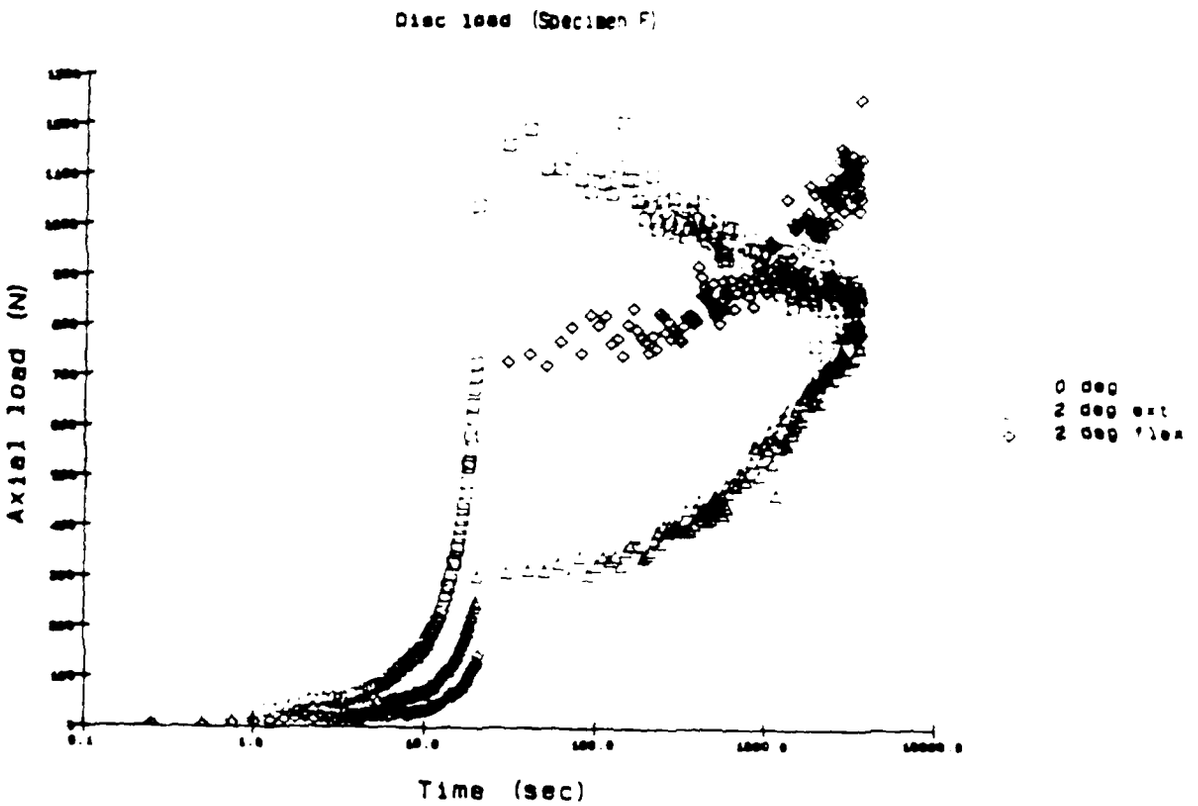

Figure 24.4 Load supported by the intervertebral joint at three sagittal rotational angle settings.

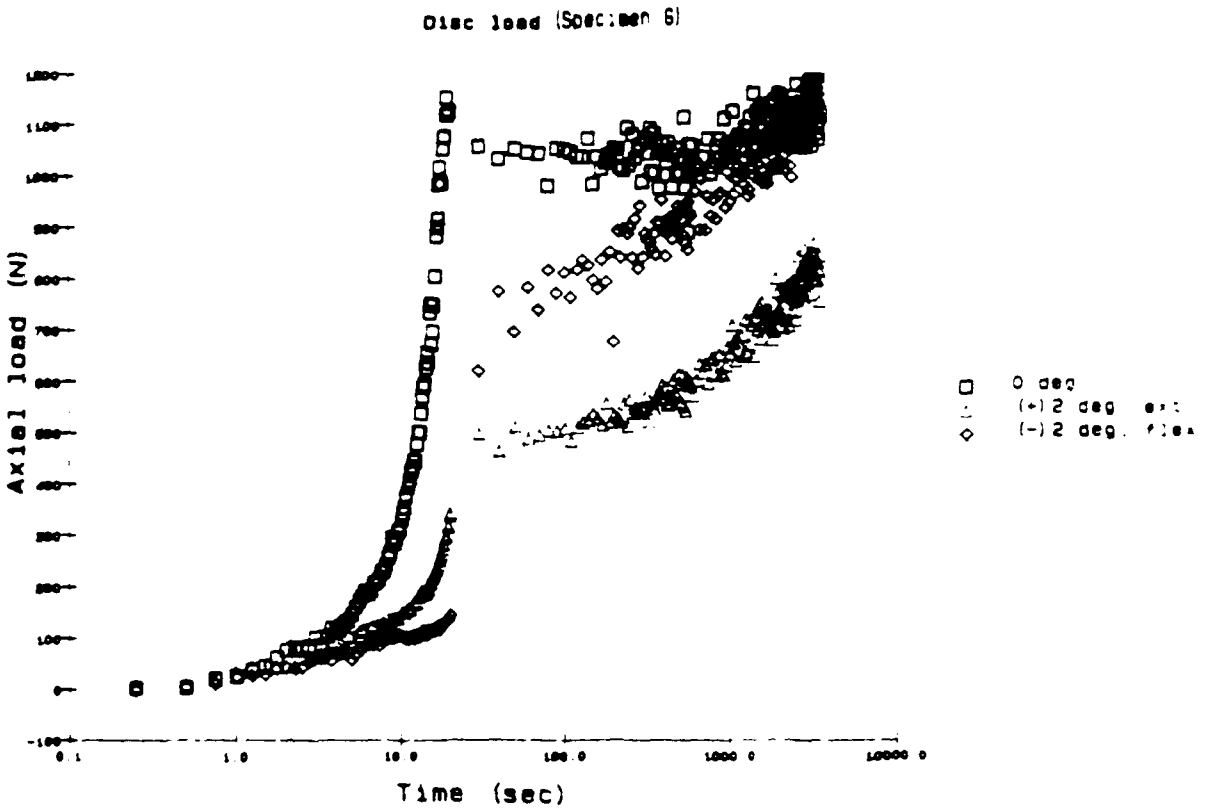

Figure:24.5 Load supported by the intervertebral joint at three sagittal rotational angle settings.

AD-A170 002 FRACTURE AND VISCOELASTIC CHARACTERISTICS OF THE HUMAN CERVICAL SPINE(U) BETH ISRAEL HOSPITAL BOTTON MASS W T EDWARDS ET AL 1986 AFOSR-TR-86-0453 2/3

UNCLASSIFIED F49620-81-K-0010 F/G 6/16 NL

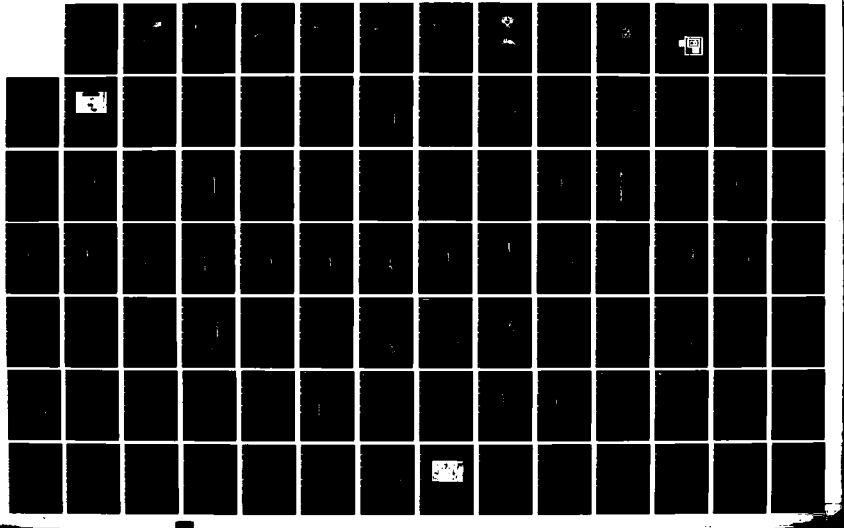

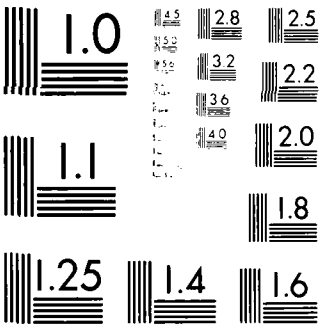

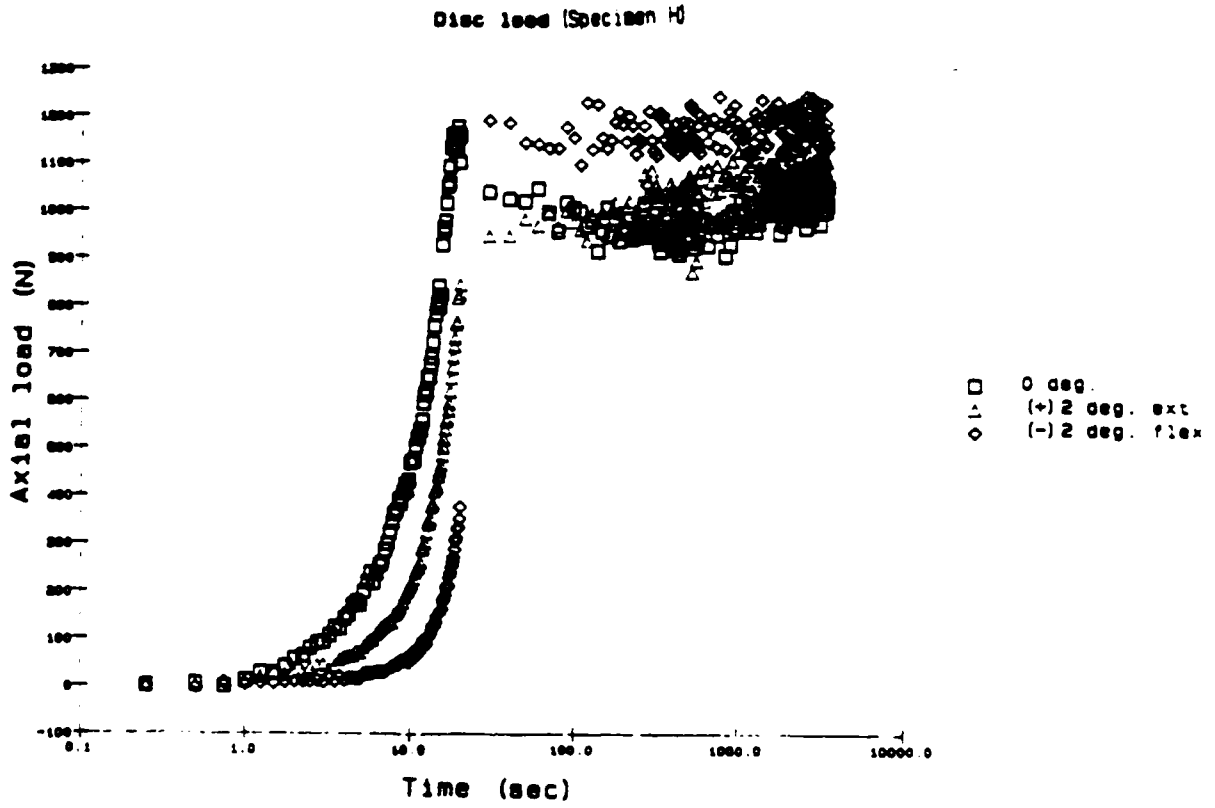

Figure:24.6 Load supported by the intervertebral joint at three sagittal rotational angle settings.

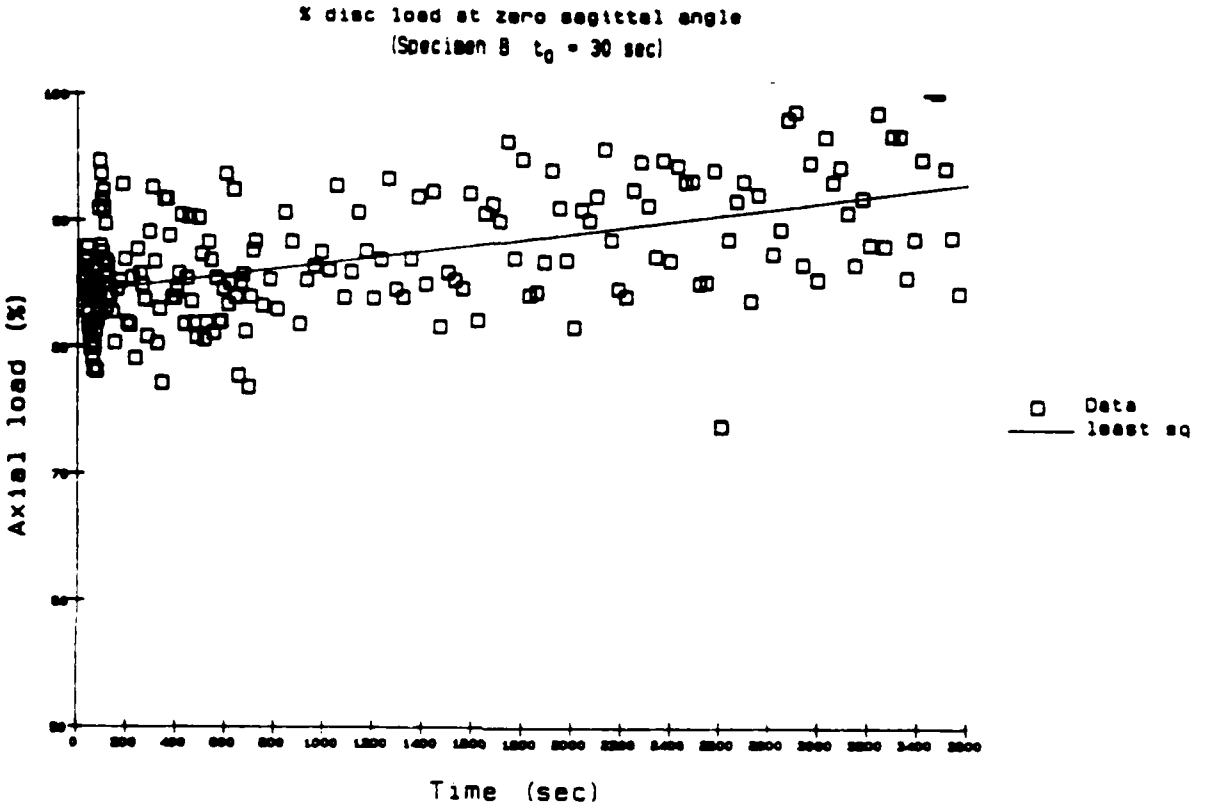

Figure:25.1 Axial load supported by the intervertebral disc.
(to:time at initial condition)

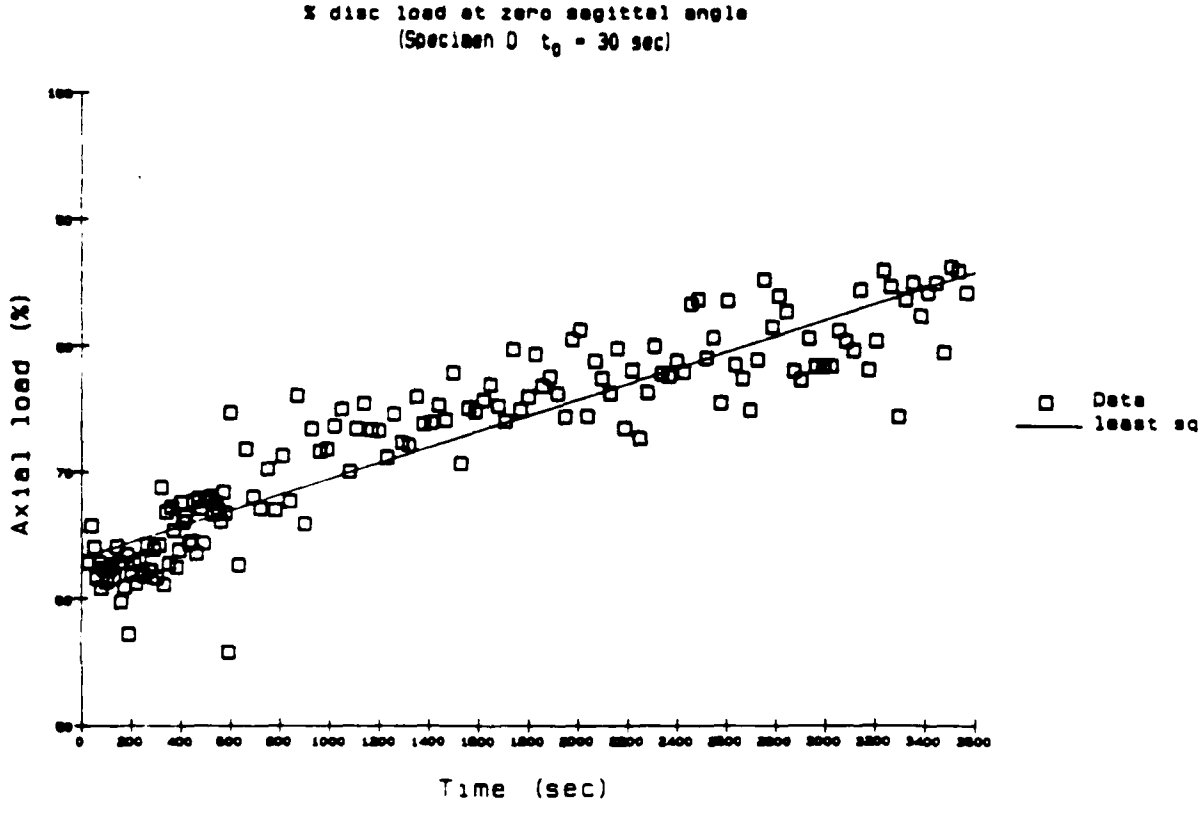

Figure:25.2 Axial load supported by the intervertebral disc.
(to: time at initial condition)

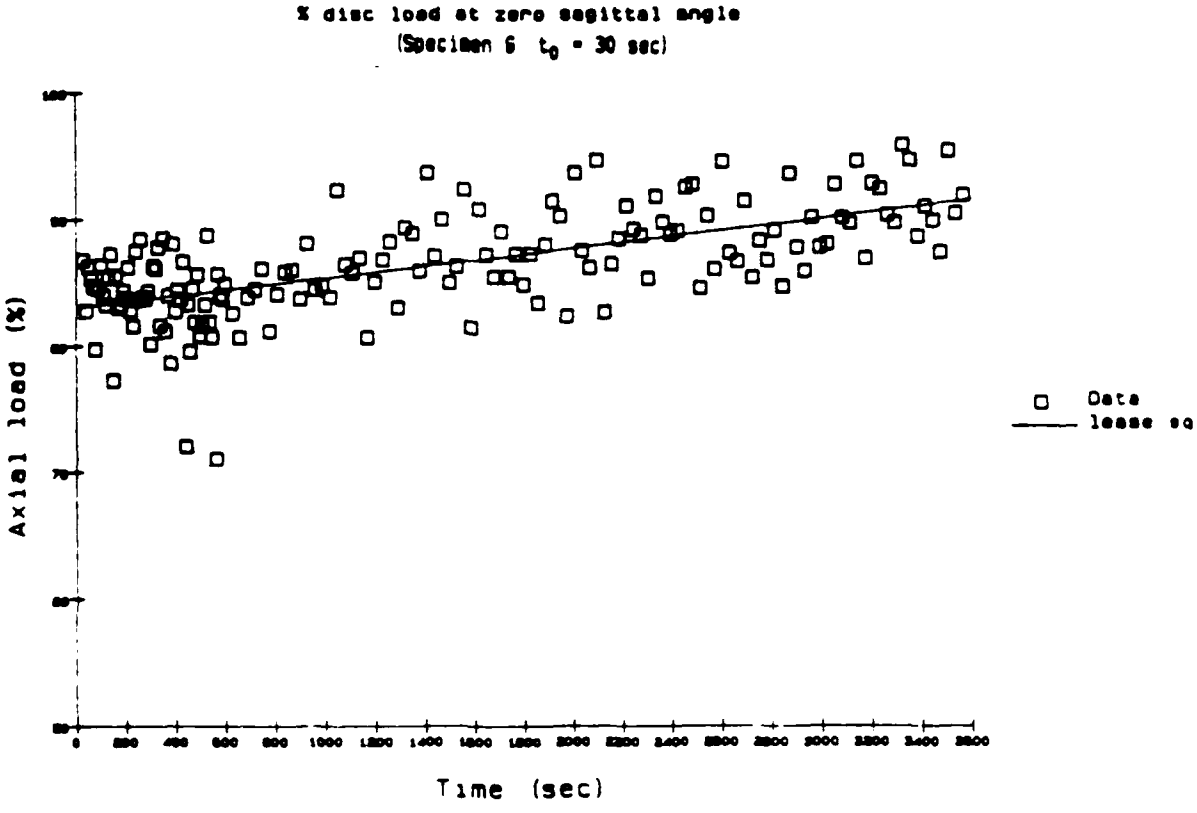

Figure:25.3 Axial load supported by the intervertebral disc.
(to: time at initial condition)

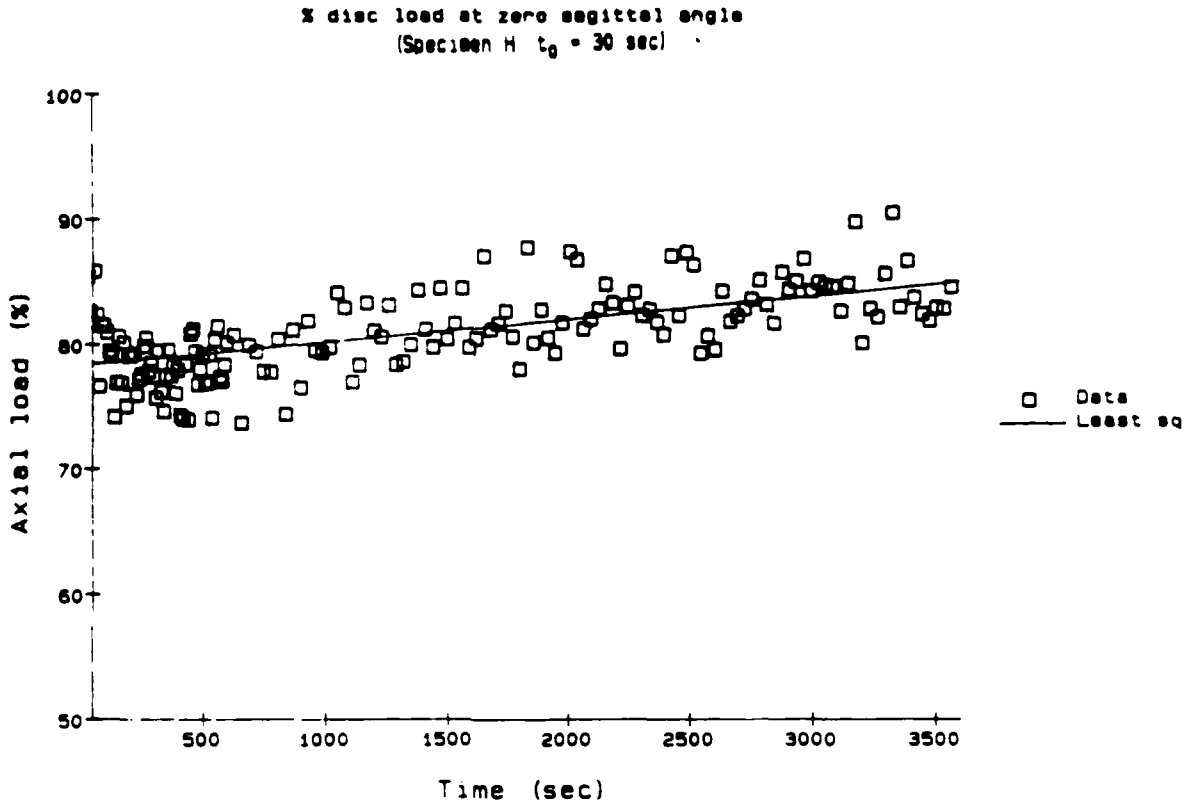

Figure:25.4 Axial load supported by the intervertebral disc.
(to: time at initial condition)

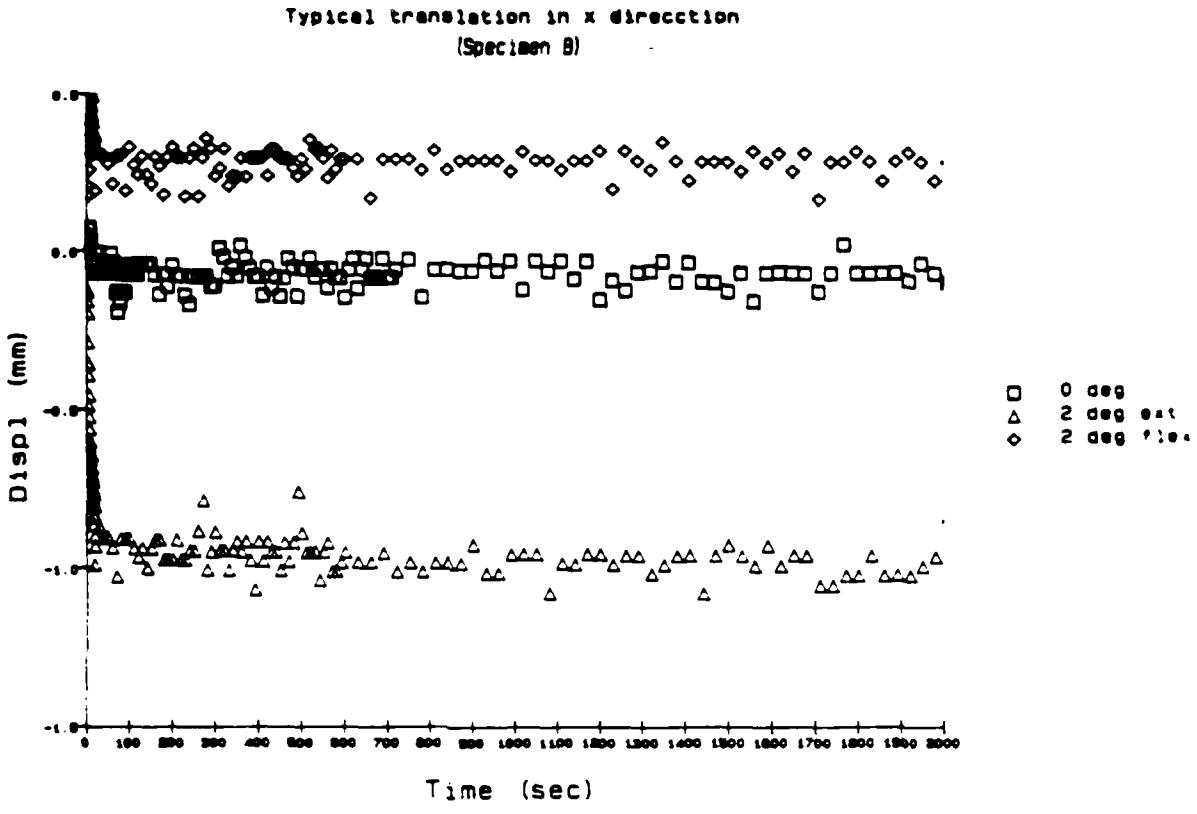

Figure:26 Typical anterior-posterior translation.

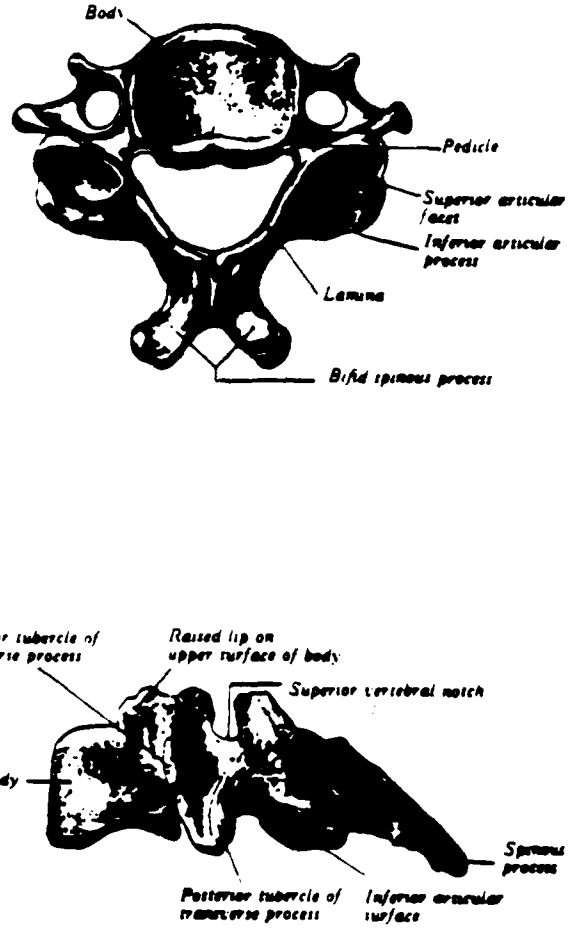

Figure:27 A typical cervical vertebra (modified from Gray's Anatomy)

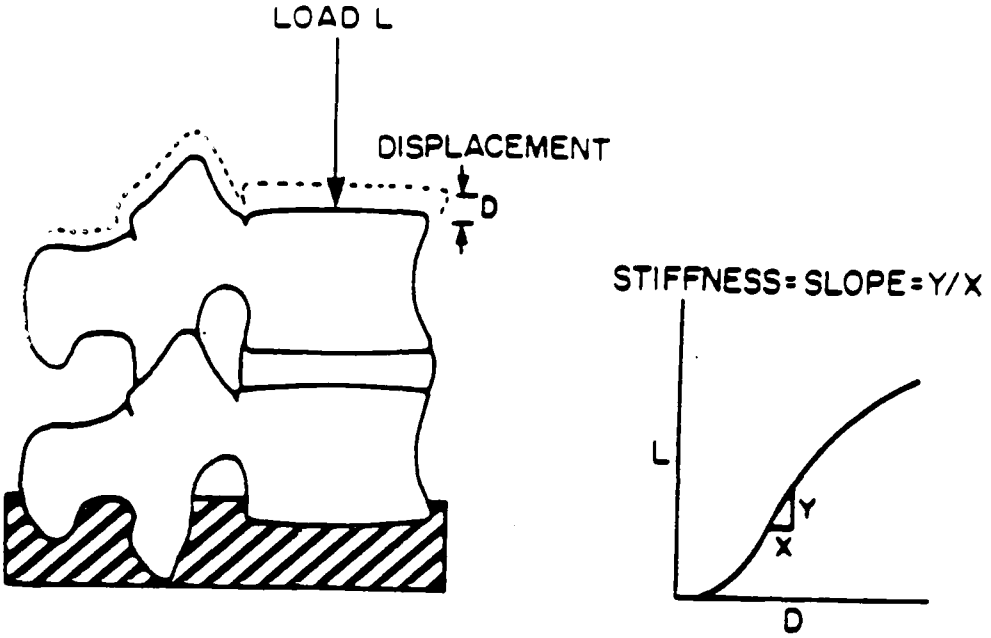

Figure 28 Load-deflection behavior of a functional spinal unit (modified from White and Panjabi, 1978)

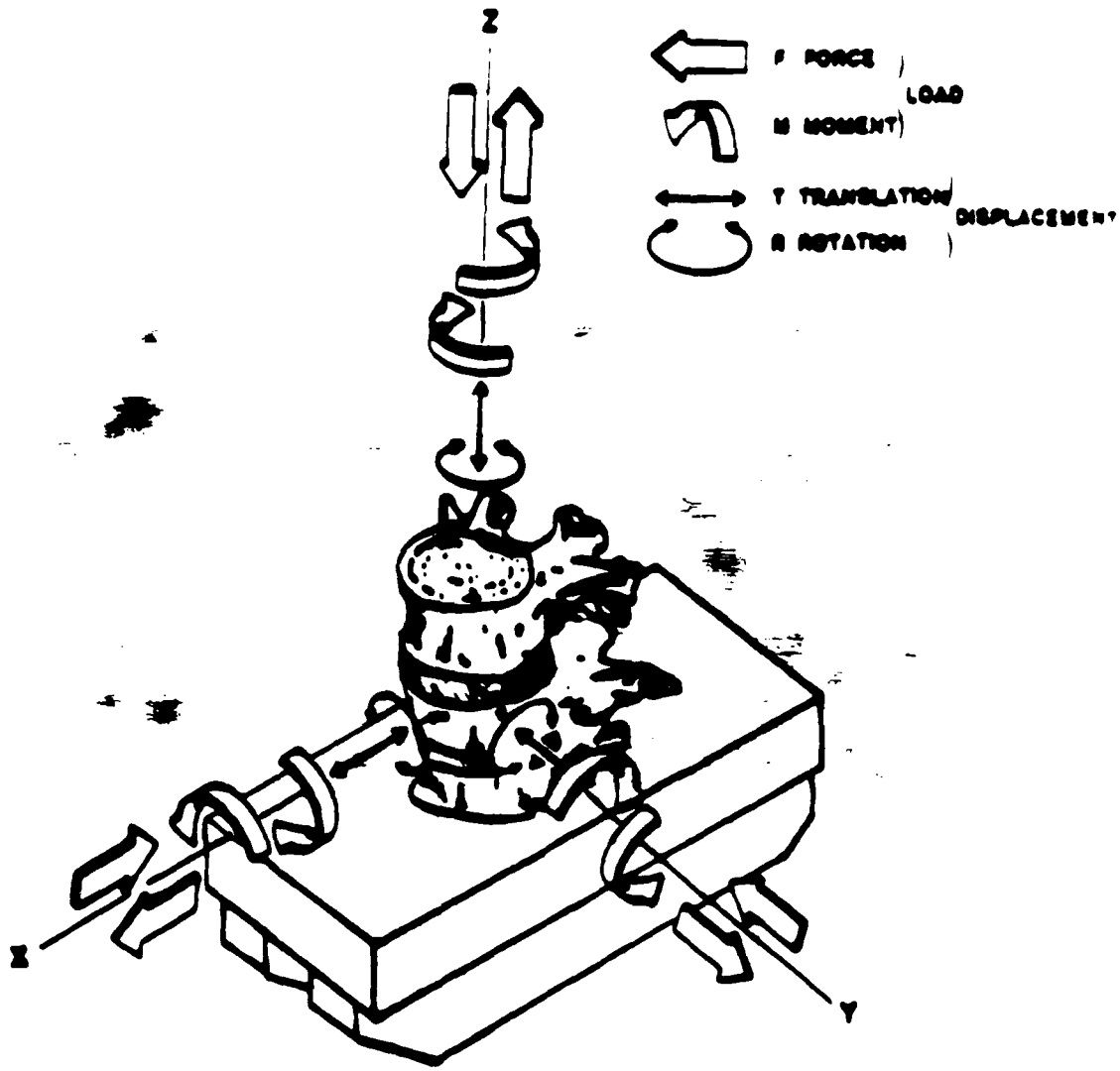

Figure:29 **Three dimensional coordinate system for the Punctional Vertebral Segment. The test stage coordinate system has it's origin at the top surface and center of the stage with axes positive in the same direction as the coordinates shown in the figure.**

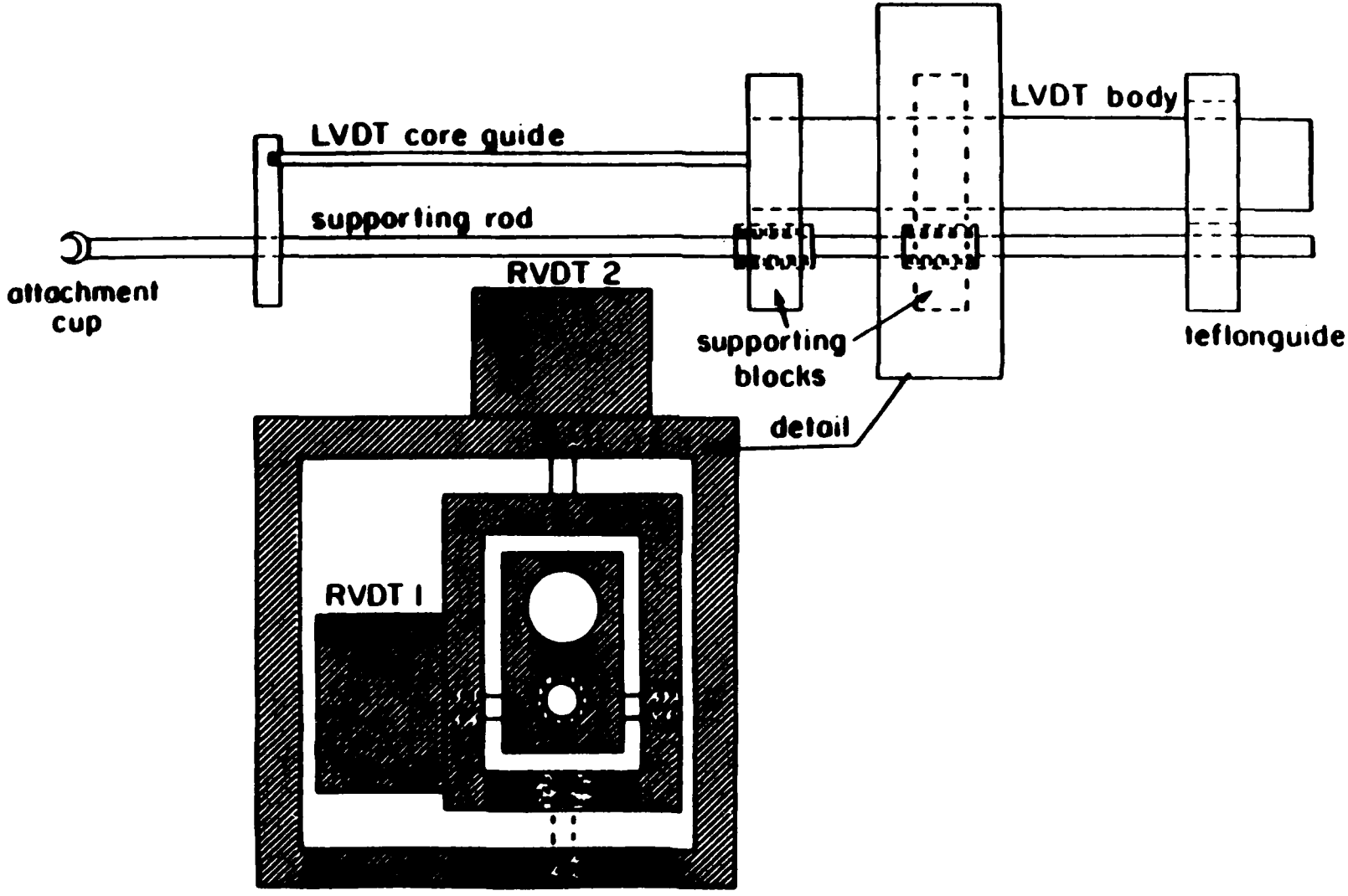

Figure:30 A transducer group consisting of one LVDT and two RVDT's and supporting structure

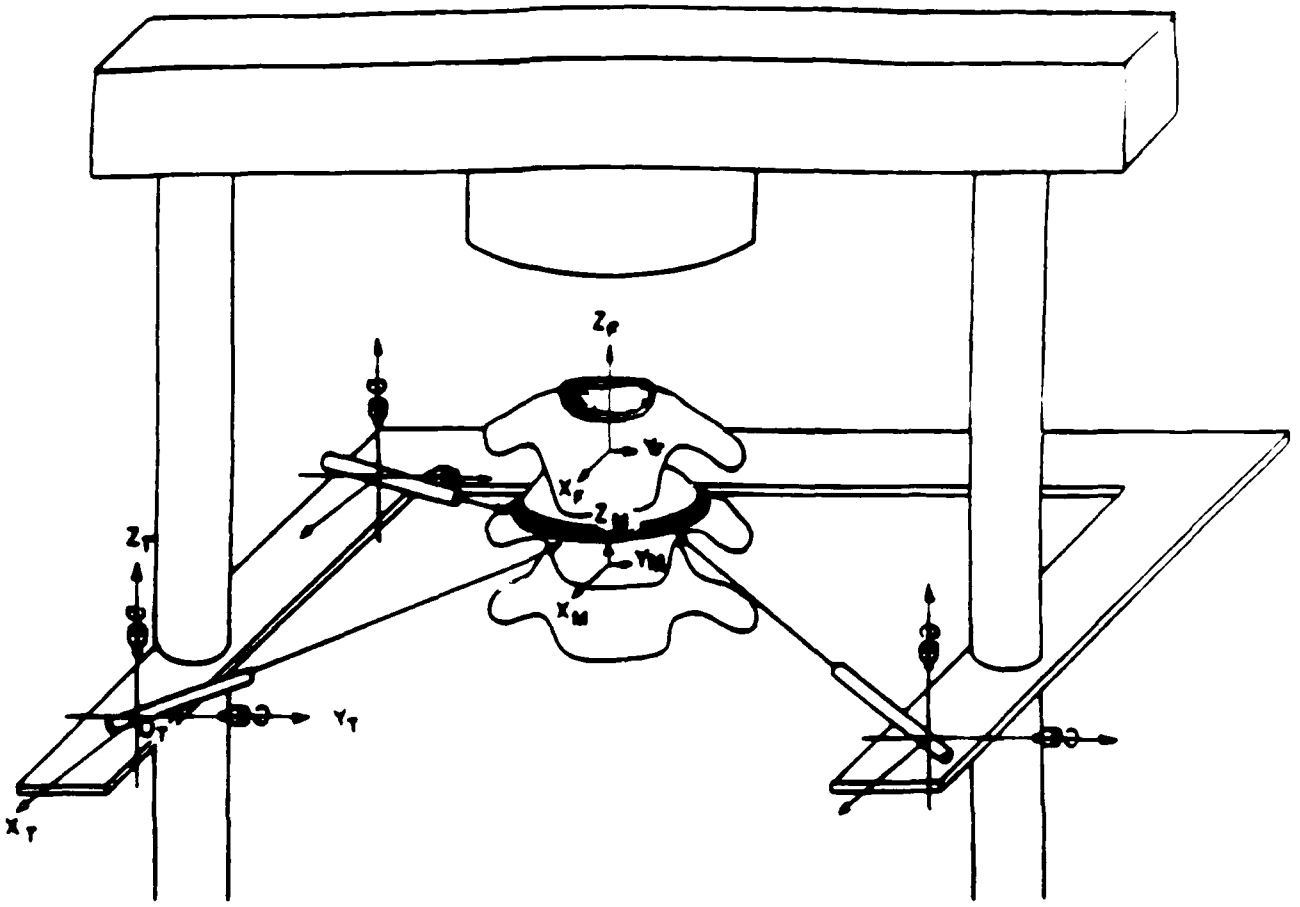

Figure:31 **Reference axes and transducer group orientation for measurement of the displacement of the moving vertebra with respect to the fixed verebra. O_T=origin of transducer group, O_M=origin of moving vertebra, O_F=origin of fixed vertebra**

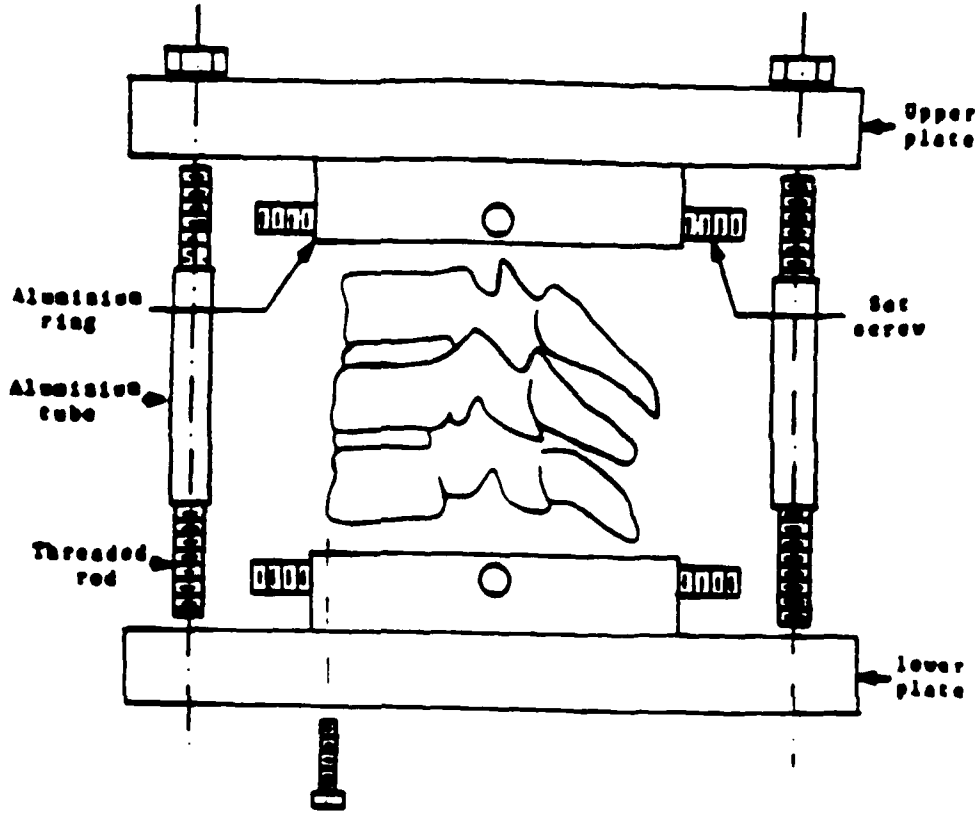

Figure:32 Test Fixture (modified from Kou, 1985)

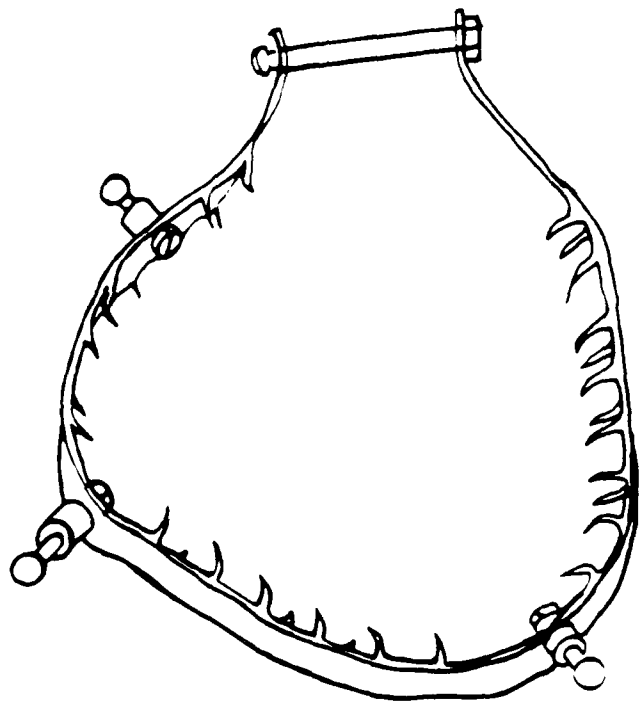

Figure:33 Specimen collar for transducer attachment

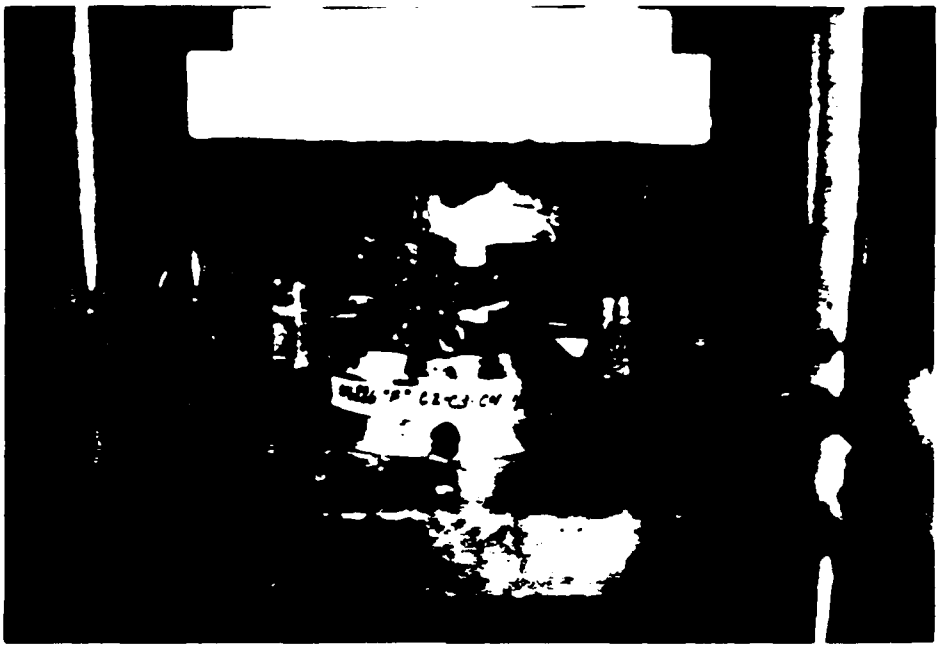

Figure:34 Test specimen, with displacement collar, on PTA

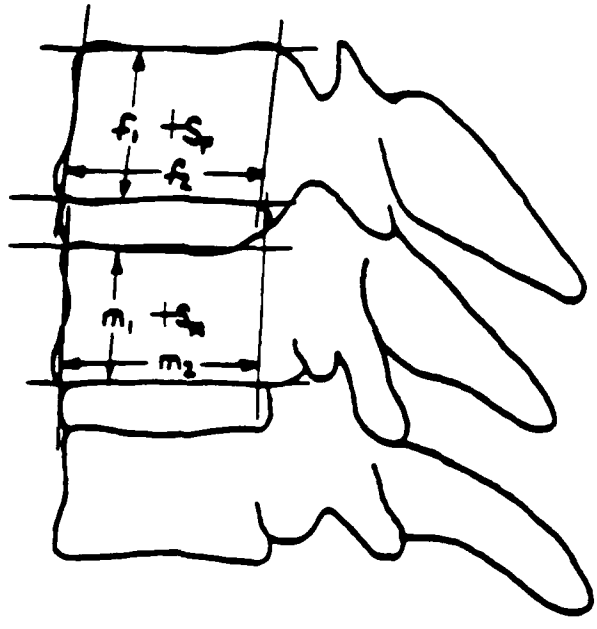

Figure:35 Geometrical parameters of the Functional Vertebral Segment

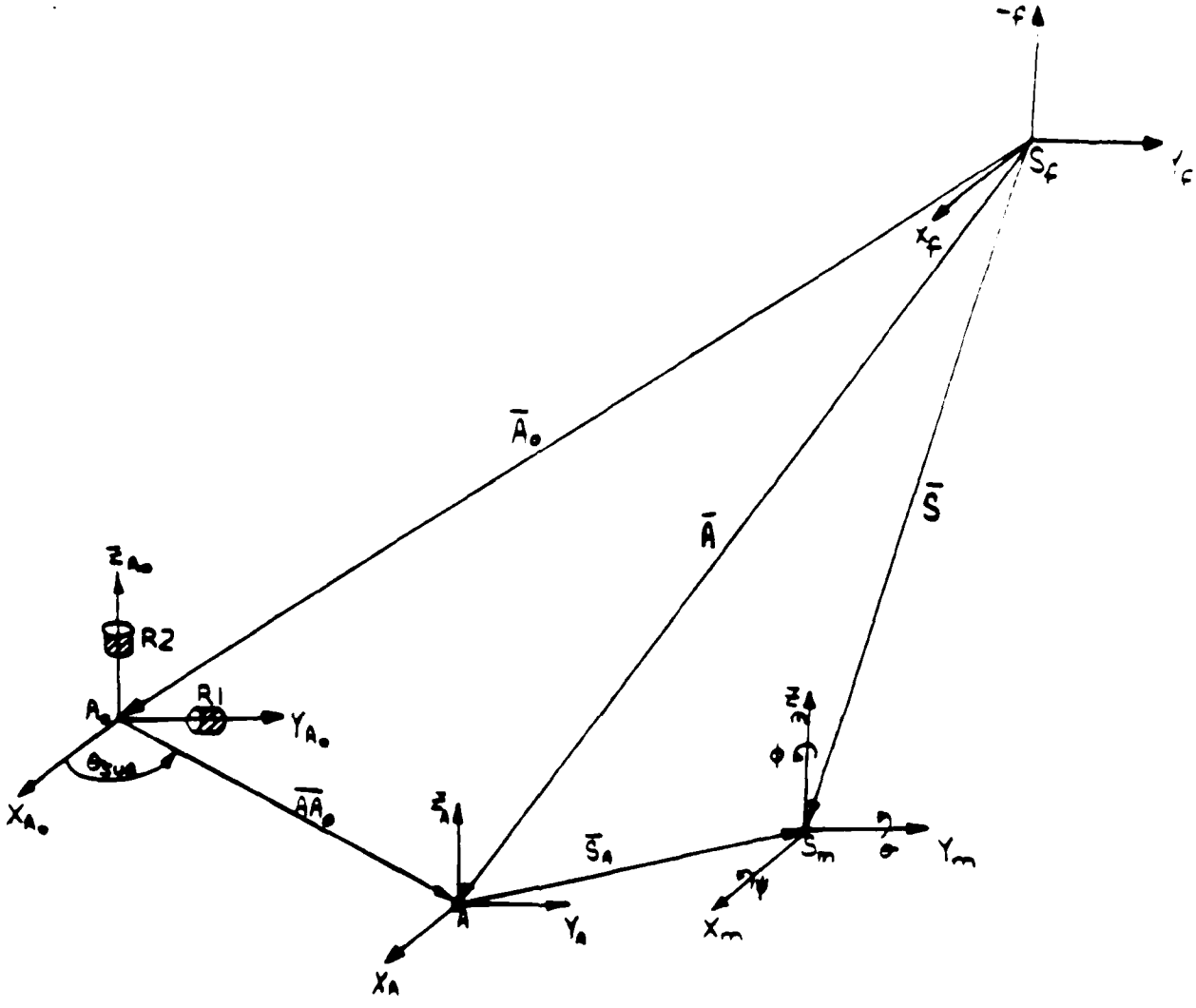

Figure:36 **Relationships between the transducer groups origin, A_o, the center of the fixed body, S_f, the center of the moving body, S_m, and a point on the specimen collar, A.**

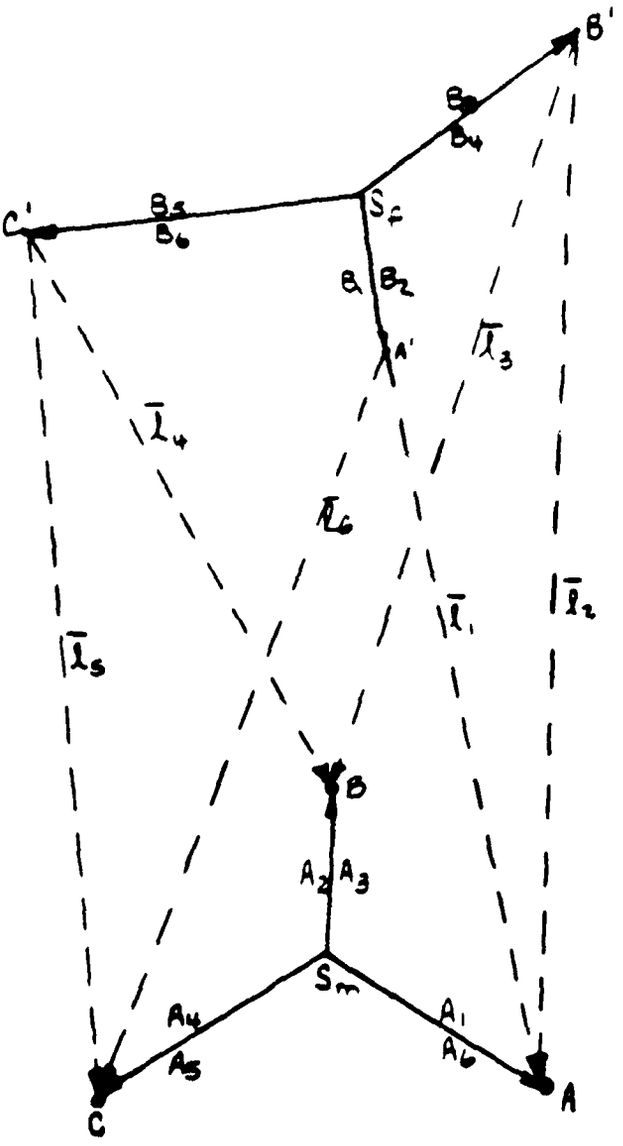

Figure:37 **The position vectors from the center of the moving body, S_m, to the three balls, A, B, and C, and from the center of the fixed body, S_f, to the points A', B', and C'.**

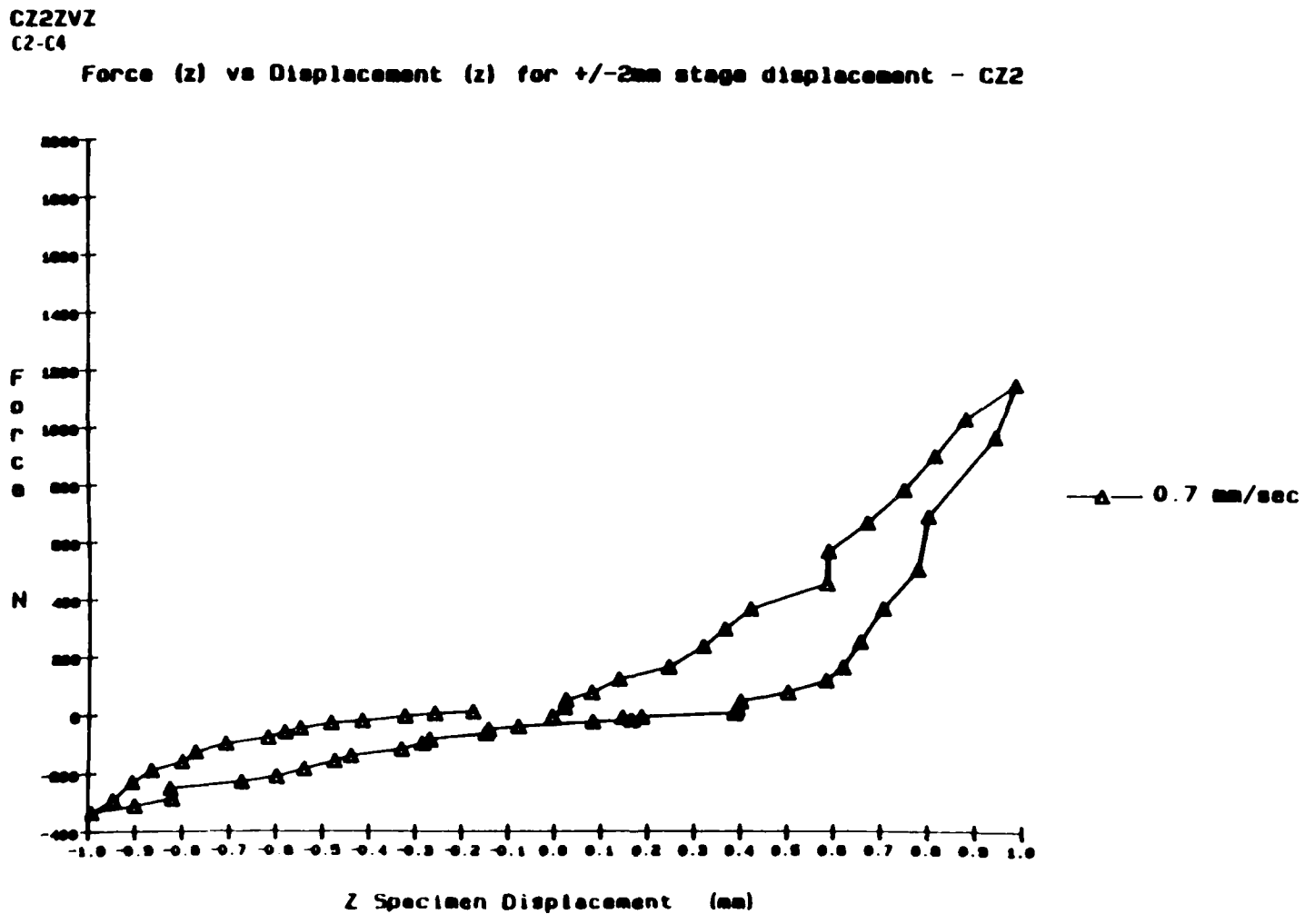

Figures:38.1-38.7 Force (z) vs displacement (z) for 7 specimens

38.1 Specimen C

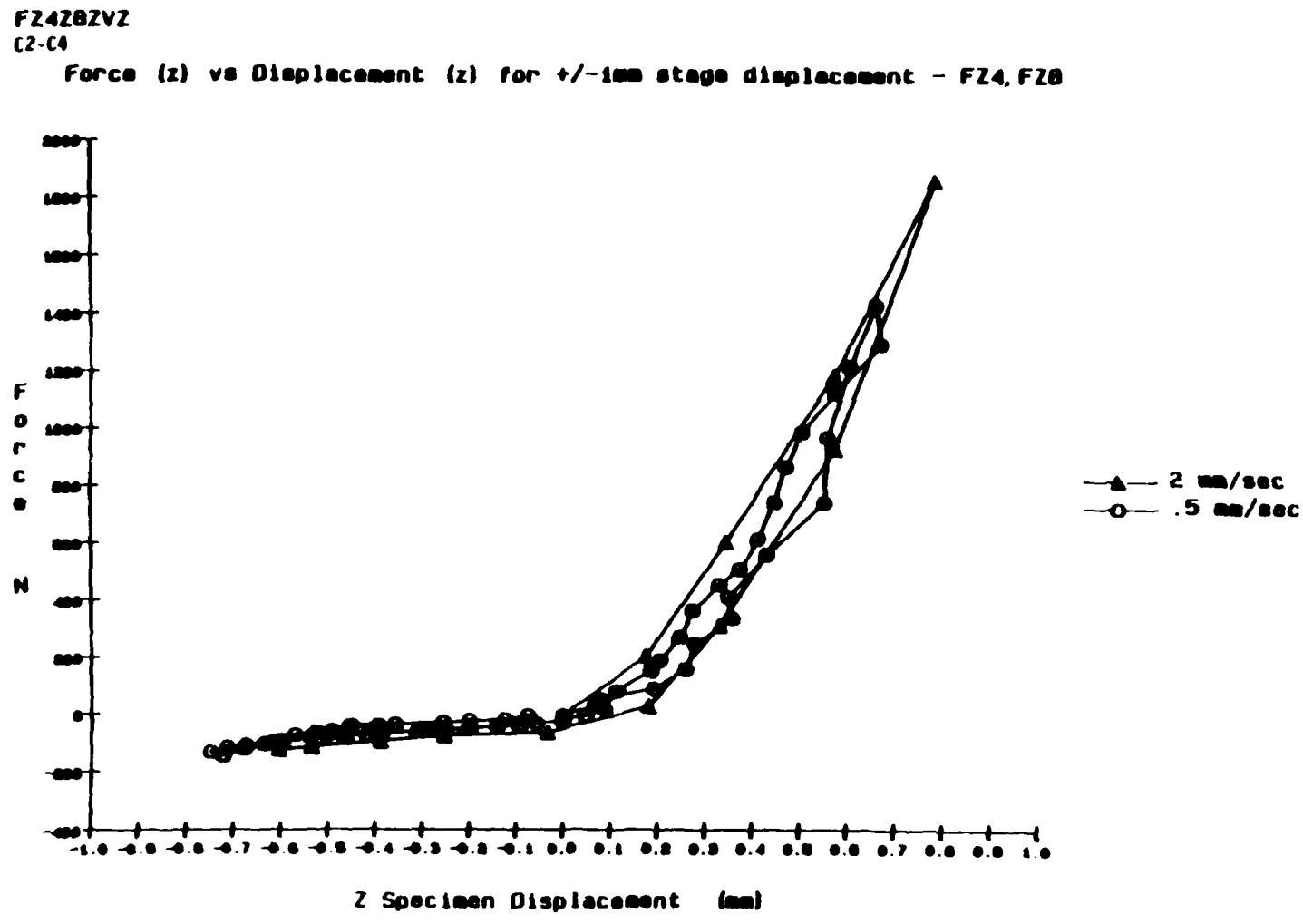

38.2 Specimen F

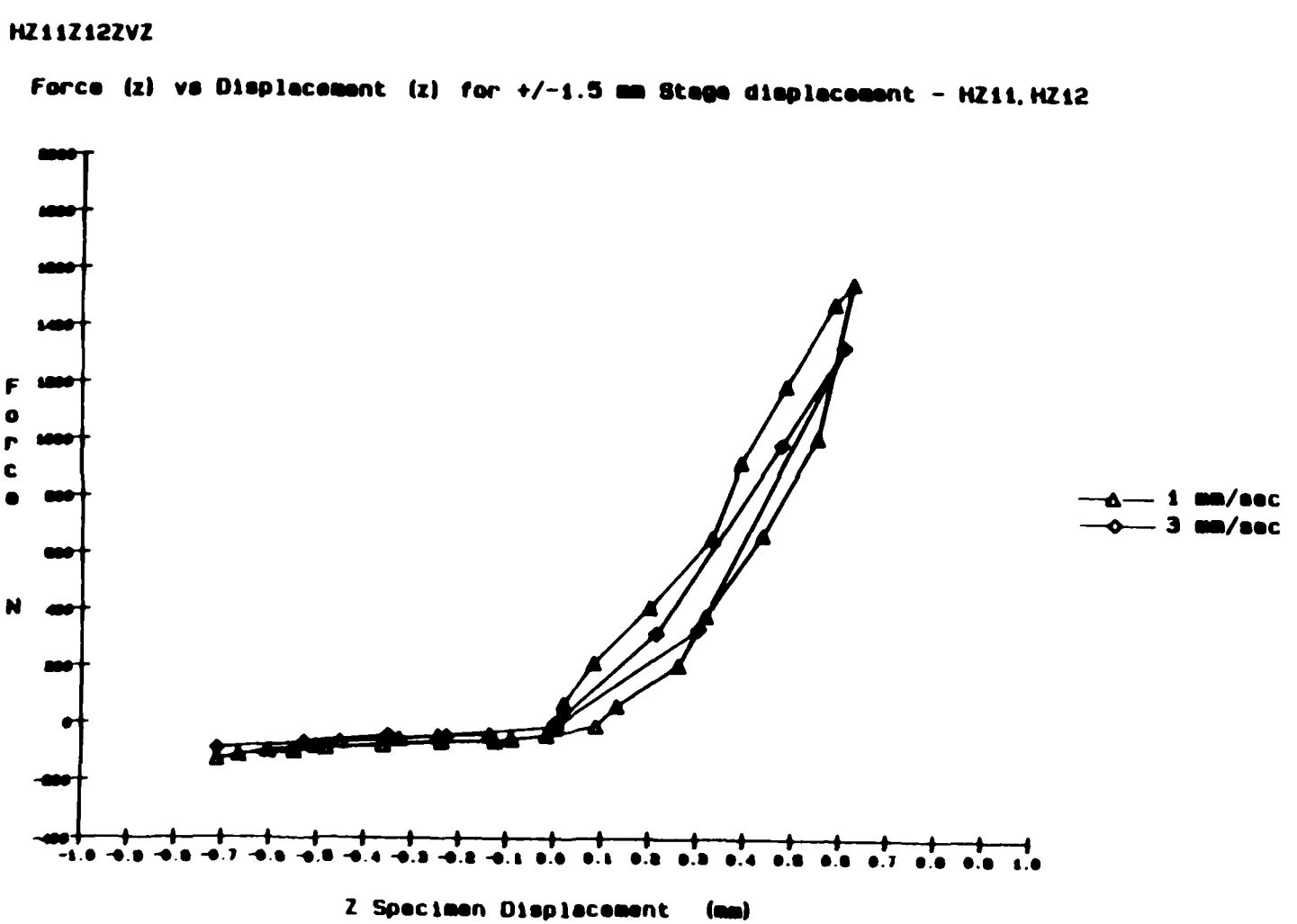

38.3 Specimen H

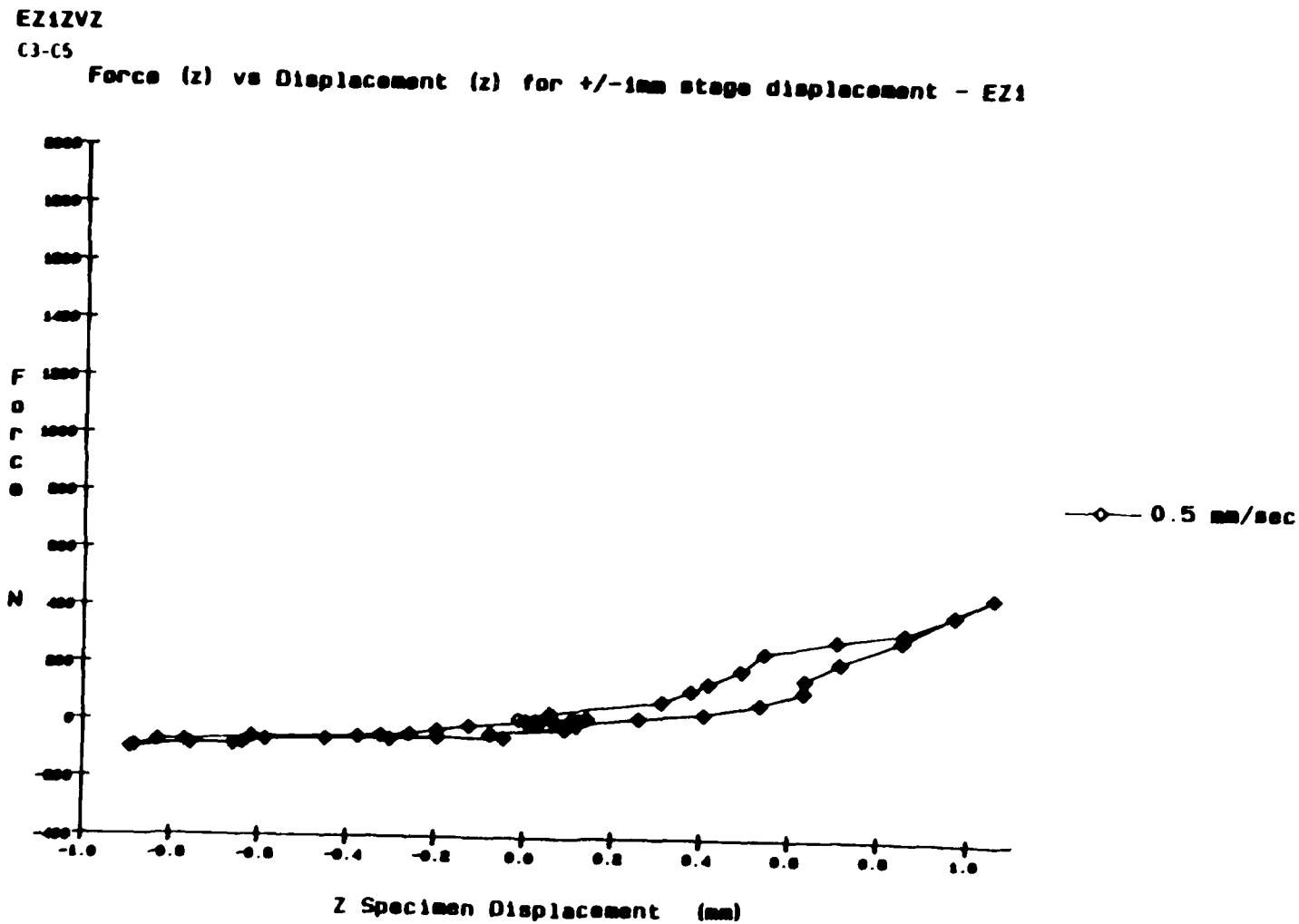

38.4 Specimen E

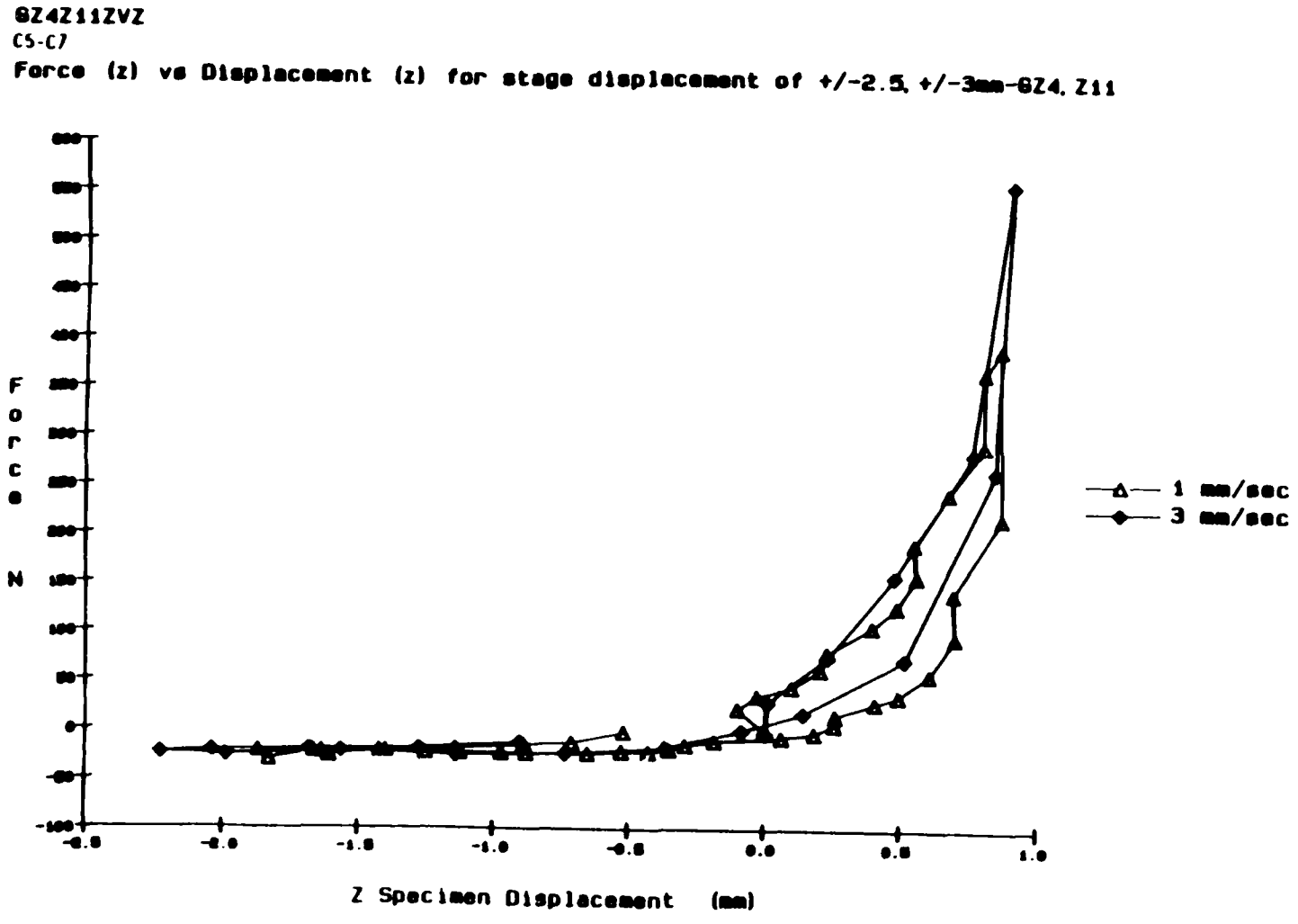

38.5 Specimen G

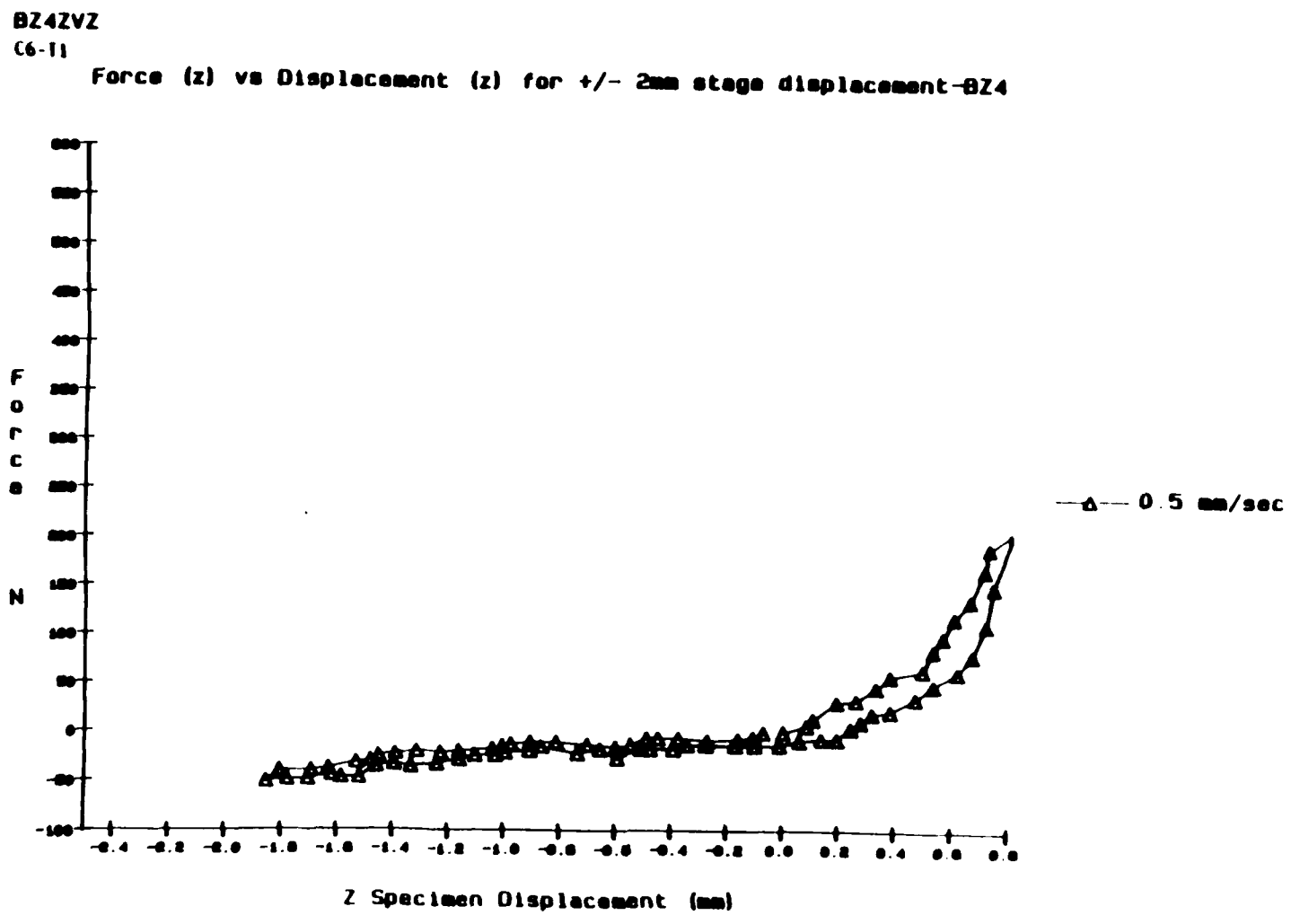

38.6 Specimen B

DZ3Z8ZVZ
C6-11

Force (z) vs Displ. (z) for +1, -2.5 mm stage displacement - DZ3, DZ8

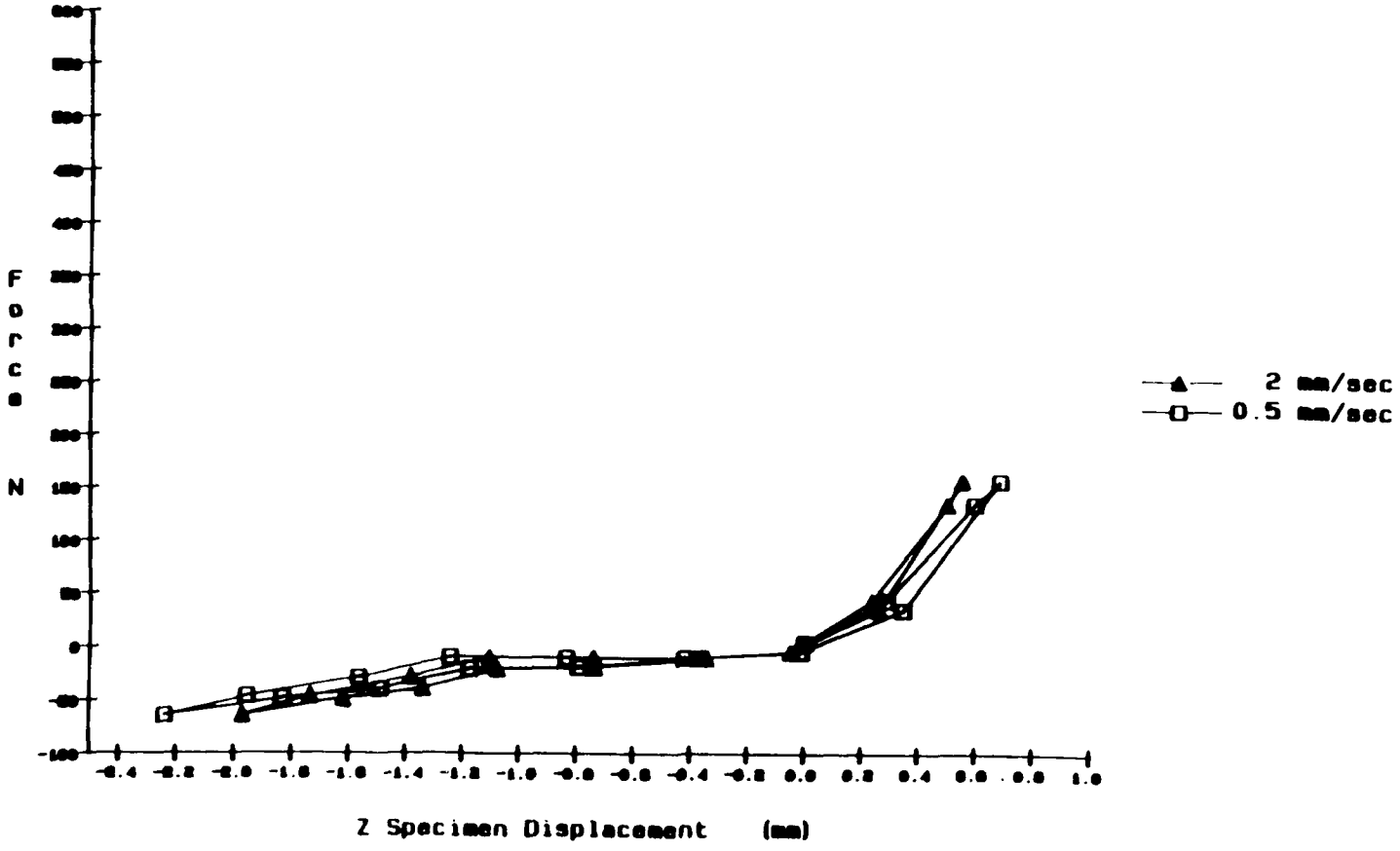

38.7 Specimen D

CZ2XZVZ

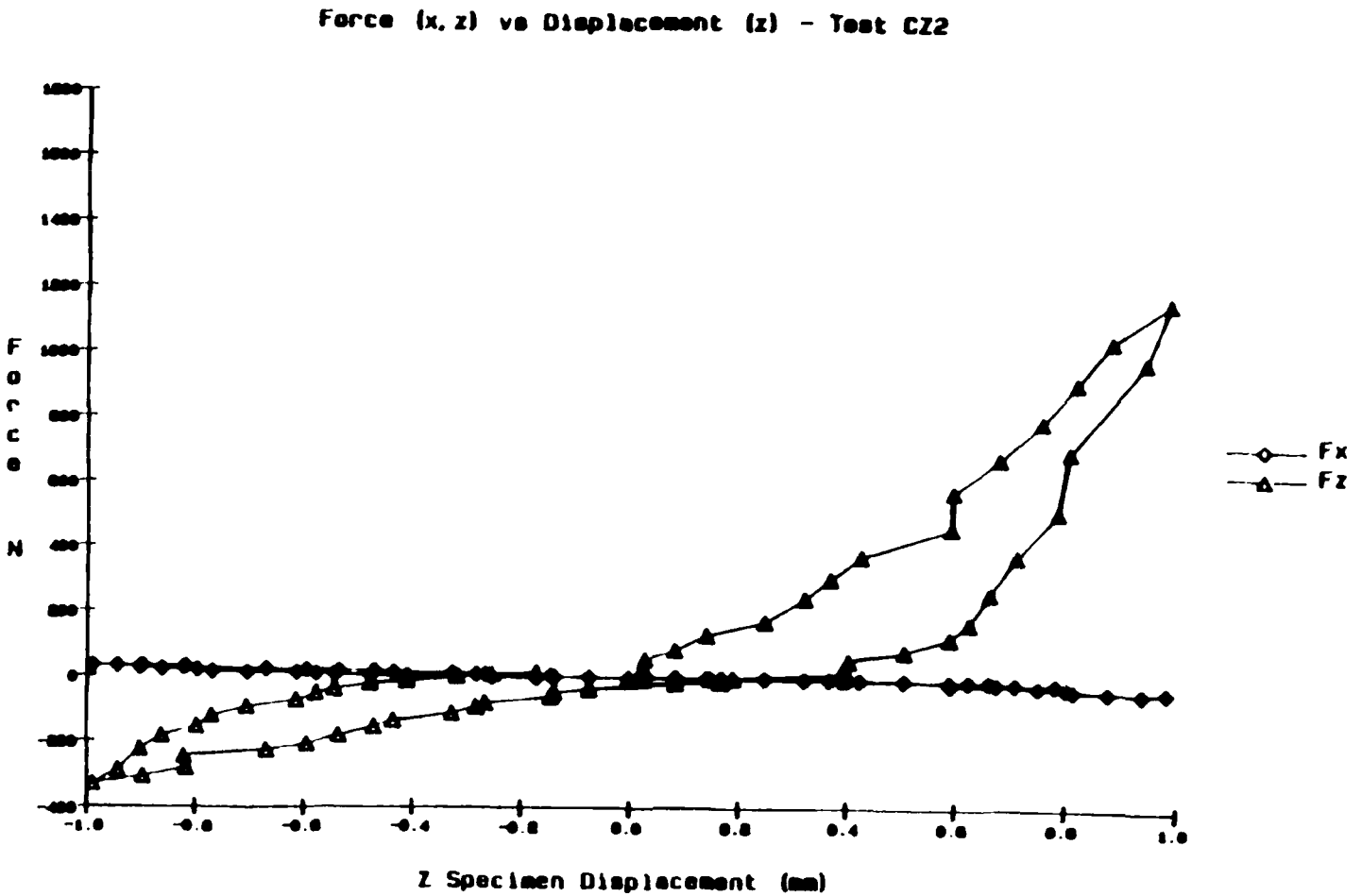

Figures:39.1-39.7 Force (x,y) vs displacement (z) for 7 specimens

39.1 Specimen C

FZ7XZVZ

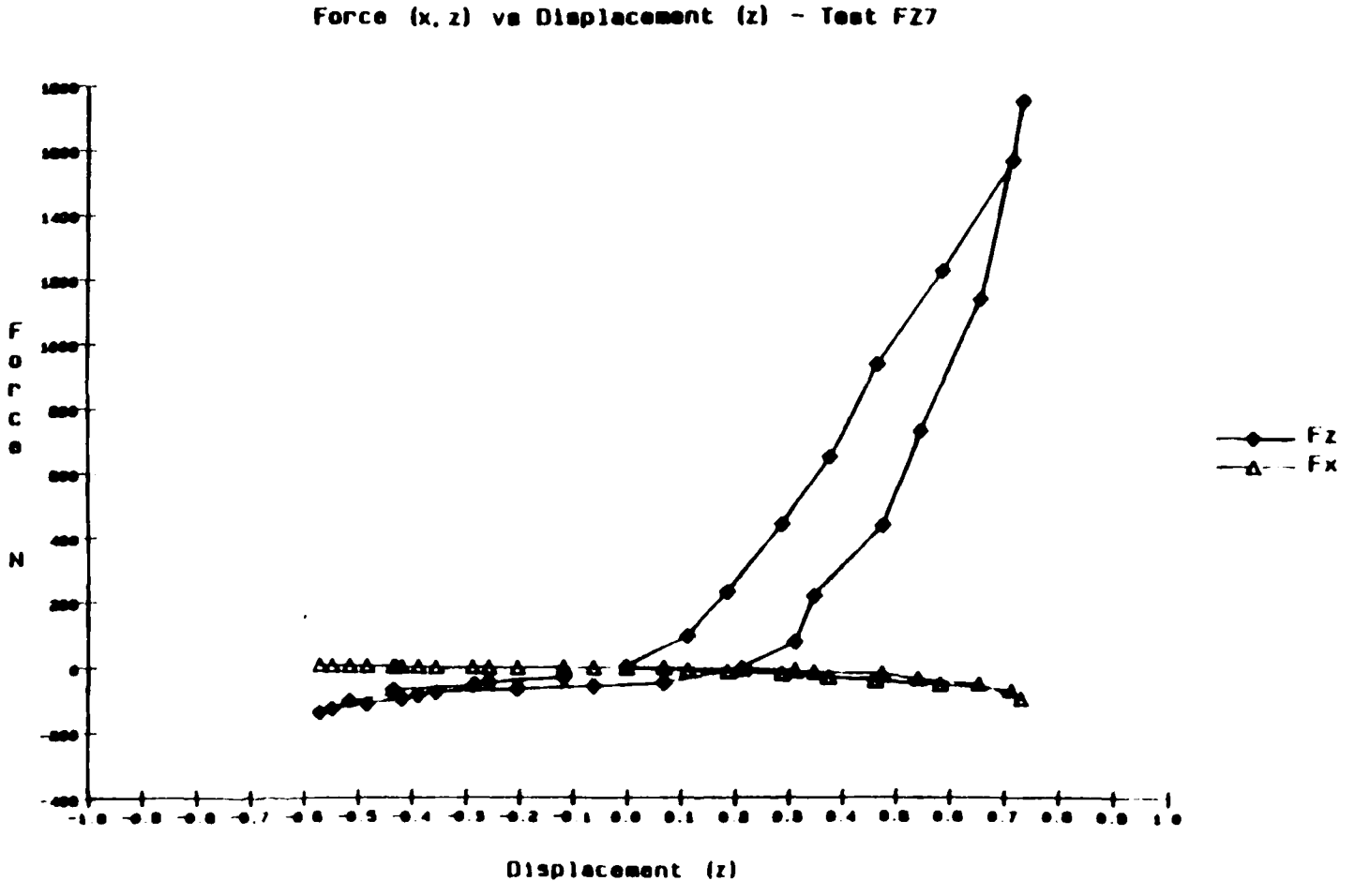

39.2 Specimen F

HZ11XZVZ

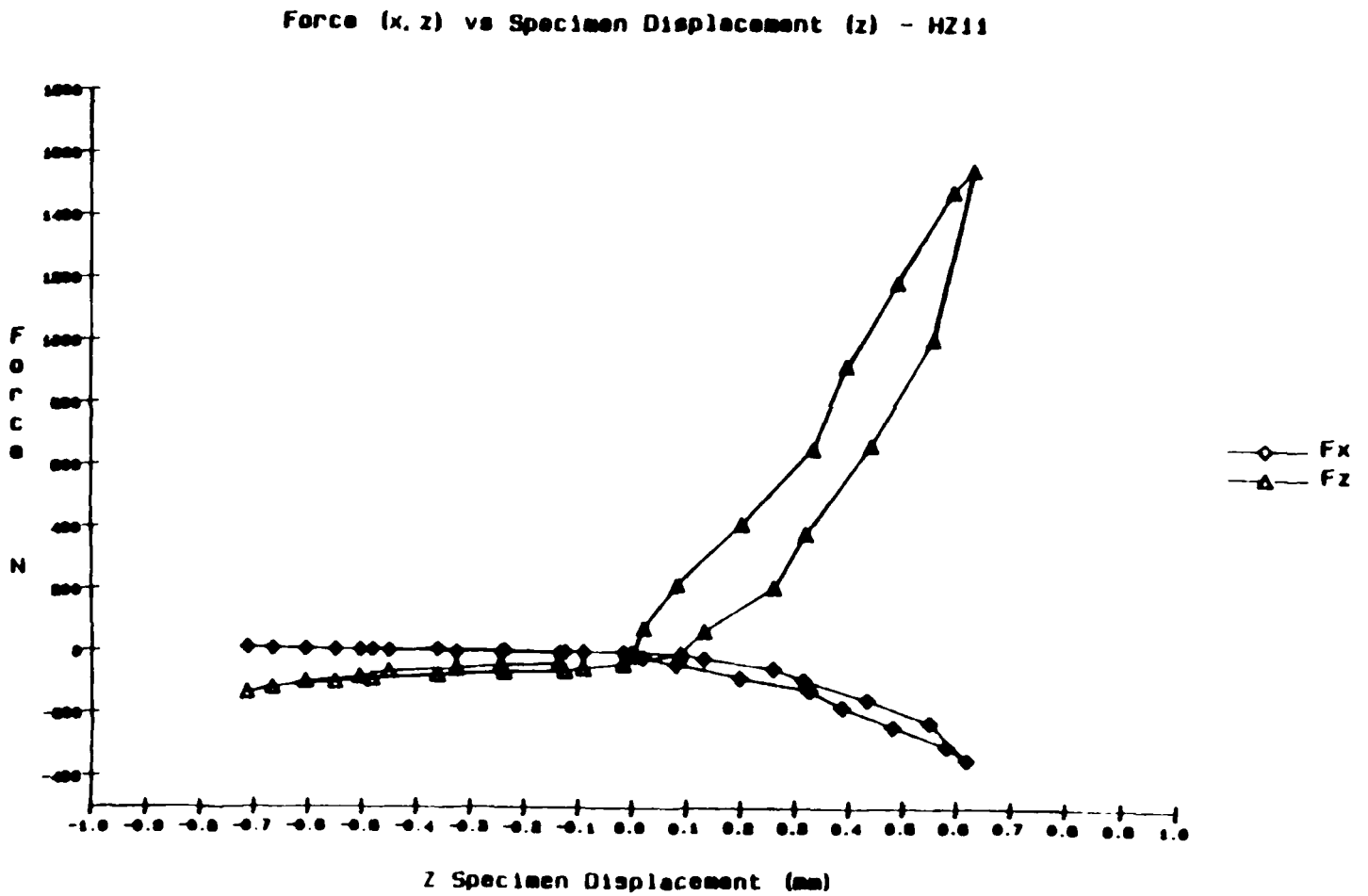

39.3 Specimen H

EZ1XZVZ

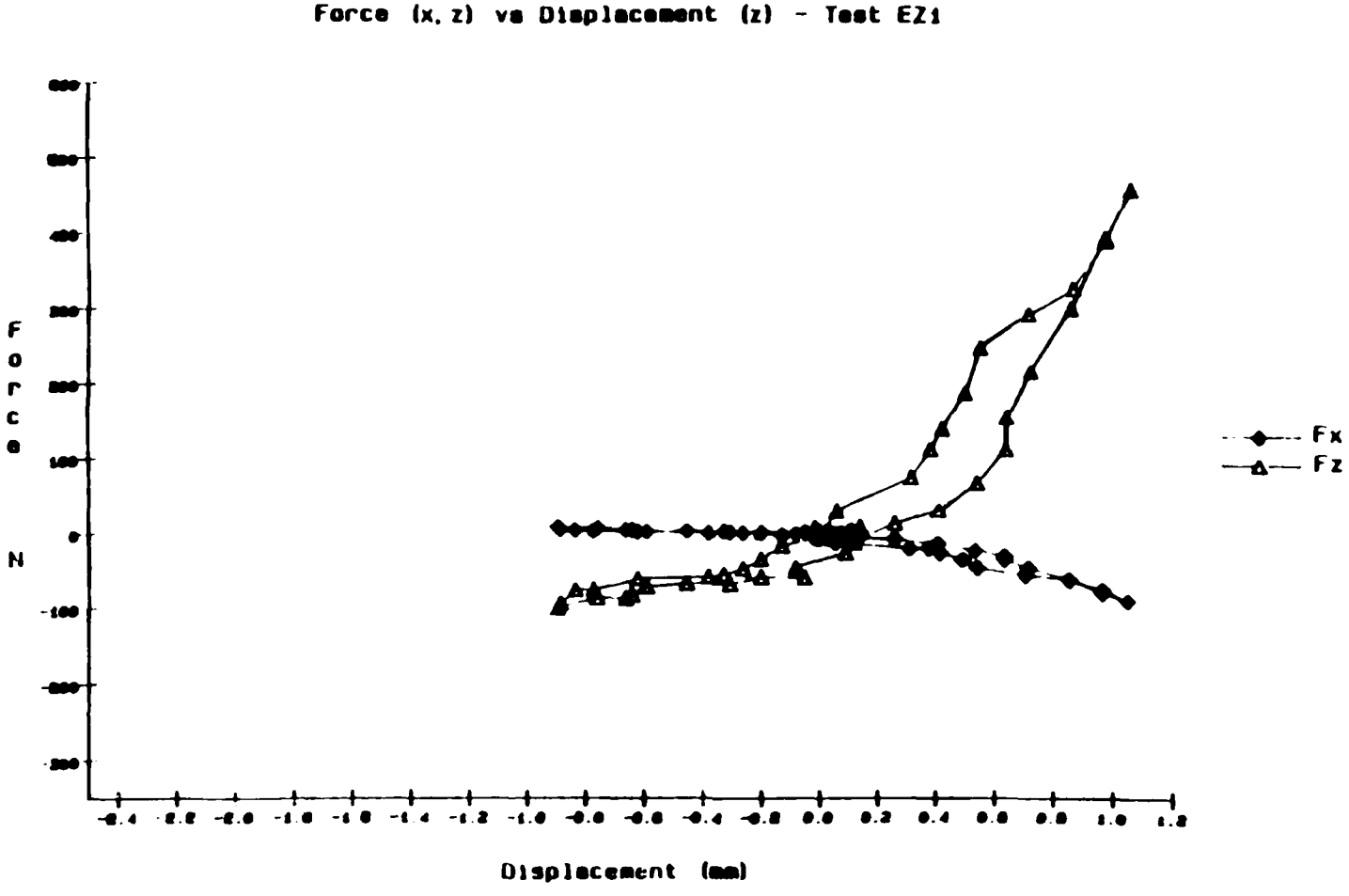

39.4 Specimen E

GZ4XZVZ

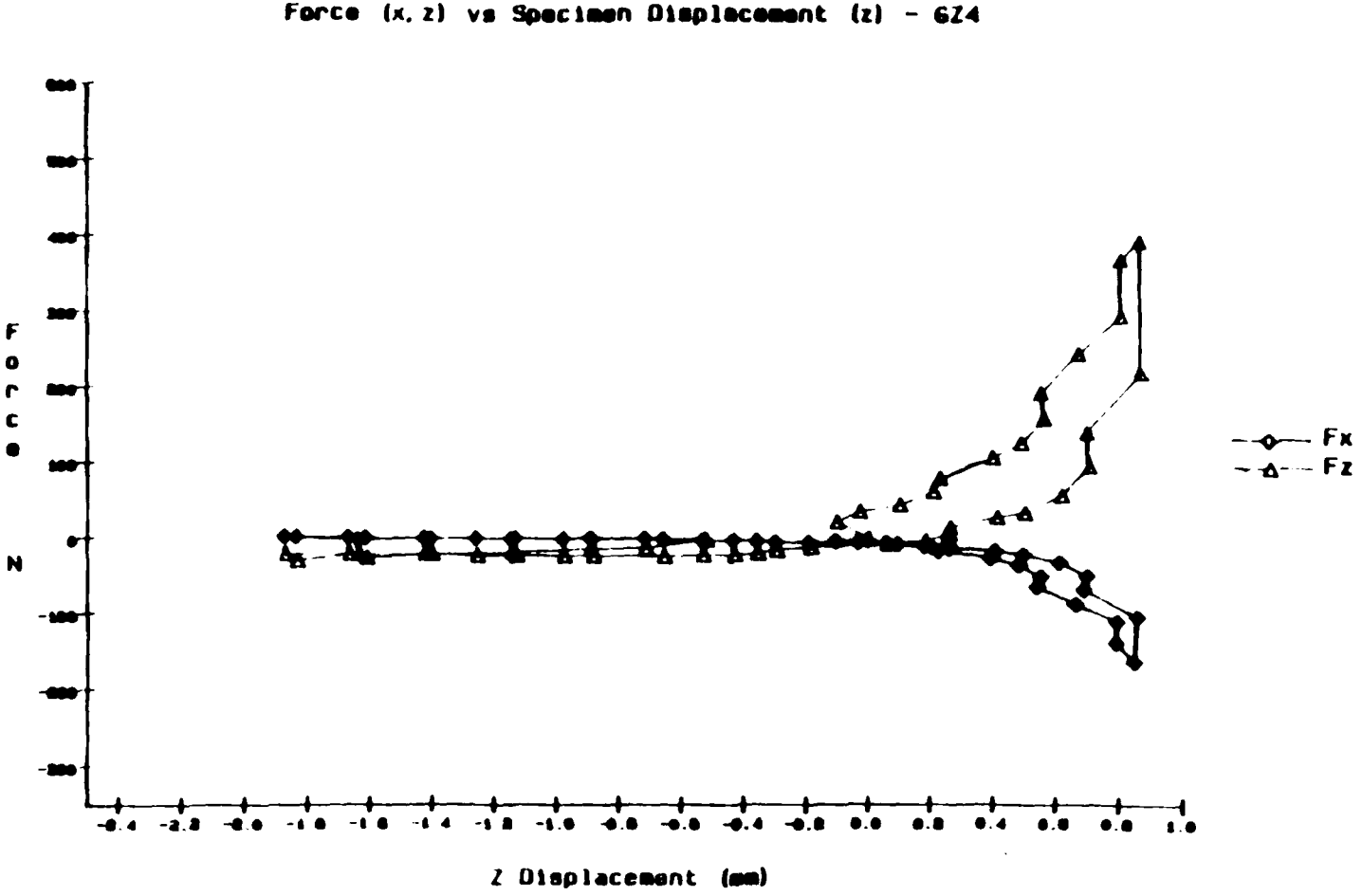

39.5 Specimen G

BZ4XZVZ

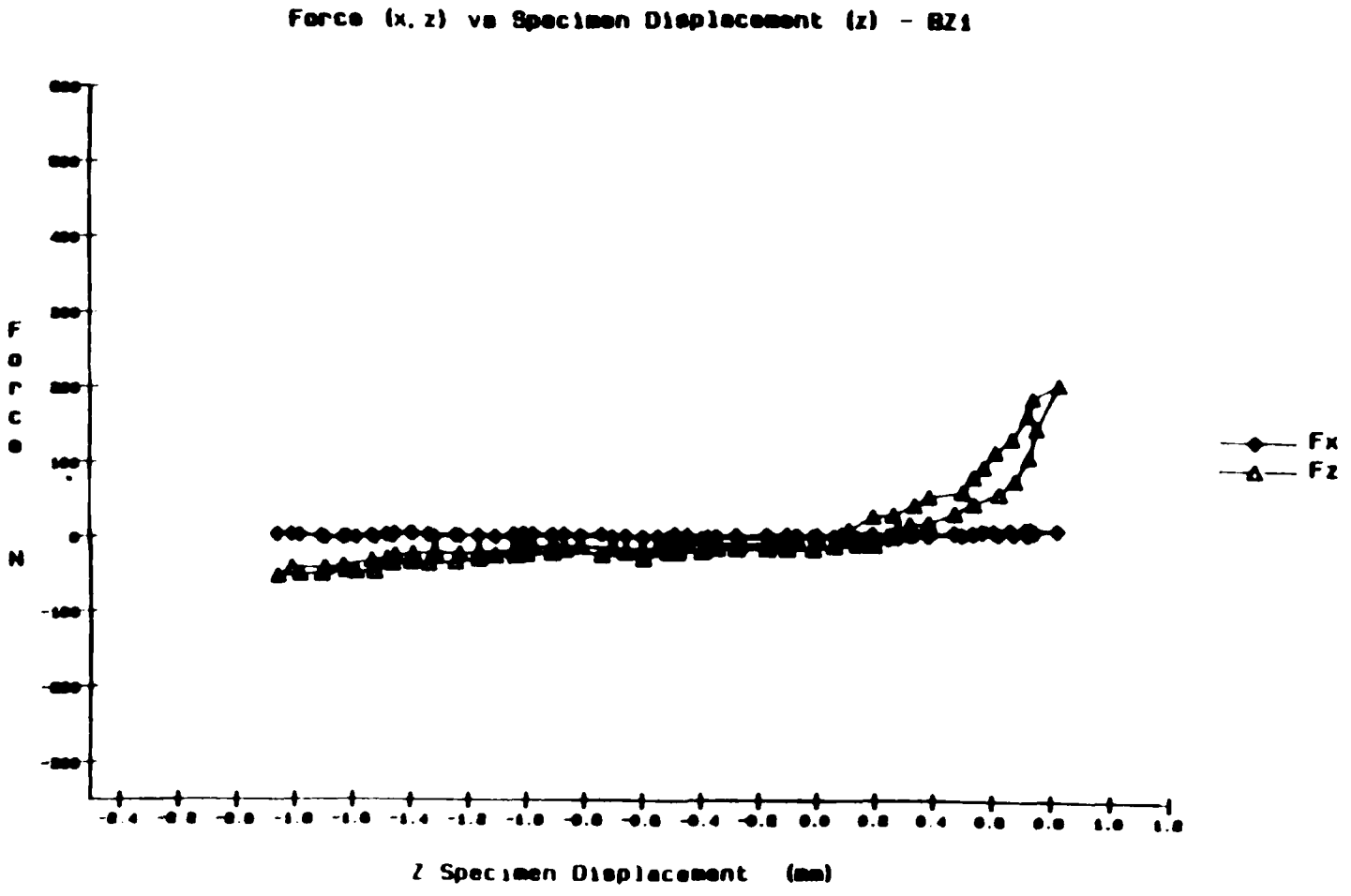

39.6 Specimen B

DZ3XZVZ

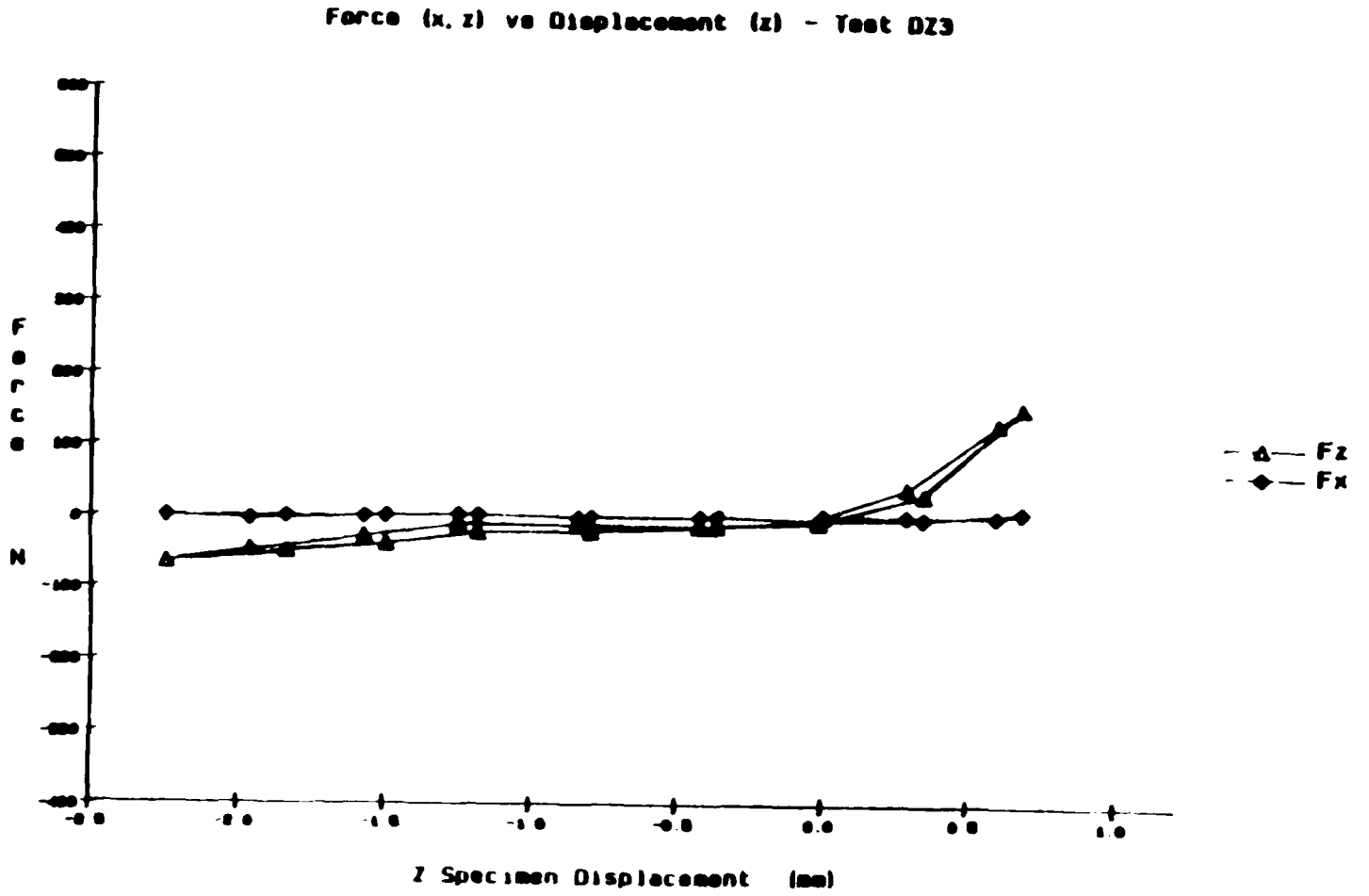

39.7 Specimen D

CZ2XYZVZTS

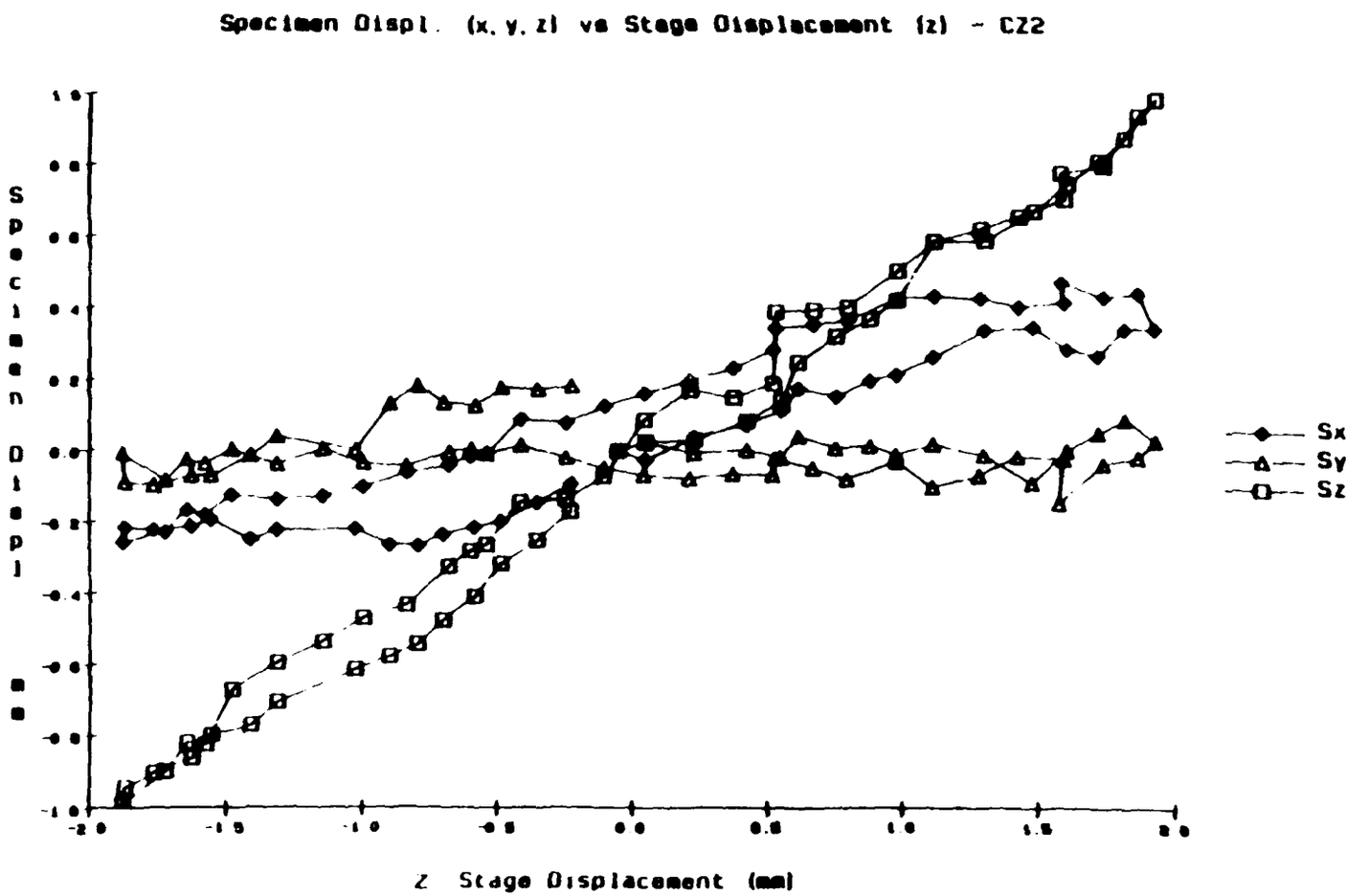

Figure:40.1-40.7 Specimen displacement (x,y,z) vs test stage displacement (z) for 7 specimens

40.1 Specimen C

FZ7XYZVZ

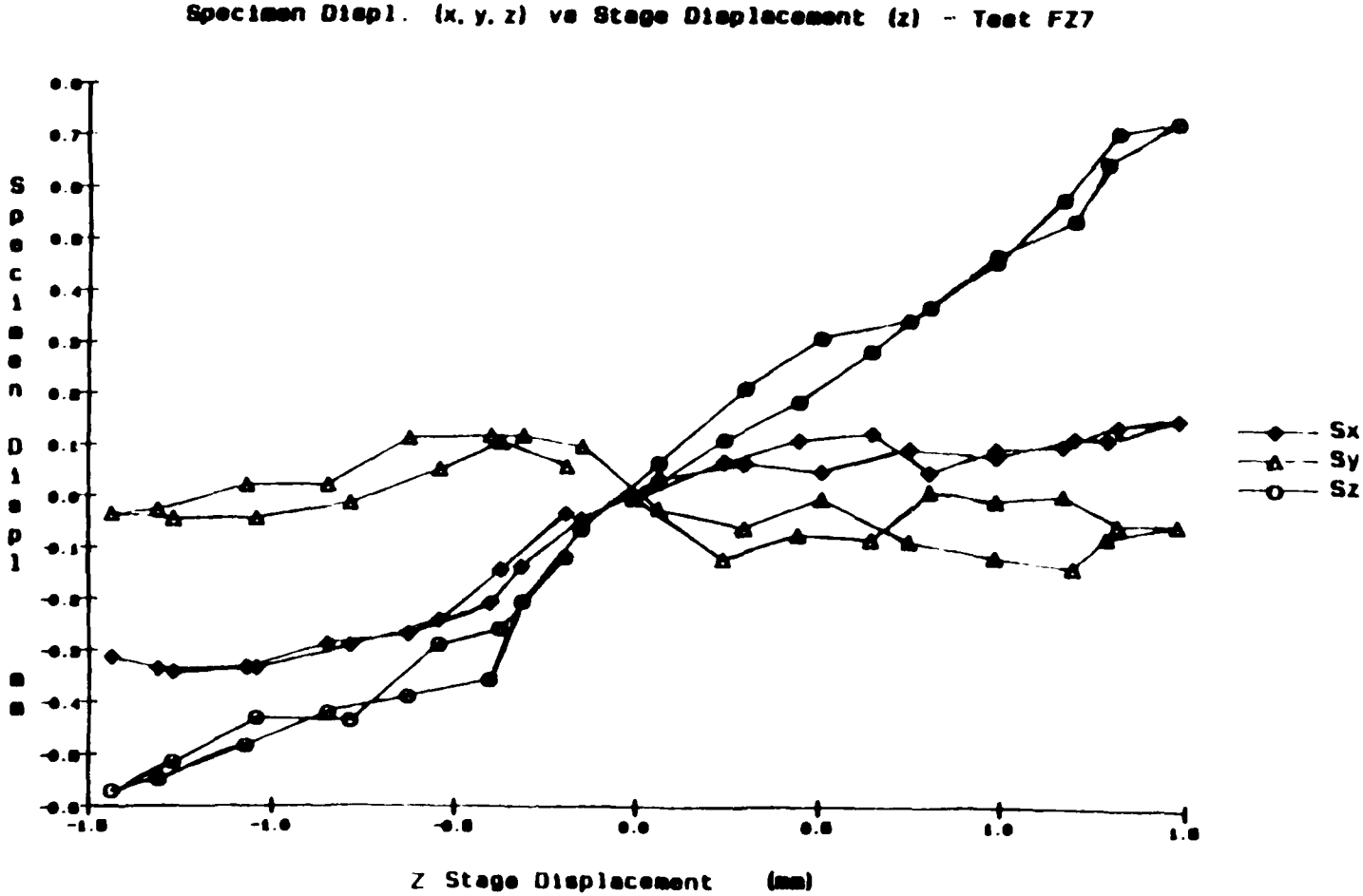

40.2 Specimen F

HZ11AXYZVTS

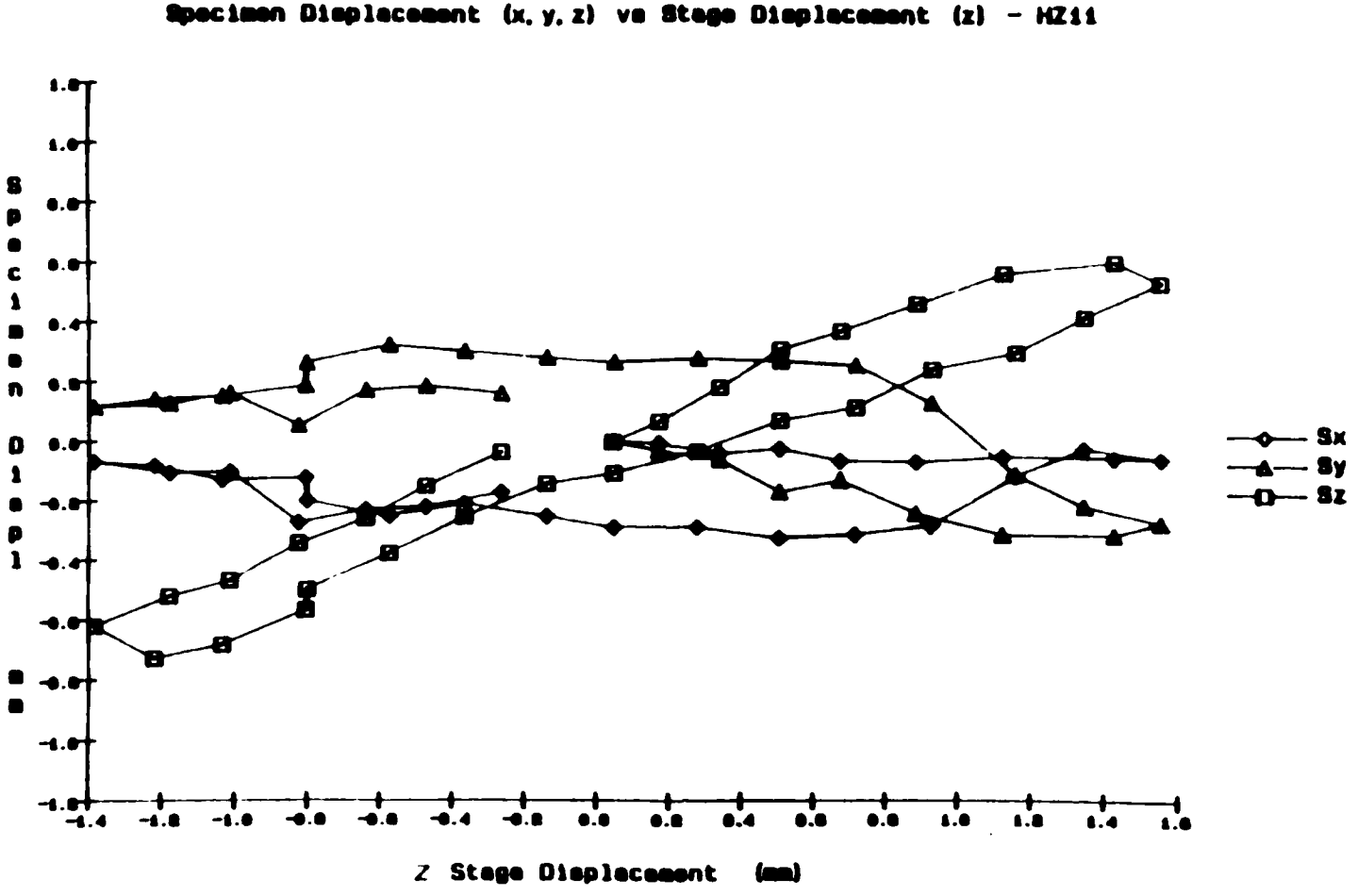

40.3 Specimen H

6Z4XYZVTS

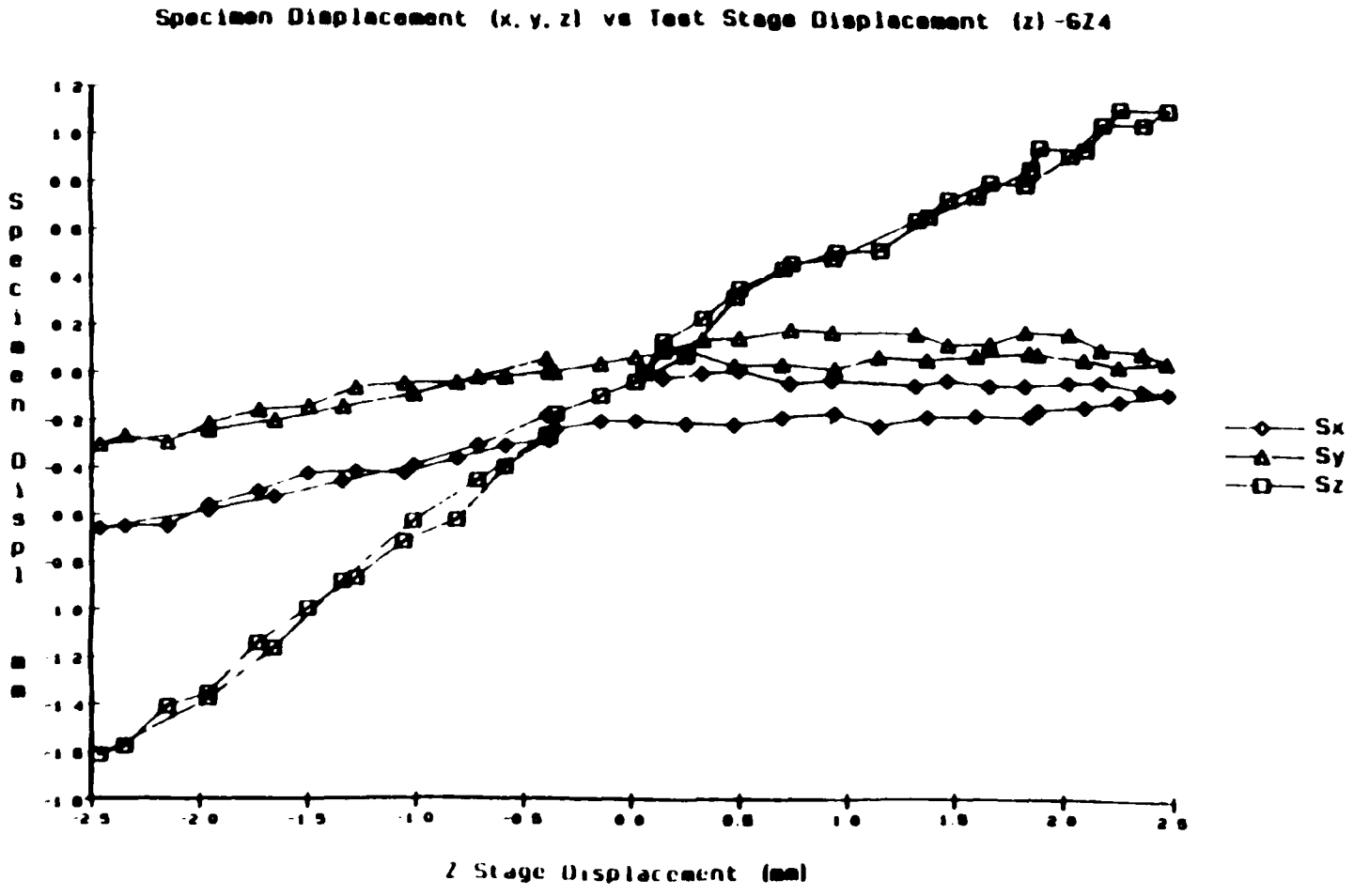

40.5 Specimen G

BZ4XYZVTS

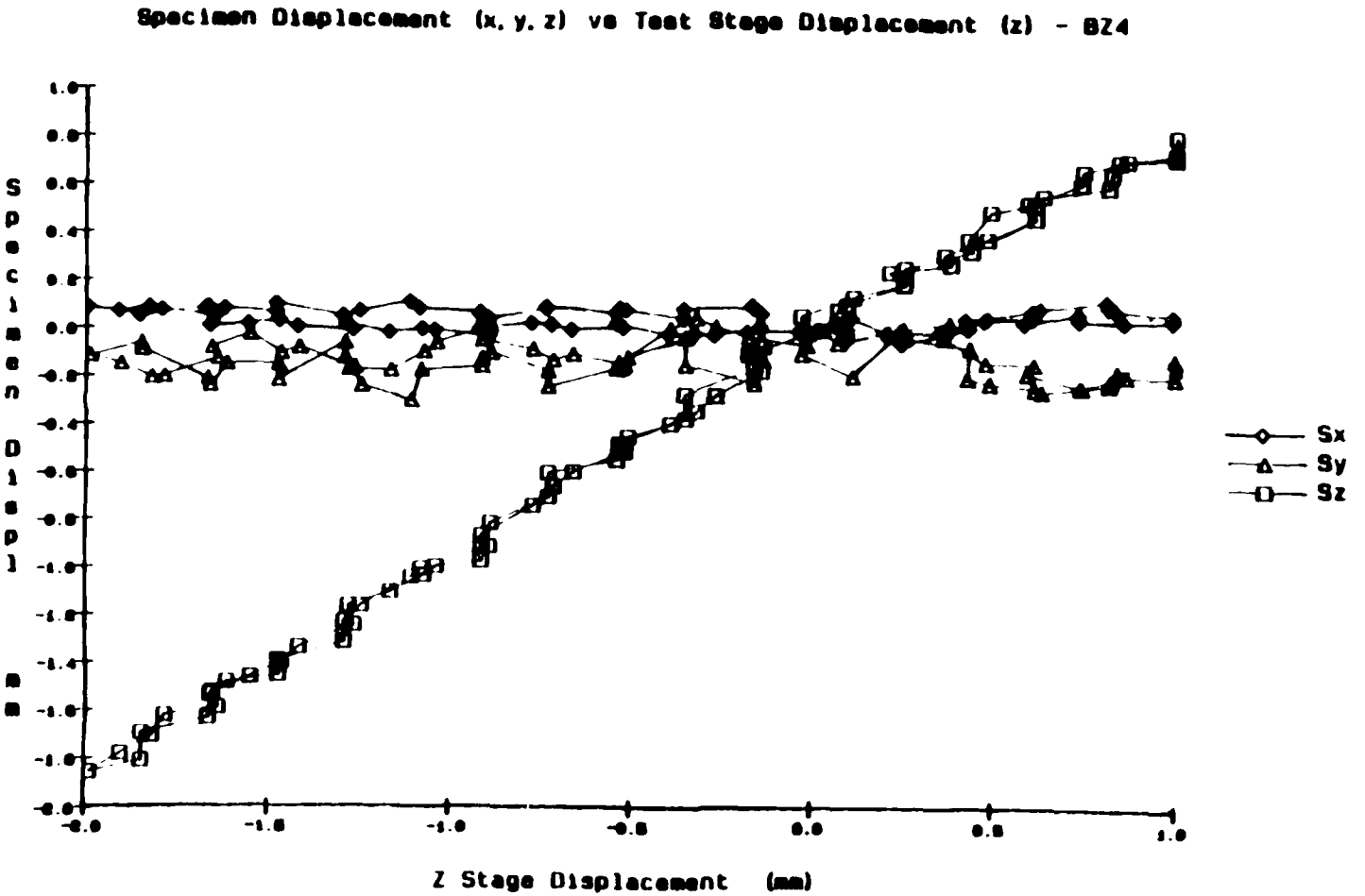

40.6 Specimen B

DZ3XYZVTS

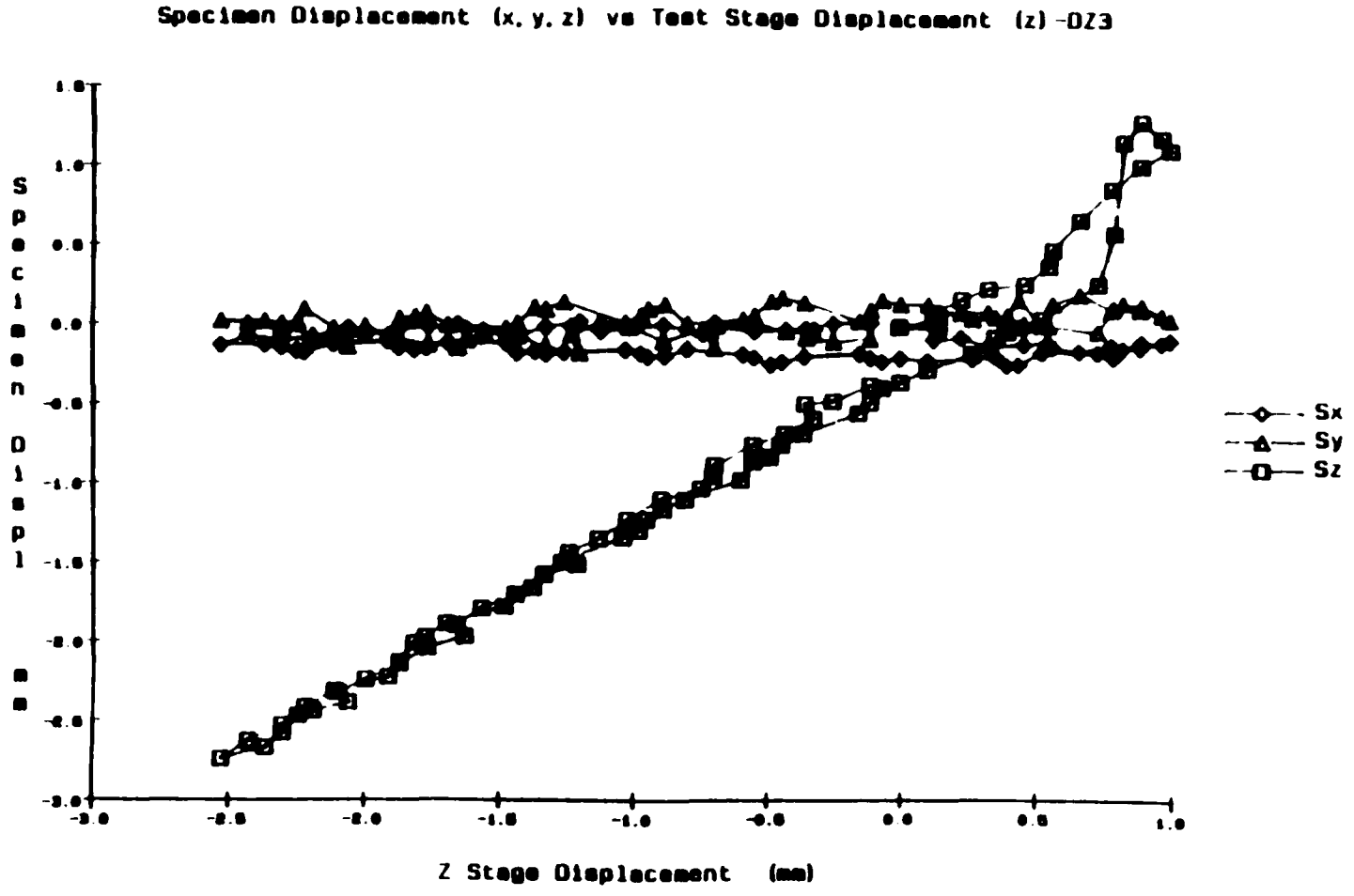

40.7 Specimen D

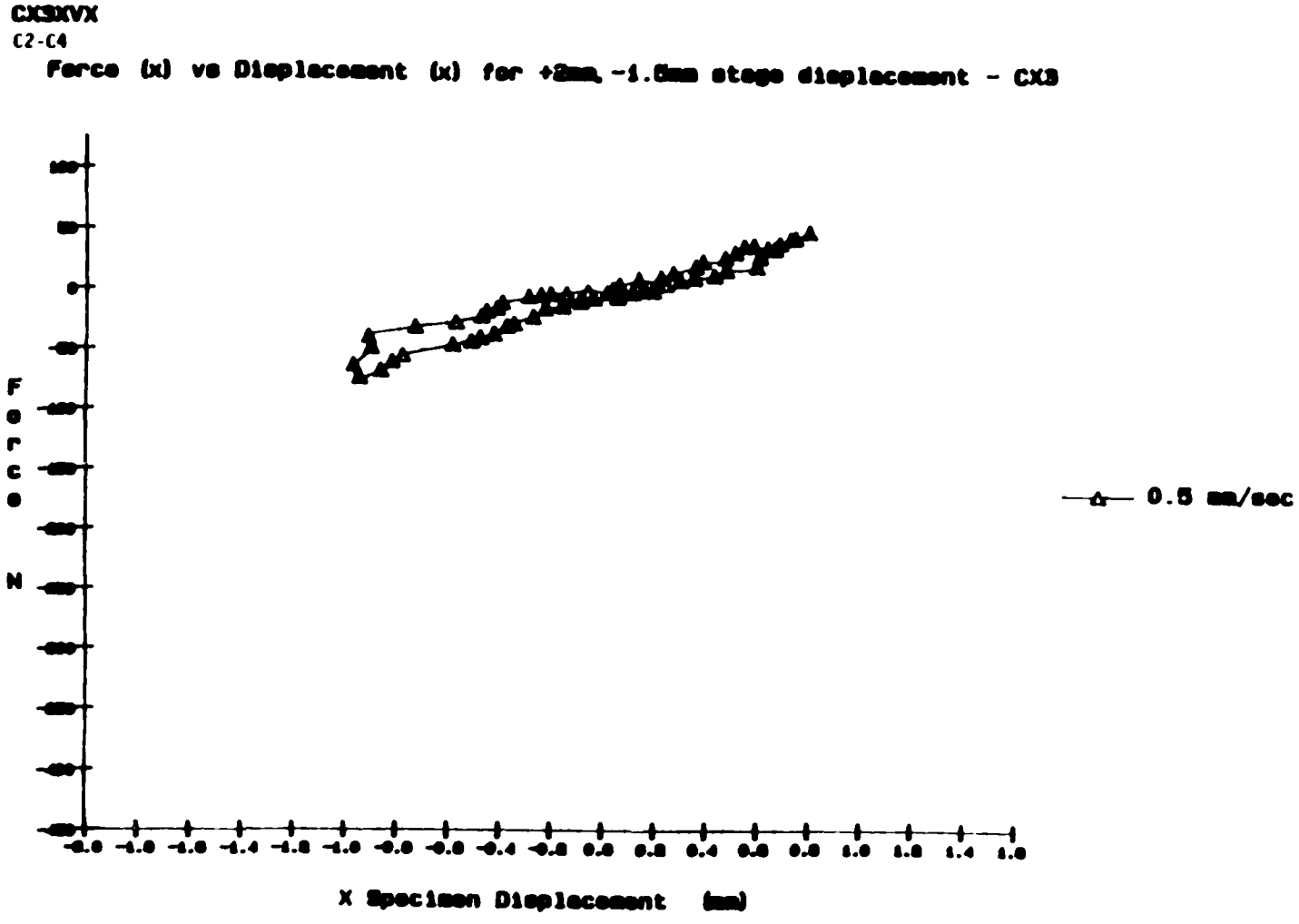

Figures:41.1-41.7 Force (x) vs displacement (x) for 7 specimens

41.1 Specimen C

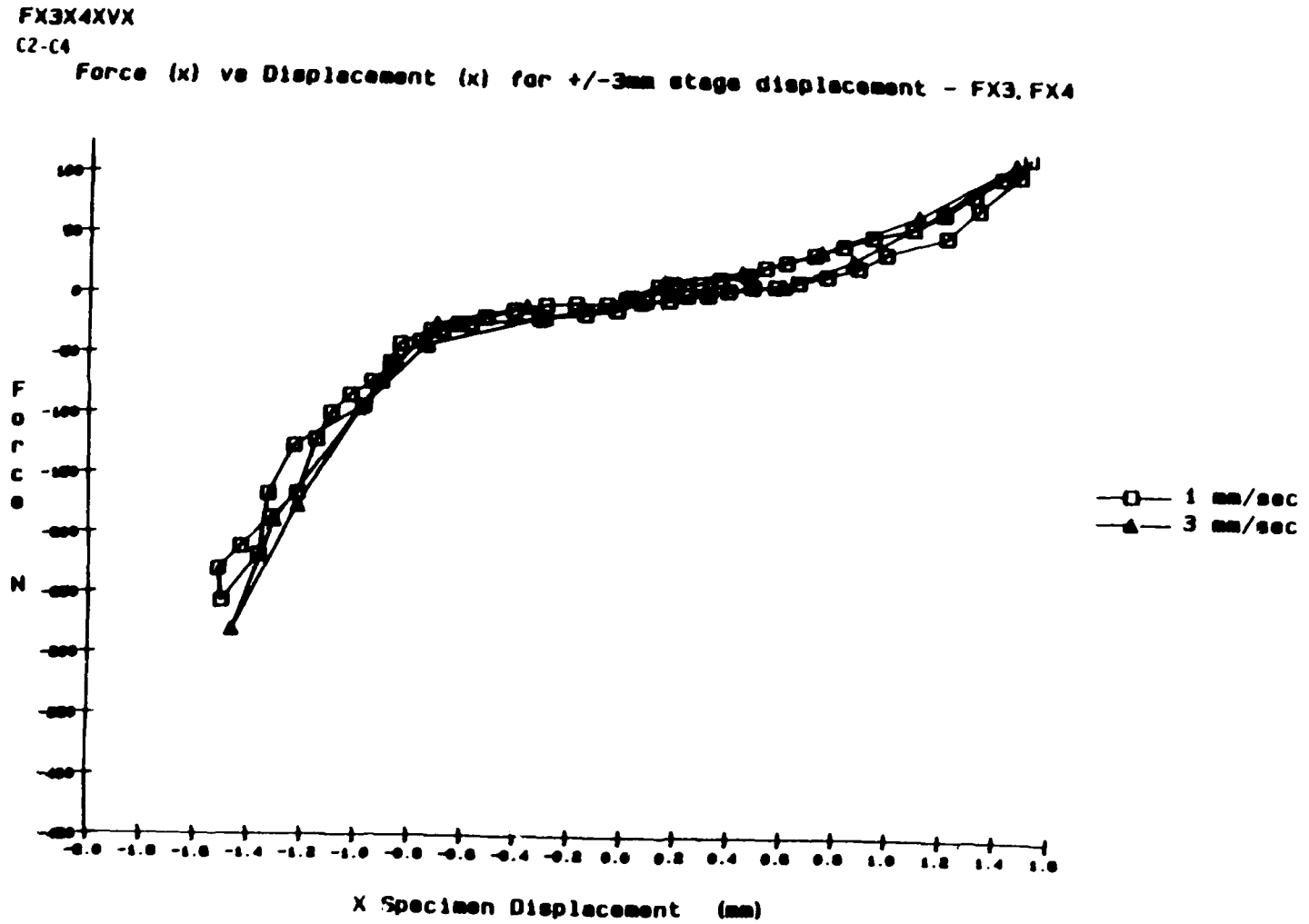

41.2 Specimen F

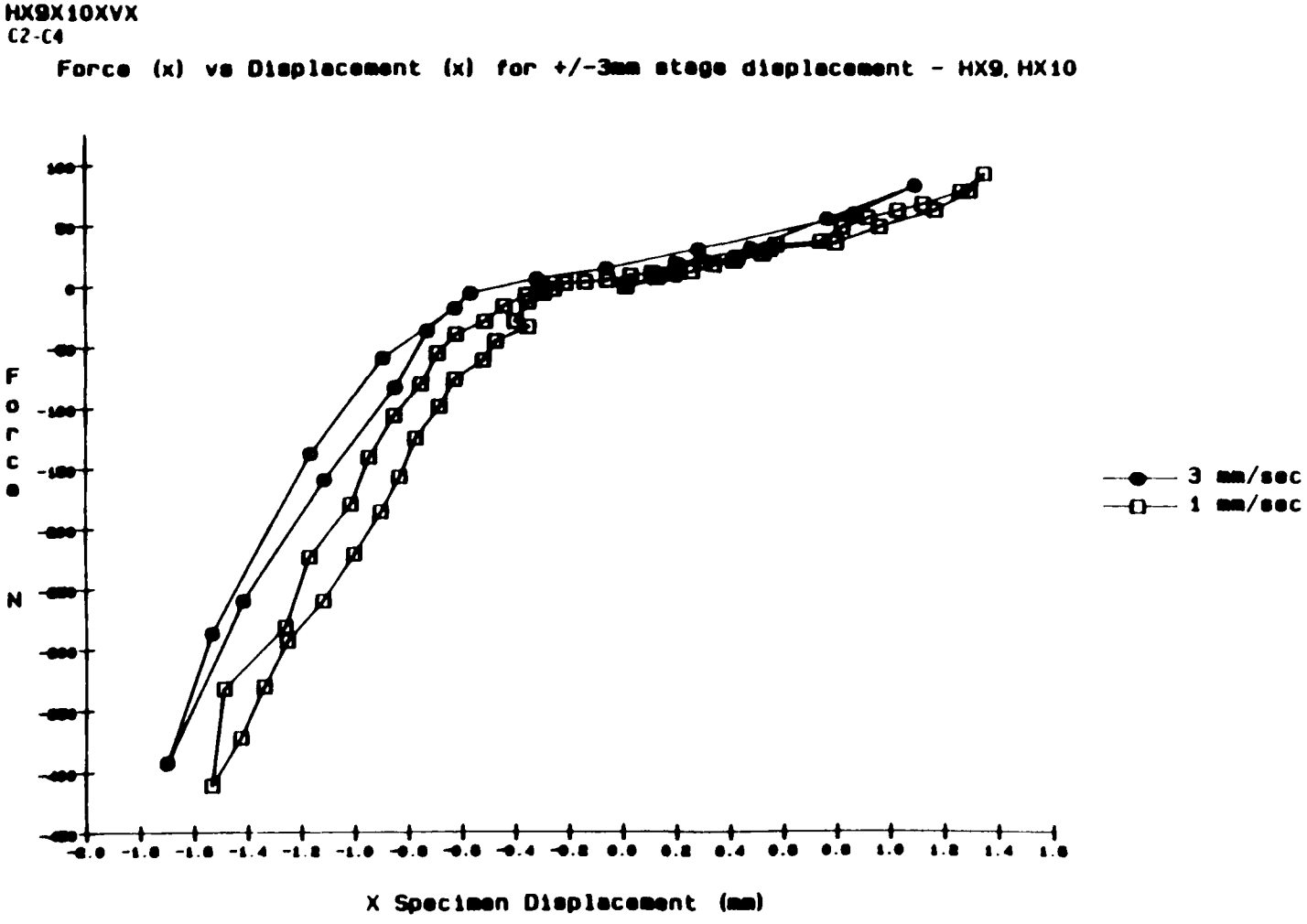

41.3 Specimen H

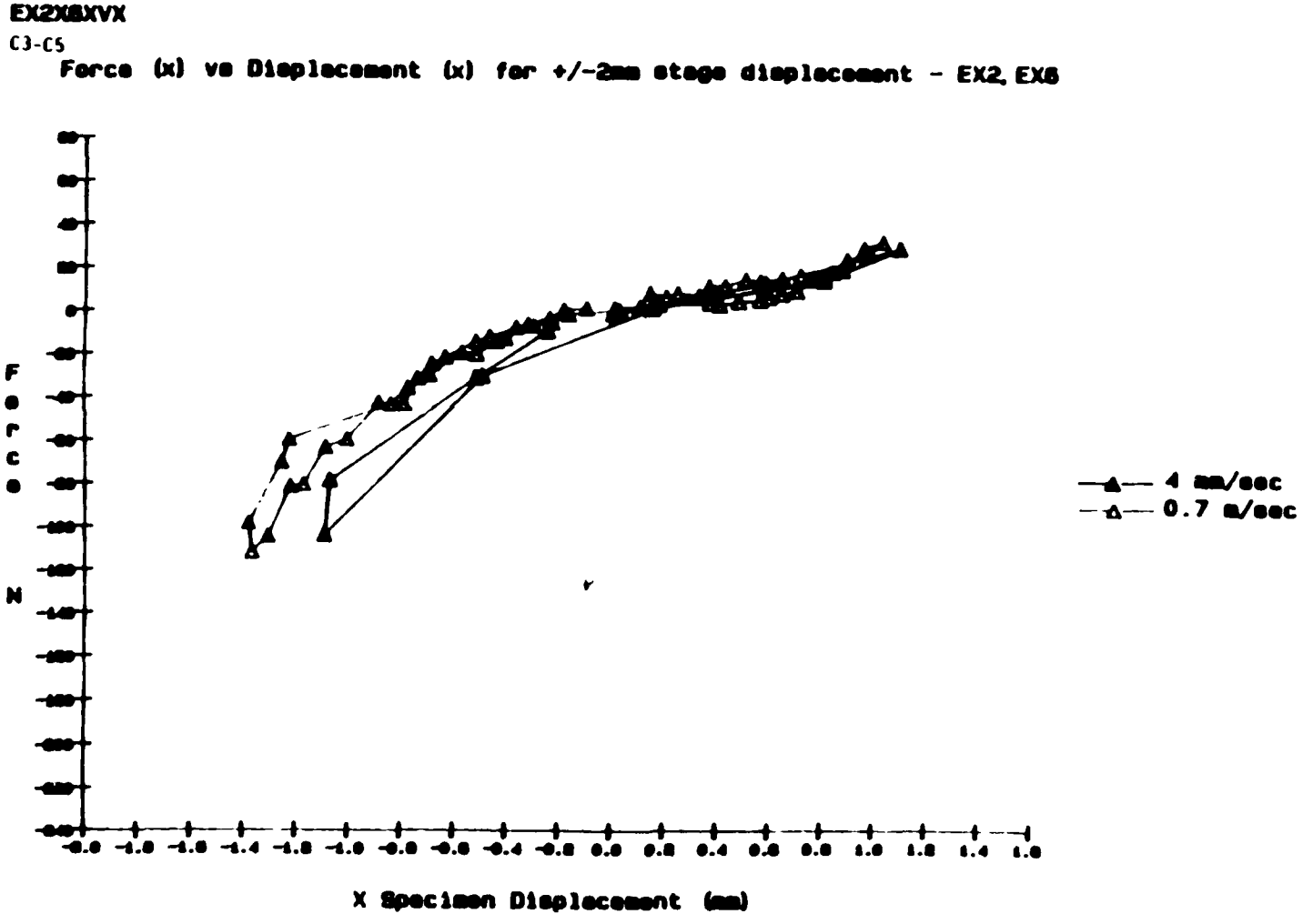

41.4 Specimen E

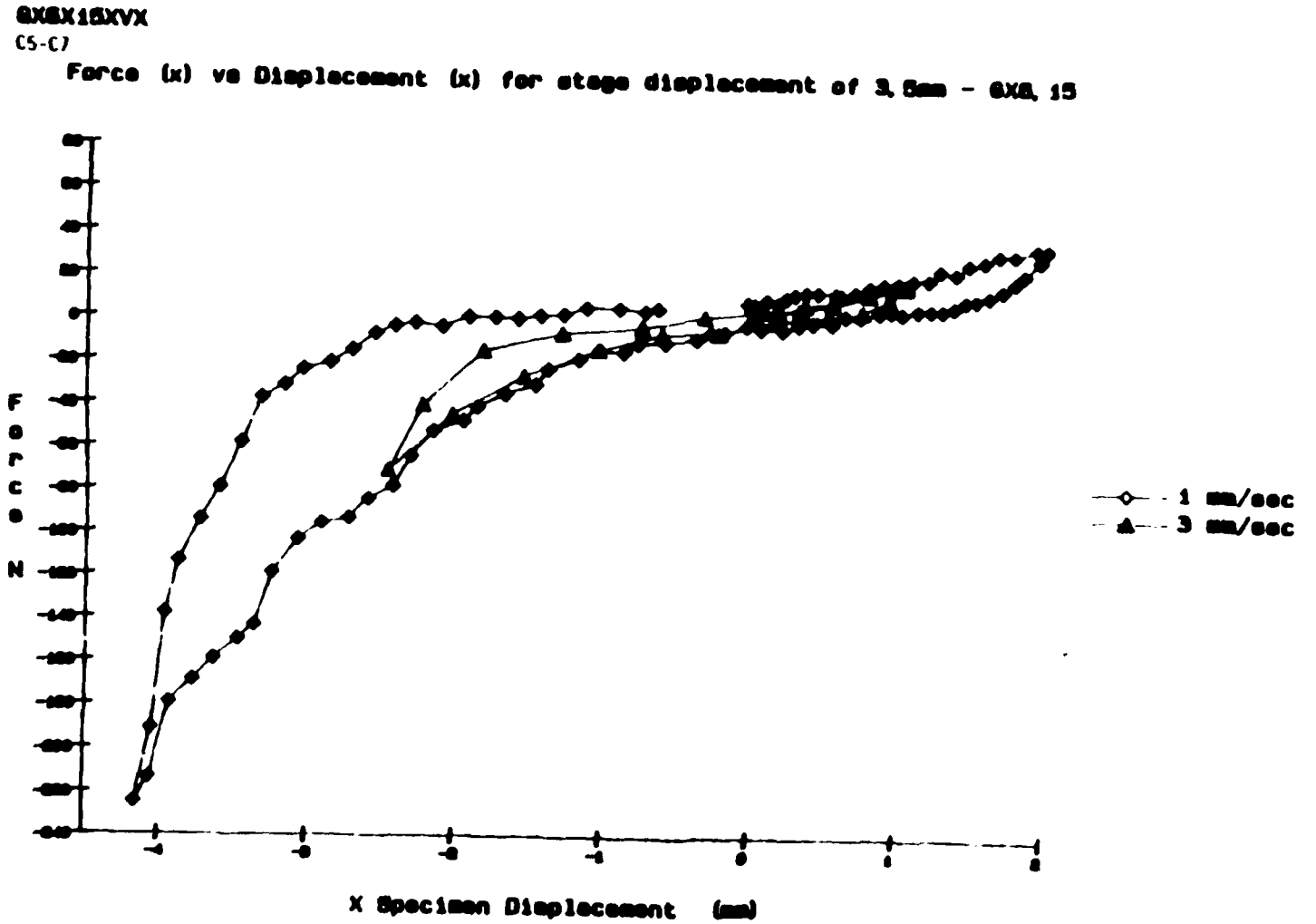

41.5 Specimen G

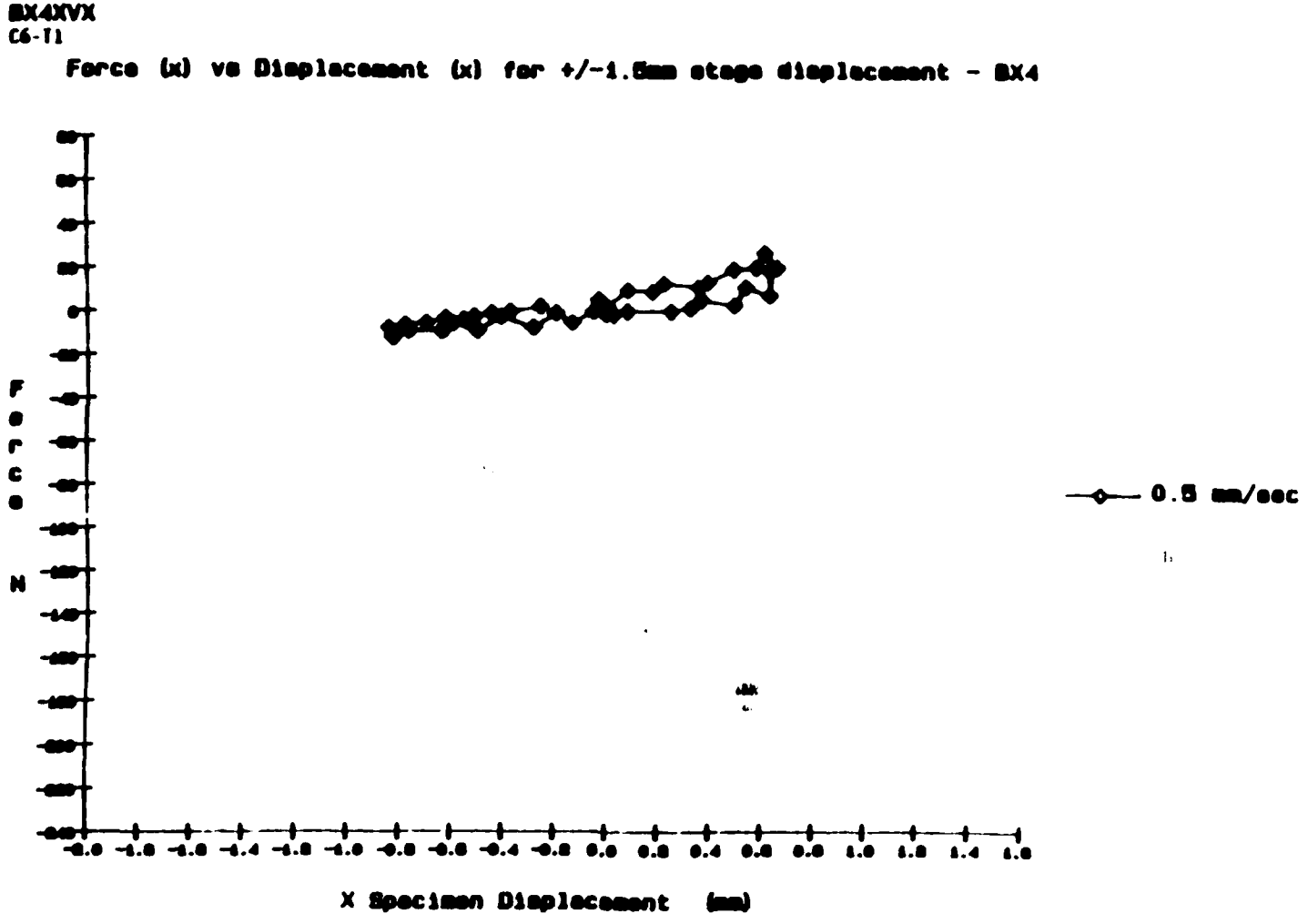

41.6 Specimen B

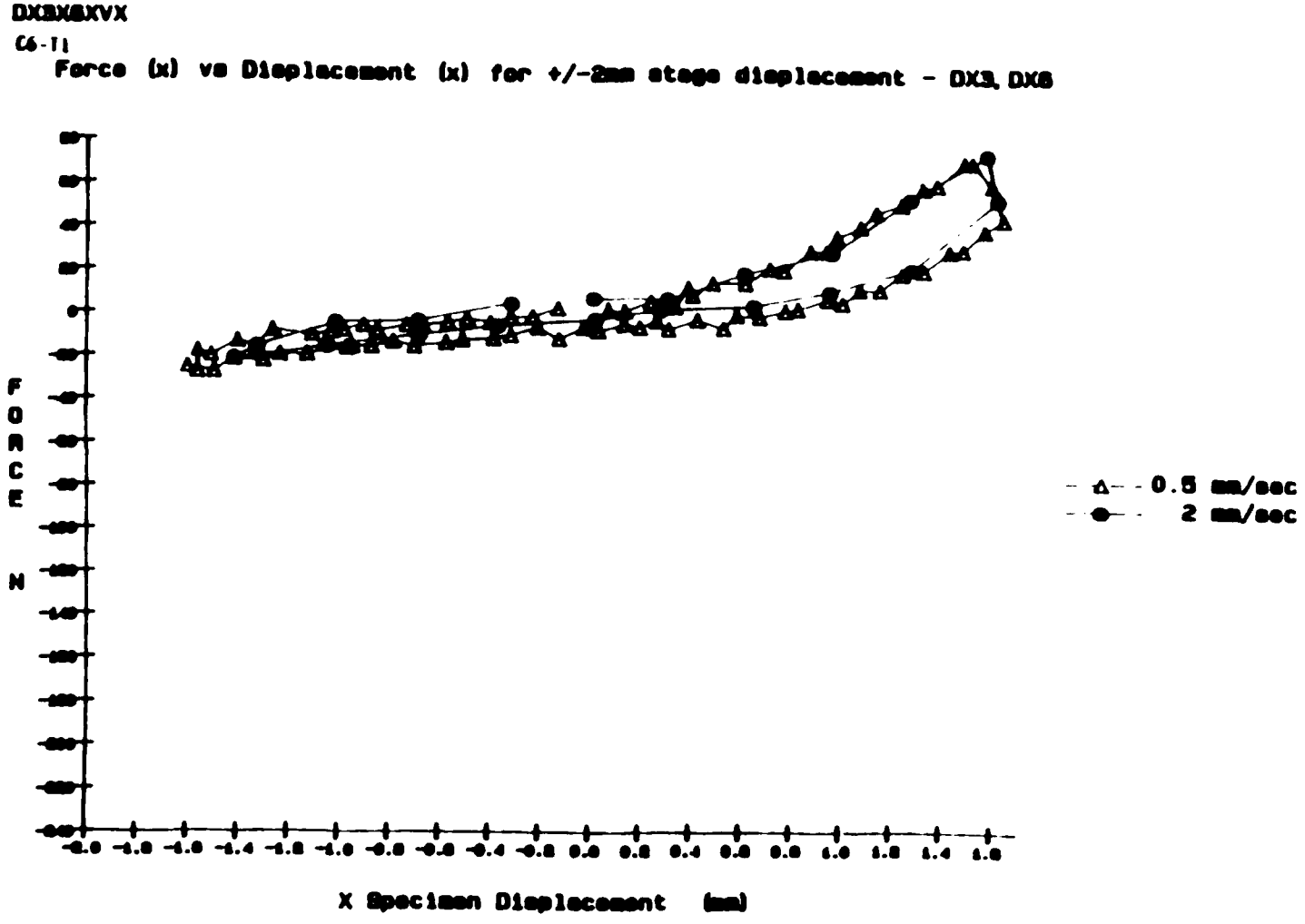

41.7 Specimen D

CX3XZVX

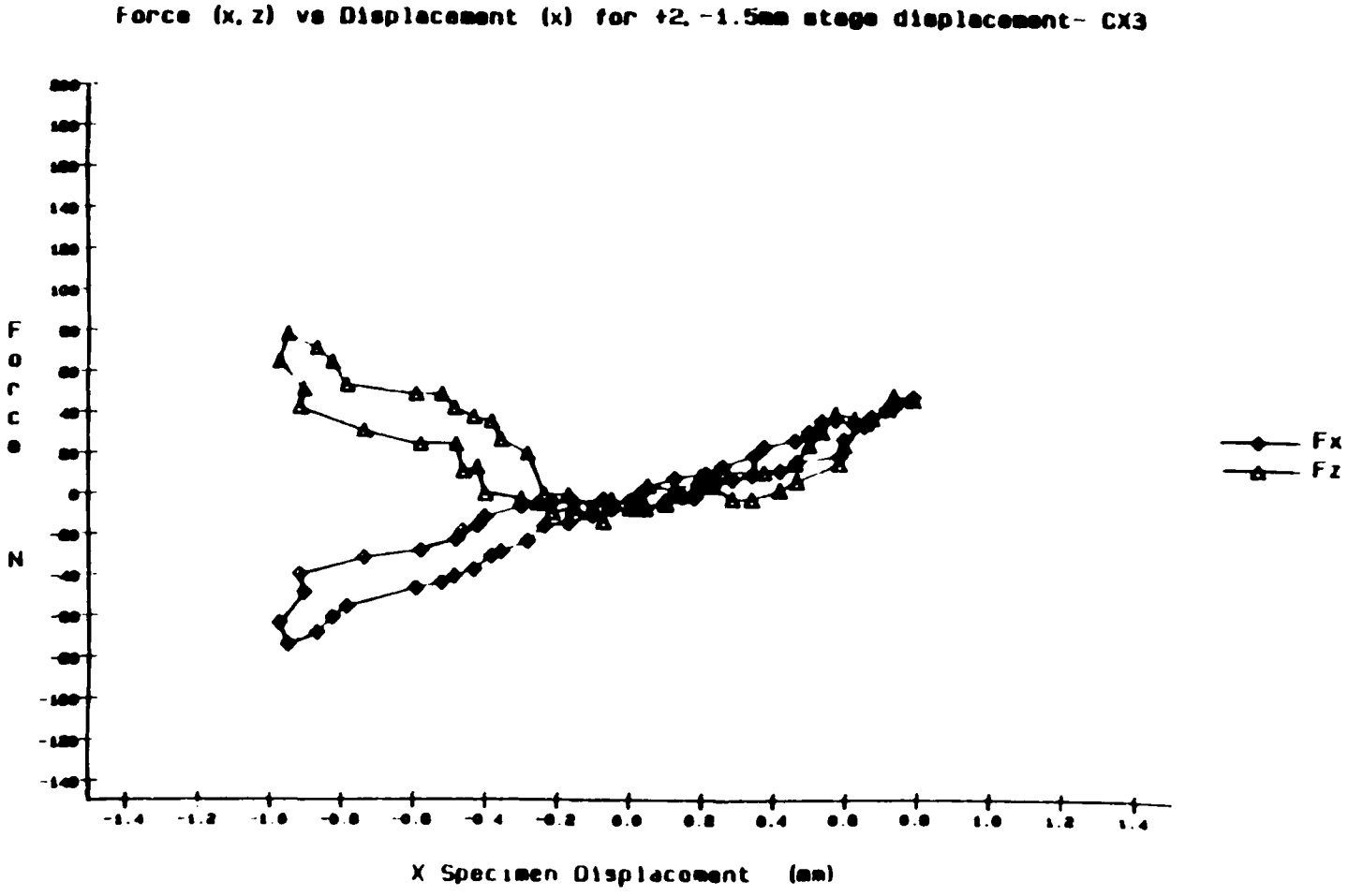

Figures:42.1-42.7 Force (x,y) vs displacement (x) for 7 specimens

42.1 Specimen C

FX3XZVX

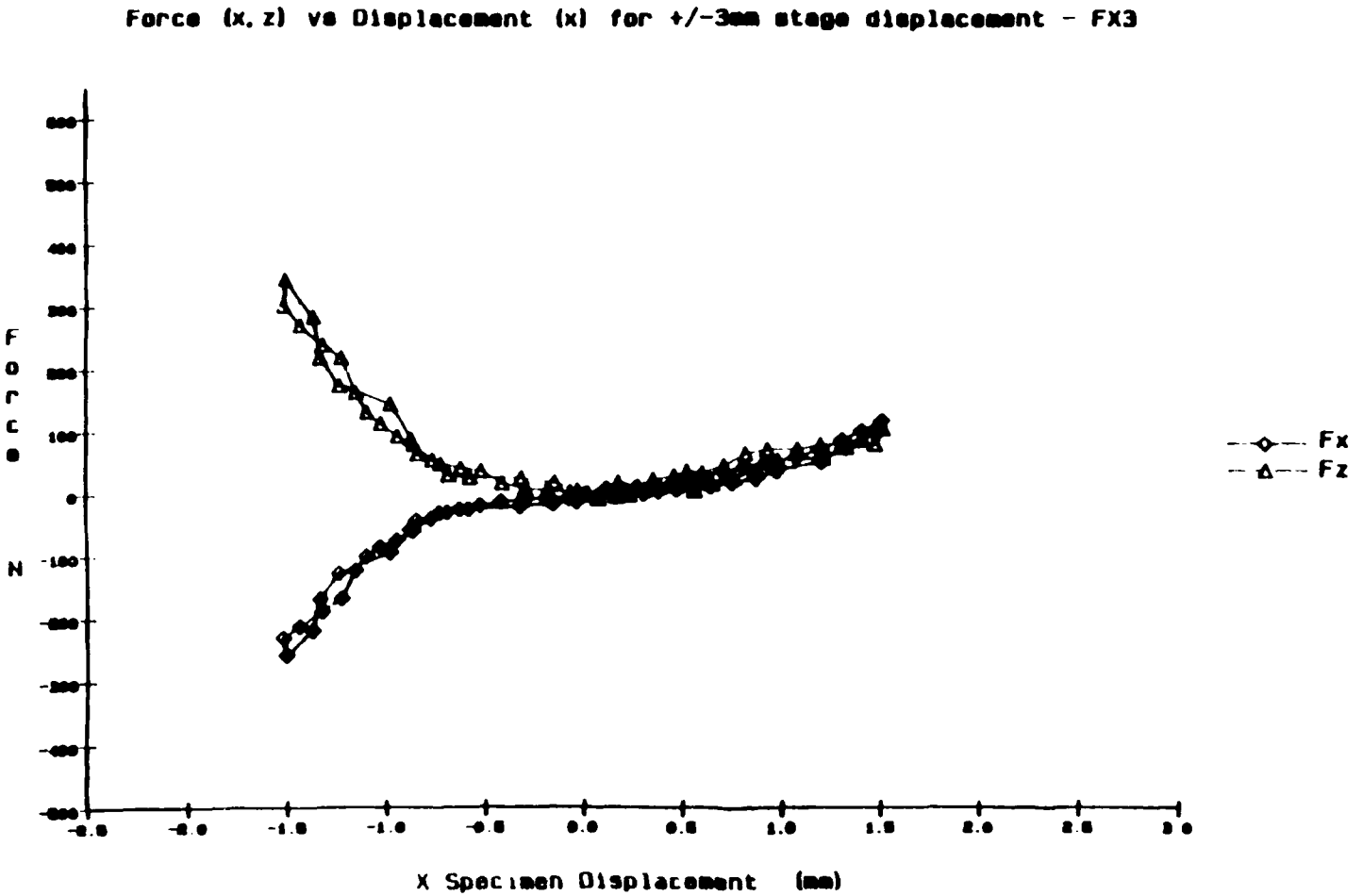

42.2 Specimen F

HX8XZVX

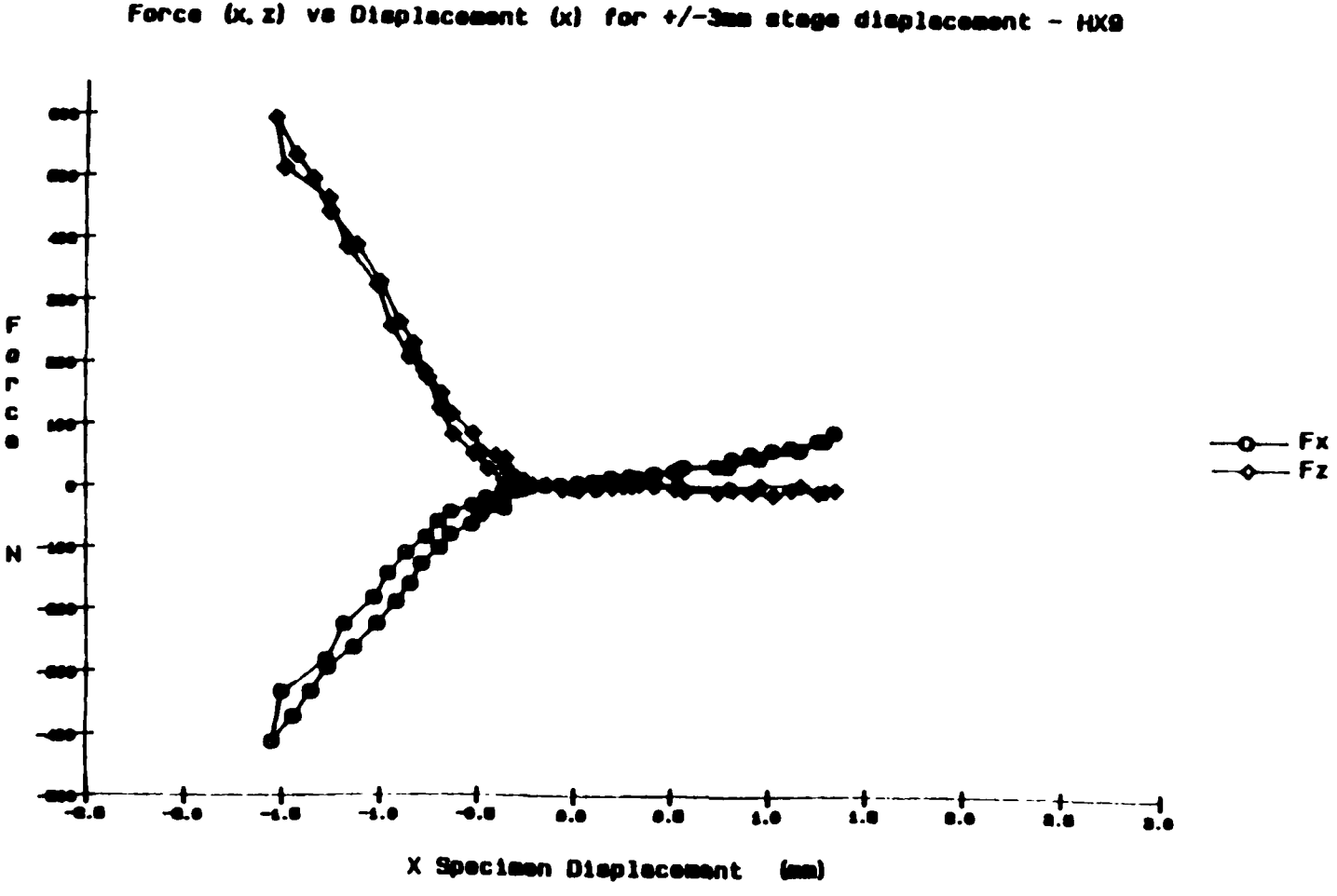

42.3 Specimen H

EX2XZVX

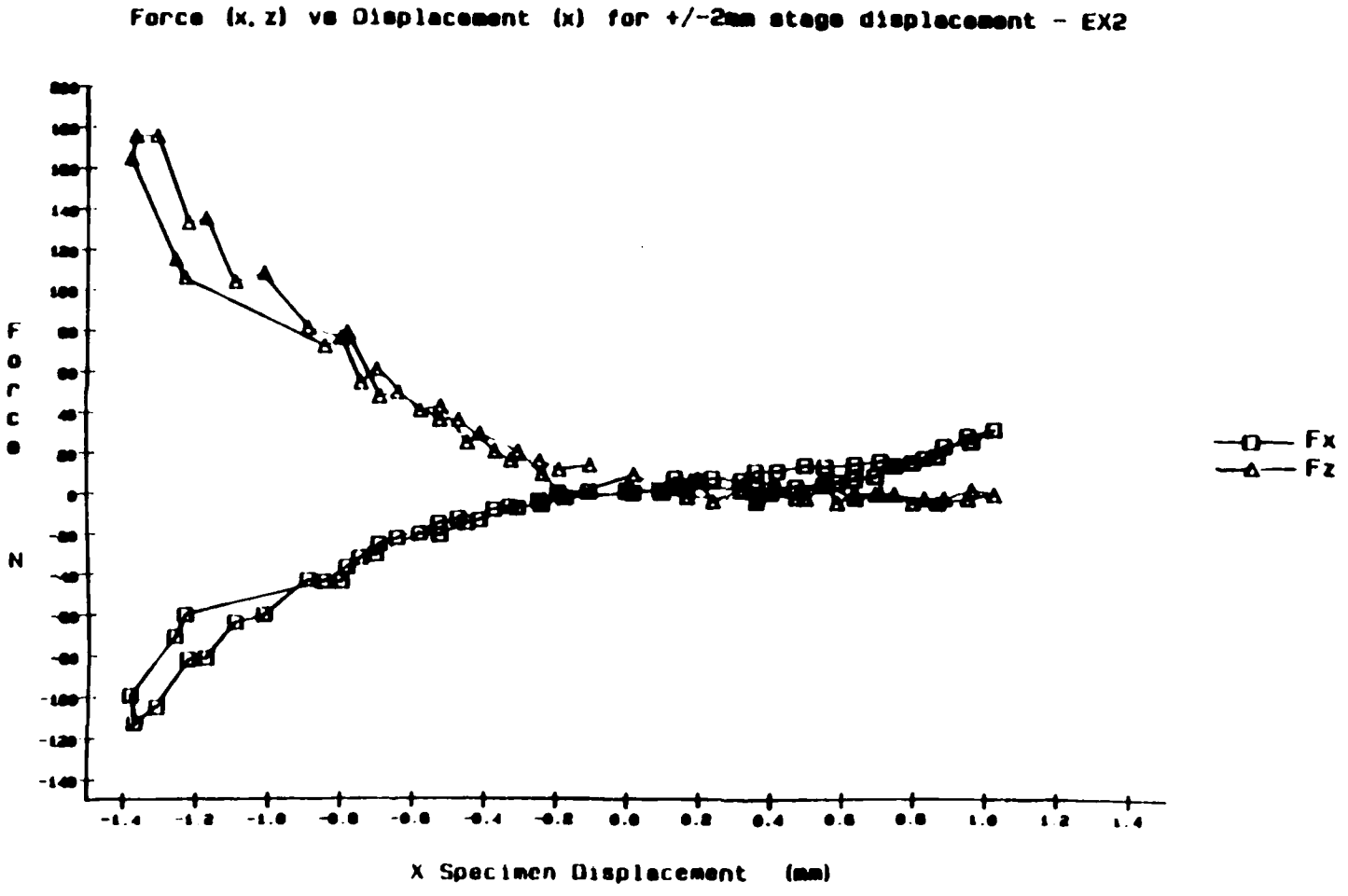

42.4 Specimen E

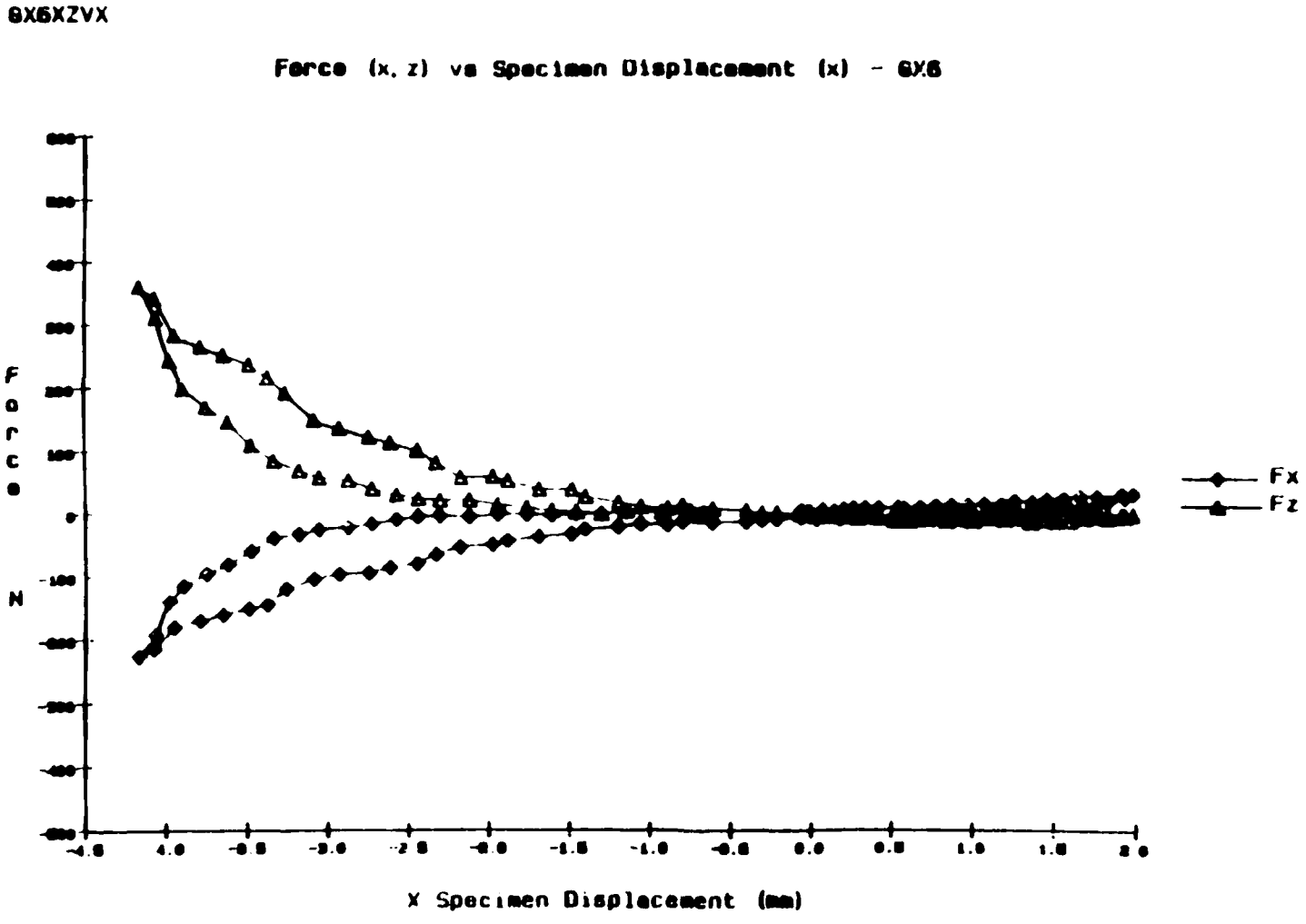

42.5 Specimen G

BX4XZVX

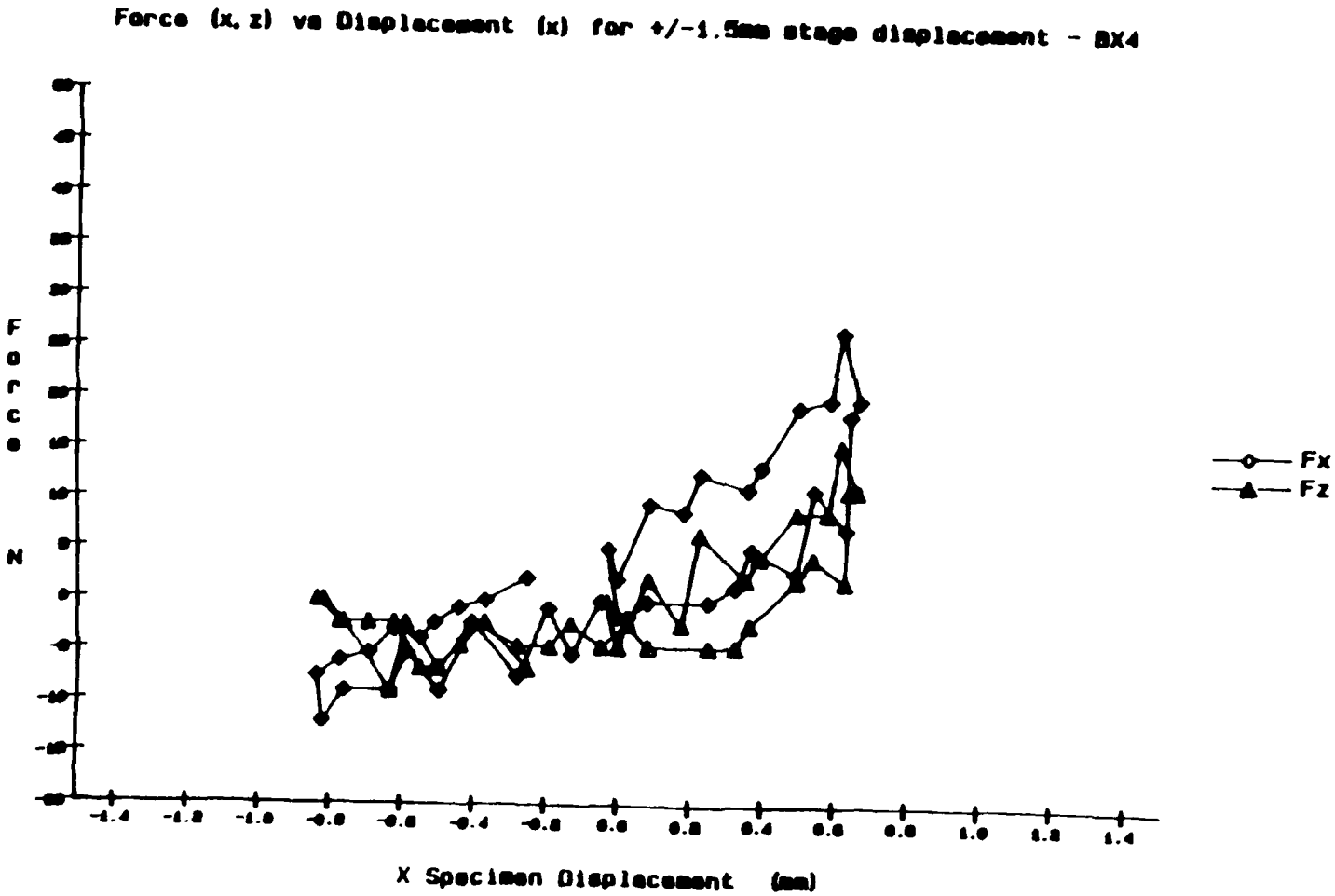

42.6 Specimen B

DX6XZVX

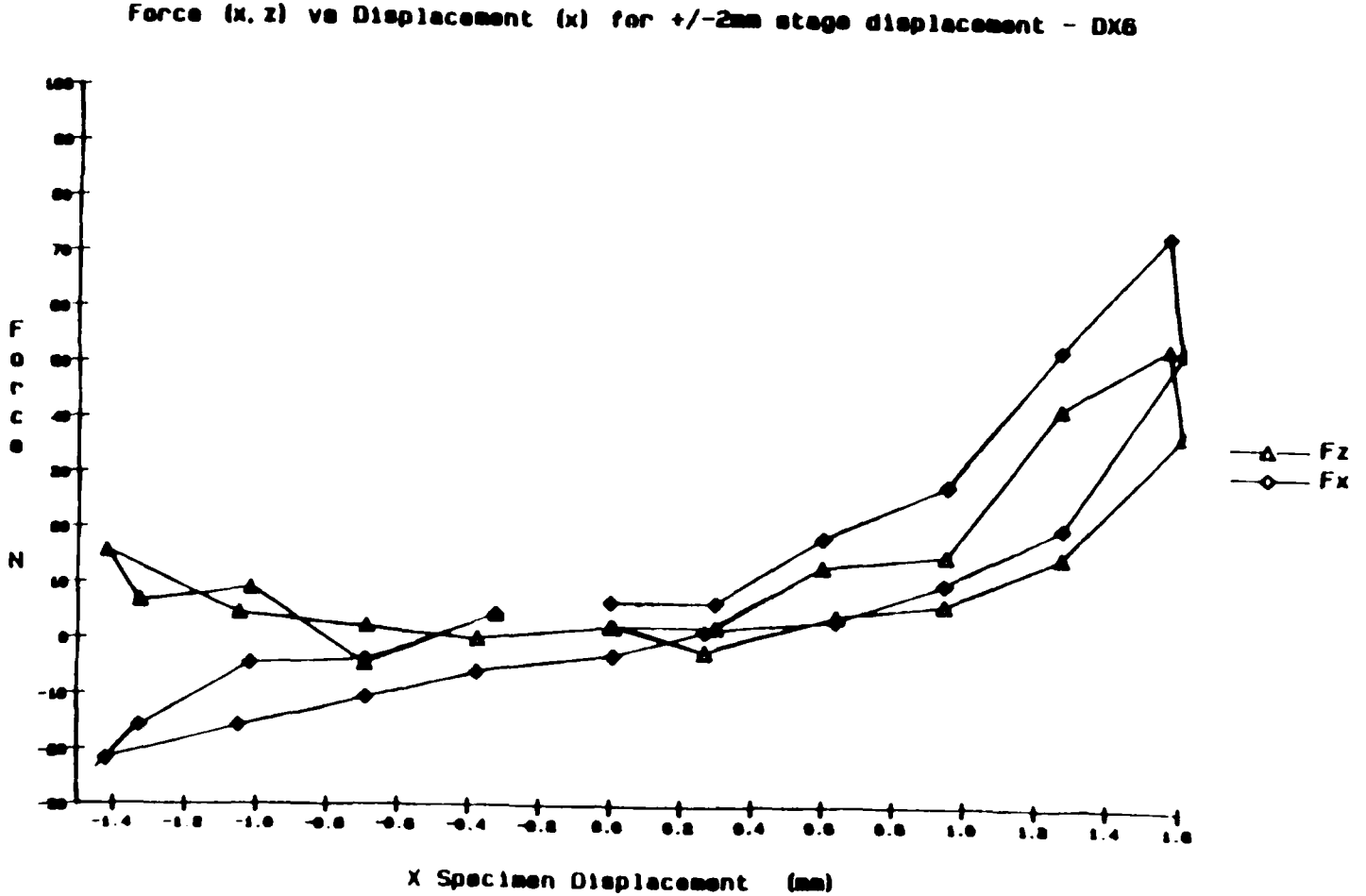

42.7 Specimen D

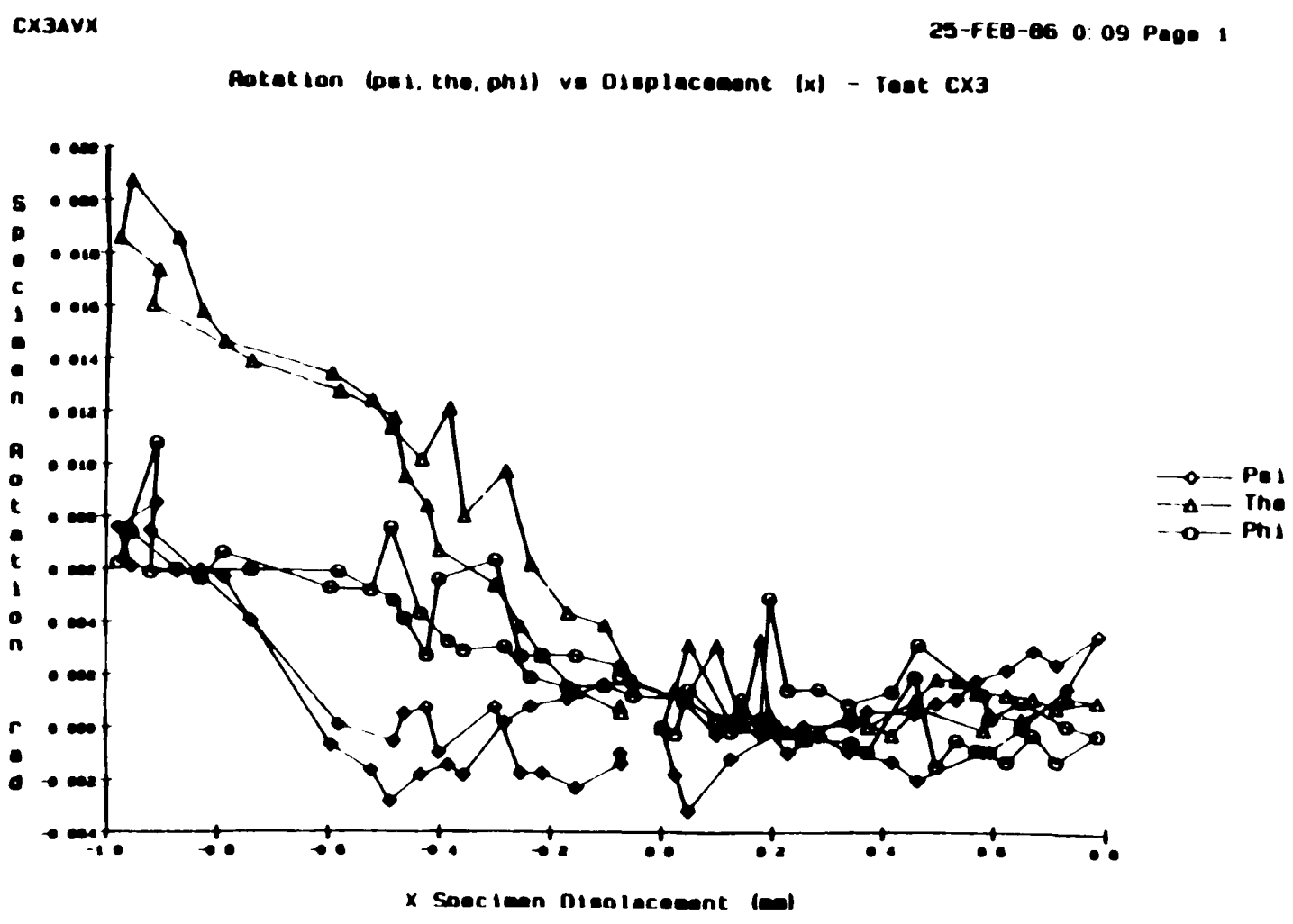

Figures:43.1-43.7 Rotation (psi, the, phi) vs displacement for 7 specimens

43.1 Specimen 1

FX3AVX

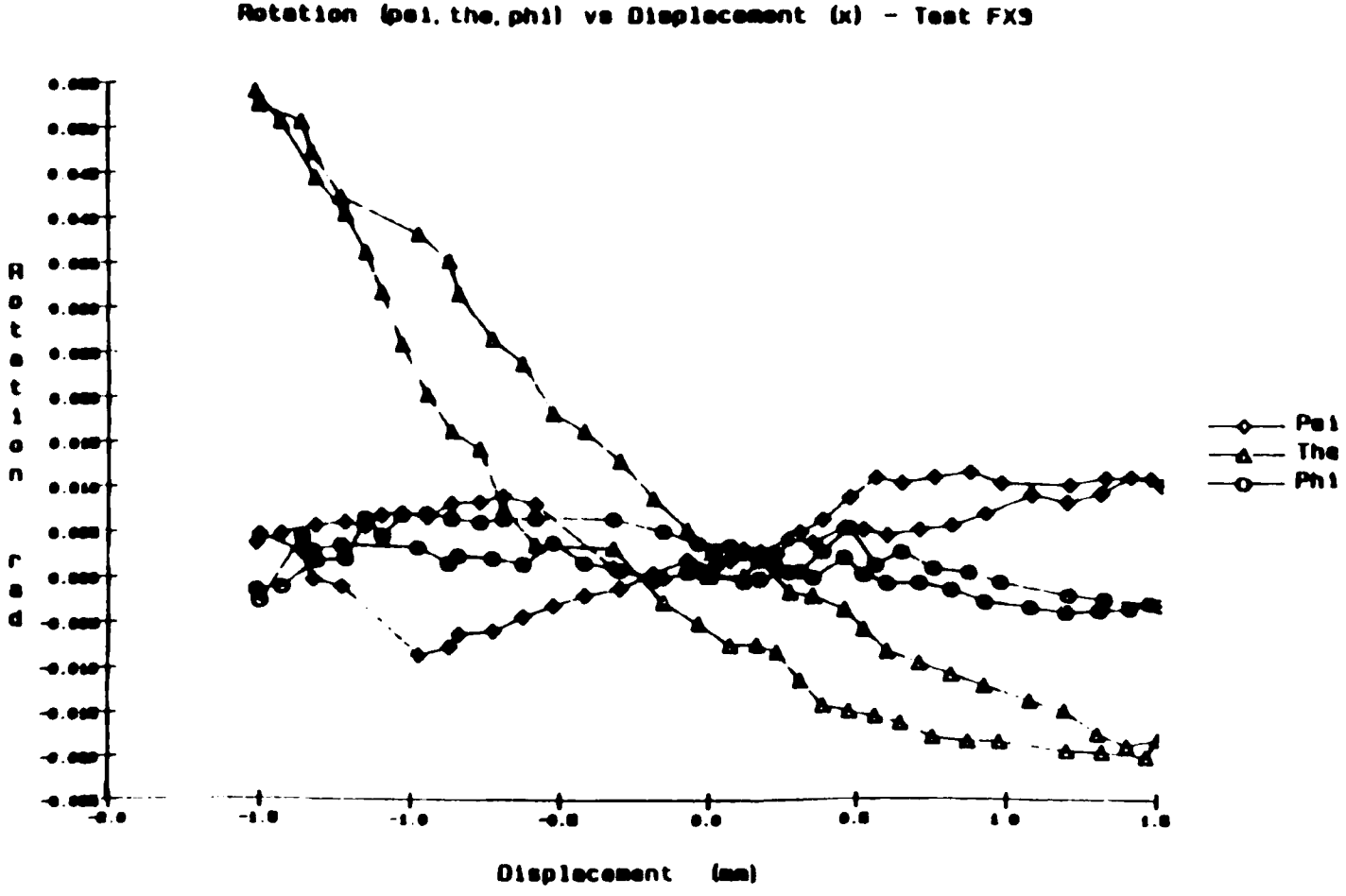

43.2 Specimen F

HX9AVX

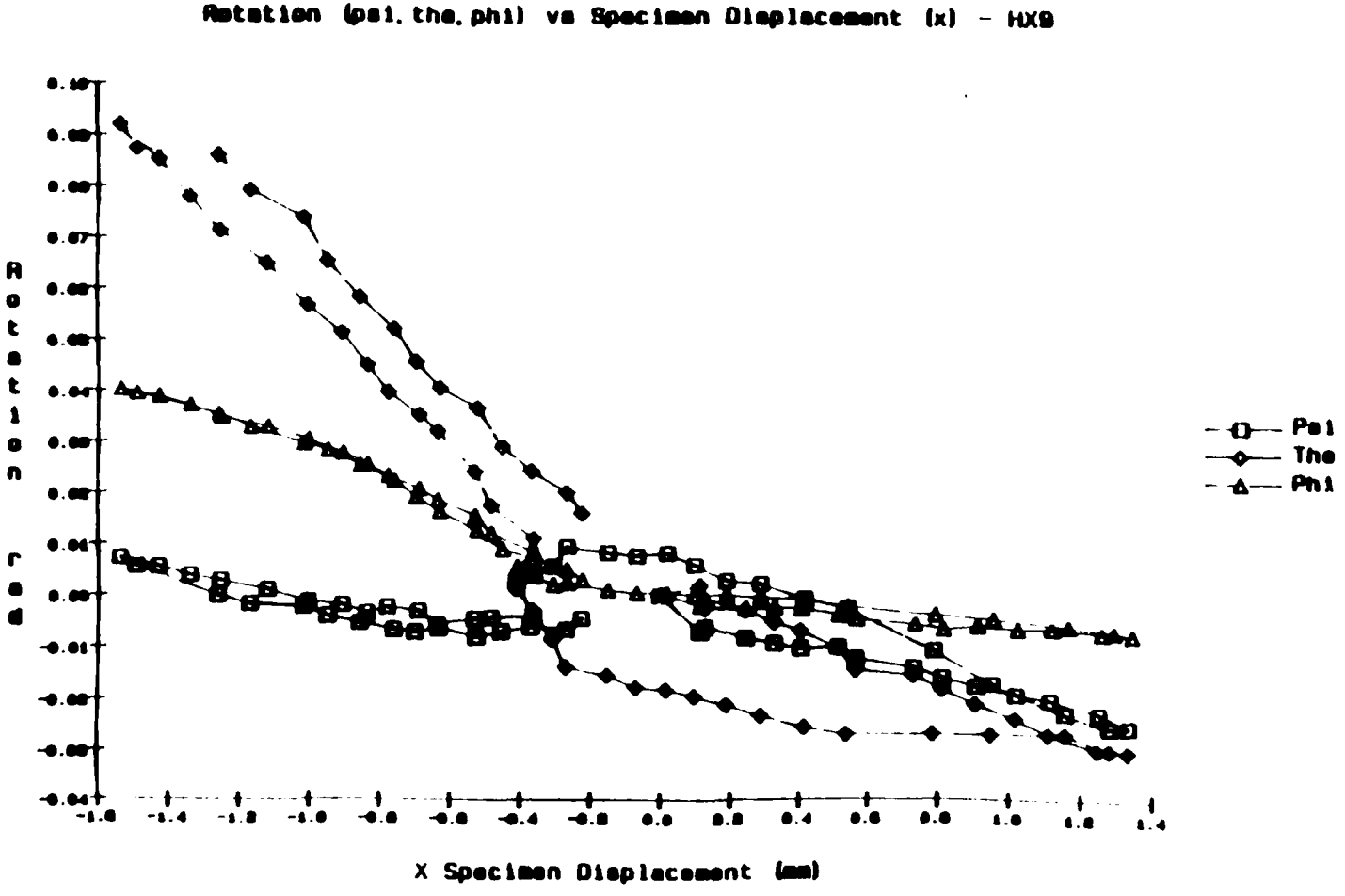

43.3 Specimen H

EX2AVX

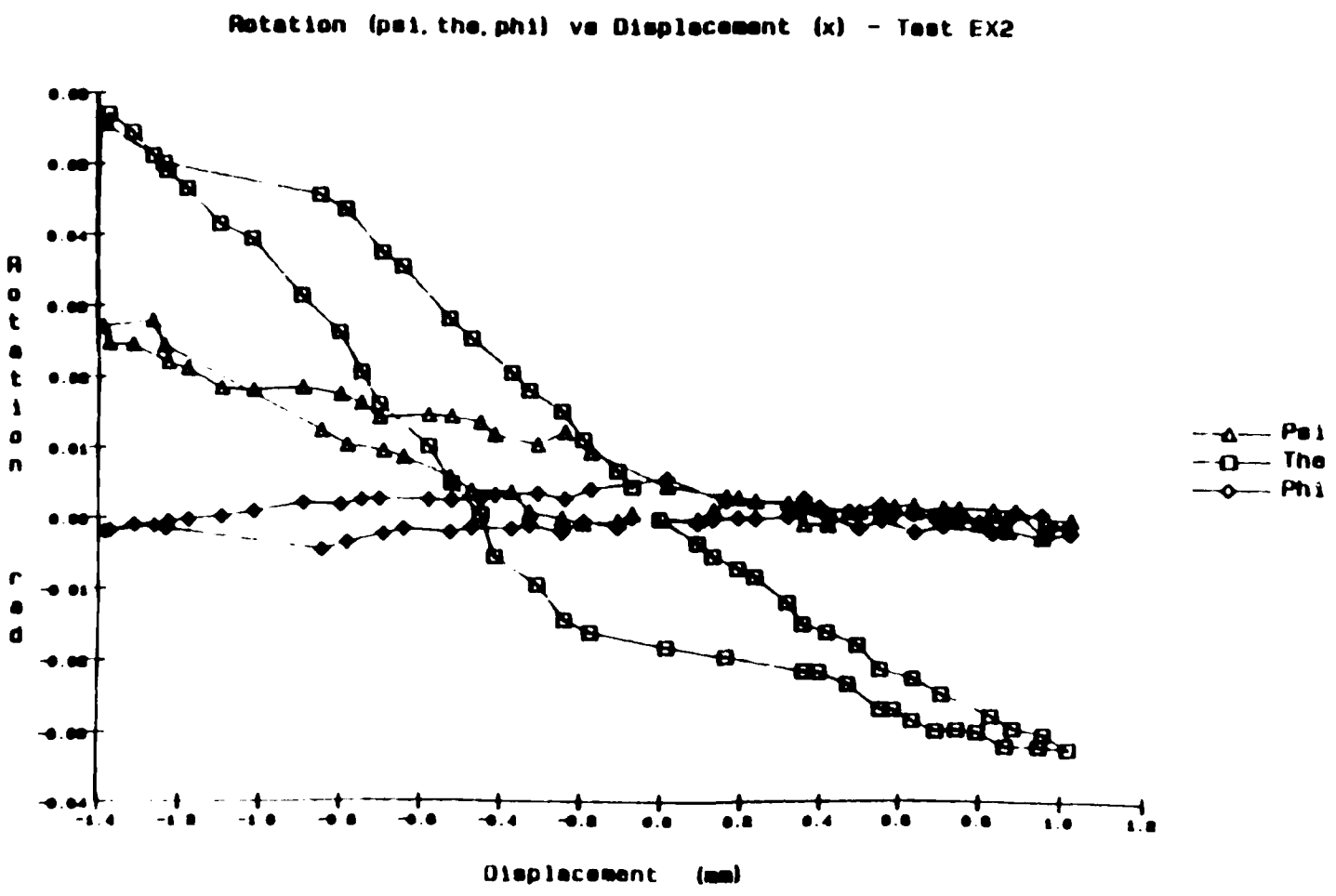

4.4 Specimen E

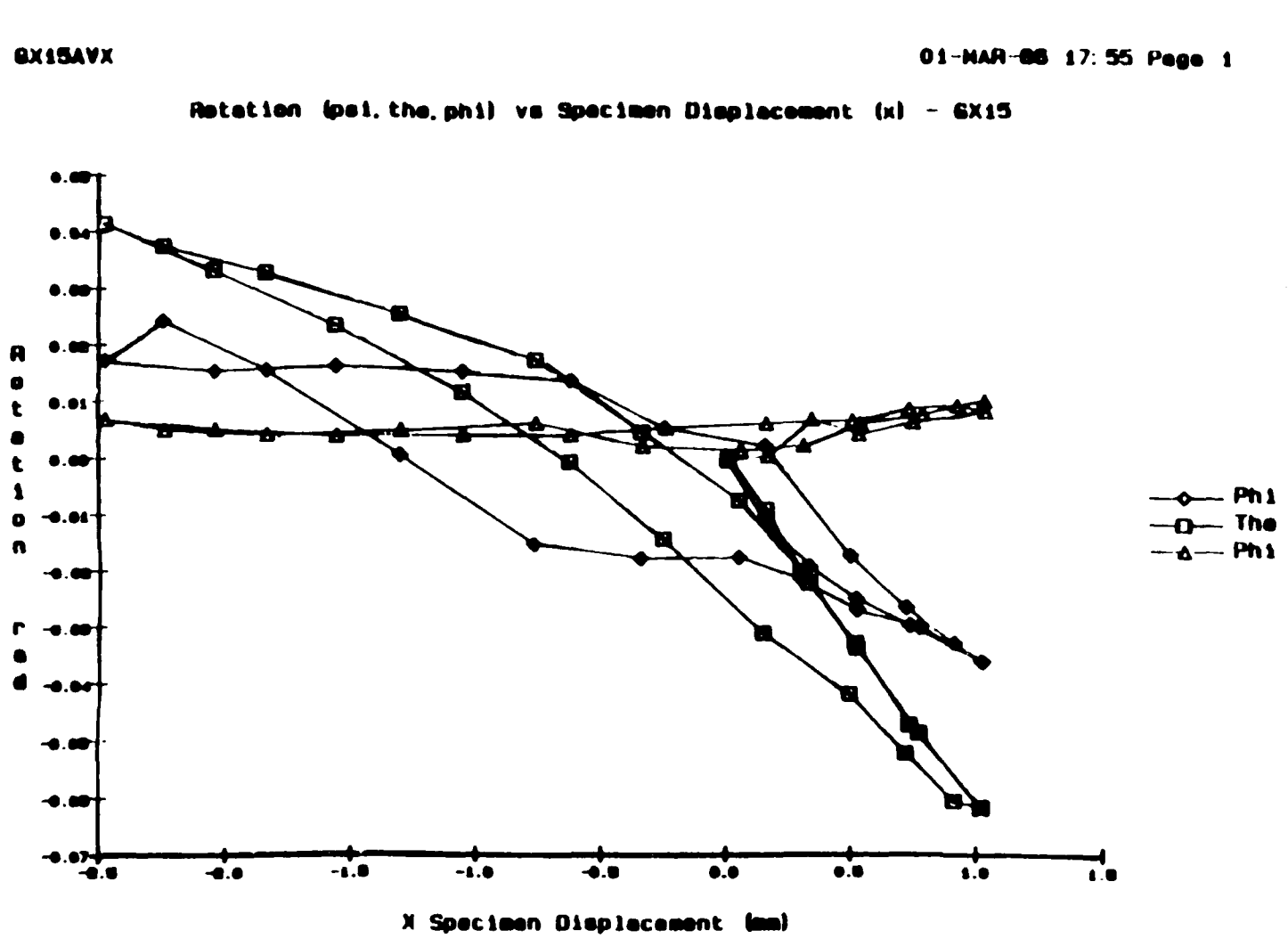

43.5 Specimen G

BX4AVX

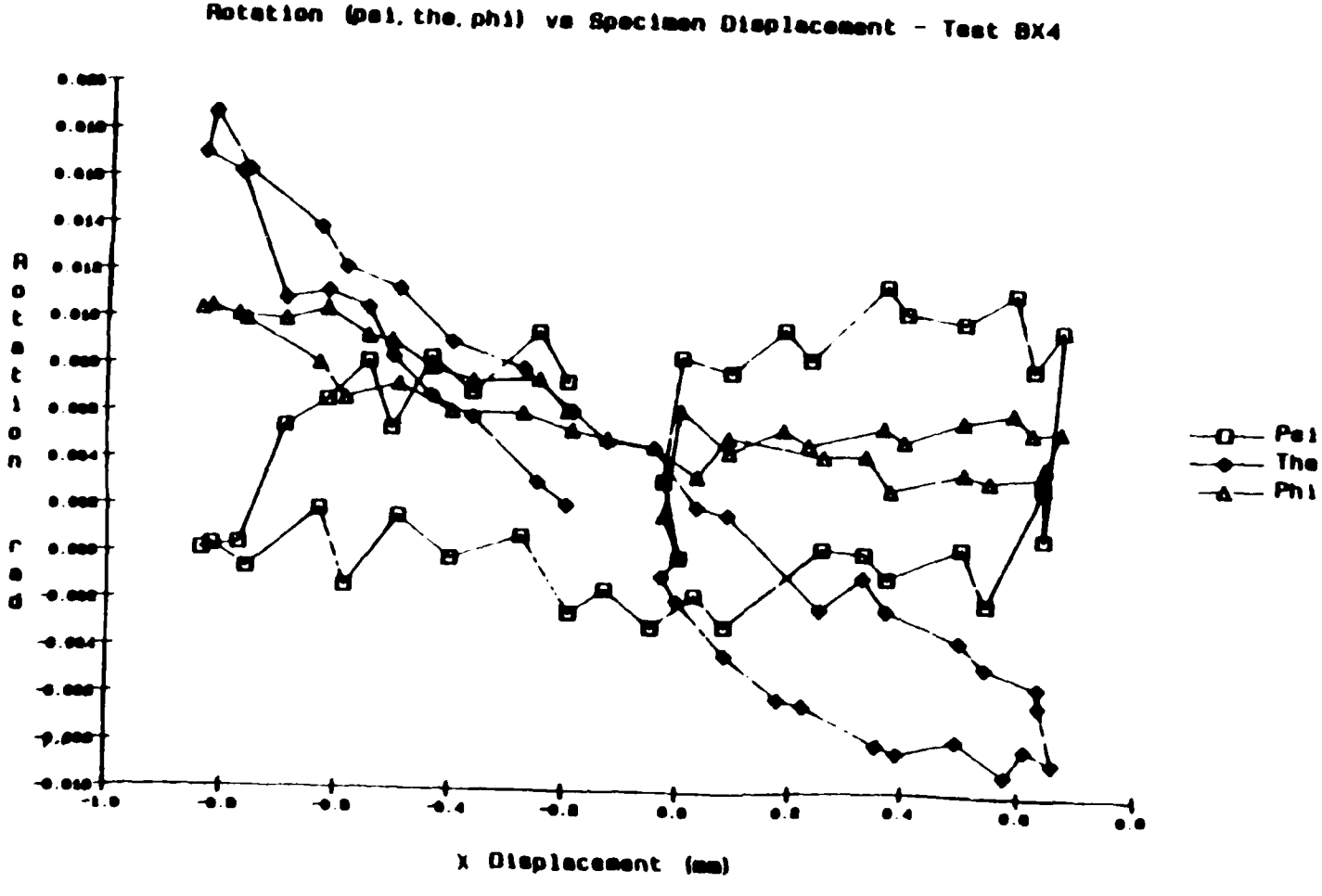

43.6 Specimen B

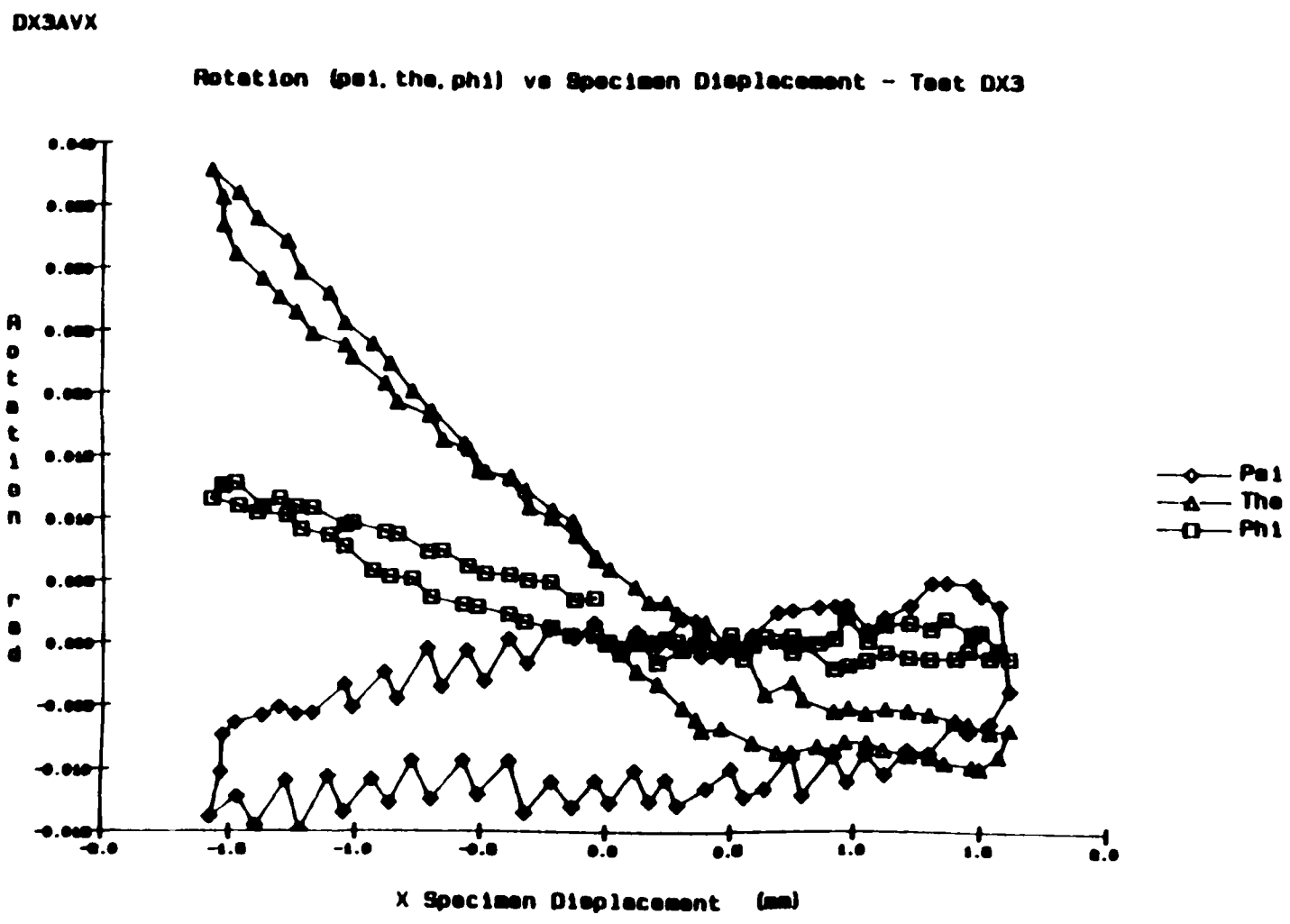

43.7 Specimen D

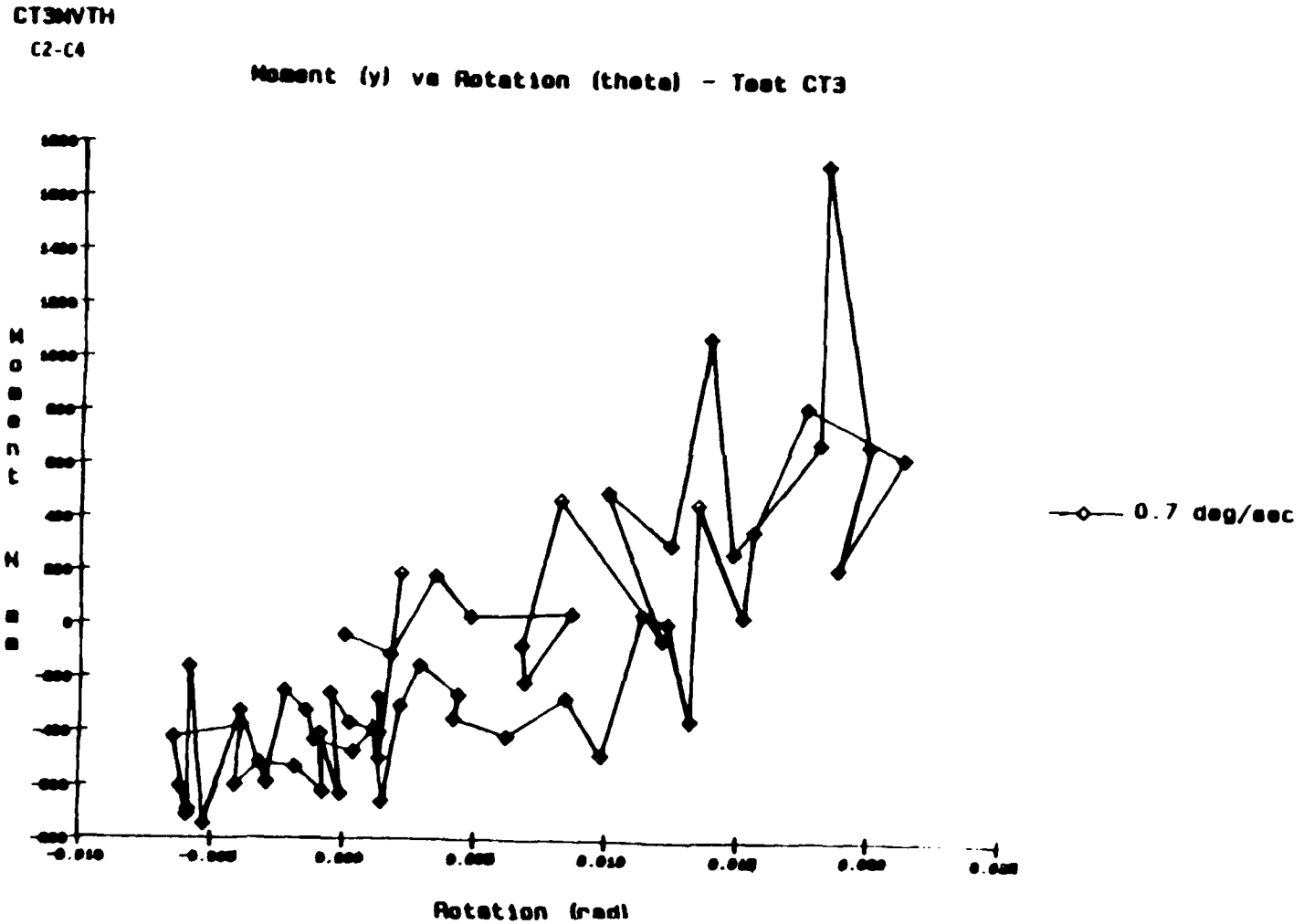

Figures:44.1-44.7 Moment (y) vs rotation (theta) for 7 specimens

44.1 Specimen C

FT6MVTH
C2-C4

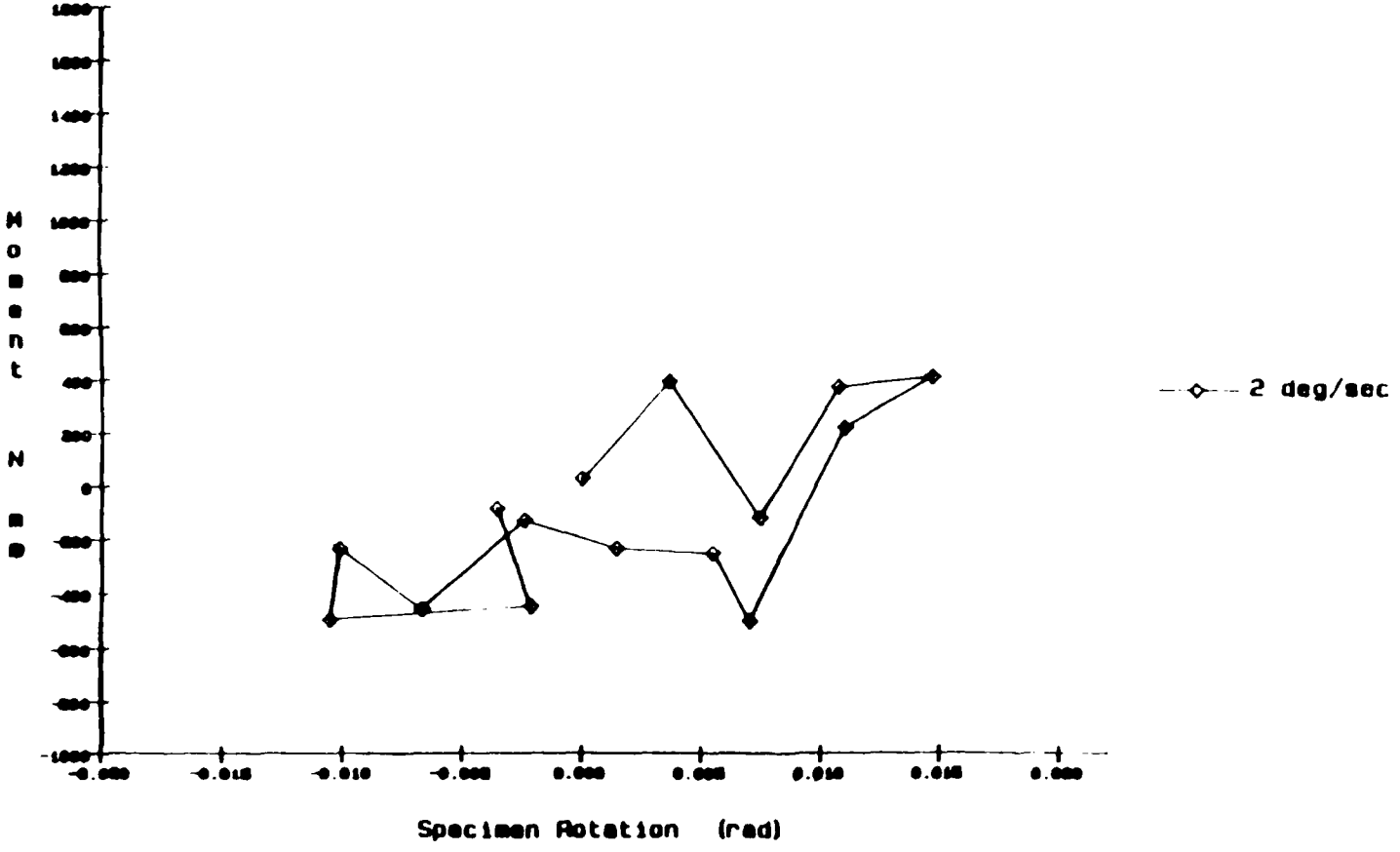

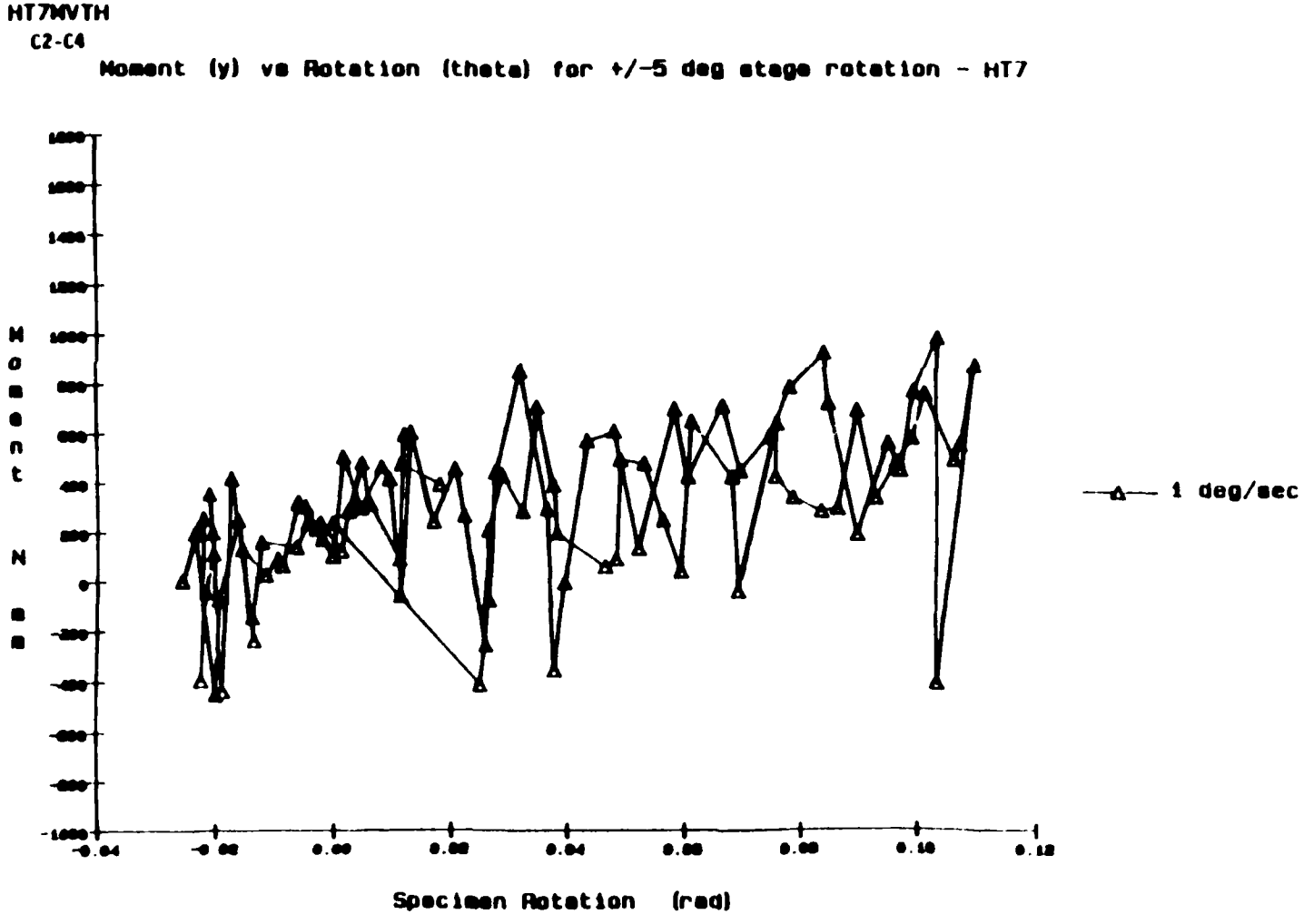

44.3 Specimen H

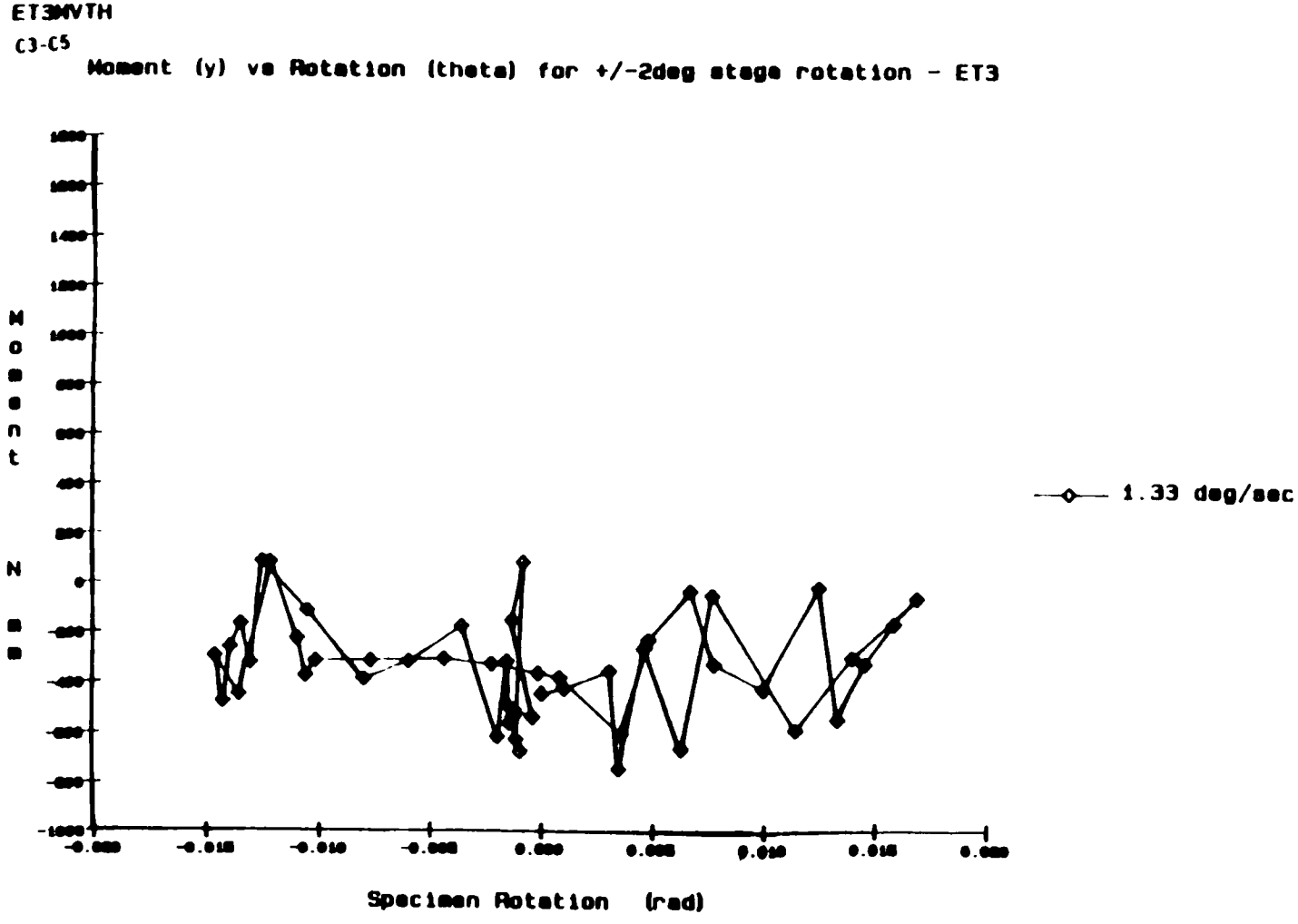

44.4 Specimen E

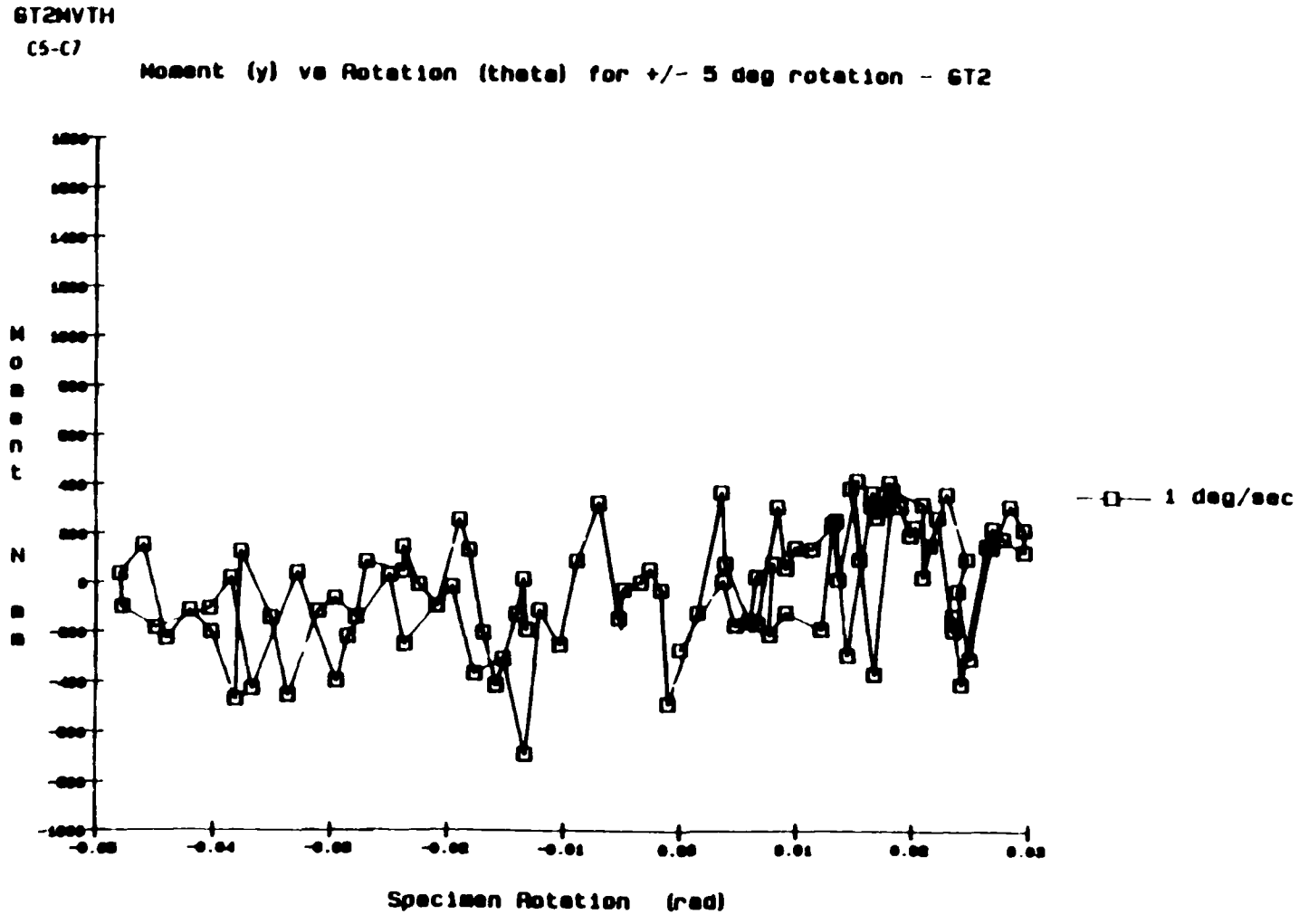

44.5 Specimen G

BT1MVTH
C6-T1

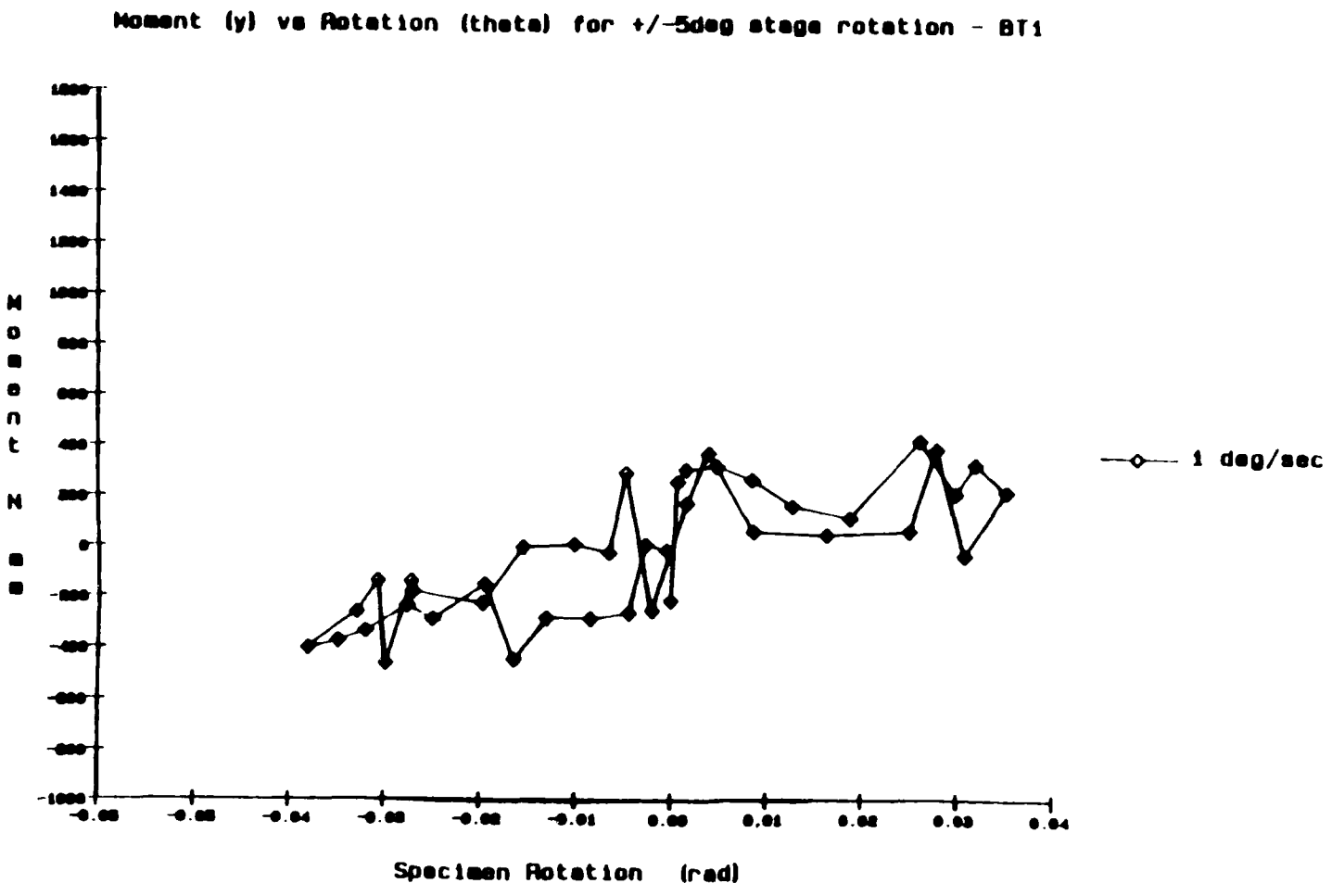

44.6 Specimen B

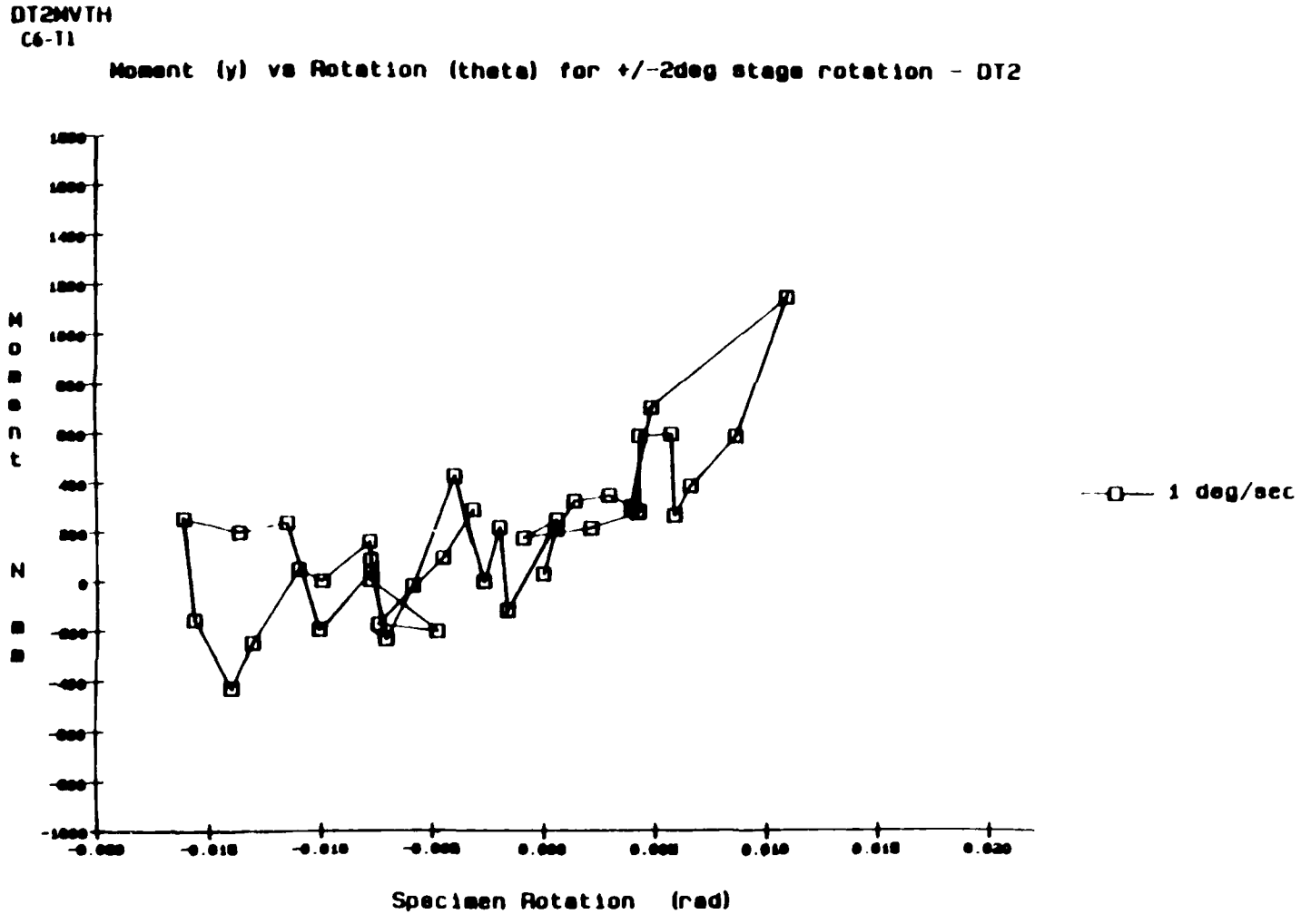
DT2MVTH
C6-T1
Moment (y) vs Rotation (theta) for +/-2deg stage rotation - DT2
Moment
N m
Specimen Rotation (rad)
1 deg/sec

CT3XZVTH

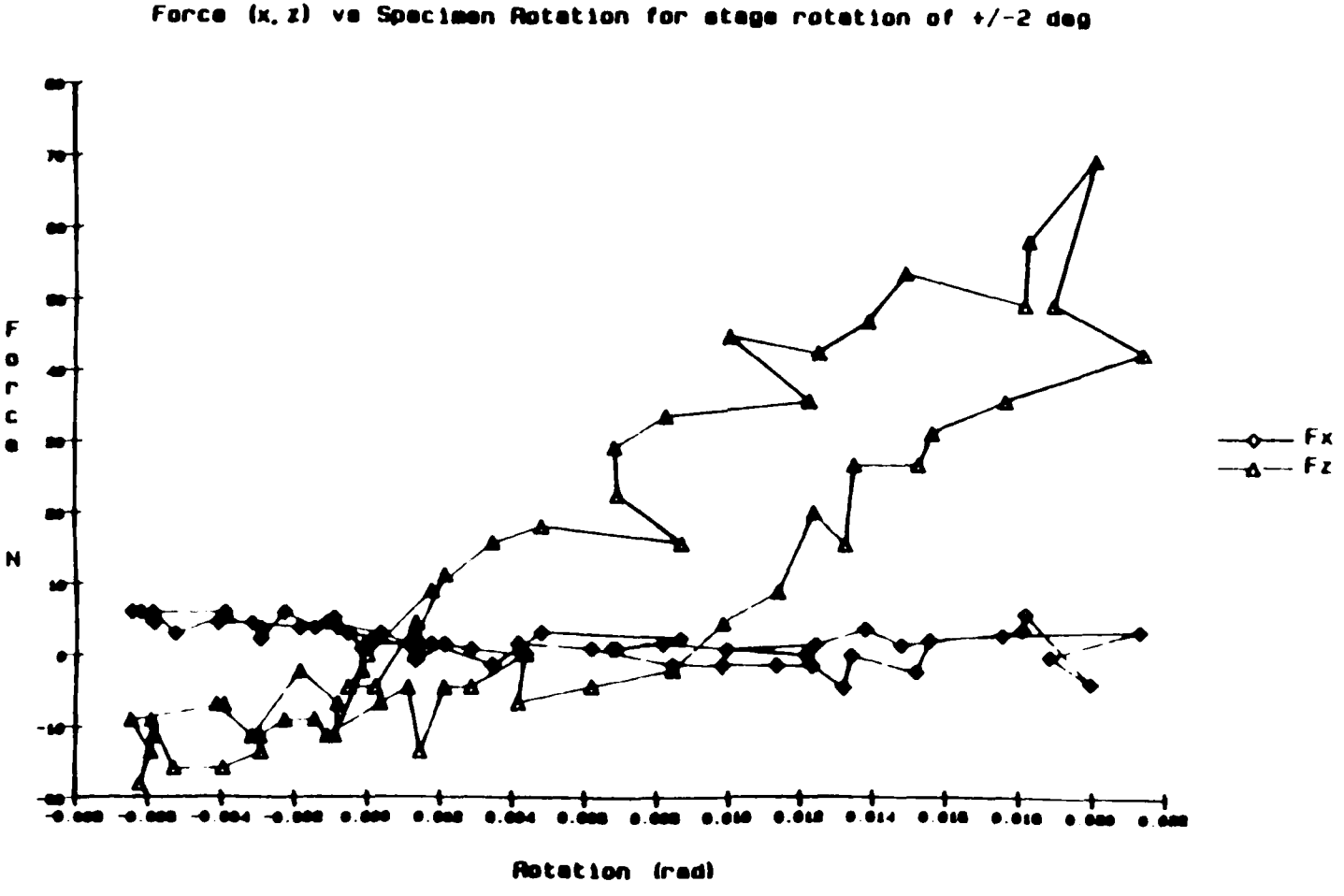

Figures:45.1-45.6 Force (x,y) vs stage rotation for 6 specimens

45.1 Specimen C

FT8XZVTH

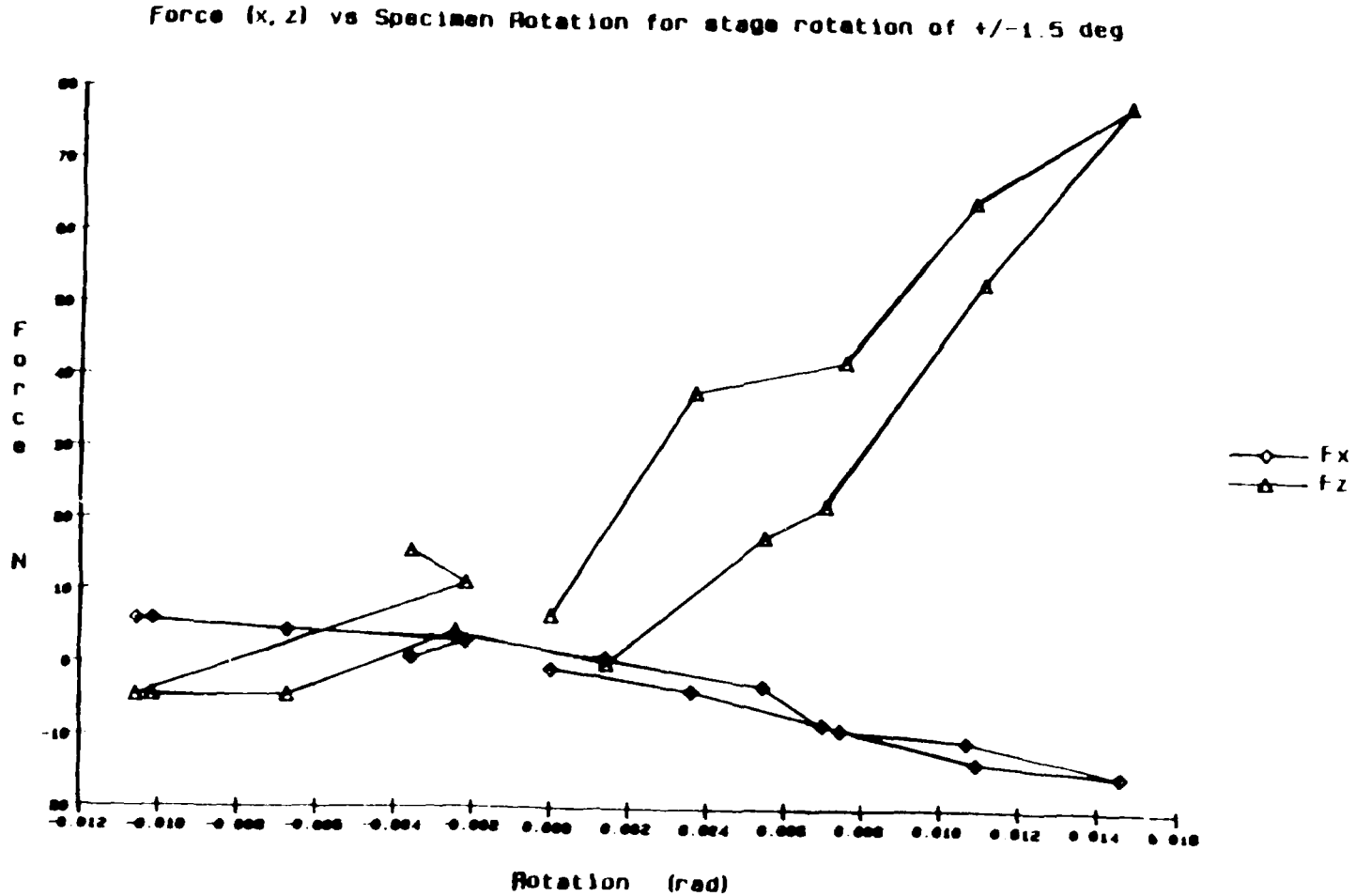

45.2 Specimen F

HT@XZVTH

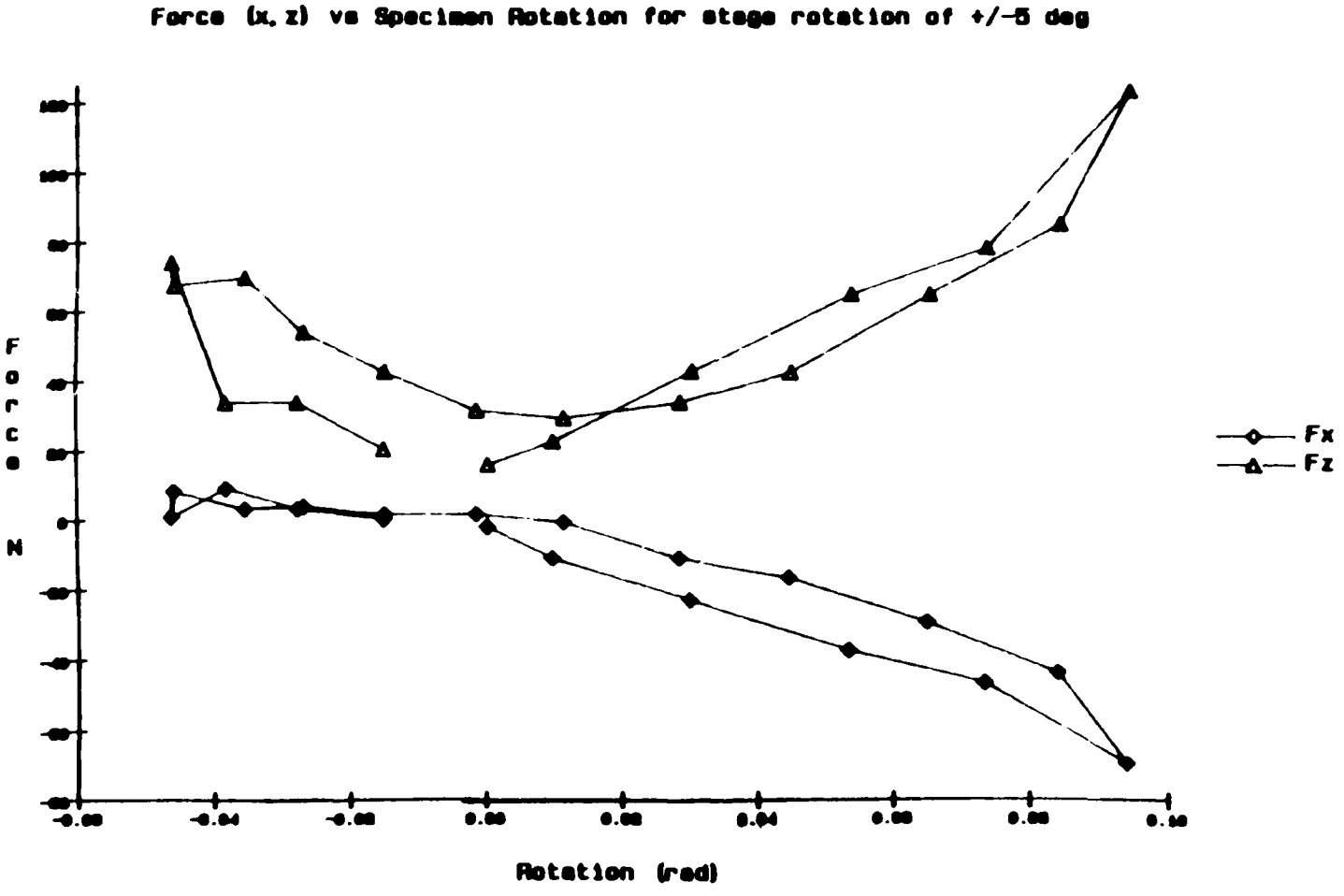

45.3 Specimen H

ET3XZVTH

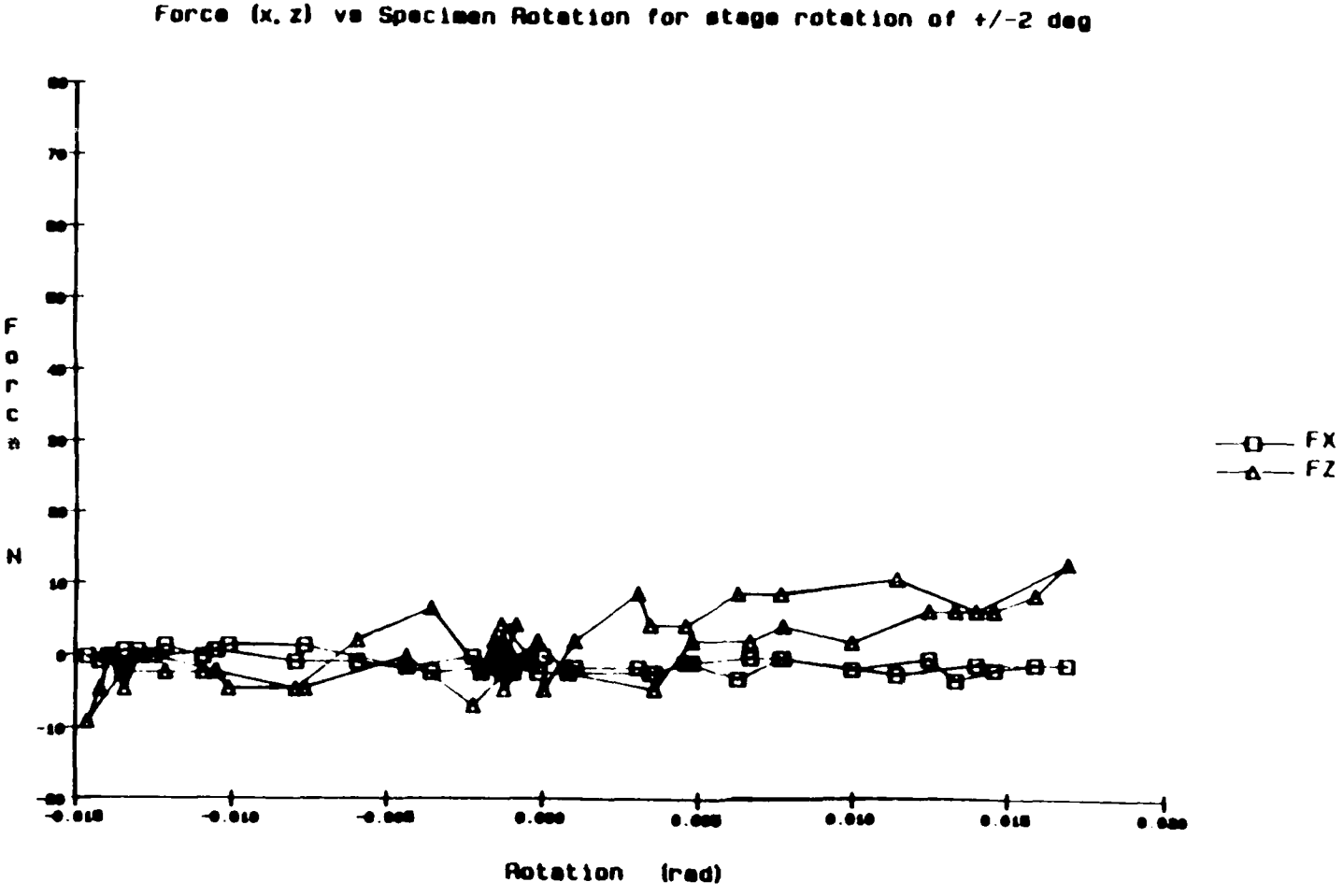

45.4 Specimen E

GT7XZVTH

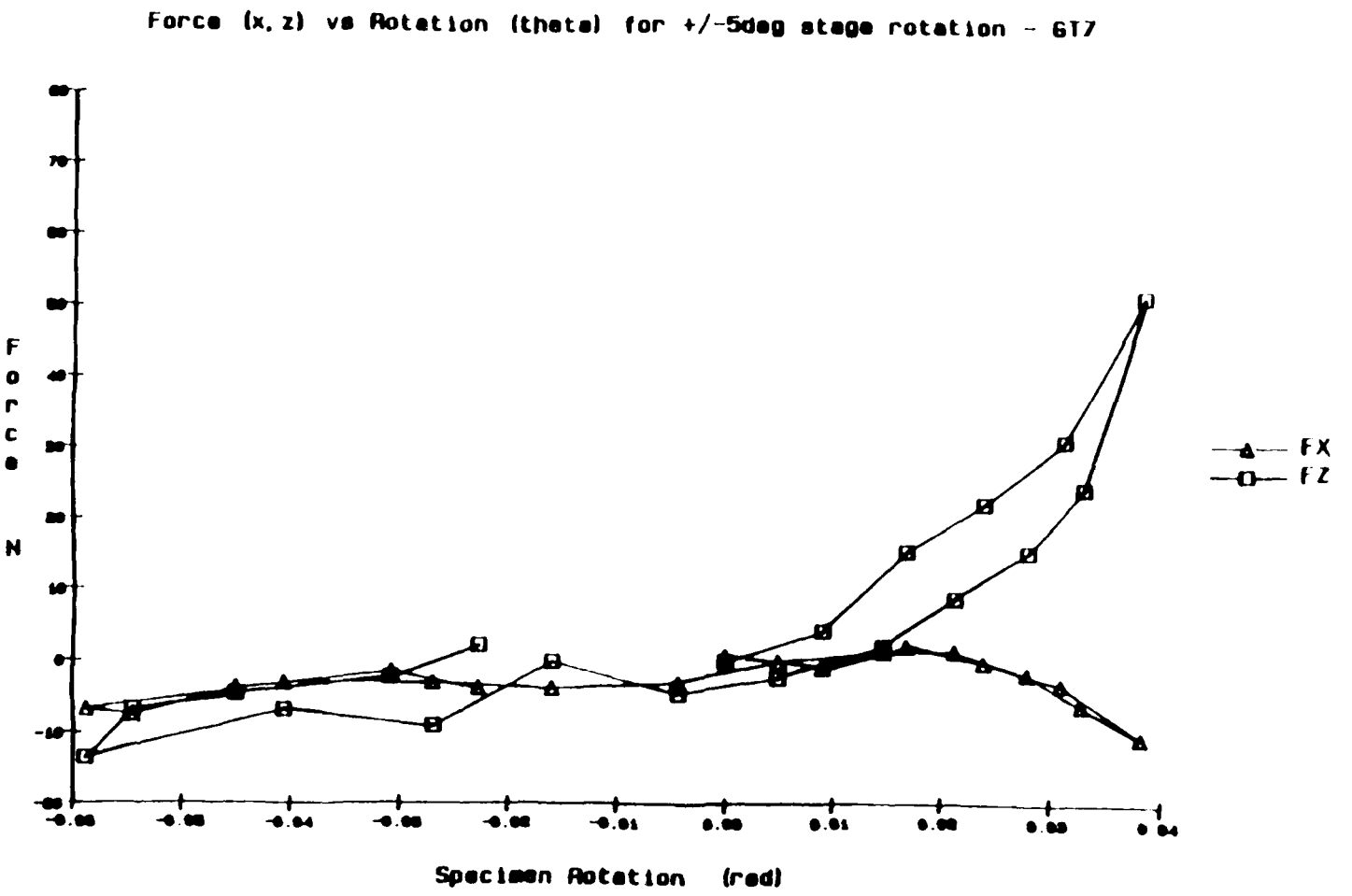

45.5 Specimen G

BT1XZ\.H

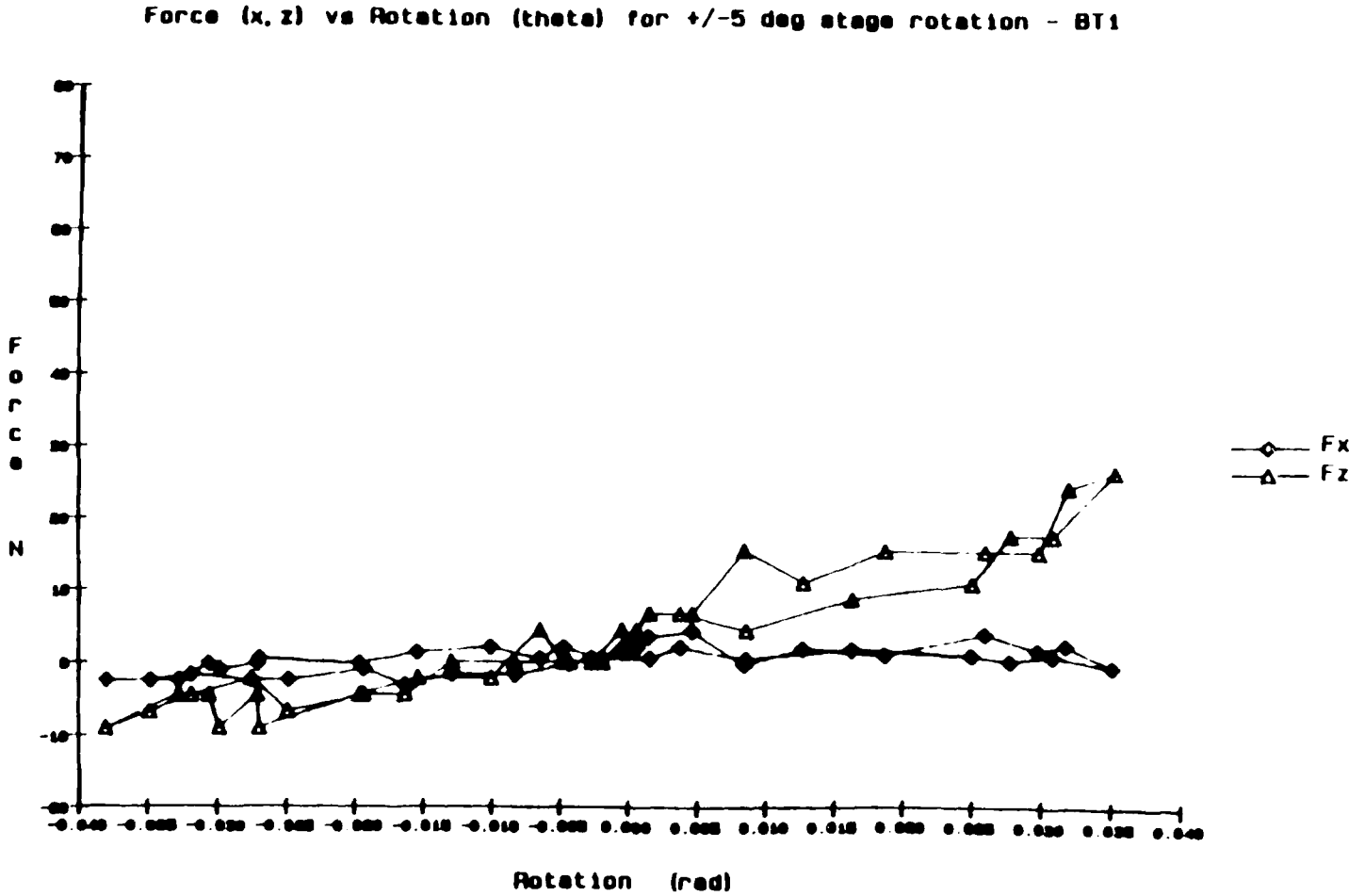

45.6 Specimen B

FT7AMVTH

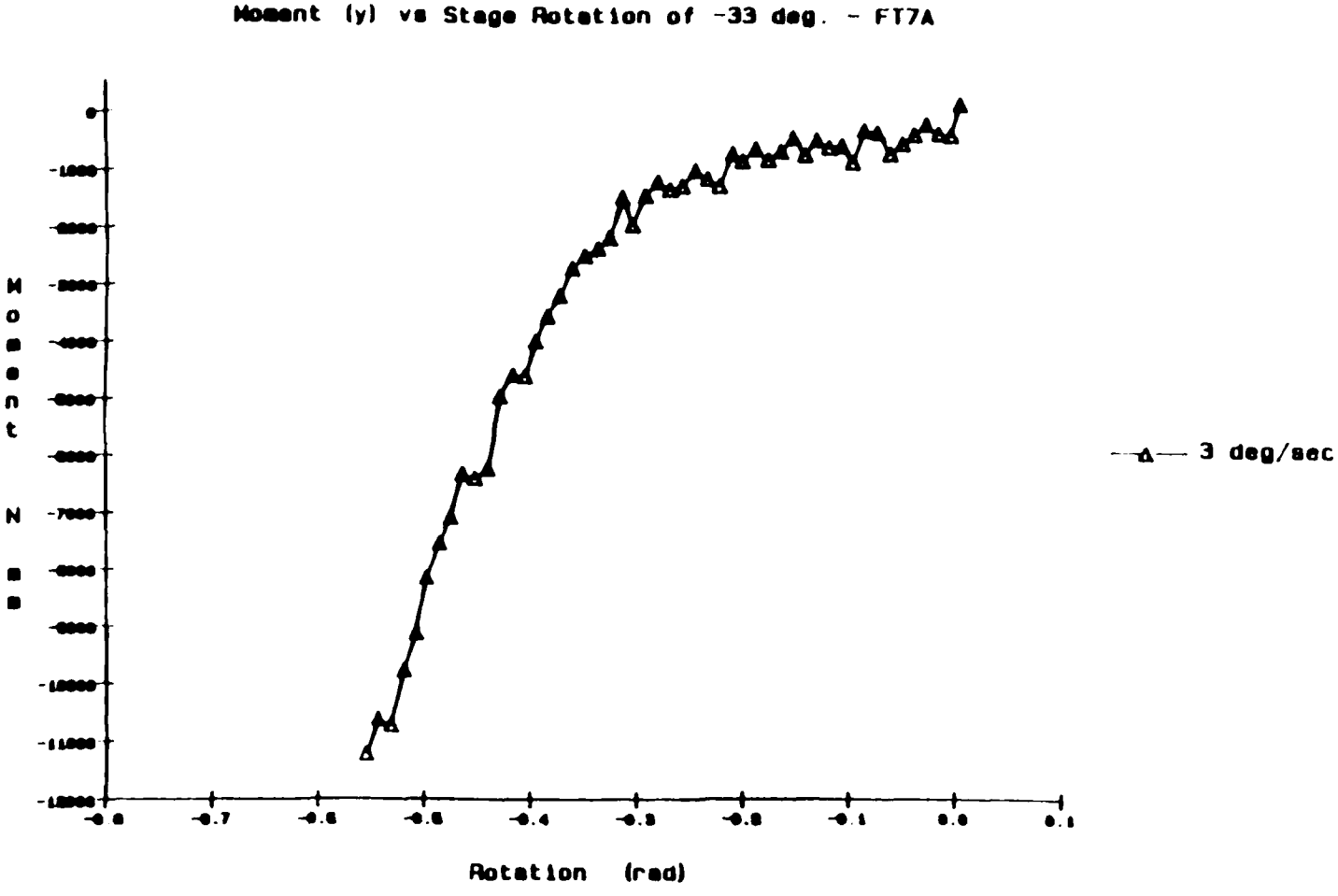

Figures:46.1-46.6 Moment (y) vs rotation (theta) at large angles for 6 specimens

46.1 Specimen F

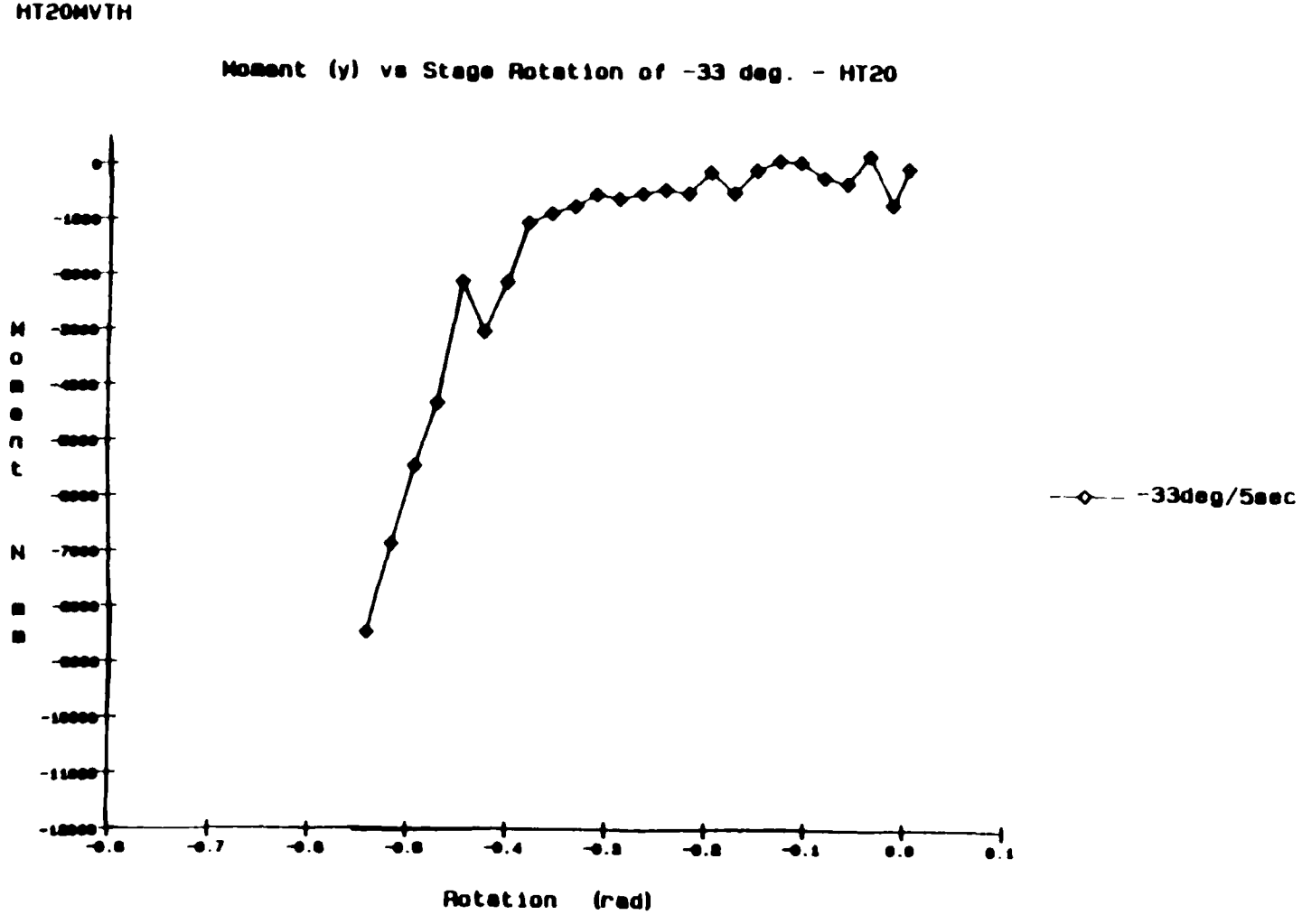

46.2 Specimen H

ET10MVTH

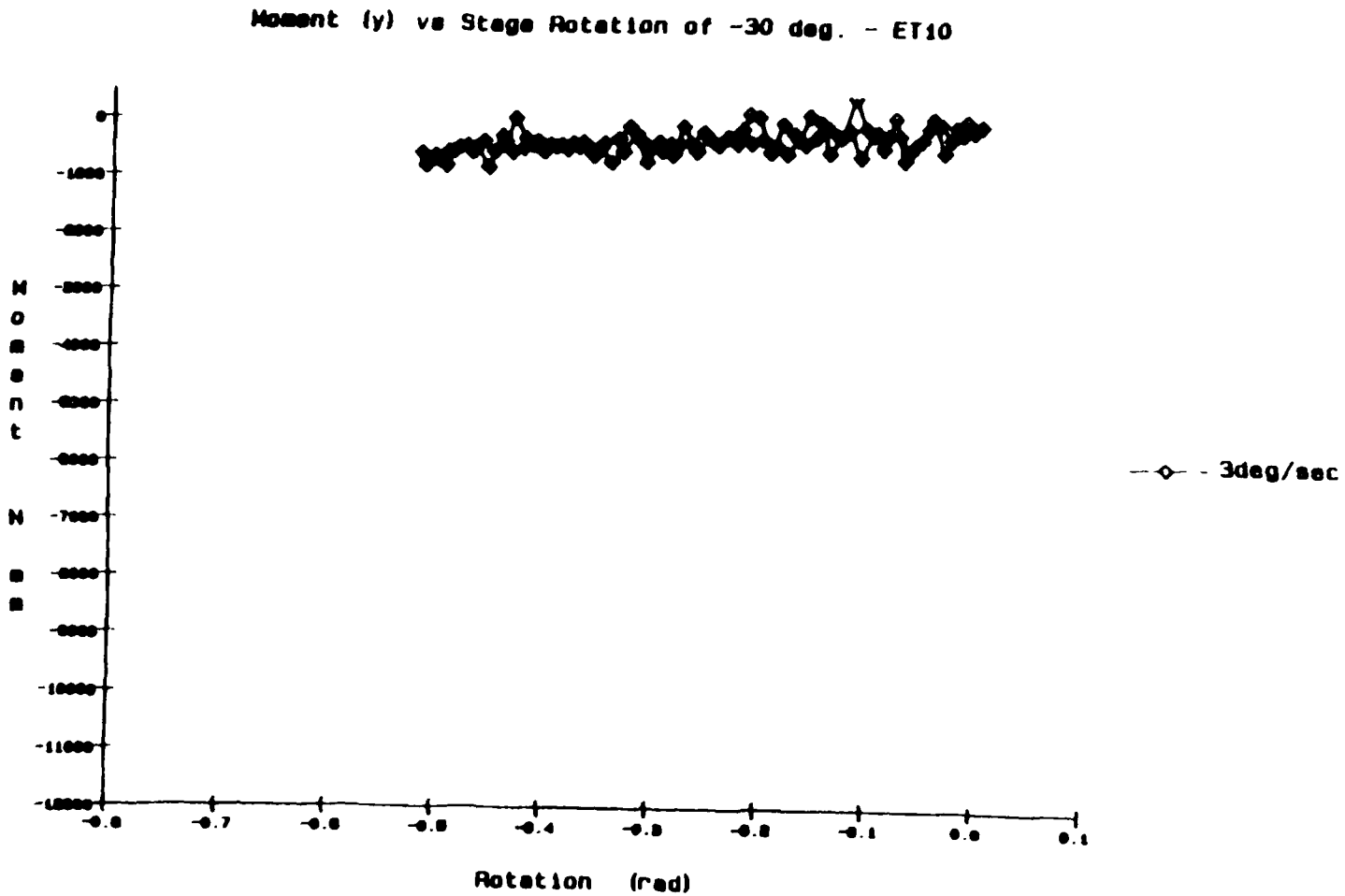

46.3 Specimen E

GT15MVTH

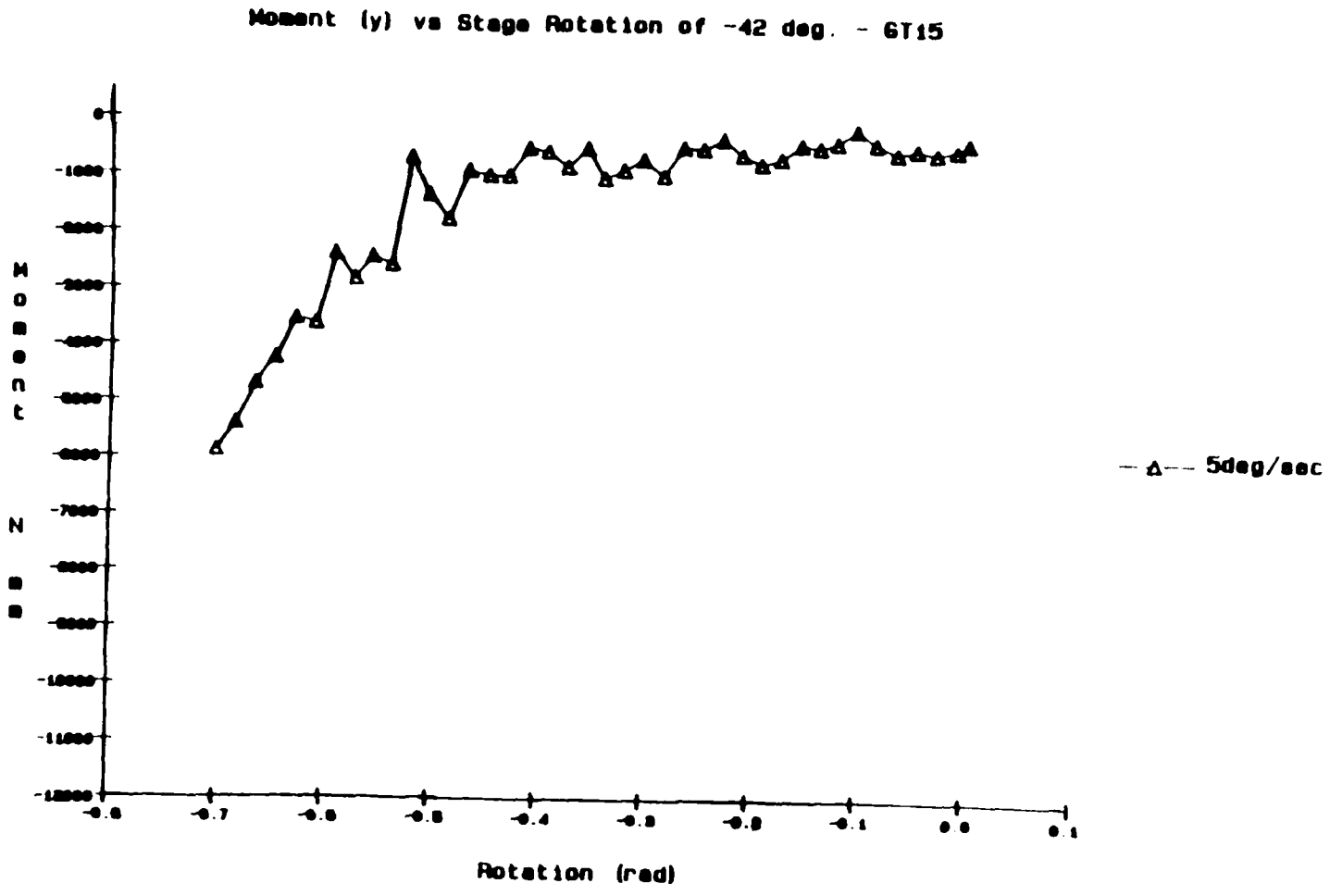

46.4 Specimen G

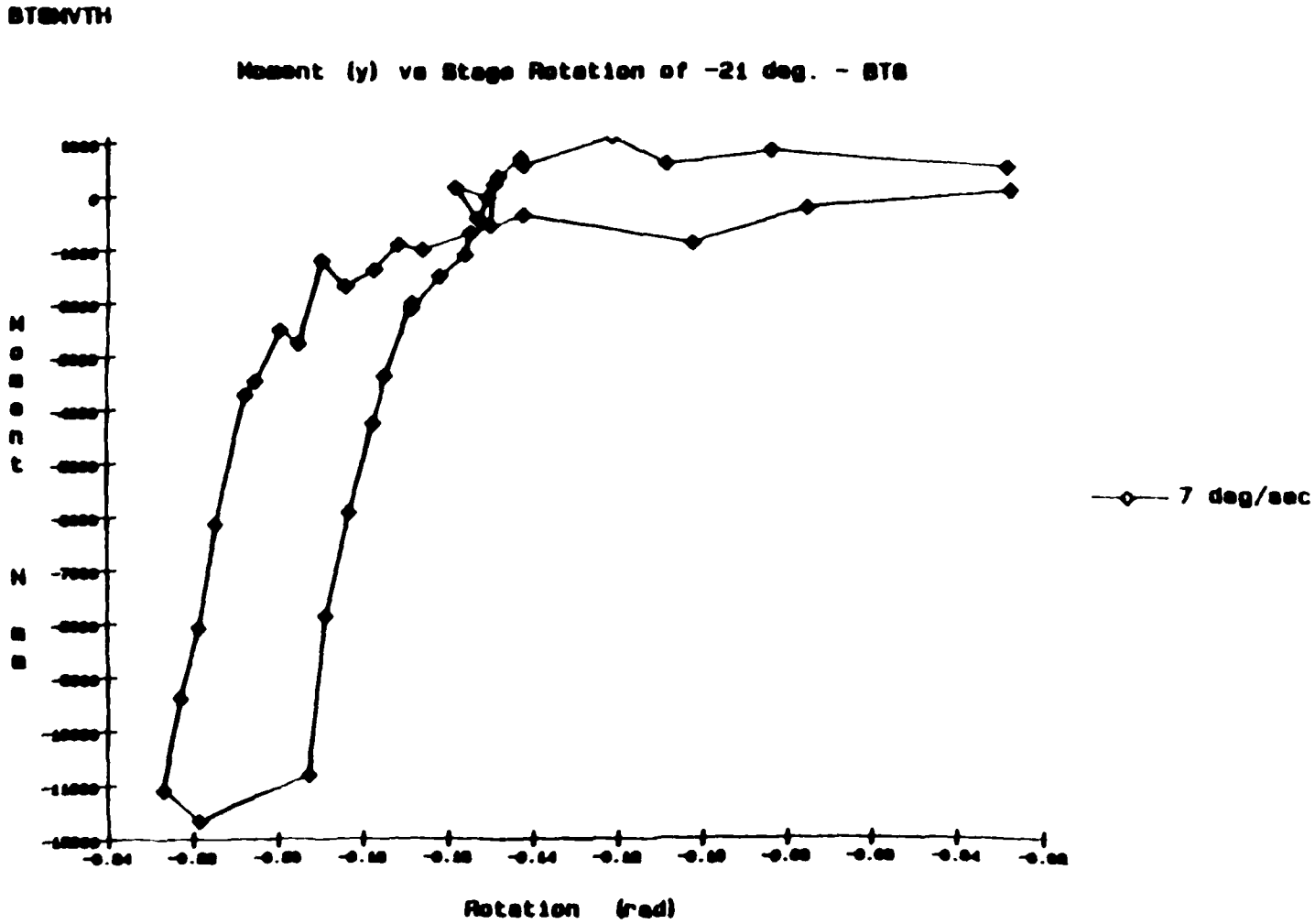

46.5 Specimen B

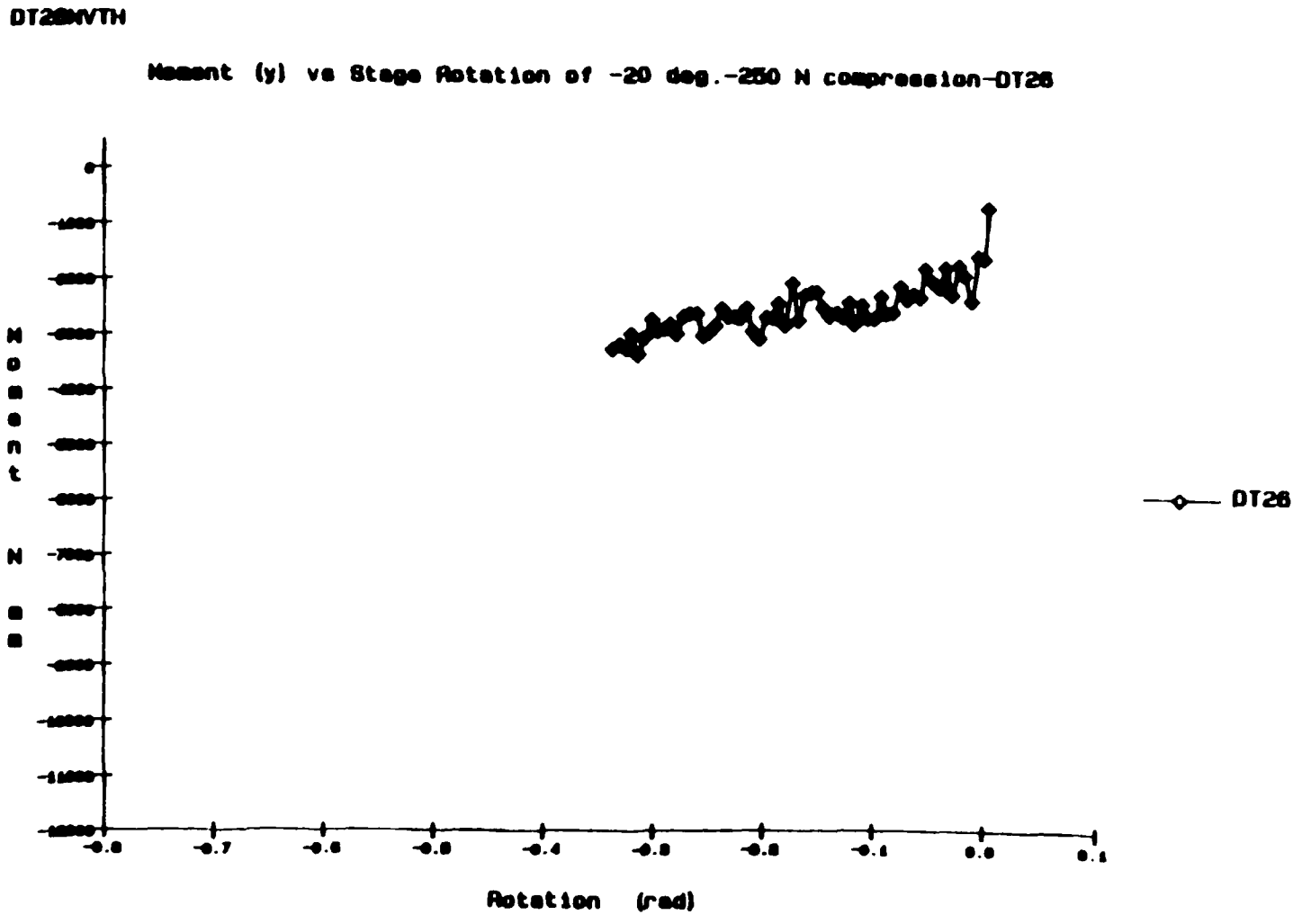

46.6 Specimen D

FT7T16MVTH

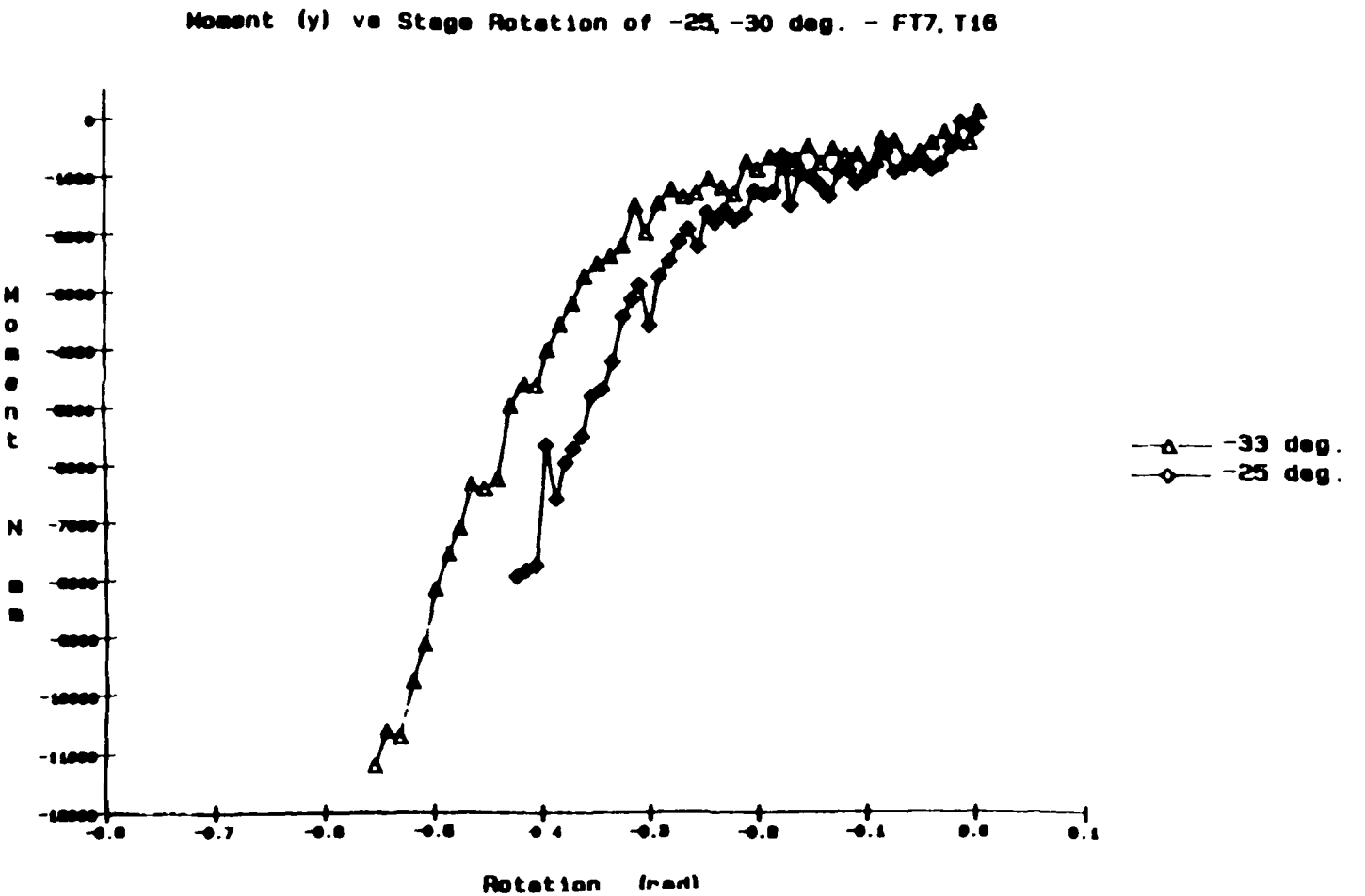

Figures 47.1-47.3 Moment (y) vs rotation (theta) at large angles for 3 specimens - 2 different angles for each specimen

47.1 Specimen F

HT181920MVTH

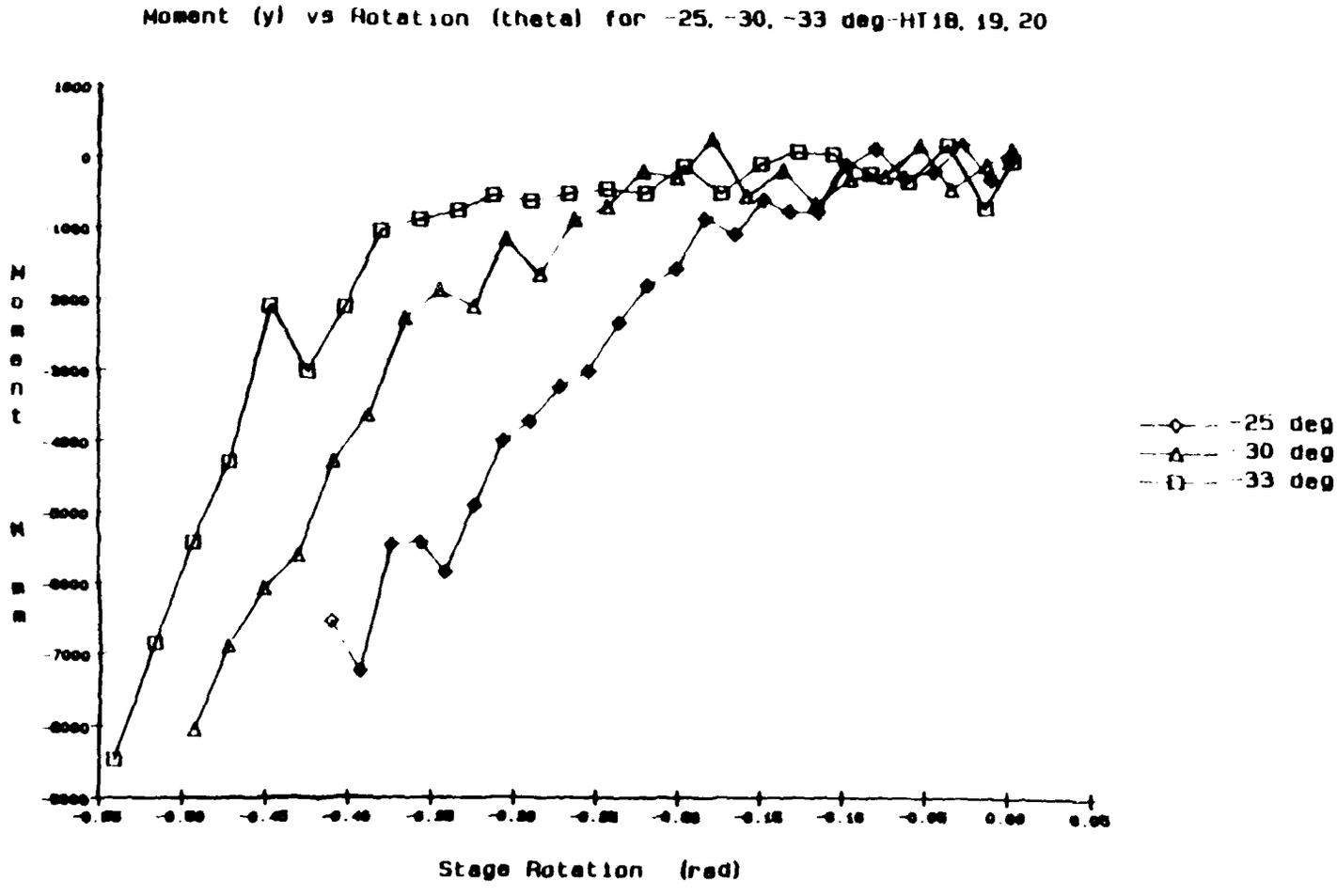

47.2 Specimen #1

GT13T15MVTH

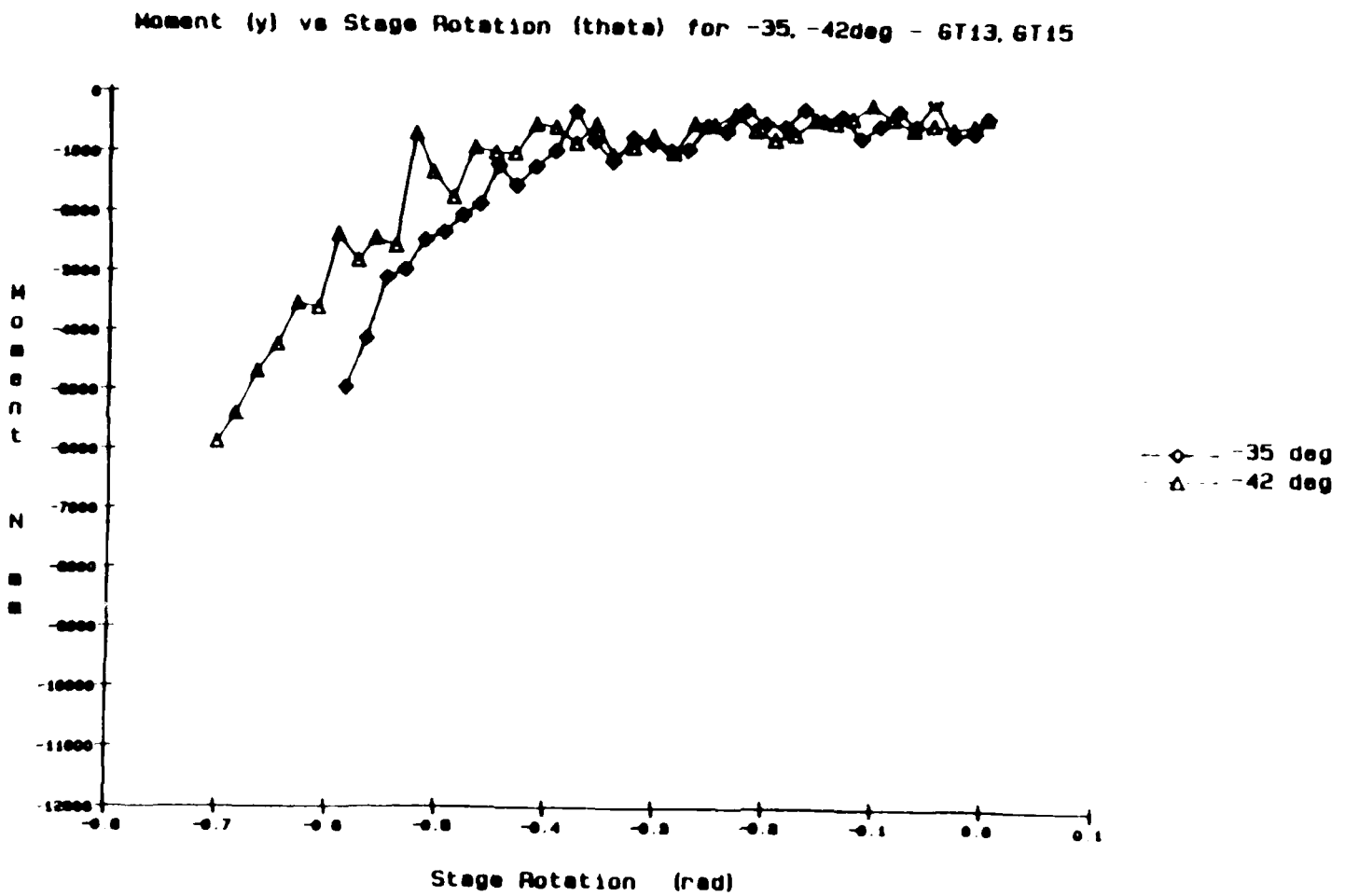

47.3 Specimen G

FT7XZVTH

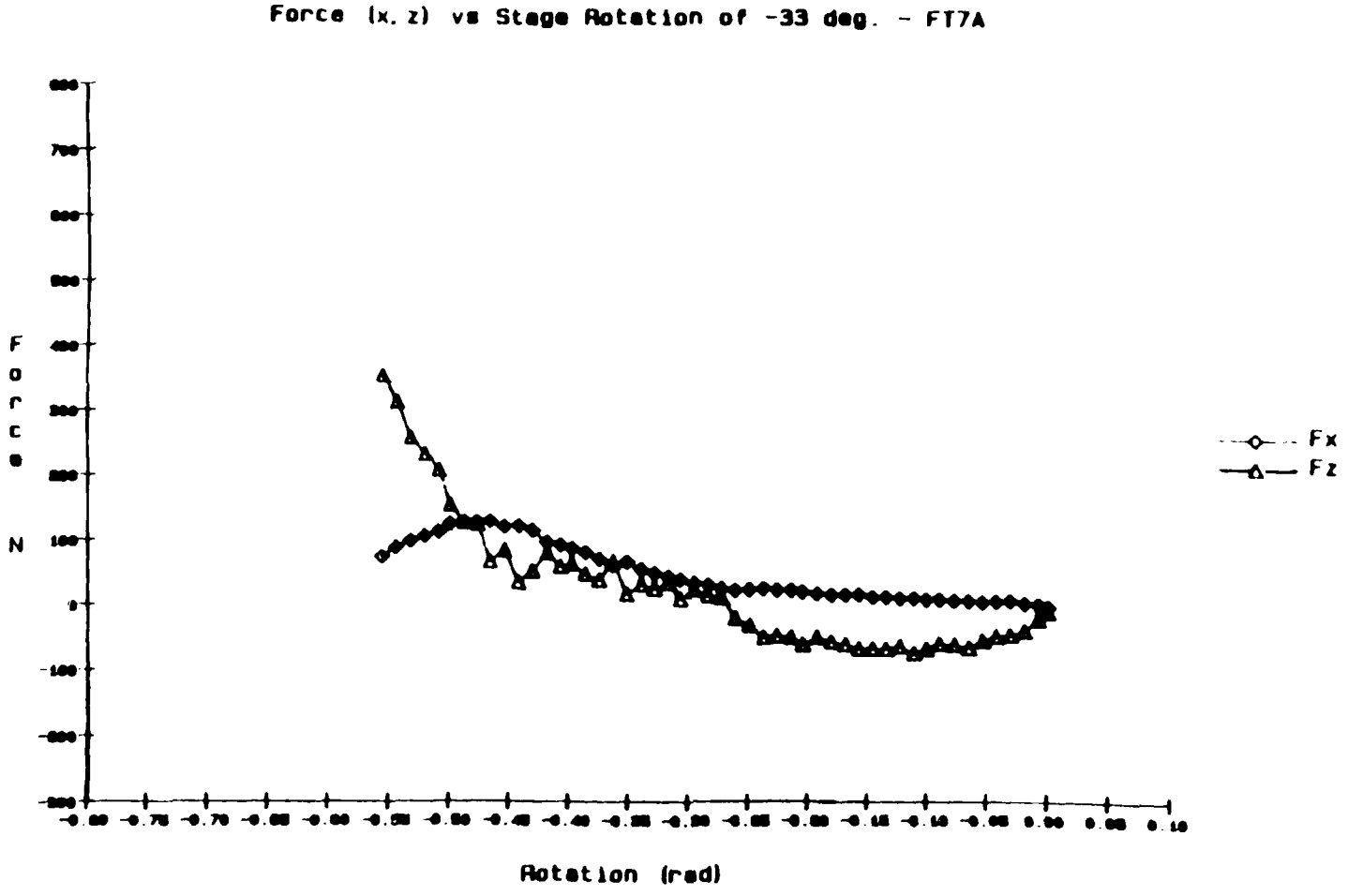

Figures:48.1-48.6 Force (x,y) vs rotation (theta) at large angles for 6 specimens

48.1 Specimen F

HT20XZVTH

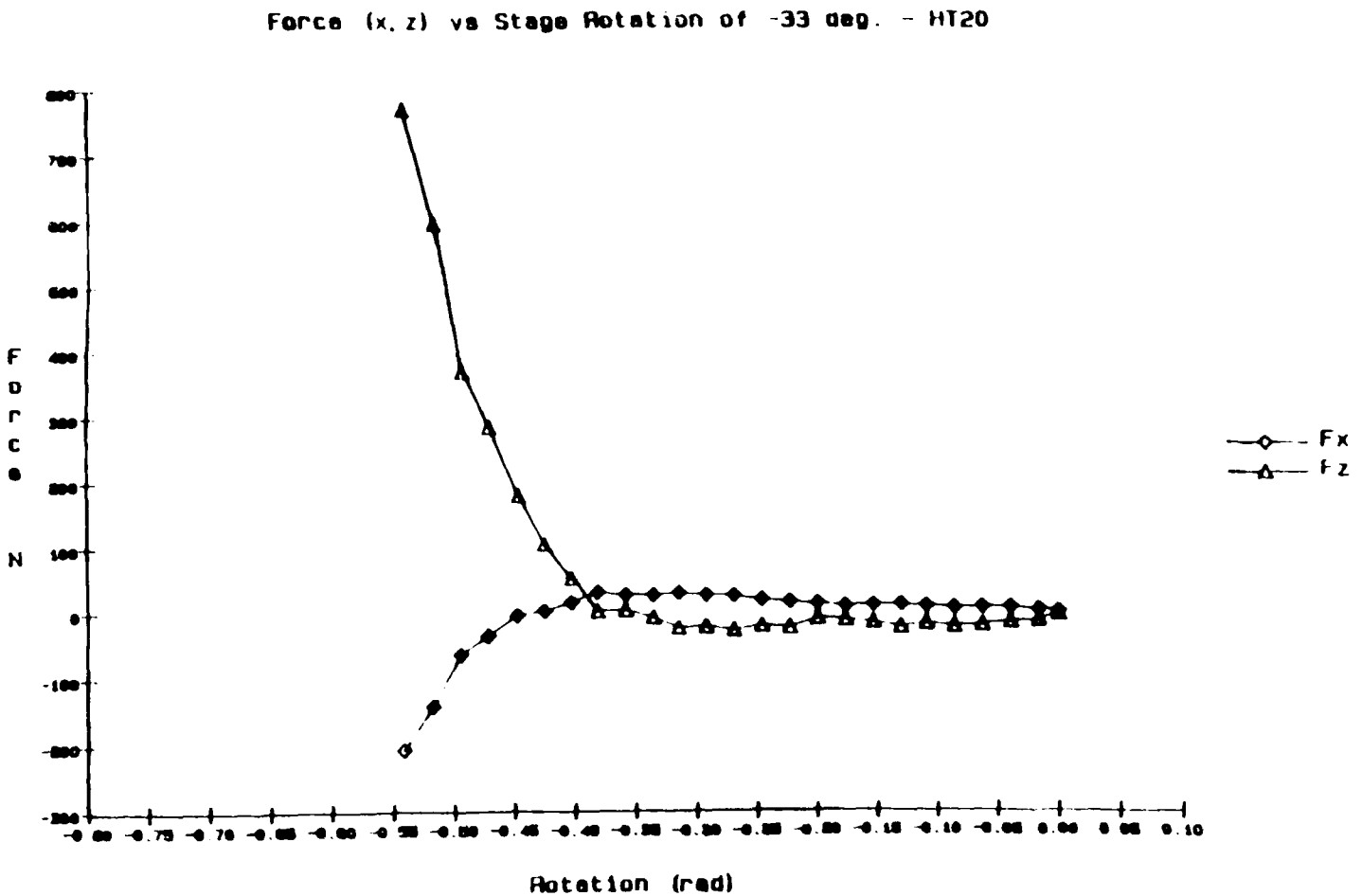

48.2 Specimen H

ET10XZYTH

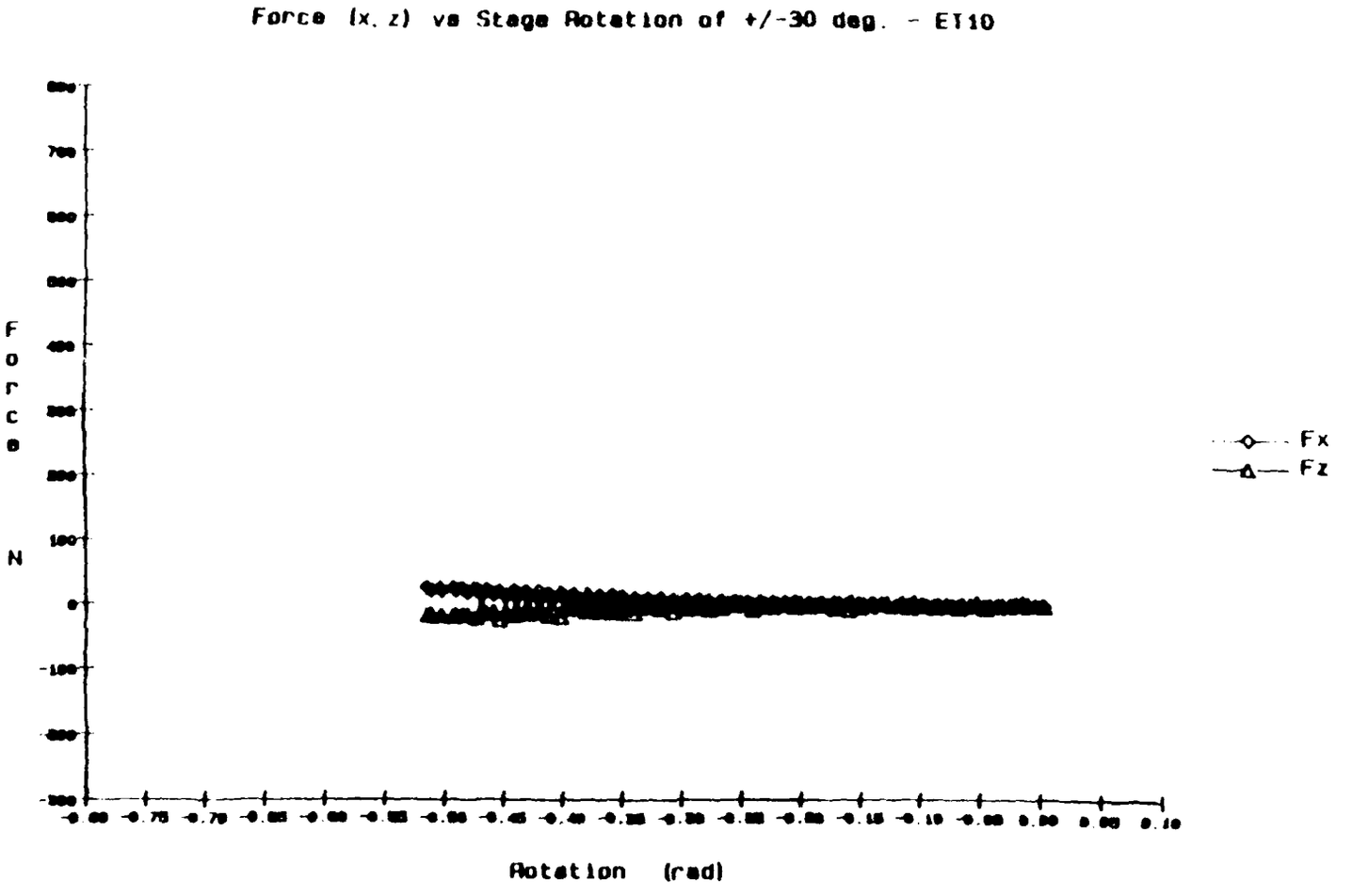

48.3 Specimen E

GT15XZVTH

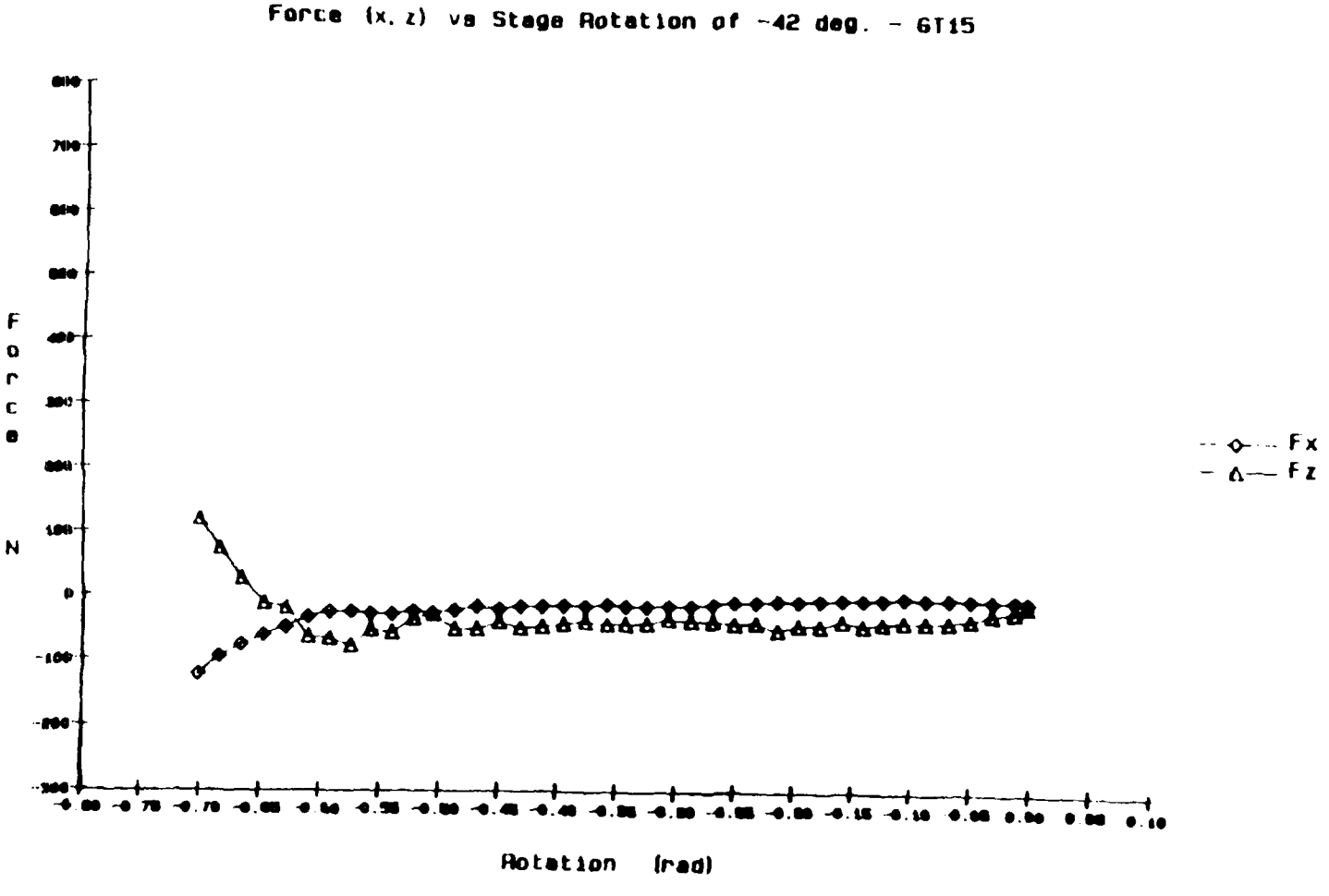

48.4 Specimen G

BT8XZVTH

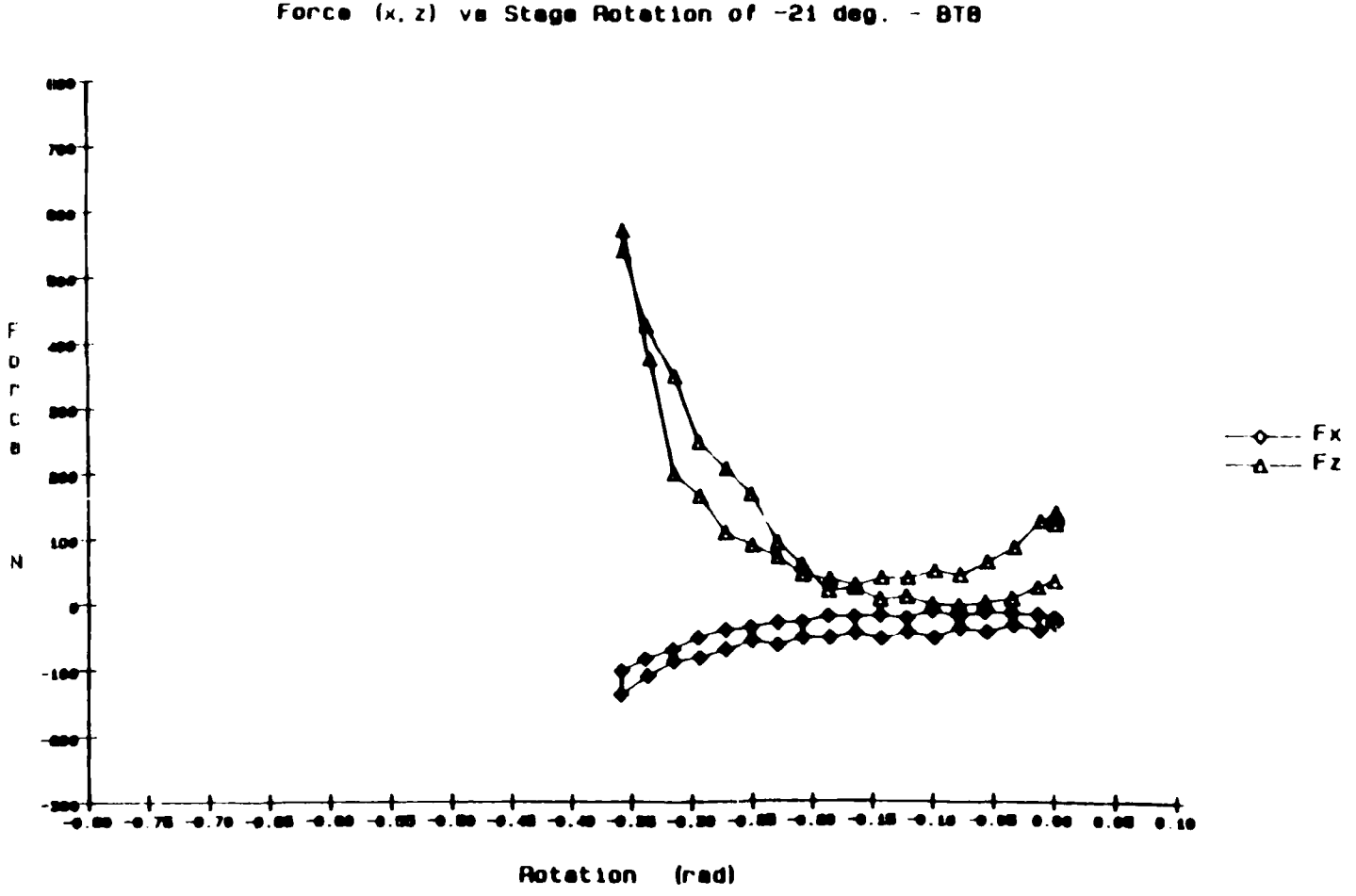

48.5 Specimen B

DT23XZVTH

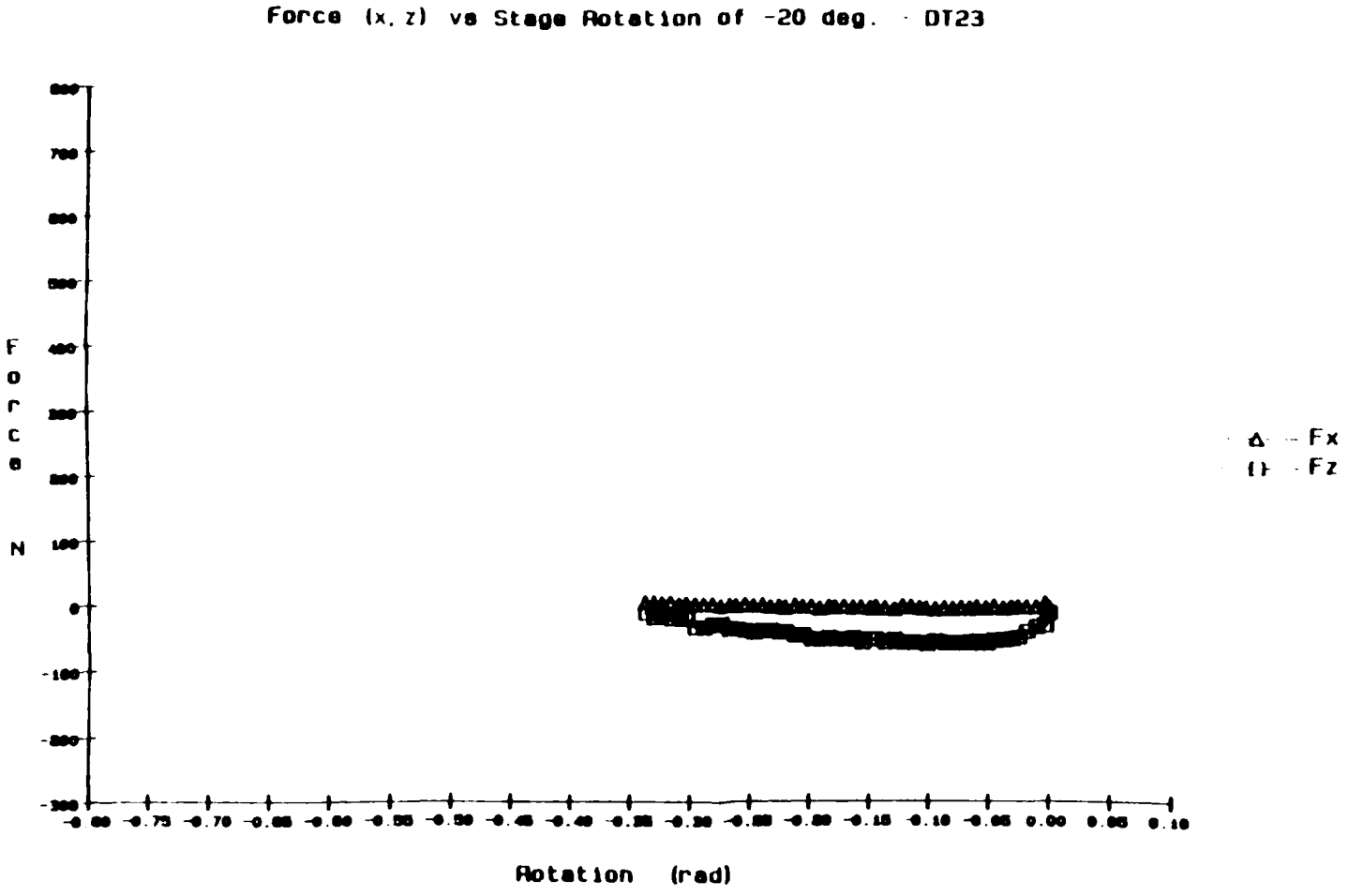

48.6 Specimen D

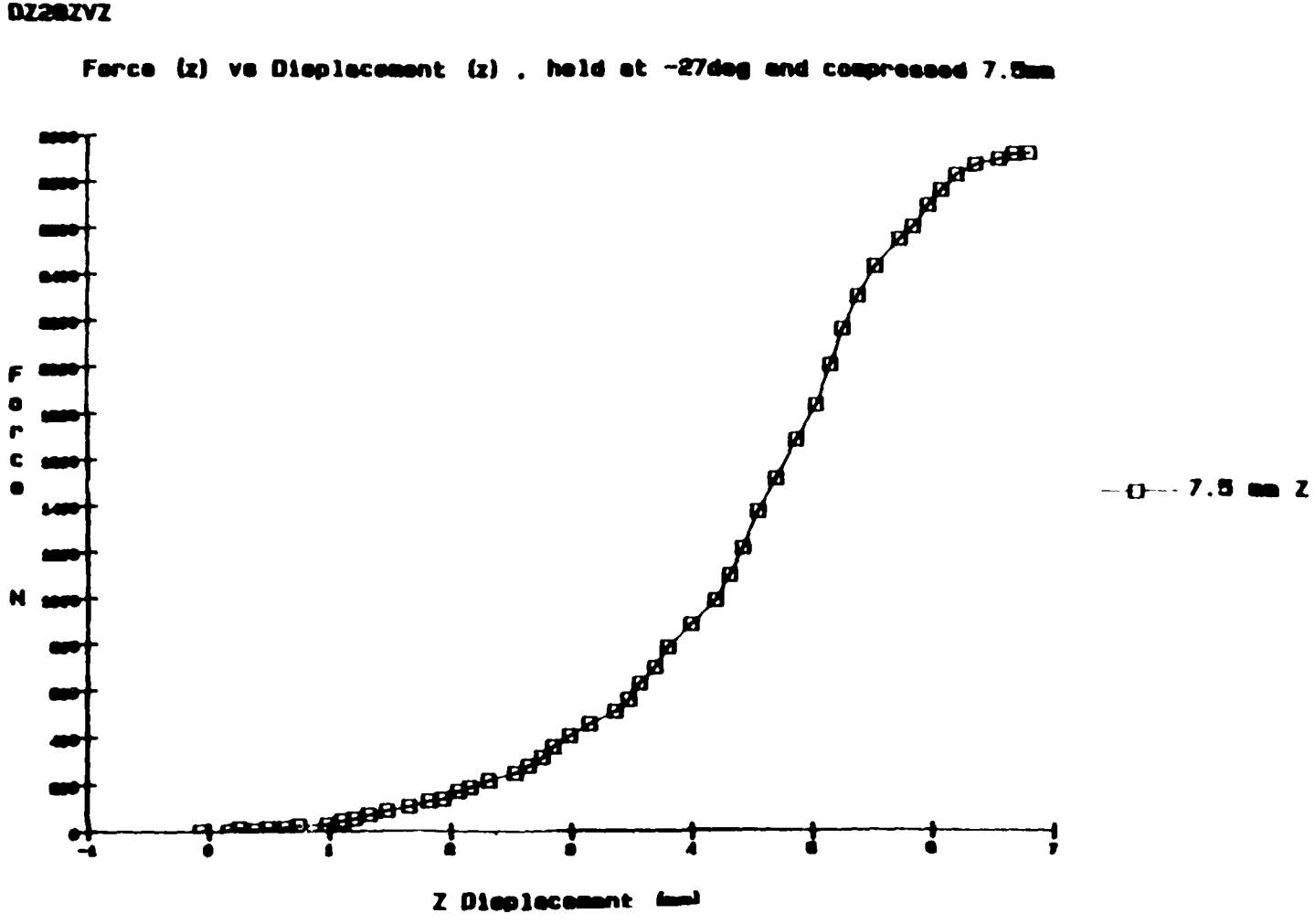

Figure:49 Force (z) vs displacement (z) while held at large angles for specimen D

LVDTCAL

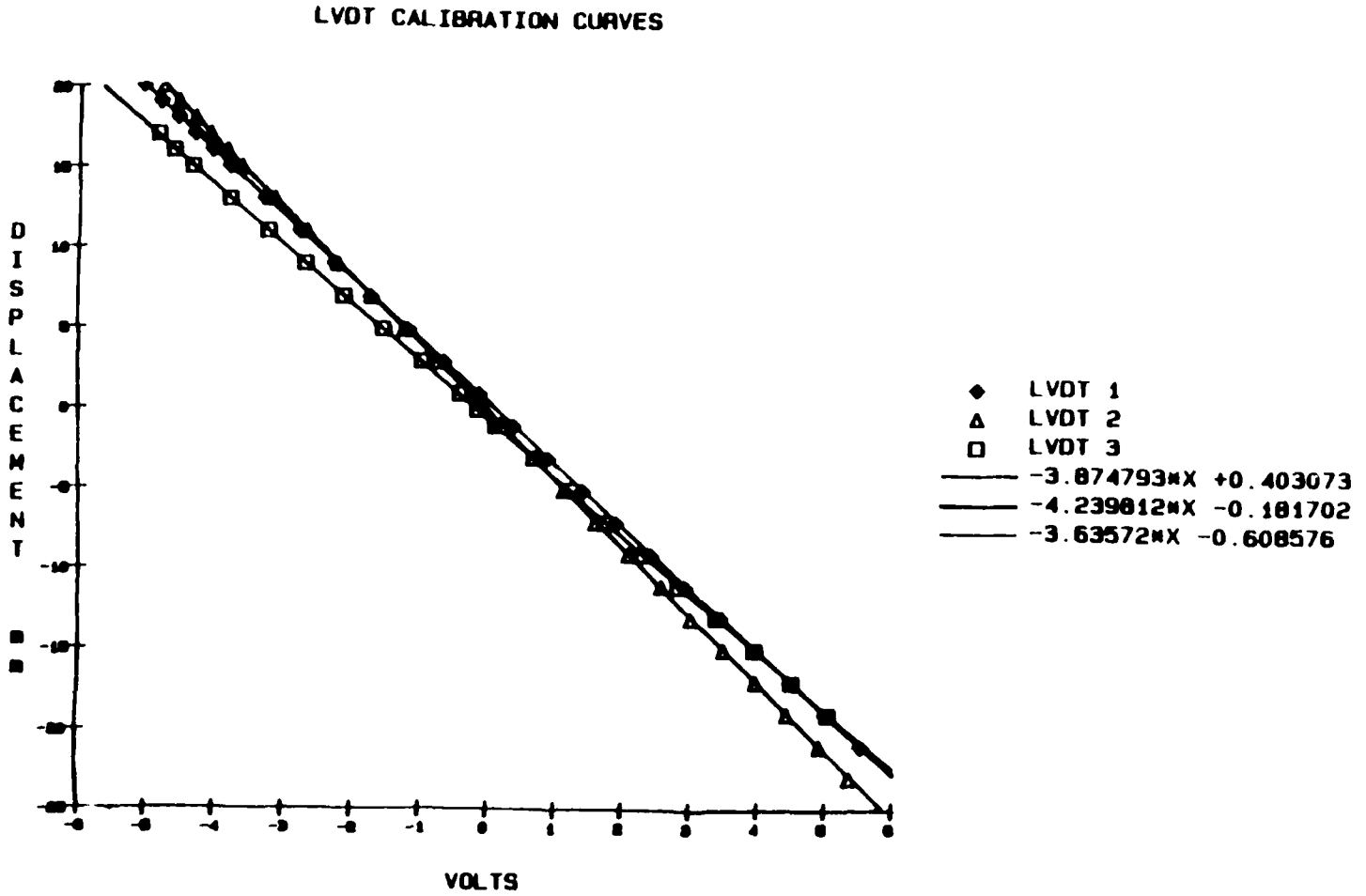

A:1 Calibration curves for 3 LVDT's

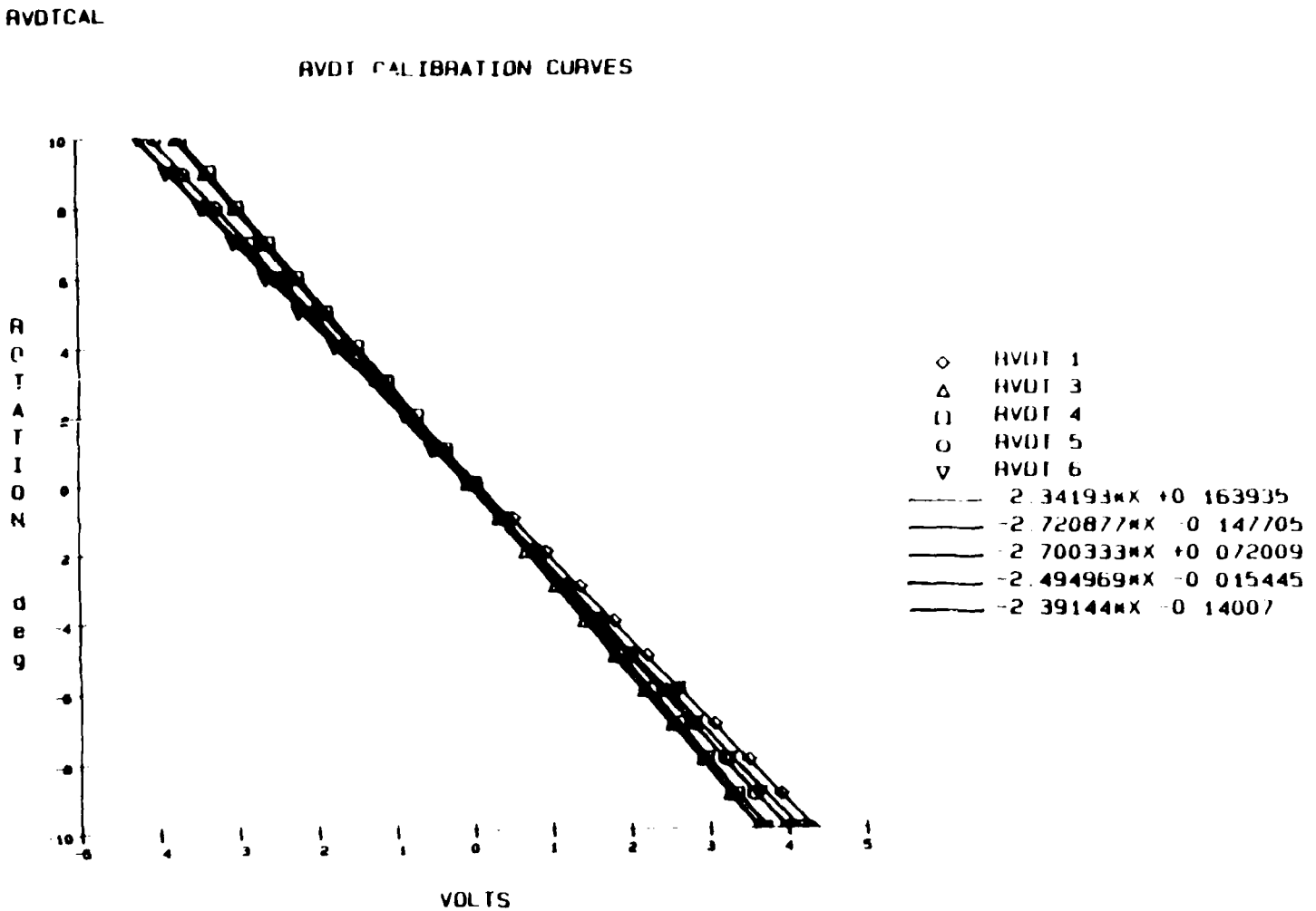

A:2 Calibration curves for 6 RVDT's

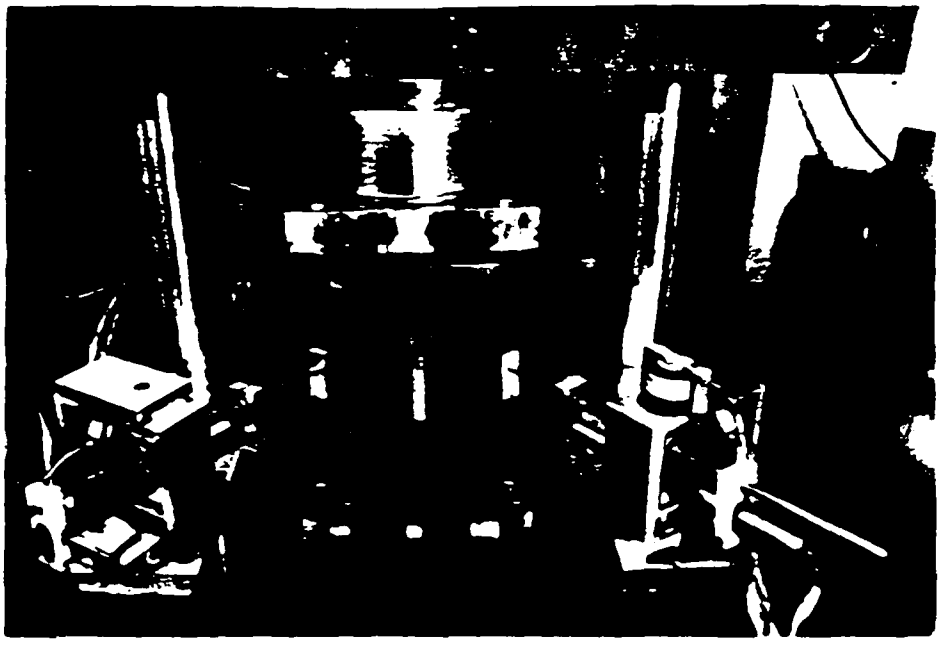

C:1 Trial collar mounted on PTA

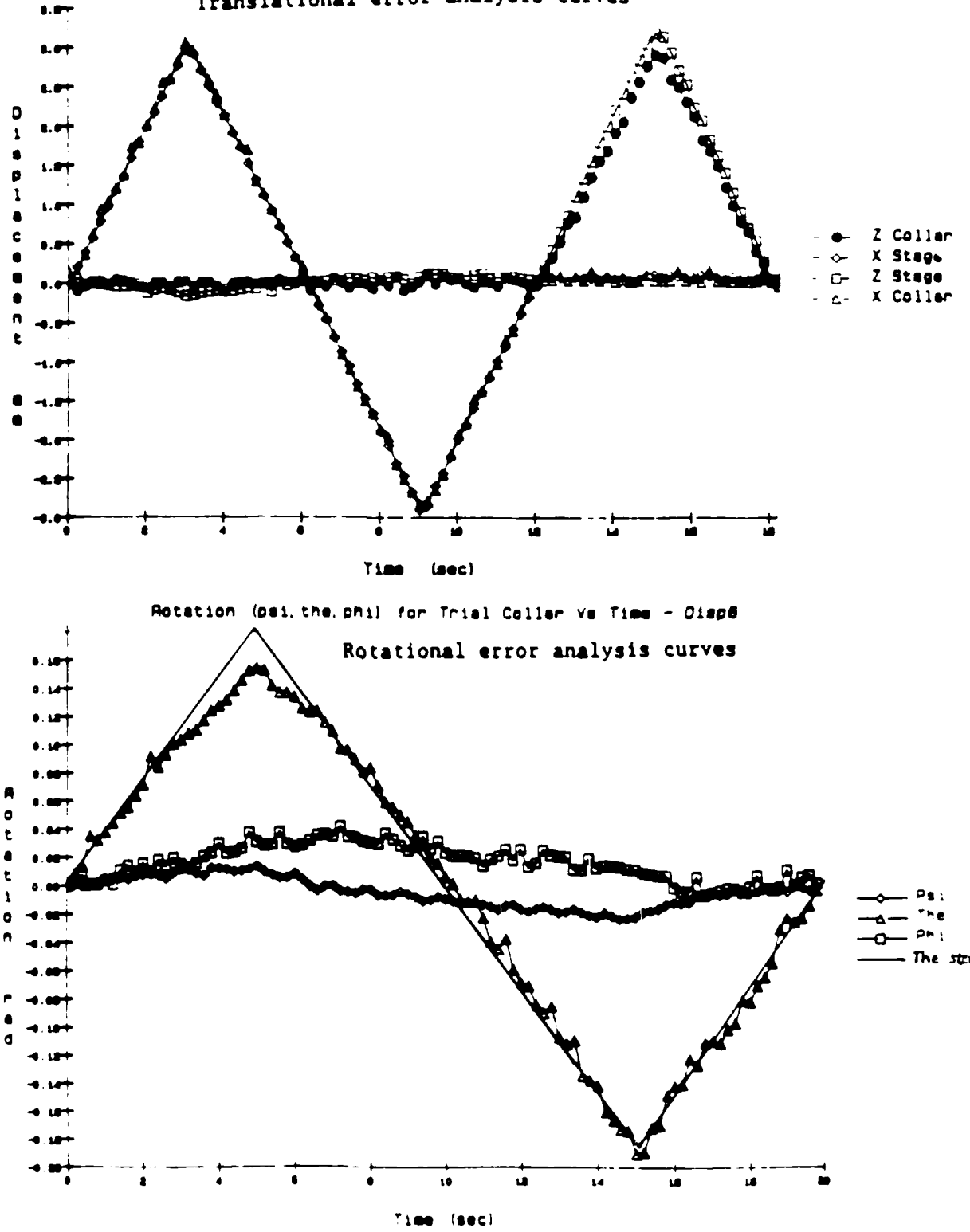

C:2 Test stage motion vs trial collar motion

0 Angle (deg)	1 Max vert range (mm)	2 Max hori range (mm)
1 0	127.00	330.20
2 10	104.14	274.32
3 20	81.28	223.52
4 30	63.50	167.64
5 40	43.18	114.30
6 50	22.86	58.42

Table:1 Range of motion of Planar Testing Apparatus.

0	Angle (deg)	1 Hori (N)	2 Vert (N)	3 Moment (N-m)
1	50	28912-34694	22240-28912	1582
2	-50	34250-36474	18682-22685	2712-2938
3				
4	40	19571-30246	27578-36029	1469-2147
5	-40	27578-34694	23130-31136	2373-2599
6				
7	30	9785-26243	32026-40477	1808-2712
8	-30	19571-31581	27133-36918	2599-2825
9				
10	20	12899-13344	19571-41366	1921-2938
11	-20	15568-27578	31136-40477	2486-2938
12				
13	10	15568-17792	37808-40477	2373-2938
14	-10	12010-23130	34694-41811	2712-2938
15				
16	0	9785-18237	37808-40922	2712-2938

Table:2 Force ranges at maximum and minimum positions for each angle along the vertical axis of the Planar Testing Apparatus.

0	Angle (deg)	1 Hori (N)	2 Vert (N)	3 Moment (N-m)
1	50	30691-31136	26688	1243-1356
2	-50	36028	20016	2825
3				
4	40	24909-25354	32026-32470	1808
5	-40	32025	25354-26688	2599
6				
7	30	18237-18682	36474-36918	2260
8	-30	14678-18237	39587-41366	2373-2599
9				
10	20	11120-11565	39142-40477	2486-2599
11	-20	19571-21350	34694-36918	2599-2825
12				
13	10	10675-14678	40477-41811	2712-2938
14	-10	15568-20016	37808-40477	2712-2938
15				
16	0	12899-18682	39587-42256	2712-2938

Table:3 Force ranges at maximum and minimum positions for each angle along the horizontal axis of the Planar Testing Apparatus.

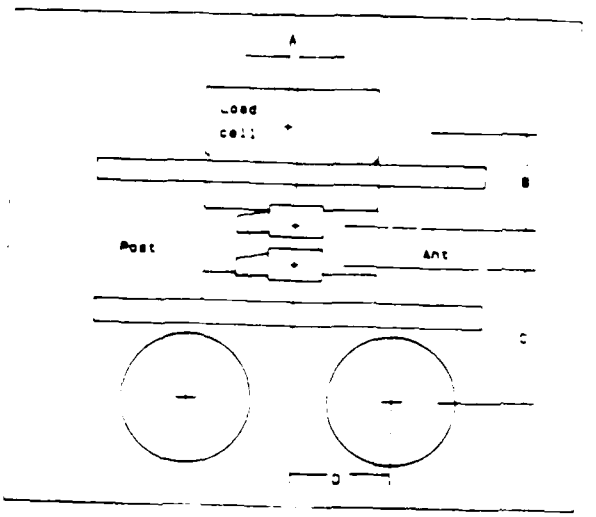

0 Test ID	1 A (mm)	2 B (mm)	3 C (mm)	4 D (mm)
1 B	18.800	119.650	108.40	52.250
2 C	48.300	107.130	111.70	24.310
3 D	49.480	114.425	104.40	18.195
4 E	44.775	108.265	113.40	25.075
5 F	42.645	114.000	109.42	29.840
6 G	42.525	114.865	112.97	29.065
7 H	40.645	114.890	95.10	34.427

Table:4 Specimen Geometry data.

Kelvin solid model

$A*(1-\exp(-(t-to)/B))+C*(1-\exp(-(t-to)/D))+E*\exp(-(t-to)/B)+(Eo-E)*\exp(-(t-to)/D)$

0 Test ID	1 to	2 Eo	3 A	4 B	5 C	6 D	7 E
1 B	14	1.10	1.3076	125.8148	0.8351	3350.1217	1.1297
2 C	40	1.83	1.0041	58.7578	2.0540	2875.5067	0.8187
3 D	18	1.55	1.0008	69.5749	1.9065	2652.5838	0.7600
4 E	14	1.10	0.9443	27.6901	1.2327	1218.5589	0.7690
5 F	30	1.98	0.9590	105.9843	2.1735	3535.8320	0.7892
6 G	19	1.57	1.0990	95.8677	2.0852	2335.9150	0.7853
7 H	18	1.49	1.0729	73.6657	1.6835	2360.4500	0.7686

Table:5 Time constant of the Kelvin Solid Model.

AD-A170 002 FRACTURE AND VISCOELASTIC CHARACTERISTICS OF THE HUMAN CERVICAL SPINE(U) BETH ISRAEL HOSPITAL BOTTON MASS W T EDWARDS ET AL 1986 AFOSR-TR-86-0453 3/3

UNCLASSIFIED F49620-81-K-0010 F/G 6/16 NL

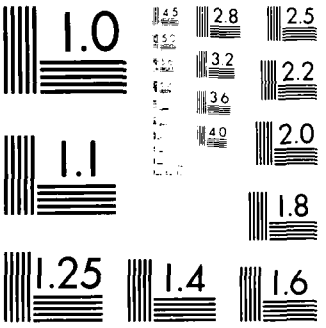

0 Test ID	1 SLOPE	2 INTERCEPT
1 B	0.002408	84.297449
2 D	0.006248	63.229373
3 G	0.002376	83.011050
4 H	0.001872	78.306532

Table:6 Linear regression of . disc load at zero sagittal angle.

Spec.	FVS	ID	Sex	Age	Weight	Cause of death
B	C6-T1	666638	M	66	110	COPD
C	C2-C4	1647185	M	52	163	Cardiomyopathy
D	C6-T1	192543	F	76	124	CVA
E	C3-C5	192543	F	76	124	CVA
F	C2-C4	616886	M	73	150	CA colon
G	C5-C7	53852	M	69	120	Myocard. infarct.
H	C2-C4	53852	M	69	120	Myocard. infarct.

Table:7 Test Specimen Information

Specimen	Level	Shear Stiffness (N/mm)		Axial Stiffness (N/mm)	
		Posterior	Anterior	Tension	Compression
C	C2-C4	35	70	325	500
F	C2-C4	125	50	260	3350
H	C2-C4	250	35	210	3500
E	C3-C5	100	30	145	500
G	C5-C7	13	25	35	200
B	C6-T1	14	27	25	250
D	C6-T1	5	30	30	360

Table:8 Specimen stiffnesses from load vs. displacement curves

APPENDIX A

Transducer Calibration

The LVDT's were calibrated using a depth gage with a resolution of 0.25 mm. The transducer group housing block was clamped to a benchtop and the depth gage was held stationary at the same height and coaxially with the LVDT support rod. The gage tip was placed in the cup on the support rods end. With the initial location of the rod tip displaced 20 mm from its position corresponding to zero voltage, the gage was turned, forcing the support rod back towards the LVDT body and towards the zero voltage location. Readings were recorded from a digital voltmeter every 2 mm for a total of 40 mm. Voltage vs. displacement was graphed and a curve was fit using an RS/1 software package (RS1 software, Bolt, Beranek, and Newman Research Systems.

The RVDT's were calibrated using a 40^{o} sector divided by radii 10 inch es in length and placed 2^{o} apart. The transducer group housing block was clamped onto the benchtop with the pivot point exactly above the origin of the sector and the LVDT body directed at 90^{o} to the housing block. The LVDT's support rod tip was aligned with each radii and the voltages recorded via a digital voltmeter. Voltage vs. rotation was graphed and a curve fit using RS/1. The calibration curves for the LVDT's and the RVDT's are given in A:1-2.

APPENDIX B

Kinematics

The components of the equations used to describe the kinematics are described in detail below.

$$[Z_s]_A = \begin{bmatrix} C\theta_{SUA} & -S\theta_{SUA} & 0 \\ S\theta_{SUA} & C\theta_{SUA} & 0 \\ 0 & 0 & 1 \end{bmatrix}$$

where C stands for cosine, S stands for sine, and θ_{SUA} is the angle of rotation of the transducer groups on the PTA bridge about the Z_{Ao} axis. This is referred to as the set-up angle.

$$[Y]_A = \begin{bmatrix} C\theta_{YA} & 0 & S\theta_{YA} \\ 0 & 1 & 0 \\ -S\theta_{YA} & 0 & C\theta_{YA} \end{bmatrix}$$

where θ_{YA} is the angle of rotation of the transducer group pivot point about the Y axis as determined by RVDT 2

$$[Z]_A = \begin{bmatrix} C\theta_{ZA} & -S\theta_{ZA} & 0 \\ S\theta_{ZA} & C\theta_{ZA} & 0 \\ 0 & 0 & 1 \end{bmatrix}$$

where θ_{ZA} is the angle of rotation of the transducer group pivot point about the Z axis as determined by RVDT 1

$$(L)_A = \begin{bmatrix} D_A \\ 0 \\ 0 \end{bmatrix}$$

where D_A is the distance (mm) from the point A_o to the point A as determined by LVDT 1

$$[R] = \begin{bmatrix} C\psi C\theta & C\psi S\theta S\phi - S\psi C\phi & C\psi S\theta C\phi + S\psi S\phi \\ S\psi C\theta & S\psi S\theta S\phi + C\psi C\phi & S\psi S\theta C\phi - C\psi S\phi \\ -S\theta & C\theta S\phi & C\theta C\phi \end{bmatrix}$$

where ψ, θ and ϕ are successive rotations of S_m about X_m, Y_m and Z_m

$$|l_i| = \sqrt{l_{ix}^2 + l_{iy}^2 + l_{iz}^2}$$

$$f(\alpha) = \begin{bmatrix} f_1(\alpha) \\ f_2(\alpha) \\ \cdot \\ \cdot \\ \cdot \\ f_6(\alpha) \end{bmatrix}$$

where $f_i(\alpha)$ is, in expanded terms,

$$\begin{aligned} f_i(\alpha) = {} & A_{i1}^2 + A_{i2}^2 + A_{i3}^2 + B_{i1}^2 + B_{i2}^2 + B_{i3}^2 + x^2 + y^2 + z^2 - \\ & |l_i|_a^2 + 2(x - B_{i1})(A_{i1}T_{11} + A_{i2}T_{21} + A_{i3}T_{31}) + \\ & 2(y - B_{i2})(A_{i1}T_{12} + A_{i2}T_{22} + A_{i3}T_{32}) + \\ & 2(z - B_{i3})(A_{i1}T_{13} + A_{i2}T_{23} + A_{i3}T_{33}) - \\ & 2(xB_{i1} + yB_{i2} + zB_{i3}) \end{aligned}$$

$$\left[\frac{\partial f(\alpha_n)}{\quad}\right] = \begin{bmatrix} \frac{\partial f_1}{\partial x} & \frac{\partial f_1}{\partial y} & \frac{\partial f_1}{\partial z} & \frac{\partial f_1}{\partial \psi} & \frac{\partial f_1}{\partial \theta} & \frac{\partial f_1}{\partial \phi} \\ \frac{\partial f2}{\partial x} & \frac{\partial f_2}{\partial y} & \frac{\partial f_2}{\partial z} & \frac{\partial f_2}{\partial \psi} & \frac{\partial f_2}{\partial \theta} & \frac{\partial f_2}{\partial \phi} \\ \cdot & \cdot & \cdot & \cdot & \cdot & \cdot \end{bmatrix}$$

$$\left[\partial\alpha_n \quad\right] \qquad \begin{vmatrix} \cdot & \cdot & \cdot & \cdot & \cdot & \cdot \\ \cdot & \cdot & \cdot & \cdot & \cdot & \cdot \\ \dfrac{\partial f_6}{\partial x} & \dfrac{\partial f_6}{\partial y} & \dfrac{\partial f_6}{\partial z} & \dfrac{\partial f_6}{\partial \psi} & \dfrac{\partial f_6}{\partial \theta} & \dfrac{\partial f_6}{\partial \phi} \end{vmatrix}$$

where f_i implies $f_i(\alpha)$ and the six expanded $f_i(\alpha_n)$ equations are

$$\frac{\partial f_i(\alpha)}{\partial x} = 2(x + A_{i1}T_{11} + A_{i2}T_{21} + A_{i3}T_{31} - B_{i1})$$

$$\frac{\partial f_i(\alpha)}{\partial y} = 2(y + A_{i1}T_{12} + A_{i2}T_{22} + A_{i3}T_{32} - B_{i2})$$

$$\frac{\partial f_i(\alpha)}{\partial z} = 2(z + A_{i1}T_{13} + A_{i2}T_{23} + A_{i3}T_{33} - B_{i3})$$

$$\frac{\partial f_i(\alpha)}{\partial \psi} = -2(x-B_{i1})(A_{i1}T_{12} + A_{i2}T_{22} + A_{i3}T_{32}) + 2(y - B_{i2})(A_{i1}T_{11} + A_{i2}T_{21} + A_{i3}T_{31})$$

$$\frac{\partial f_i(\alpha)}{\partial \theta} = 2(x - B_{i1})(-A_{i1}S\theta C\psi + A_{i2}S\phi C\theta C\psi + A_{i3}C\phi C\theta C\psi) + 2(y - B_{i2})(-A_{i1}S\theta S\psi + A_{i2}S\phi C\theta S\psi + A_{i3}C\phi C\theta S\psi) - 2(Z - B_{i3})(A_{i1}C\theta + A_{i2}S\phi S\theta + A_{i3}C\phi S\theta)$$

$$\frac{\partial f_i(\alpha)}{\partial \phi} = 2(x - B_{i1})(A_{i2}T_{31} - A_{i3}T_{21}) + 2(y - B_{i2})(A_{i2}T_{32} - A_{i3}T_{22}) + 2(z - B_{i3})(A_{i2}T_{33} - A_{i3}T_{23})$$

APPENDIX C

Error Analysis

To determine the accuracy of the equations for the three translations and three Eulerian rotations, along with the accuracy of the displacement hardware, a trial displacement collar was constructed. Three balls were attached to a lead cylinder which was positioned at the center of the PTA test stage. The balls were at a known height and at known positions with respect to the center of the stage. The cups on the LVDT support rod tips were linked to the balls, exactly as if the collar were on a specimen Figure C:1. The test stage was displaced by three mm along the X and Z axes and by three degrees about the Y axis. The translation and rotation data generated by the displacement software were compared to the input data. The results for uniaxial command displacements are shown graphically in Figure C:2. Maximum errors of 0.4 mm for test stage translations of 3 mm and 1.2^{o} for stage rotations of 10^{o} resulted. The error in translation affects the measured rotation angle.

APPENDIX D

Expanded Figures 38.1-38.7, 39.1-39.7, 40.1-40.7

CZ2ZVZ

C2-C4

Force (z) vs Displacement (z) - Test CZ2

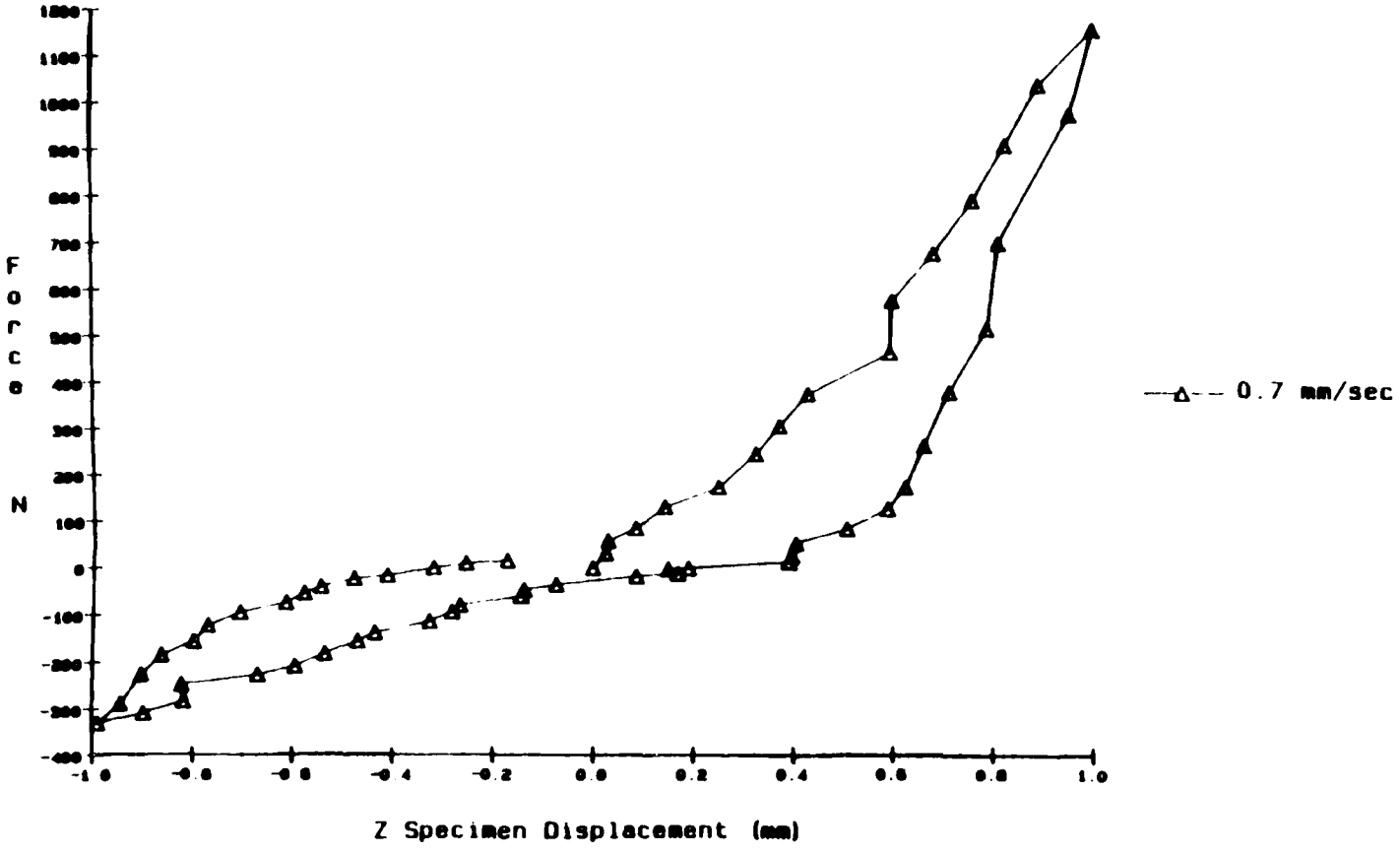

FZ6Z7Z8ZVZ

C2-C4 Force (z) vs Displacement (z) - 3 rates - FZ4, FZ7, FZ8

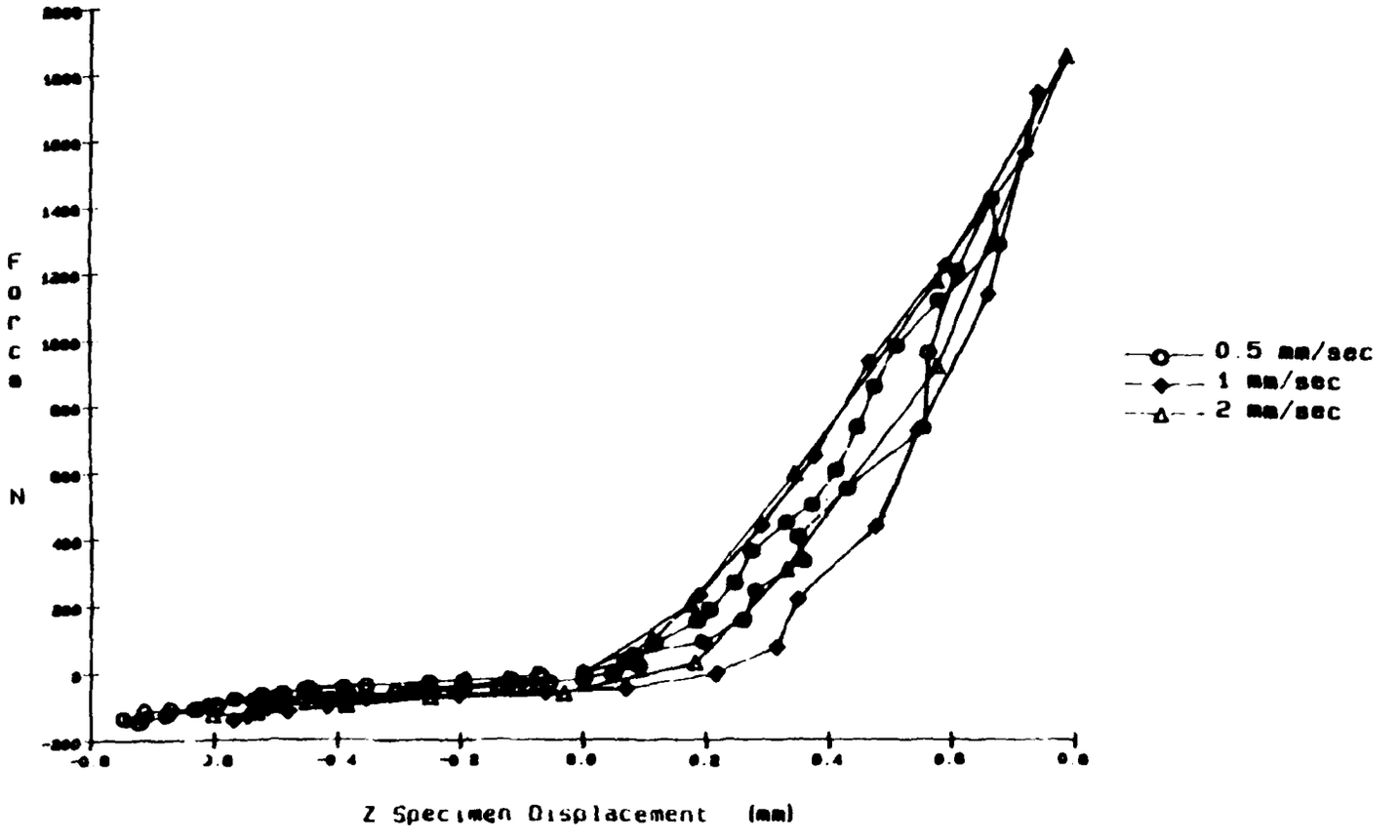

HZ11Z12ZVZ
C2-C4

Force (z) vs Displacement (z) for +/-1.5 mm Stage displacement - HZ11, HZ12

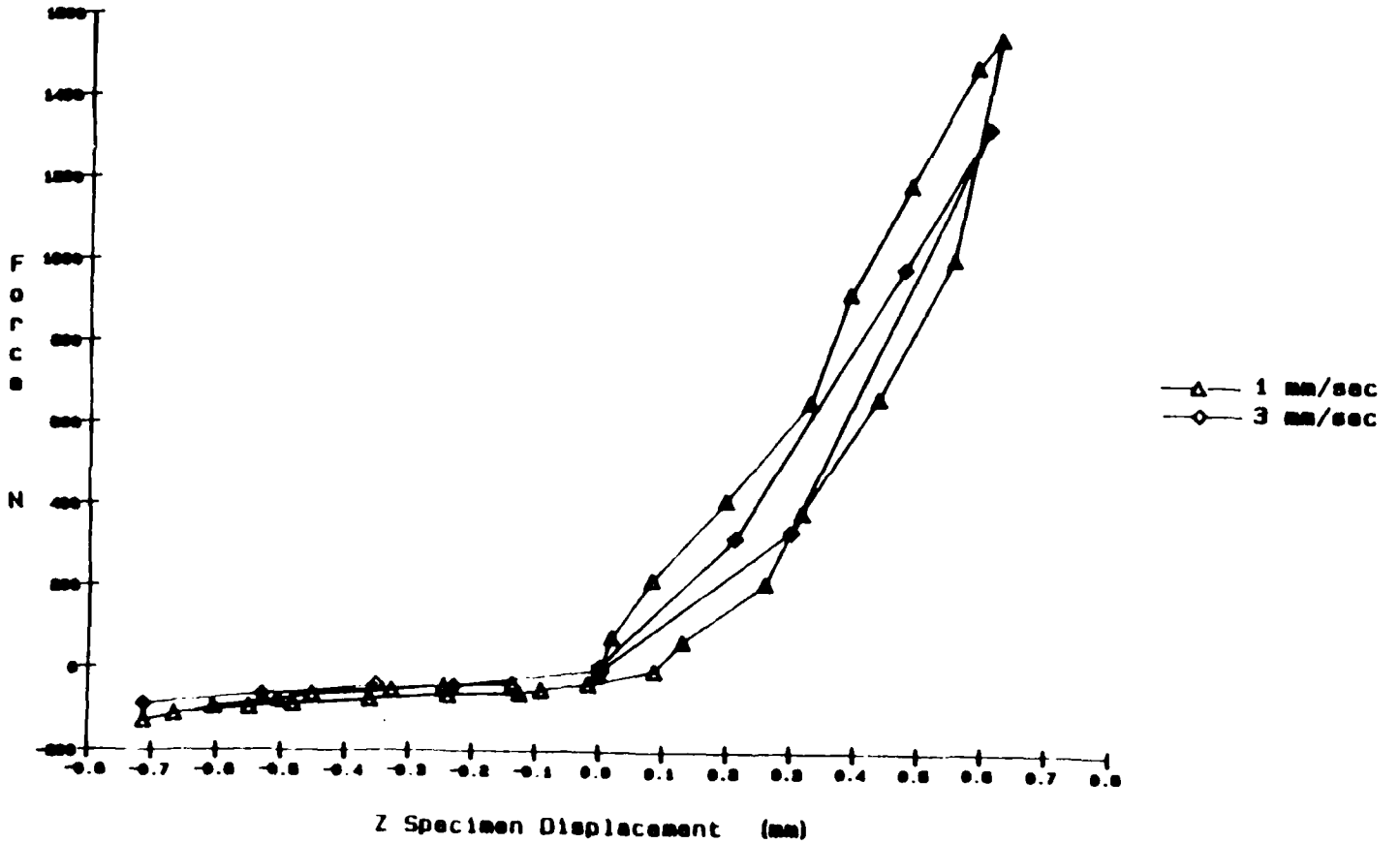

EZ1Z

Force (z) vs Displacement (z) for +/-1mm stage displacement - EZ1

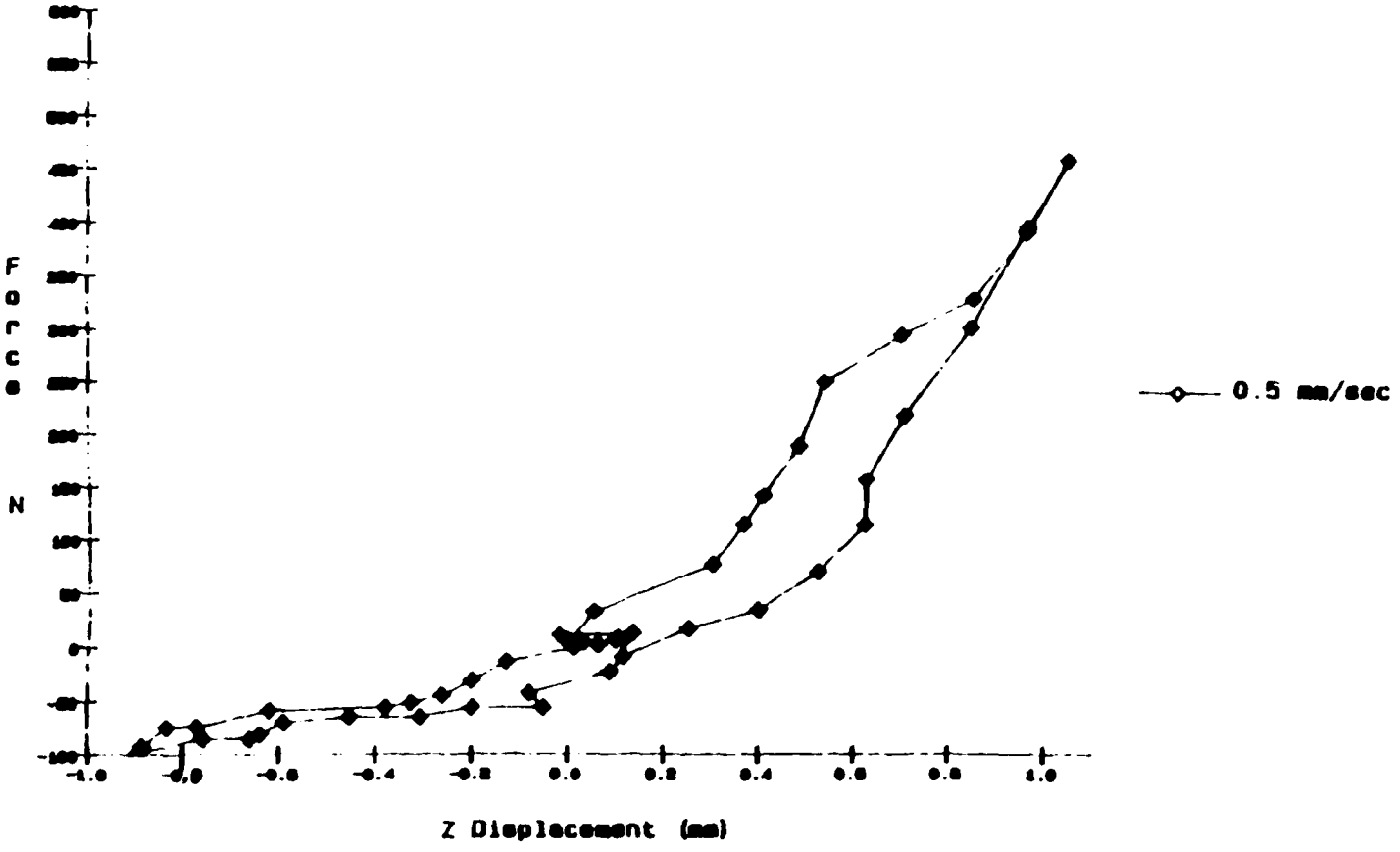

GZ4Z11VZ

C5-C7

Force (z) vs Displacement (z) - 2 rates: Tests GZ4, GZ11

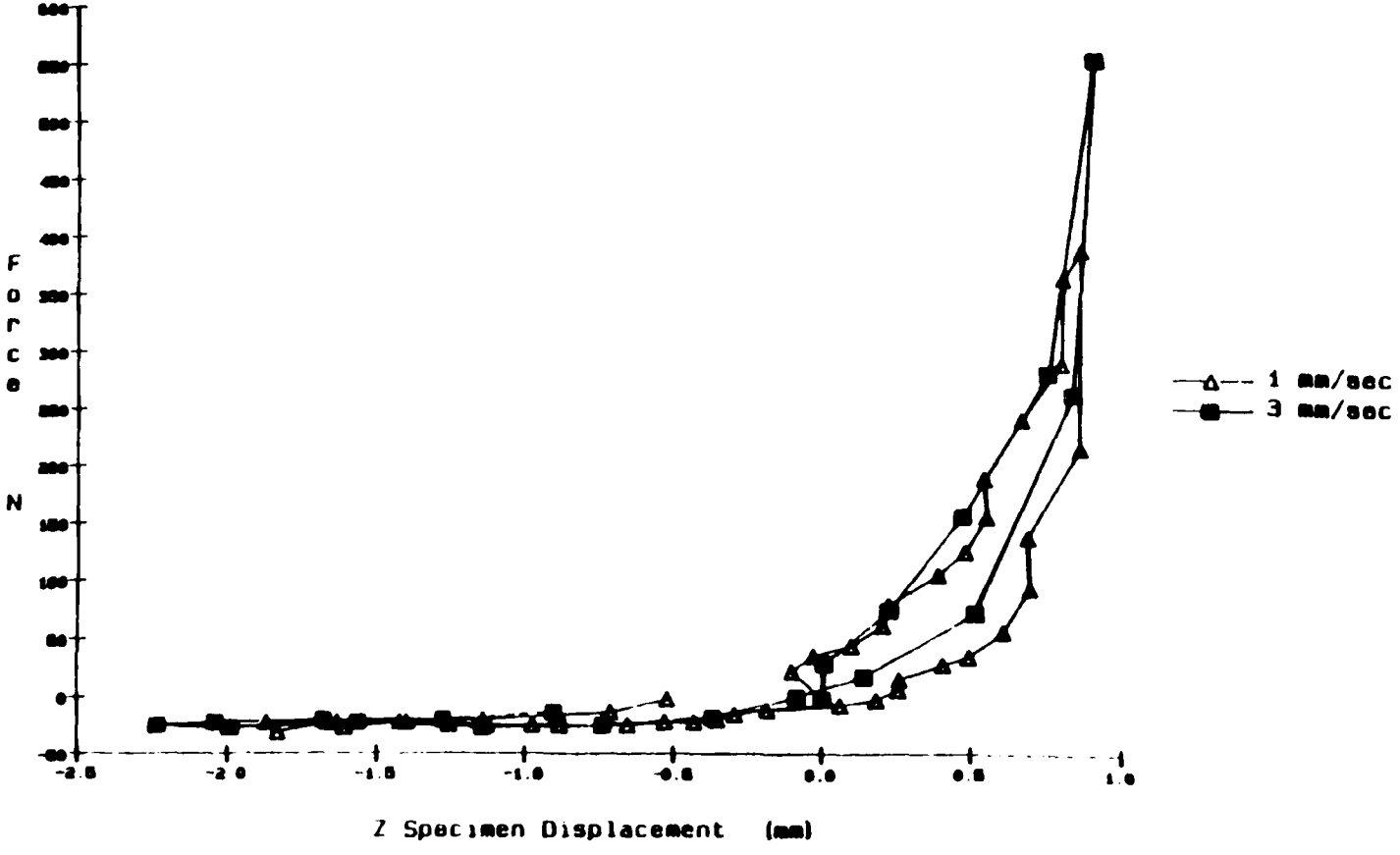

BZ4ZVZ

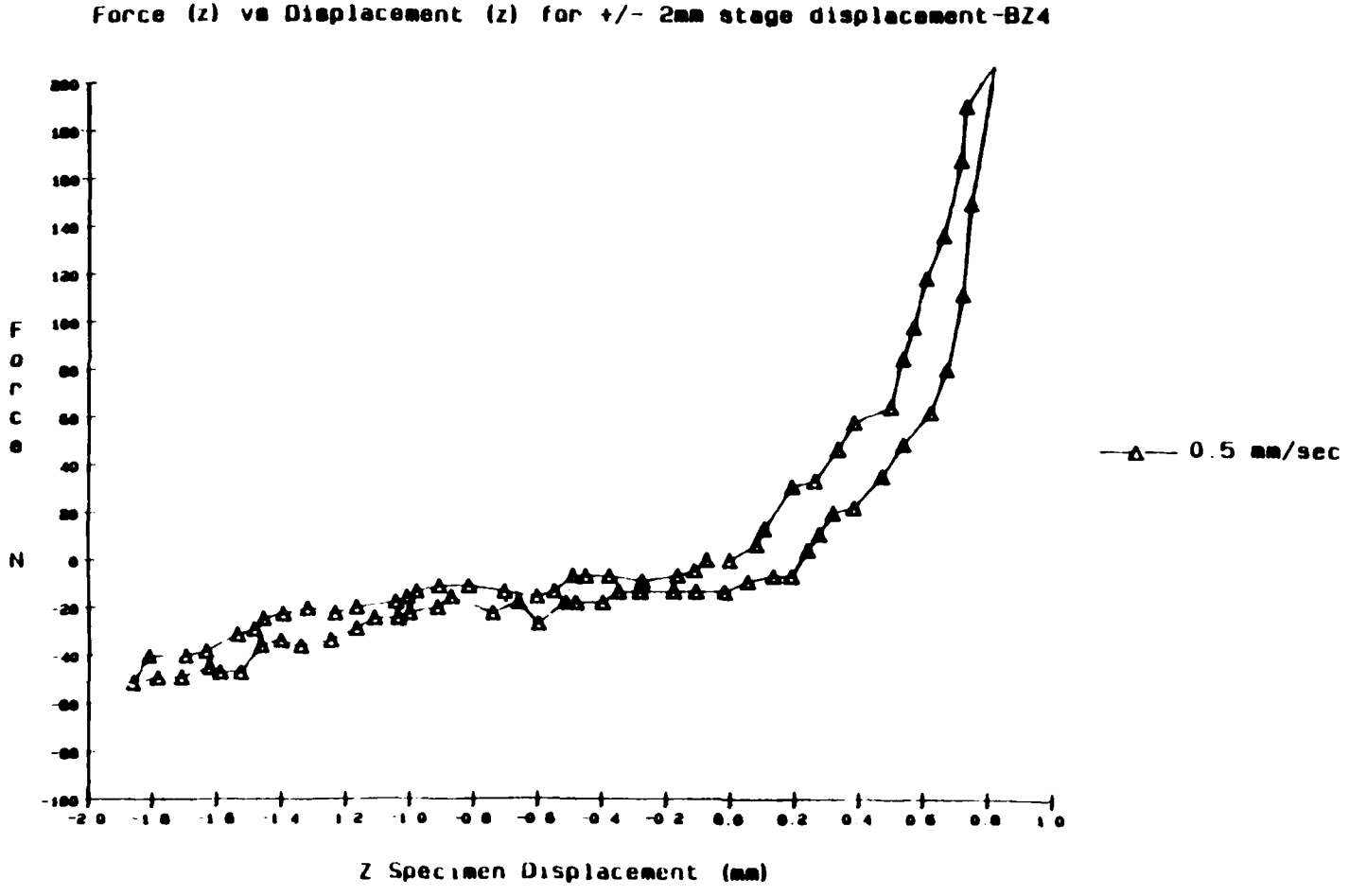
Force (z) vs Displacement (z) for +/- 2mm stage displacement-BZ4
F
o
r
c
e
N
-2.0
-1.8
-1.6
-1.4
-1.2
-1.0
-0.8
-0.6
-0.4
-0.2
0.0
0.2
0.4
0.6
0.8
1.0
Z Specimen Displacement (mm)
0.5 mm/sec

DZ3Z8ZVZ

Force (z) vs Displ. (z) for +1, -2.5 mm stage displacement - DZ3, DZ8

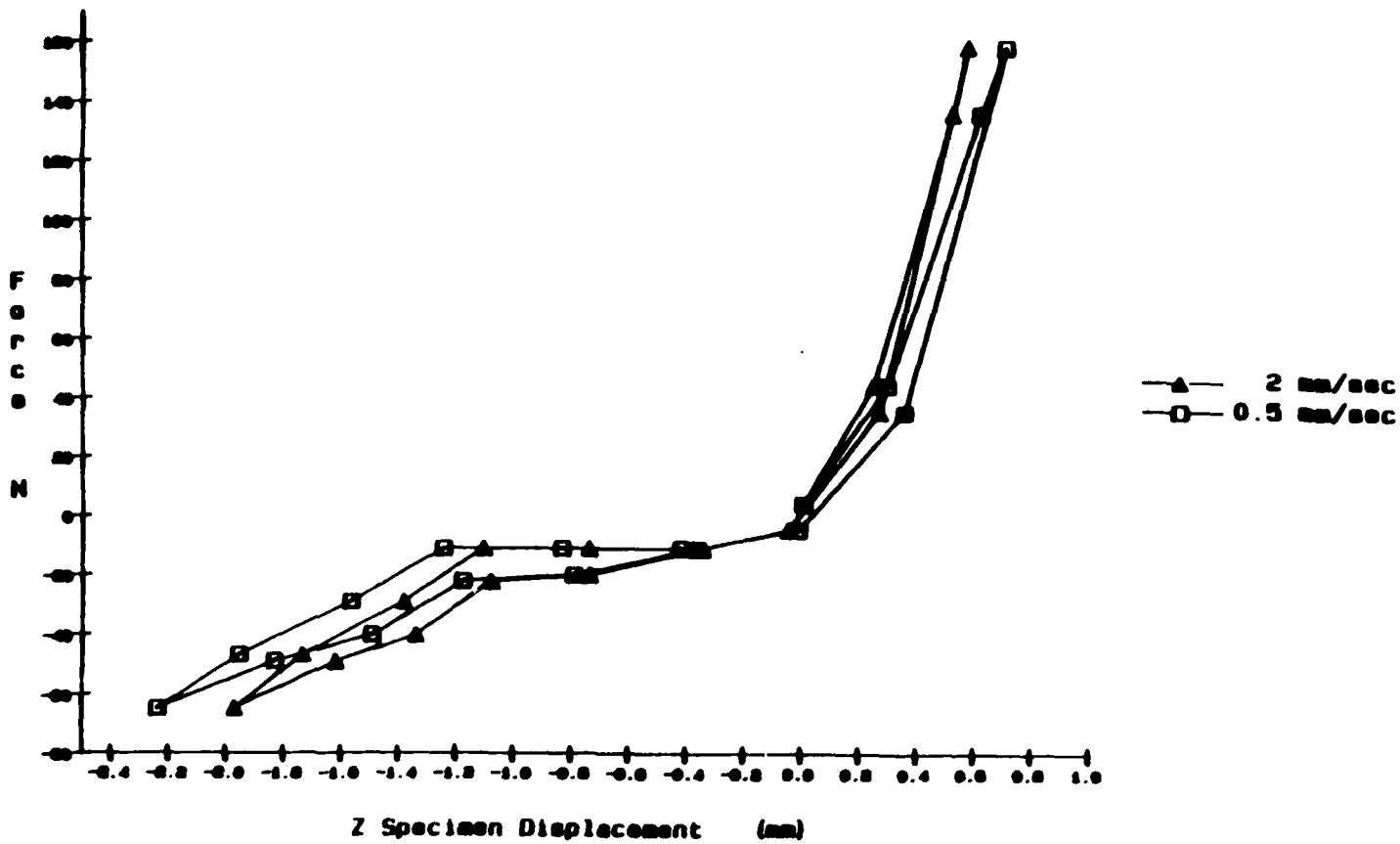

CZ2XZVZ

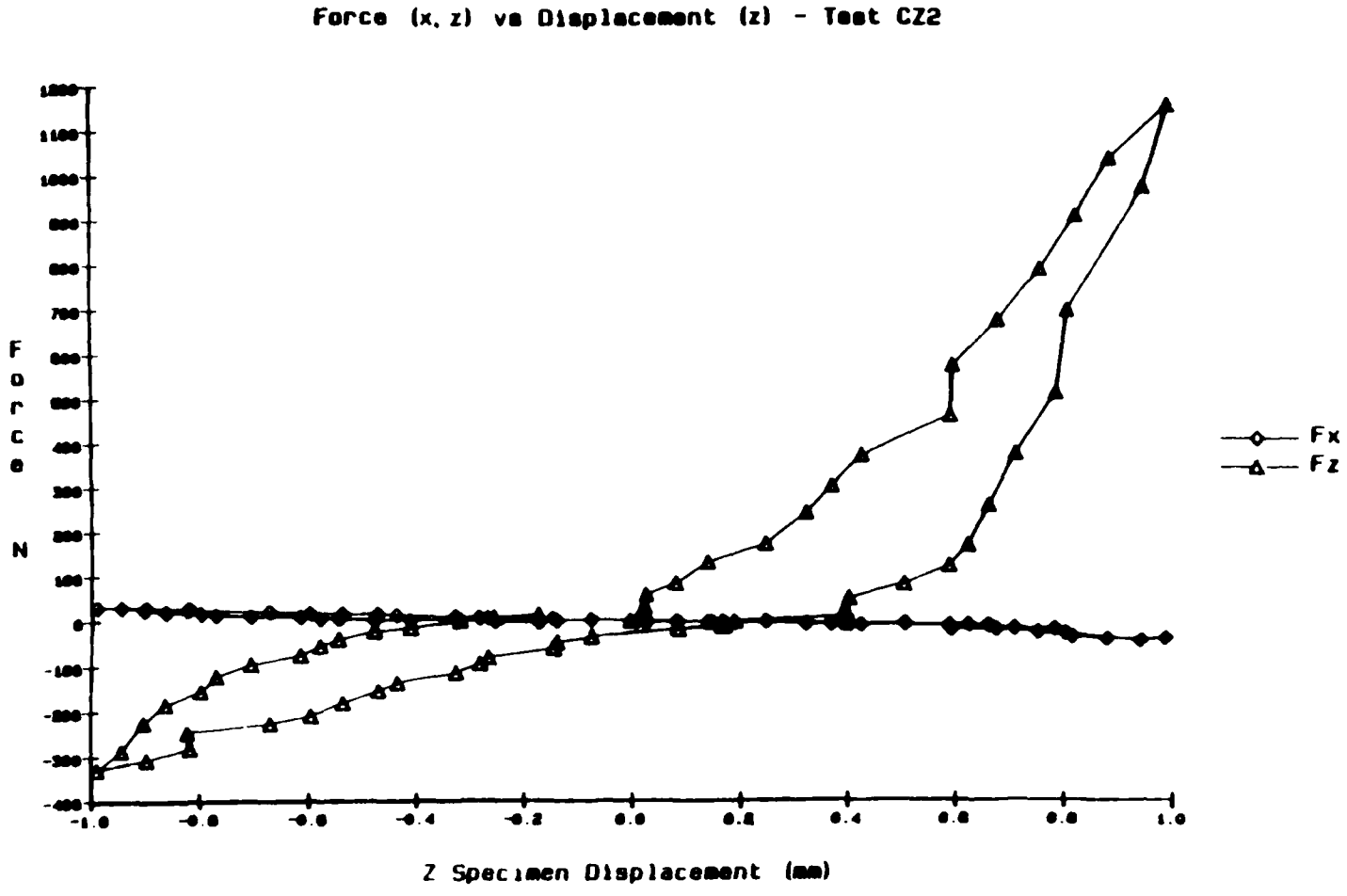
Force (x, z) vs Displacement (z) - Test CZ2
Force N
Z Specimen Displacement (mm)
Fx
Fz

FZ7XZVZ

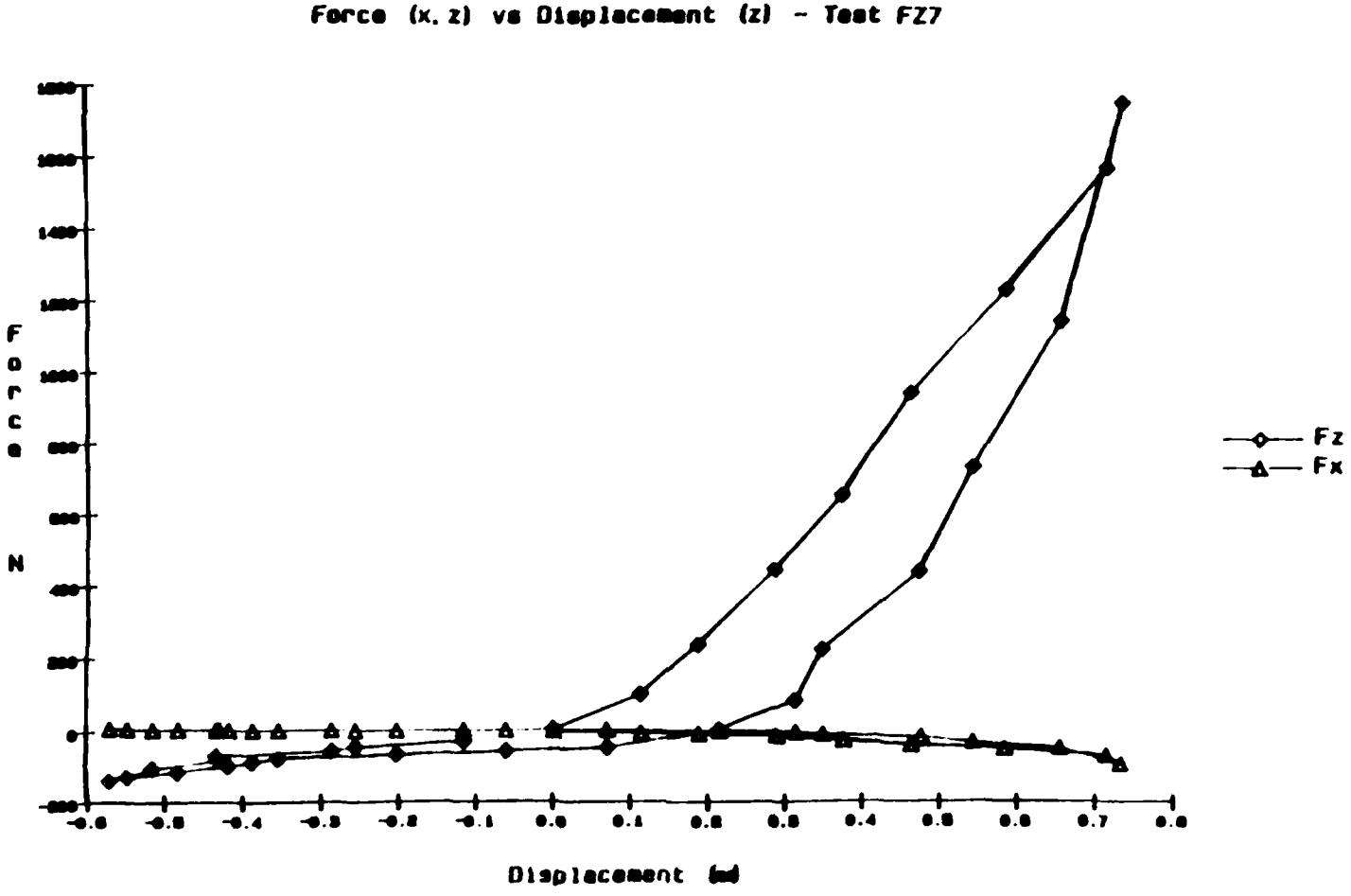
Force (x, z) vs Displacement (z) - Test FZ7
Force
N
Displacement (m)
Fz
Fx

HZ11XZVZ

Force (x, z) vs Specimen Displacement (z) - HZ11

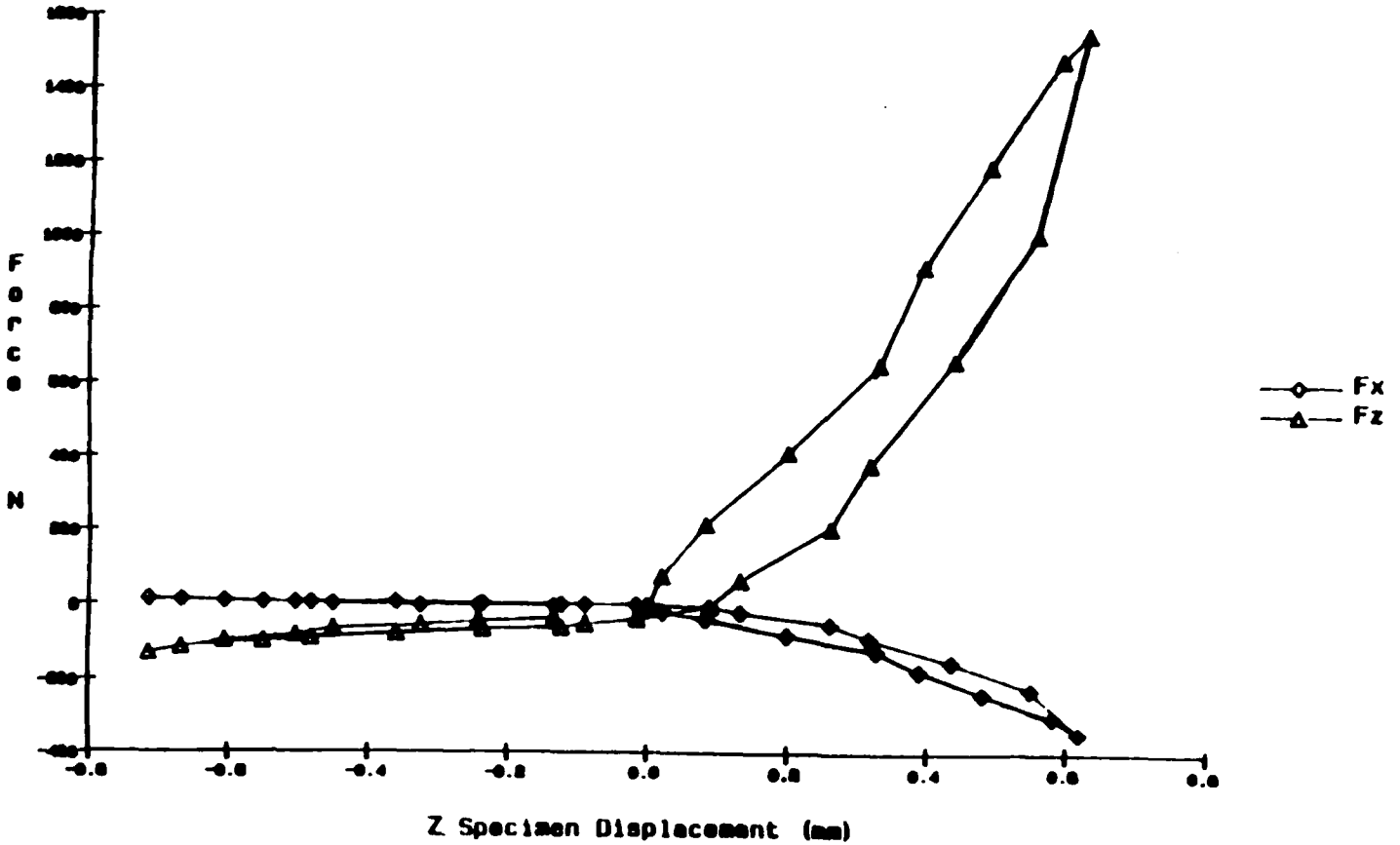

EZ1XZVZ

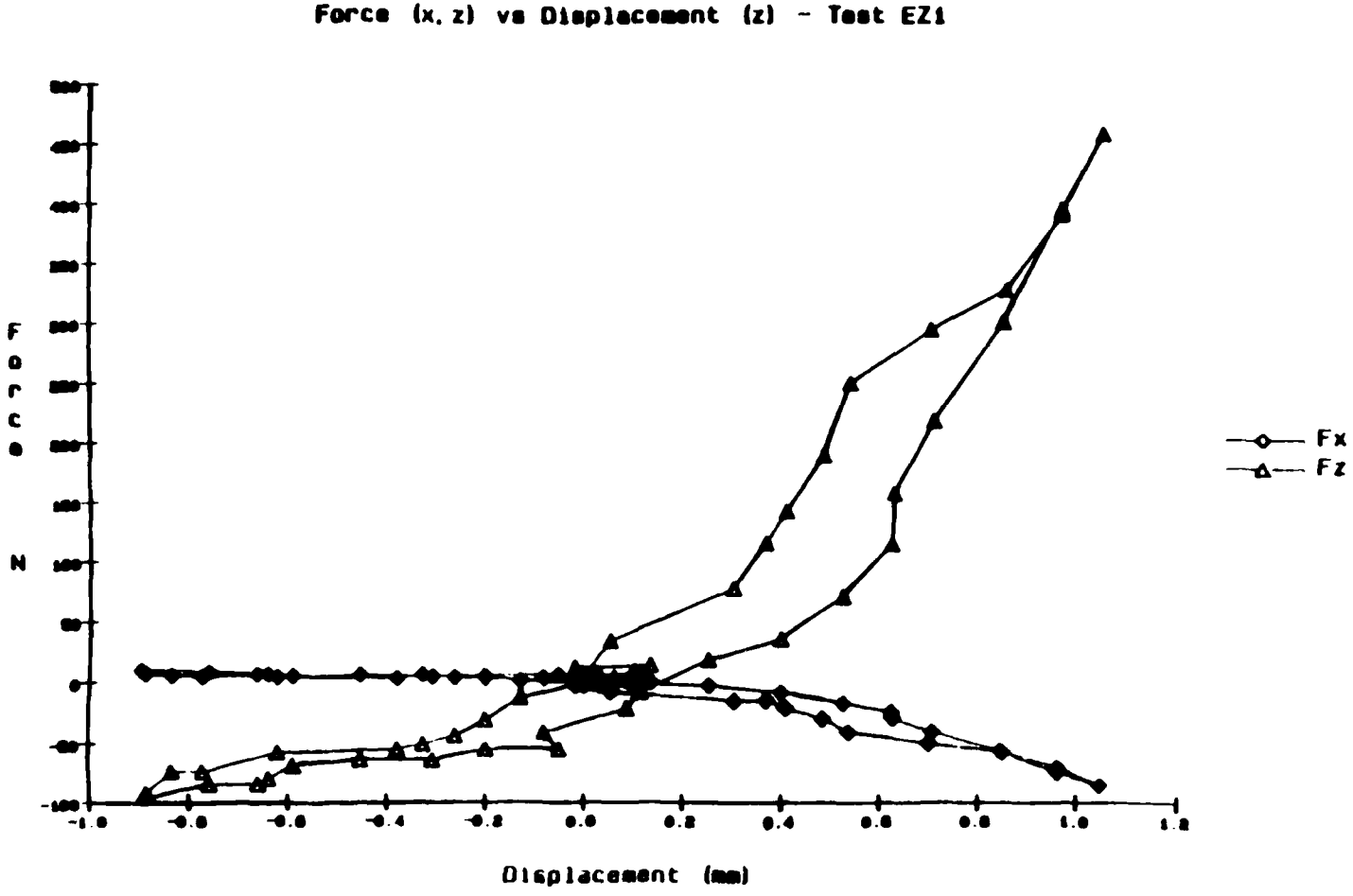
Force (x, z) vs Displacement (z) - Test EZ1
Force
N
Displacement (mm)
Fx
Fz

8Z4XZVZ

Force (x, z) vs Specimen Displacement (z) - 8Z4

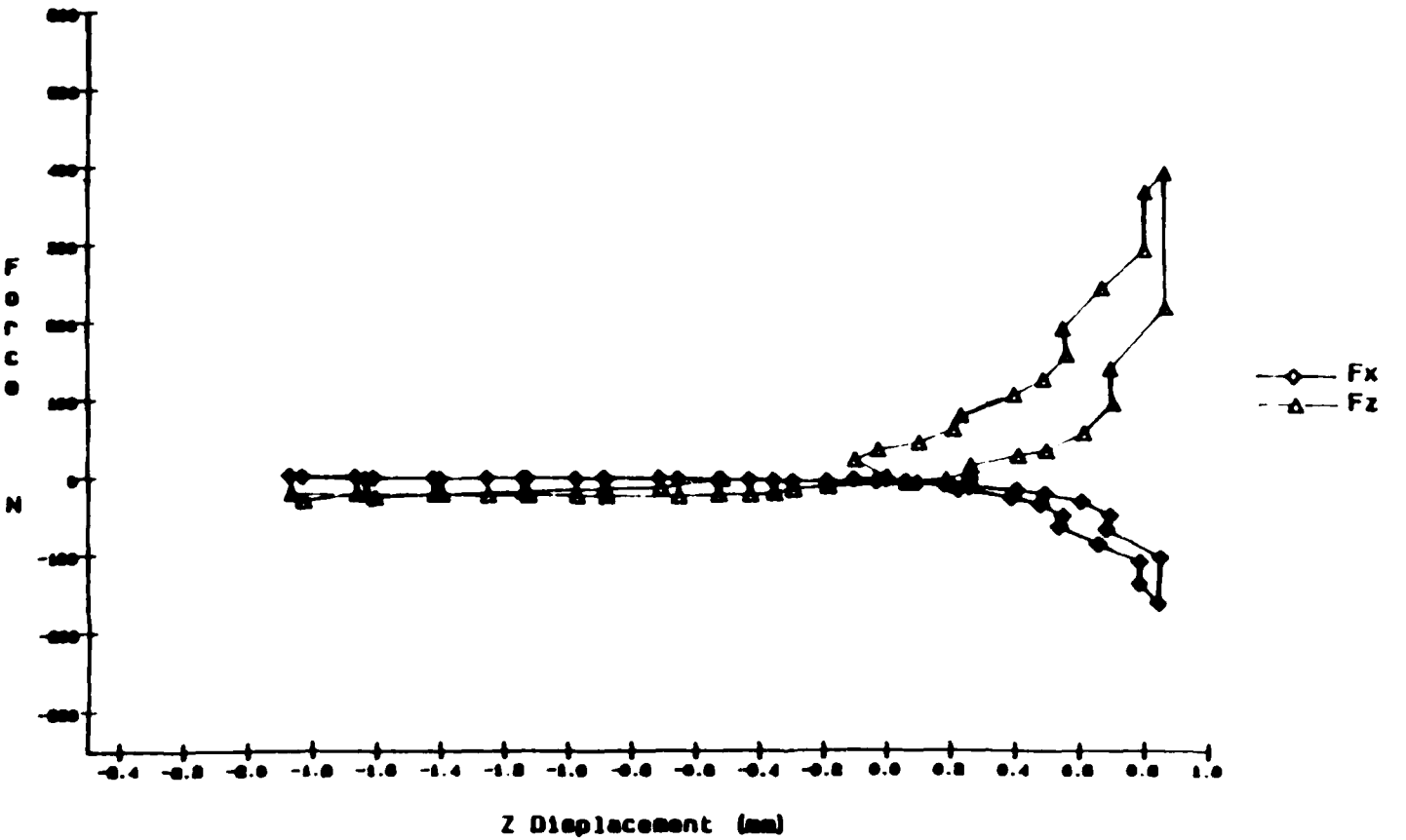

BZ4XZVZ

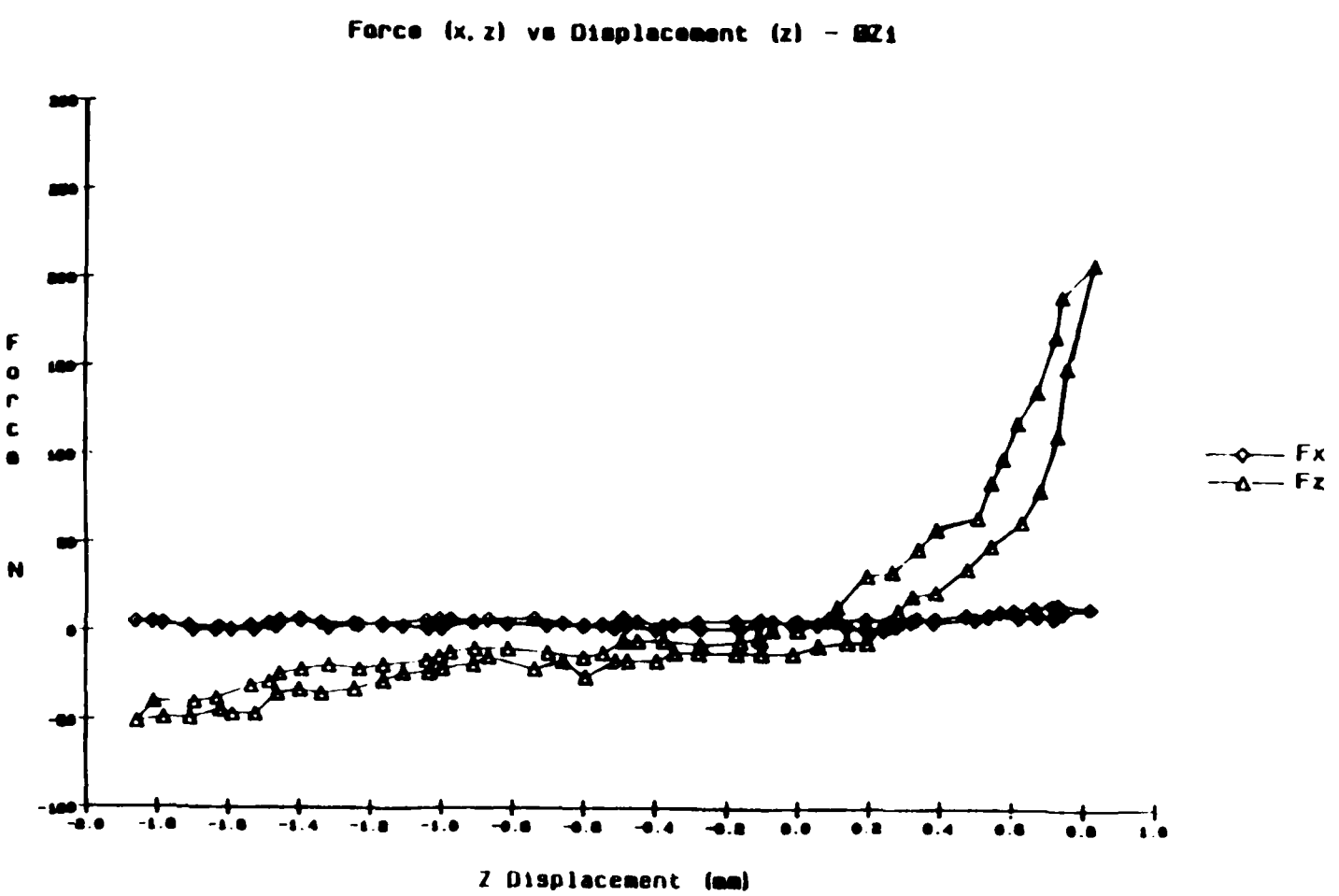
Force (x, z) vs Displacement (z) - BZ1
Force
N
Z Displacement (mm)
Fx
Fz

DZ3XZVZ

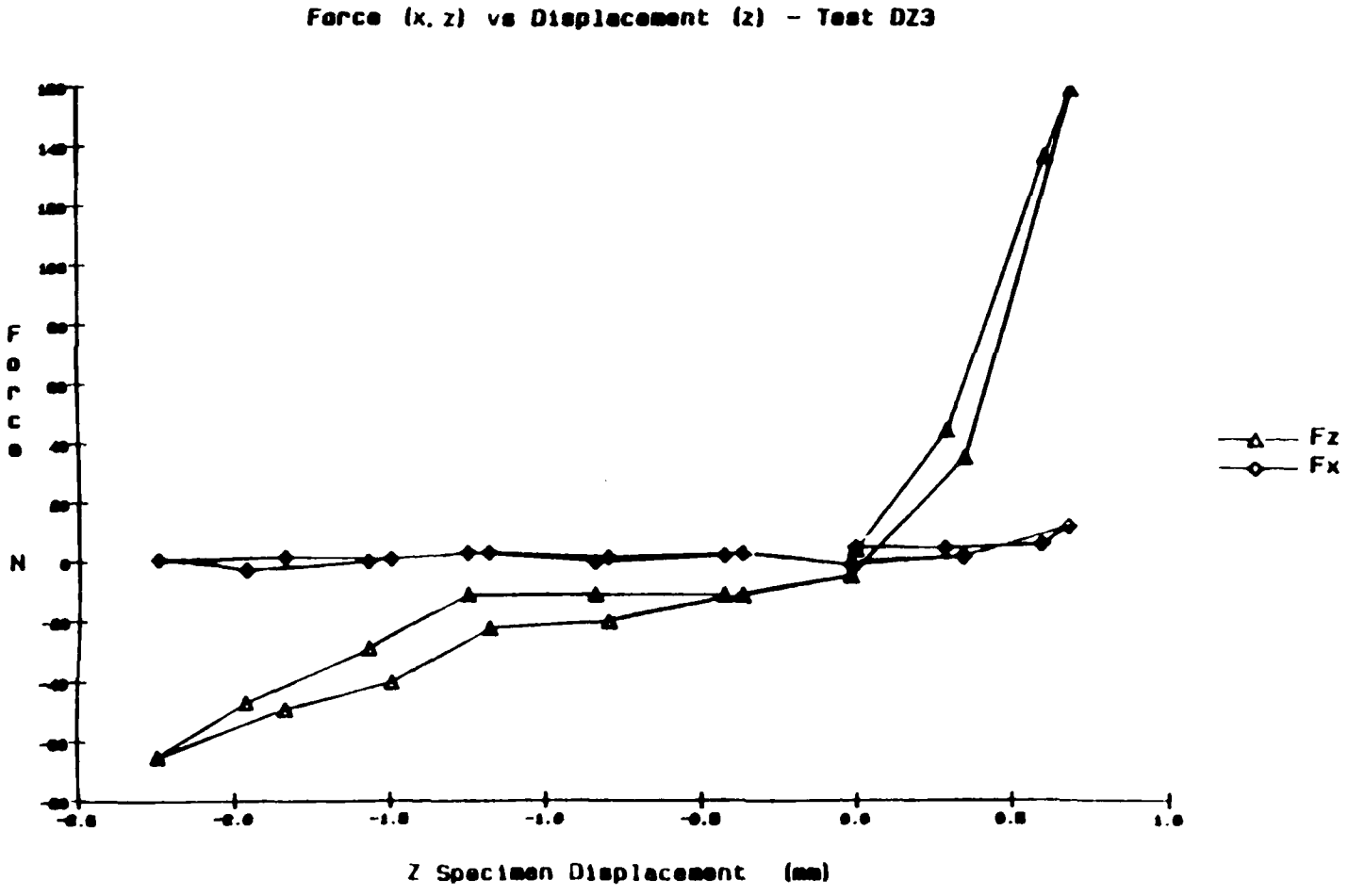
Force (x, z) vs Displacement (z) - Test DZ3
Force
N
Z Specimen Displacement (mm)
Fz
Fx

CX3XVX

C2-C4

Force (x) vs Displacement (x) - Test CX3

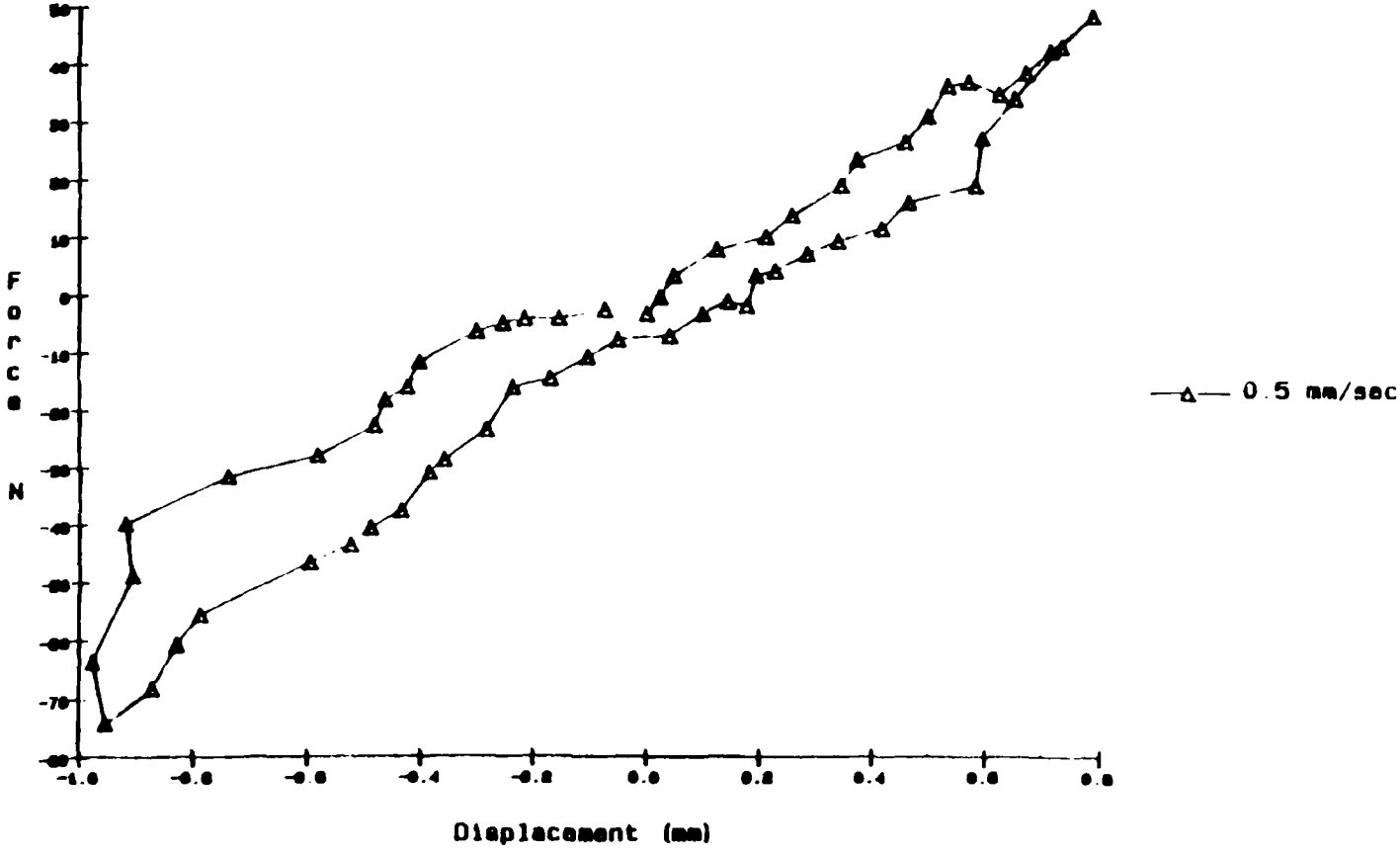

FX3X4VX
C2-C4

Force (X) vs Displacement (x) -2 rates-Tests FX3, FX4

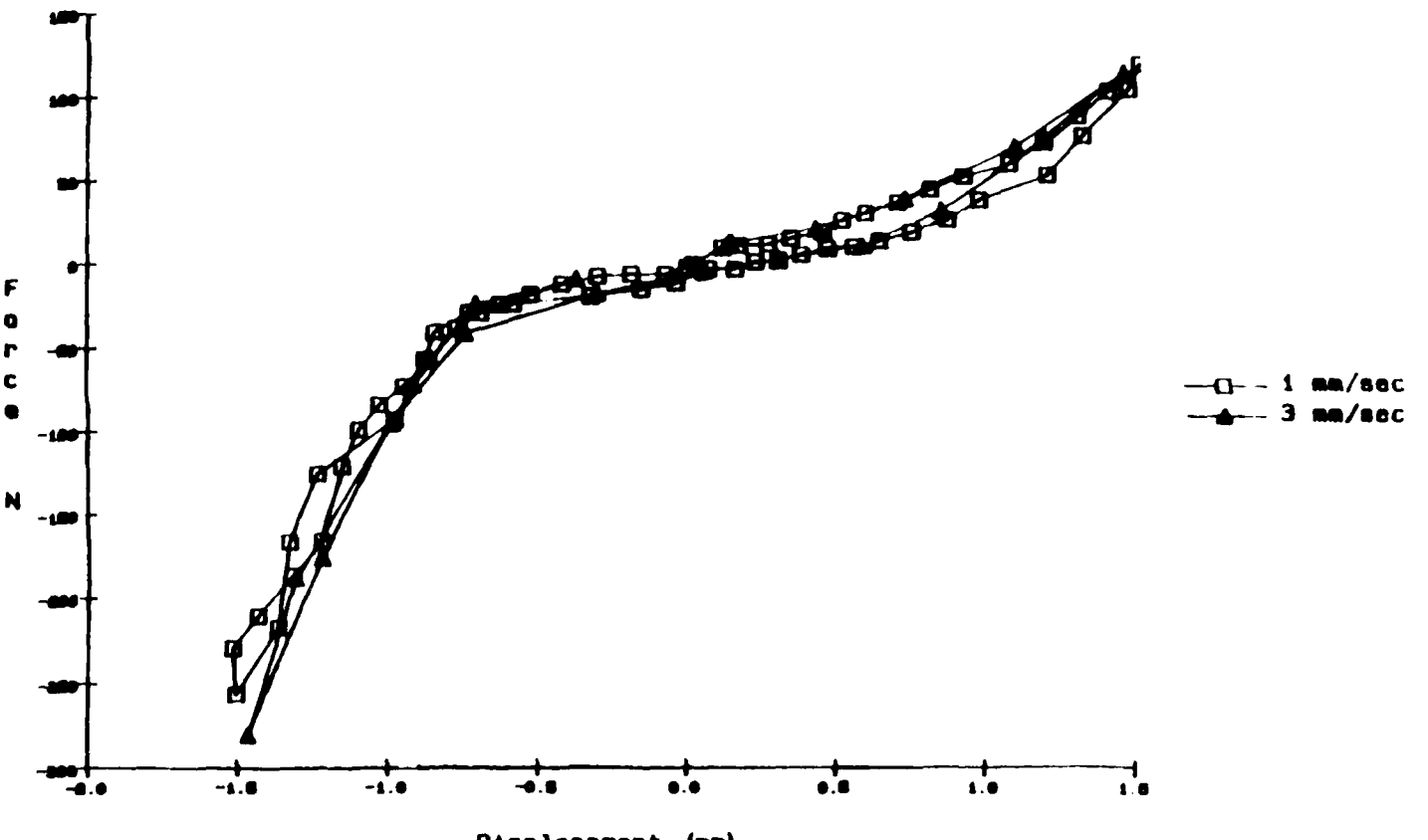

HX9X10XVX
C2-C4

Force (x) vs Displacement (x) for +/-3mm stage displacement - HX9, HX10

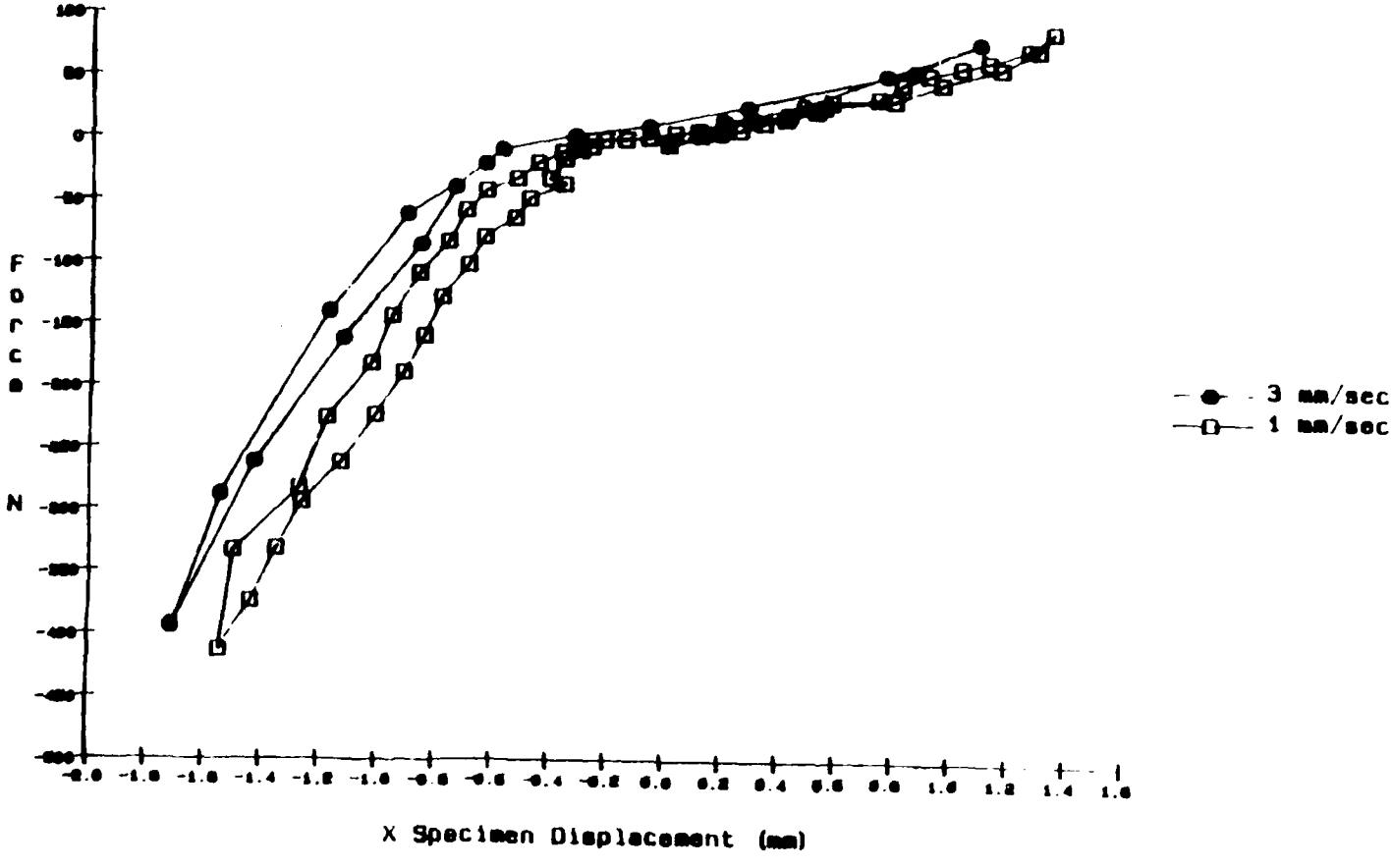

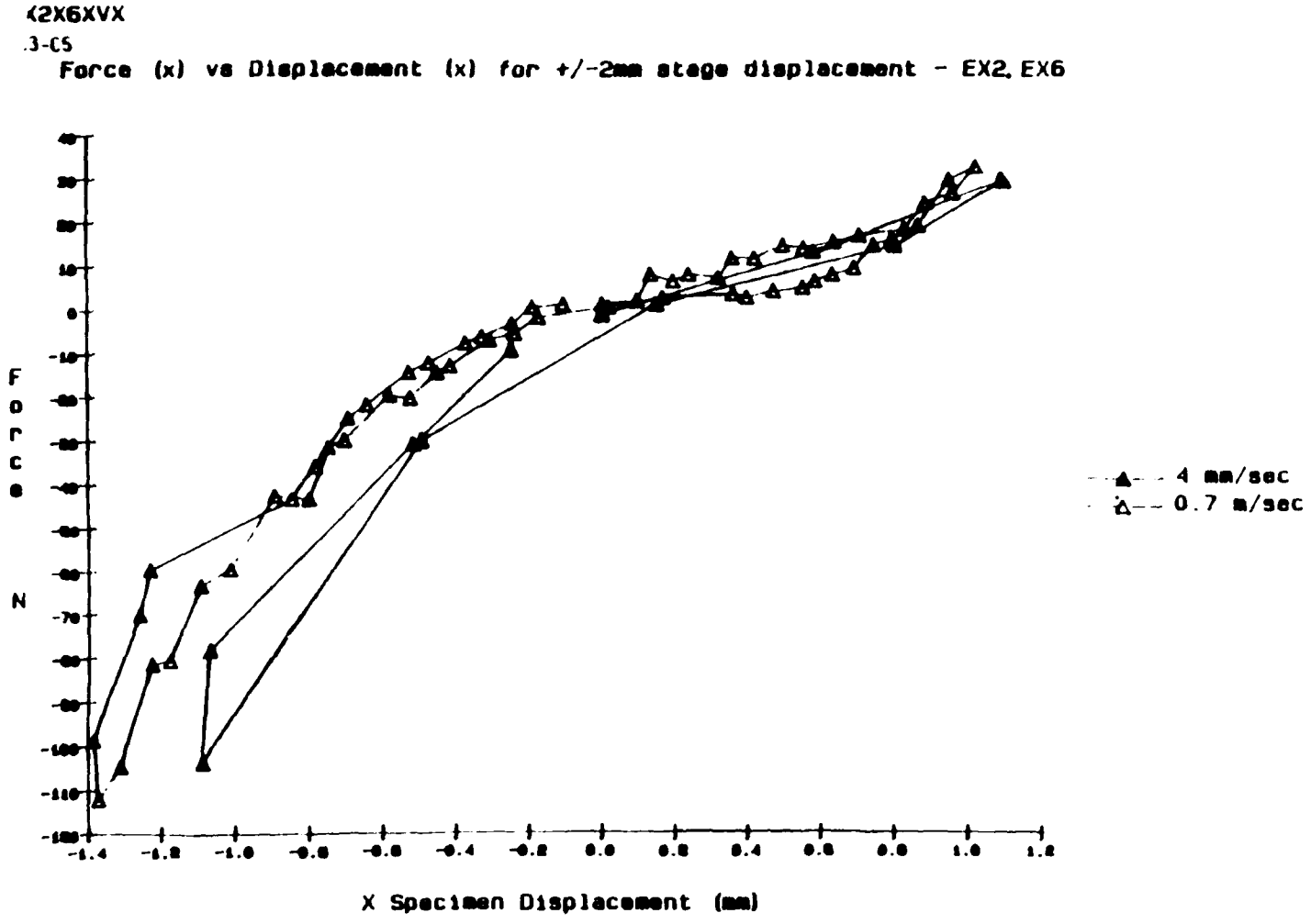
(2X6XVX
.3-C5
Force (x) vs Displacement (x) for +/-2mm stage displacement - EX2, EX6
F
o
r
c
e
N
-1.4
-1.2
-1.0
-0.8
-0.6
-0.4
-0.2
0.0
0.2
0.4
0.6
0.8
1.0
1.2
X Specimen Displacement (mm)
4 mm/sec
0.7 m/sec

GX6X15XVX
C5-C7

Force (x) vs Displacement (x) for stage displacement of 3.5mm-6X6.X15

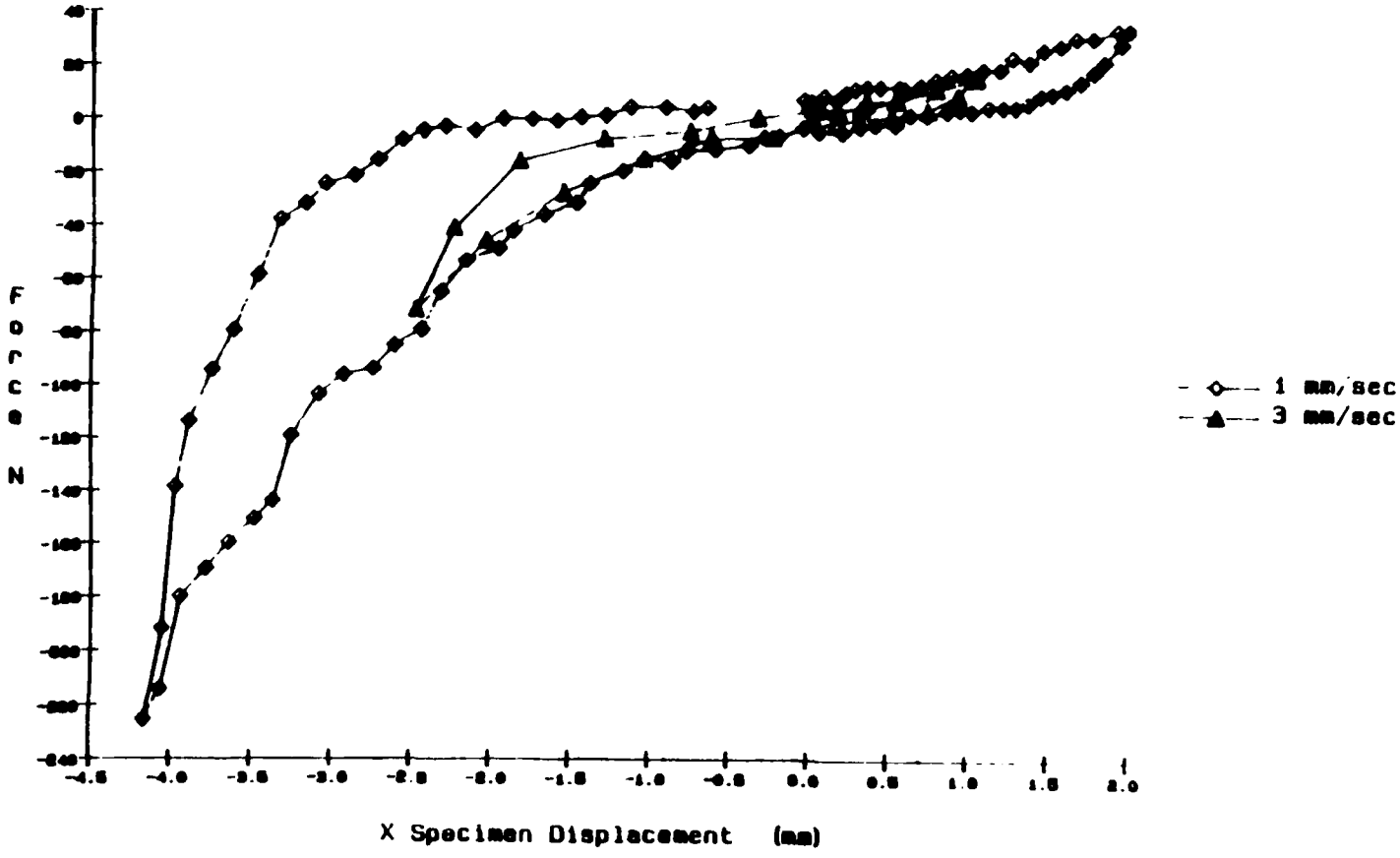

BX4EXX
C6-T1

Force (x) vs Displacement (x) - Test BX4

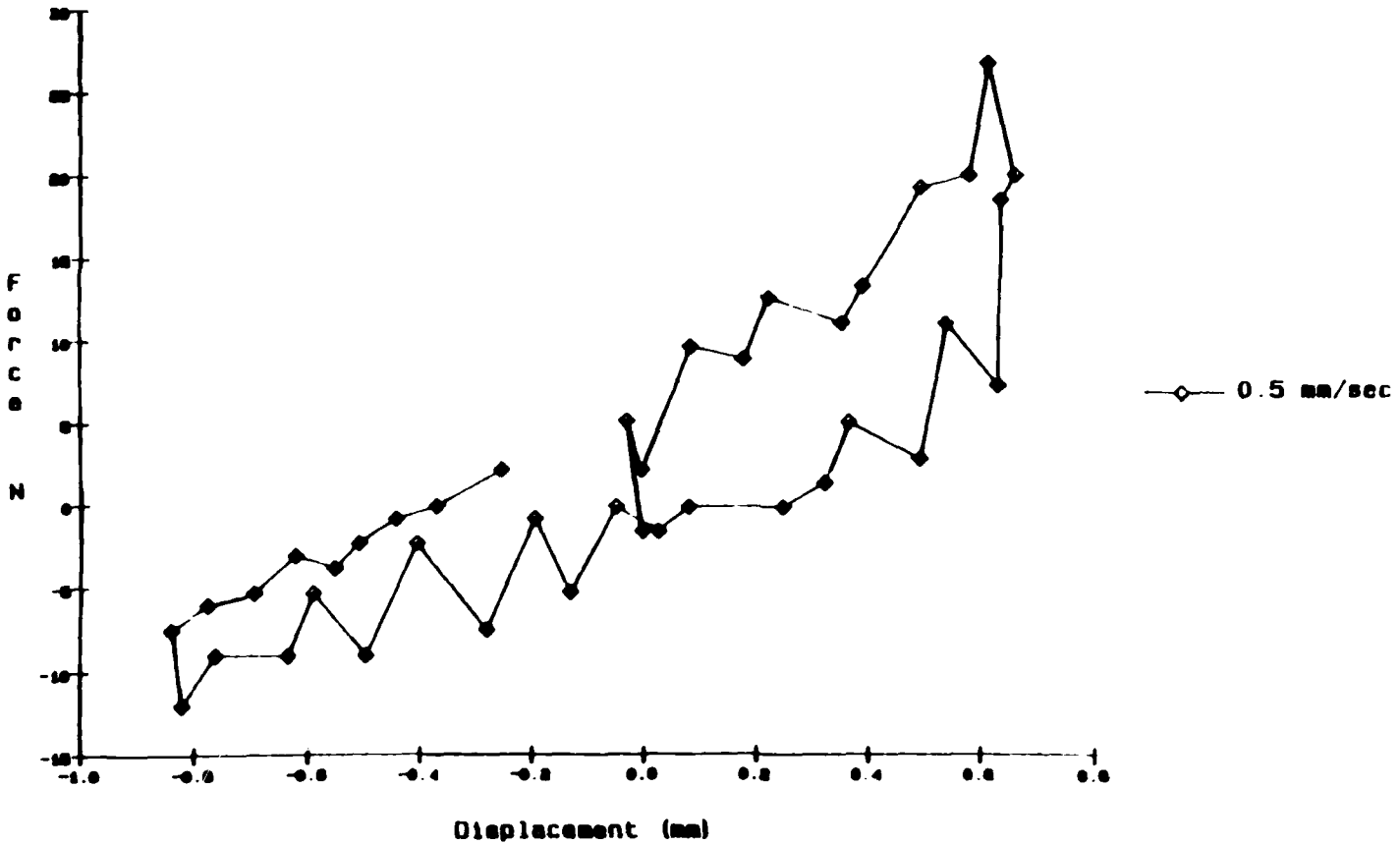

END

DTIC

8-86